

Márcia Raquel da Silva e Sousa Vagos

A computational study of Atrial Fibrillation mechanisms at the cardiomyocyte level

Thesis submitted for the degree of Philosophiae Doctor

Department of Informatics
Faculty of Mathematics and Natural Sciences

Simula Research Laboratory



2020

© Márcia Raquel da Silva e Sousa Vagos, 2020

*Series of dissertations submitted to the
Faculty of Mathematics and Natural Sciences, University of Oslo
No. 1234*

ISSN 1234-5678

All rights reserved. No part of this publication may be reproduced or transmitted, in any form or by any means, without permission.

Cover: Hanne Baadsgaard Utigard.
Print production: Reprosentralen, University of Oslo.

Preface

This is my thesis for the degree of *Philosophiae Doctor* at the Department of Informatics at the University of Oslo. Is it the result of four years of work at Simula Research Laboratory, within the European project AFib-TrainNet. I am very grateful to have been given the opportunity to work in this project, and to be part of such an exciting network. It was an enriching experience to work alongside with such inspiring researchers.

I would like to express my gratitude for all the support and fruitful discussions I had with my supervisors, Dr. Molly Maleckar, Dr. Hermenegild Arevalo, and Prof. Joakim Sundnes. I also appreciate the opportunity I had to collaborate with Dr. Jordi Heijman and Prof. Ulrich Schotten and the time spent at Maastricht University. I would also like to thank my colleagues at Simula and the students of the network, who were an endless source of enthusiasm, support and fun.

I am also immensely grateful for all the support I had from my family and close friends, who were understanding and always helpful during the most difficult moments. Finally, I would also like to show my appreciation for Simula's Administration, who were always very kind and helpful with both technical and personal matters.

The research presented here is conducted under the supervision of Prof. Joakim Sundnes, Dr. Hermenegild Arevalo, and Dr. Molly Maleckar. The thesis is a collection of four papers, within the common theme of computational modelling in Atrial Fibrillation. The papers are presented in chronological order, with the exception of the second paper, and are preceded by an introductory chapter that provides a framing and motivation for the work.

•Márcia Raquel da Silva e Sousa Vagos
Oslo, August 2020

List of Papers

Paper I

Márcia R. Vagos, Ilsebeth G. M. van Herck, Joakim Sundnes, Hermenegild J. Arevalo, Andrew G. Edwards and Jussi T. Koivumäki ‘Computational Modeling of Electrophysiology and Pharmacotherapy of Atrial Fibrillation: Recent Advances and Future Challenges’. In: *Frontiers in Physiology* **9** (2018), DOI: 10.3389/fphys.2018.01221.

Paper II

Márcia R. Vagos, Hermenegild Arevalo, Bernardo Lino de Oliveira, Joakim Sundnes, and Mary M. Maleckar ‘A computational framework for testing arrhythmia marker sensitivities to model parameters in functionally calibrated populations of atrial cells’. In: *Chaos* **27** (2017), DOI: 10.1063/1.4999476.

Paper III

Márcia R. Vagos, Hermenegild Arevalo, Jordi Heijman, Ulrich Schotten, and Joakim Sundnes. ‘A novel computational model of the rabbit atrial cardiomyocyte with spatial calcium dynamics’. *Submitted for publication in Frontiers in Physiology*.

Paper IV

Márcia R. Vagos, Hermenegild Arevalo, Jordi Heijman, Ulrich Schotten, and Joakim Sundnes. ‘A computational study of the effects of rapid atrial pacing-induced remodeling on calcium wave propagation in rabbit atrial cardiomyocytes’. *In preparation*.

Contents

Preface	i
List of Papers	iii
Contents	v
1 Introduction	1
1.1 Motivation	1
1.2 Cardiac anatomy and function	3
1.3 Cardiac electrophysiology	6
1.4 The role of calcium cycling	8
1.5 AF pathophysiology	13
1.6 Cardiac alternans	15
1.7 APD restitution	22
1.8 Models of cardiac electrophysiology	23
1.9 Sensitivity Analysis	33
1.10 Summary of Papers	35
References	36
Papers	50
I Computational Modeling of Electrophysiology and Pharmacotherapy of Atrial Fibrillation: Recent Advances and Future Challenges	51
II A computational framework for testing arrhythmia marker sensitivities to model parameters in functionally calibrated populations of atrial cells	103
II.1 Introduction	104
II.2 Methods	106
II.3 Results	109
II.4 Discussion	118
II.5 Conclusions and future directions	121
References	122
III A novel computational model of the rabbit atrial cardiomyocyte with spatial calcium dynamics	127
III.1 Introduction	129
III.2 Methods	130
III.3 Results	136

Contents

III.4	Discussion	140
III.5	Conclusions	143
III.A	Na ⁺ -Ca ²⁺ exchanger model	143
III.B	Serca2a model	144
III.C	Ca ²⁺ buffers	144
III.D	Initial conditions	145
III.E	Selected population	145
	References	145
IV	A computational study of the effects of rapid atrial pacing-induced remodeling on calcium wave propagation in rabbit atrial cardiomyocytes	151
IV.1	Introduction	152
IV.2	Methods	154
IV.3	Results	157
IV.4	Discussion	163
IV.5	Conclusions	164
	References	165

Chapter 1

Introduction

Contents

1.1	Motivation	1
1.2	Cardiac anatomy and function	3
1.3	Cardiac electrophysiology	6
1.4	The role of calcium cycling	8
1.5	AF pathophysiology	13
1.6	Cardiac alternans	15
1.7	APD restitution	22
1.8	Models of cardiac electrophysiology	23
1.9	Sensitivity Analysis	33
1.10	Summary of Papers	35
	References	36

1.1 Motivation

Atrial fibrillation (AF) is the most common sustained arrhythmia in humans. It is estimated that 1–2% of the population suffer from this condition, and its prevalence is expected to increase with population ageing [1]–[3], posing a huge burden to healthcare.

AF is characterized by the rapid irregular beating of the atria, which ultimately leads to insufficient blood supply to the ventricles. AF is a progressive heart condition which presents three main disease stages: paroxysmal, persistent and permanent [4]. Paroxysmal AF starts with the occurrence of a sudden episode of rapid, arrhythmic activity in the atria, and is usually self-terminating within 48 h. After that point spontaneous conversion becomes significantly less likely [1]. If AF continues to progress for over 7 days it becomes persistent, and may require termination by cardioversion [1]. As AF progresses it becomes more resistant to both standard pharmacological and electrical anti-arrhythmic treatment [5]. If AF persists for over an year, which is designated long-standing persistent AF, the patient is prescribed rhythm control strategies. However, if treatment is not pursued AF is said to be chronic or permanent. Although not fatal in itself, AF can lead to other potentially deadly conditions, such as stroke [3], [6], [7], and congestive heart failure [6], [8], [9]. Additionally, AF susceptibility is exacerbated by co-morbidities and precedent risk factors, such as hypertension, cardiac failure, diabetes, and ventricular hypertrophy [2].

Currently available therapies have limited efficacy and often pose the risk of secondary heart conditions. For instance, the use of anti-arrhythmic drugs can potentially generate ventricular arrhythmias [10] and severe extra-cardiac

1. Introduction

toxicities [1]. Despite the considerable progress made in recent decades towards understanding the pathophysiology of AF, many aspects of the mechanisms of disease still remain poorly understood. Furthermore, the development of new therapies has been hampered by gaps in our understanding how AF initiates and progresses, as well as by the lack of accurate disease models in which new treatments can be tested.

The development of computational models of cardiac myocytes, tissues, and whole hearts have considerably advanced our understanding of cardiac electrophysiology and disease mechanisms. In particular, computational models have greatly contributed to the study of atrial arrhythmias, such as AF, and provided new insight into atrial function across healthy and diseased states [11]–[14]. In particular, computational models spanning the various length scales of the atria, from the sub-cellular, to cellular, and to organ levels, have been key in dissecting the role of atrial structures, anatomy and physiology on different levels of atrial function, which are often difficult and impossible to assess experimentally.

For instance, models of single myocytes have helped clarify the implication of altered electrophysiological properties and signalling pathways to arrhythmogenesis. Tissue and organ level models in turn have allowed to simulate electrical propagation in the heart and the structure-function relationship of different tissue components. Thus, computational modelling provides a more holistic and detailed approach to assessing the dynamics of cardiac diseases than what can be achieved by clinical and experimental observations alone. Measurement modalities, such as the electrocardiogram (ECG) and mapping techniques allow to record large amounts of electrical activation data in the heart which is essential for characterization of heart conditions. However, they have limited capacity to infer on the underlying mechanisms that give rise to the observed activation patterns. Although computational models extensively depend on experimental and clinical data, they go one step beyond by allowing to integrate these data at a higher level and by finding new links between processes at different time and length scales.

Computational models have also been useful for testing new treatment hypotheses, such as simulating the outcomes of novel drug targets [14]. Such developments have the potential for create a high impact on the pharmaceutical industry by allowing fast and cost-effective drug screening with minimal animal testing cost. Furthermore, animal models have long been an important source of experimental and clinical data, which has motivated the development of dedicated models to different animal species, such as the rat, rabbit, canine, pig, and goat. Thus, the development of computational models of human and other animal species has further contributed to the advancement of *in silico* clinical trials, as evinced by the CiPA Initiative [15].

It is important to note, however, that although useful and comprehensive, mathematical models intrinsically are biased by the experimental data they are built upon, which in often cases is obtained from a particular species, group of individuals, or specific region in the heart. Therefore, computational models should be employed within a well-defined scope of application, and results should

be critically analysis with regards to model assumptions and limitations. Models are always only representations of a subset of biophysical processes, and thus do not provide the whole picture of the system they aim to emulate. Therefore, models are continuously being developed and validated against new data and experimental findings to improve their accuracy and predictive capabilities.

The work presented in this doctoral dissertation has therefore been motivated by the need to improve our understanding of AF via computational modeling, and in particular to assess the basic cellular level mechanisms that affect calcium handling, and to evaluate its role in electrophysiological properties of atrial myocytes. The next sections of this chapter will provide a general description of the structure, function and electrophysiology of the atria, as well as an introductory overview of single cell cardiac electrophysiological models, including modeling of ionic currents and the calcium handling system. A more comprehensive overview of the state-of-the-art in atrial and AF modeling will be given in Chapter 2. This chapter will also cover instabilities in the calcium handling system, cardiac alternans, and restitutions curves which together provide a framing for Chapters II, III, and IV. Finally, I will give an overview of some basic methods for sensitivity analysis of single cell models of cardiac electrophysiology, an emerging field within cardiac modeling that has been shown to be useful in both uncovering mechanisms underlying model behaviors, and in guiding the model development procedure itself. This overview will provide a framing for the methodologies used in Chapters II and III.

1.2 Cardiac anatomy and function

The heart is one of the most important organs in the body, whose main function is to pump blood into the vascular system. The heart is essentially a muscle that contracts and relaxes at every heartbeat. It contains four chambers: the left and right ventricles and the left and right atria (Figure 1.1). The atria are the two uppermost chambers and are responsible for regulating blood flow into the ventricles. The right atrium receives blood from the superior vena cava, the inferior vena cava, the anterior cardiac veins and smallest cardiac veins and the coronary sinus, and sends it into the right ventricle. The right ventricle in turn pumps the blood into the pulmonary vein and into the lungs. The blood returns to the left atrium from the left and right pulmonary veins, and is pumped into the left ventricle which then sends out the blood to the system circulation through the aorta.

At rest conditions, the contribution of the atria to the filling of the ventricles is relatively low, about 10%, but during increased hemodynamic load atrial contraction increases to accommodate for the higher blood pressure, accounting for about 20-30% of the ventricle filling [16].

The cardiac muscle, also known as the myocardium, is composed of multiple myofibers, each containing a large number of heart cells, or cardiomyocytes (1.2(a-b)). Cardiac cells are excitable, i.e. they are capable of generating electrical activity when stimulated. For the myocardium to contract effectively,

1. Introduction

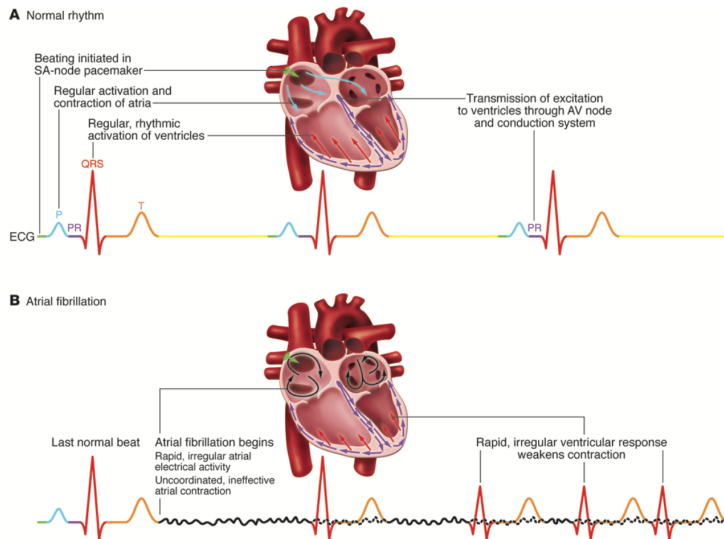


Figure 1.1: Heart anatomy, electrical propagation, and typical electrocardiograph wave shape in normal rhythm (A), and Atrial Fibrillation (B). [17].

all cardiomyocytes must contract in a synchronous manner. That requires the coordinated activation of the cardiac cells, and this coordination is made possible by connections among the cardiomyocytes, called gap junctions (Figure 1.2(c)). These connections allow electrical signals to rapidly propagate from myocyte to myocyte and throughout the heart triggering contraction, which allows the myocardium to effectively operate as a uniform syncytium. Thus, in the myocardium, much like in other muscular tissue, electrical and contractile activity are inherently associated, in what is termed ‘excitation-contraction coupling’.

Contraction initiates at the cardiomyocyte level, and carried out by specialized intracellular structures called myofibrils. These are composed of bundles of myofilaments, composed of long protein chains that are laid in parallel with the cell axis (Figure 1.2(c)), and slide over each other to produce mechanical contraction and relaxation. These macromolecular structures constitute the backbone of the contractile machinery in cardiomyocytes, shortening and expanding at every beat, and possibly constitute about 60% of the cell volume [18].

Atrial and ventricular myocytes share several structural and electrophysiological characteristics. However, there are also important differences which translate into their somewhat different functional roles. Atrial myocytes are in general smaller than ventricular myocytes, and have specific electrophysiology.

Electrical stimulation in the heart is generated at the SA node, a small region located in the posterior wall of the right atrium. The SA node is composed

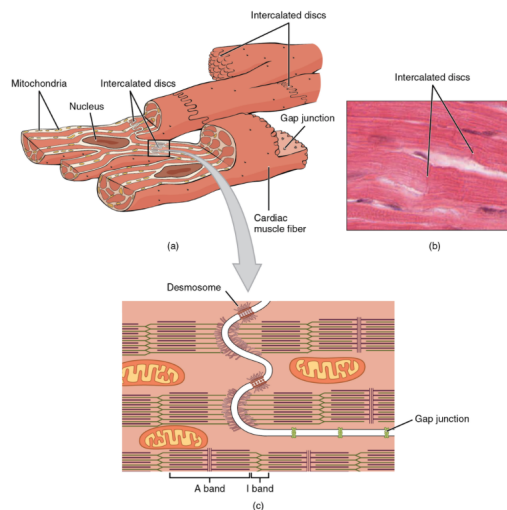


Figure 1.2: (a) Schematic representation of the ultrastructure of cardiac muscle tissue, showing myofibrils contained individual cardiomyocytes. (b) A micrograph of cardiac muscle tissue; (c) A close in on the sub-cellular structure of a cardiomyocyte, representing the myofilaments, mitochondria, and the intercalated disk containing gap junctions, and desmosomes. Obtained from [17].

of myocyte with self-excitability properties (Figure 1.1A). These myocytes are appropriately called ‘pace-maker’ cells, since they are responsible for establishing the autonomic pacing of the heart. The pace-maker cells generate electrical signals which then propagate downstream throughout the atria and into the ventricles, as illustrated in Figure 1.1A. Under normal conditions, the SA node is triggered at a steady pace – the heart rate – ensuring a regular and continuous beating of the myocardium.

Although all cardiomyocytes are excitable, the atria and the ventricles rely on specialized structures organized as conducting bundles for rapid electrical propagation. This ensures a rapid and synchronous contraction of the myocardium. In healthy hearts, the electrical signals propagate from the SA node first across the right atrium, and into left atrium, reaching the atrio-ventricular node, a small region connecting the conducting bundles of the atria with those of the ventricles. The electrical signals then continue to propagate into the ventricles through the His bundles and finally into the Purkinje fibers, triggering them to contract and pump out blood (Figure 1.1A).

In each beat the myocardium contracts (systole), pumping out the blood, and subsequently relaxes (diastole) to be ready to be filled again. The heart rate adapts to hemodynamic conditions in the body, for example due to increased physical activity, stress, or disease. The cardiac output of the heart is increased by regulating force of contraction – inotropic response –, the rate of contraction – chronotropic response –, or the velocity of electrical conduction – dromotropic

1. Introduction

response. Positive chronotropic response results from increasing the trigger rate of the SA node.

1.3 Cardiac electrophysiology

Electrical activity in cardiac myocytes is mediated by the opening and closing of ion channels and transporters located at the cell membrane, also called the sarcolemma. These are transmembrane macromolecules which allow selective movements of ions in and out of the cell, thus effectively maintaining ionic concentration gradients, necessary for a stable transmembrane potential. The flow of ions across the membrane cause fluctuations of the transmembrane potential, that is the *action potential* (AP), which trigger a cascade of signalling pathways inside the myocyte. The most relevant of such events is the release of large amounts of calcium ions into the cytosol, ultimately leading to cell contraction. The transient variations in transmembrane potential are ‘sensed’ by adjacent myocytes and triggers new APs (Figure 1.3).

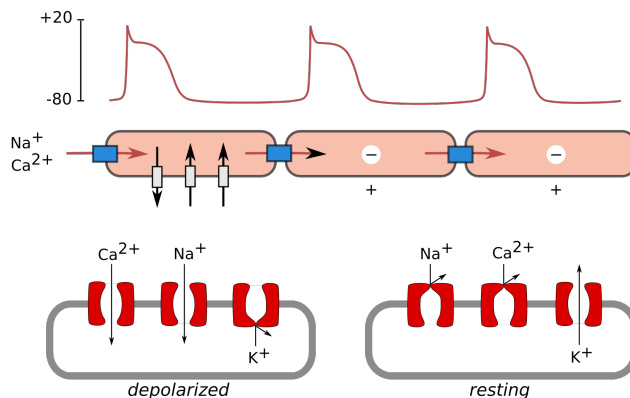


Figure 1.3: Action potentials propagate along adjacent myocytes through movement of ions which create activating currents. When a cell is stimulated, fast sodium channels open allowing a rapid inflow of Na^+ into the cytosol. This inward flow of positive ions causes the membrane to become depolarize, eventually reaching the threshold voltage for activation of the voltage-sensitive Ca^{2+} channels, which open to let Ca^{2+} ions to flow in. Simultaneously, K^+ channels open allowing in outward current to flow and bring the membrane back to the repolarized state.

A number of ion channels and transporters are expressed in the cardiac tissue, and their main function is to mediate the transport of Na^+ Ca^{2+} K^+ , as well as Cl^- across the sarcolemma. Concentrations of Na^+ and Ca^{2+} are much greater in the intra- than in the extracellular medium, whereas K^+ is more predominant inside the cell. Differences in the expression levels of ion channels and structural differences in their subunits dictate the observable diversity in AP morphologies

across species, individuals, and heart regions. In humans, as well as in many other animal species, myocytes express the fast sodium channel (I_{Na}), L-type Ca^{2+} channels (I_{CaL}), sodium-calcium exchanger (I_{NCX}), sodium-potassium pump (I_{NaK}), a transient outward current (I_{to}), a n inward rectifier current (I_{K1}), and rapidly (I_{Kr}) and slowly (I_{Ks}) activating delayed rectifier potassium channels (see Figure 1.4A).

When the channels open, ions flow across the membrane down their electrochemical gradients. It is the synchronous opening and closing of ion channels that produces the AP, thus they are essential to maintain rhythmicity and contractility in cardiac myocytes. Therefore, their function is tightly regulated by a multitude of cellular processes. Ion channels are both time- and voltage-sensitive, which means that they are activated when the transmembrane potential reaches a certain threshold value, and inactivate after a certain time period (normally a few tens to a few hundred ms). Some ion channels are additionally modulated by local ionic concentrations. For instances, L-type calcium channels (LTCC) are inactivated by the rise of intracellular Ca^{2+} concentration.

Upon stimulation, Na^+ channels rapidly open allowing a large current to flow inwards, which cause a sudden rise in membrane potential – *depolarization*. The I_{Na} current is active in phase 0 of the AP (Figure 1.4B). Almost simultaneously, K^+ channels open allowing ions to flow outwards and balance out the depolarizing Na^+ current. This cause transmembrane potential to drop back to more negative levels – *repolarization*–, giving rise to phases 1 through 4 of the AP. The peak of the AP is followed by a slower opening of the LTCC, and the inflow of Ca^{2+} ions contributes to a prolongation of membrane depolarization and is visible as a plateau on the AP (phase 2).

As mentioned, AP morphologies in cardiac myocytes vary considerably, as each myocyte has a unique ‘signature’ of ion channel structures and distribution throughout the membrane. However, most AP shapes share the same four phases depicted in Figure 1.4B. Thus, AP morphologies have been consistently characterized by a few metrics. Four of the most common ones are: (1) AP duration (APD), the time from the peak of the AP to a certain repolarization threshold; (2) upstroke velocity, which is the rate of voltage increase from the onset of the AP to the peak; (3) AP amplitude (APA), defined as the peak voltage (most depolarized state) minus the voltage at the onset of the AP; and (4) the resting membrane potential (RMP), which is the voltage level at ‘rest’. These metrics are schematically represented in Figure 1.4C.

1. Introduction

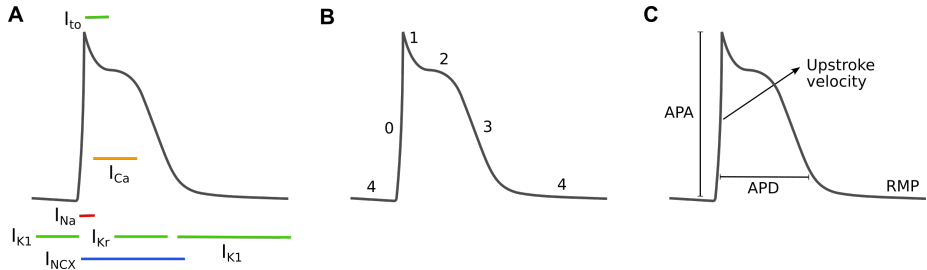


Figure 1.4: ((A) Most predominant ionic currents in human cardiac myocytes and their activity span during the AP. (B) The four phases of the action potential. (C) Representation of four common metrics to describe action potential shape: action potential duration (APD), upstroke velocity, action potential amplitude (APA), and the resting membrane potential (RMP).

1.4 The role of calcium cycling

Calcium is the single most important ionic species in cardiac myocytes since it mediates a large number of cellular processes, from membrane depolarization, to several signalling pathways, to cell apoptosis, and most importantly, to mechanical contraction. Thus, it is crucial for the cell to maintain a tight control over the intracellular concentrations of Ca^{2+} in order to maintain vital functions.

There are different mechanisms by which cardiac myocytes maintain Ca^{2+} homoeostasis and ensure adequate Ca^{2+} availability. The normal Ca^{2+} concentration inside the cytosol is $\sim 0.1 \mu\text{M}$, in contrast with the $\sim 1 \text{ mM}$ found in the extracellular medium. This steep concentration gradient across the cell membrane gives the cell the ability to rapidly increase its intracellular Ca^{2+} concentration via passive inflow of ions through calcium channels. The influx of Ca^{2+} through the LTCC is, however, not sufficient to trigger full cell contraction. Instead, the majority of intracellular Ca^{2+} in myocytes is located inside specialized Ca^{2+} storages, mainly the sarcoplasmic reticulum (SR), where Ca^{2+} is kept at around $100 \mu\text{M}$ [19], [20], and the mitochondria. When an AP is elicited, I_{CaL} triggers the release of a large amount of Ca^{2+} from the SR, which causes a rapid increase of the cytosolic Ca^{2+} levels, that is the *calcium transient* (CaT).

Ca^{2+} is released from the SR via specialized transporters called the ryanodine receptors (RyR), which are distributed over the entire SR membrane. They are organized into clusters, termed ‘calcium release units’ (CRUs) of varying numbers of RyRs, from a few tens to a few hundreds [21]. Clusters have been shown to be laid out in a tight regular 2D lattice at the dyad junction, juxtaposed by an heterogeneous array of LTCC across the dyadic space of about 15 nm [21], [22]. This complex of RyRs and LTCCs is commonly referred to as the ‘couplon’. RyRs in close proximity with the sarcolemma directly interact with the LTCCs, and this physical coupling sensitizes the RyRs to Ca^{2+} and facilitates activation by I_{CaL} [23]. These are termed ‘junctional’ RyRs.

The couplon is a region of elevated calcium concentration from which Ca^{2+} diffuses out towards adjacent CRUs not in direct contact with LTCCs. These are termed ‘non-junctional’ RyRs or CRUs. The diffusion of Ca^{2+} triggers the release of more Ca^{2+} from the SR, and this self-amplifying process is often referred to as ‘calcium-induced calcium release’ (CICR). Computational modeling has suggested that RyRs are sensitive only to elevations of calcium in the nano-domain surrounding the CRU. This ‘local control’ hypothesis [24] proposes that the control of SR Ca^{2+} release is facilitated by a graded recruitment of independent and stochastic Ca^{2+} release events from a single RyRs, designated ‘calcium sparks’ [25]–[27]. Sparks are stochastic events of RyR opening, with the combination of multiple sparks forming the CaT [25]. The rate of Ca^{2+} sparks also increases with increasing SR Ca^{2+} content. Thus end-diastolic Ca^{2+} overload can significantly increase the probability of spontaneous Ca^{2+} release events [28].

The same amount of Ca^{2+} that is released into the cytosol must be removed to restore intracellular Ca^{2+} levels before the onset of the next beat. If intracellular Ca^{2+} levels remained constant, the myocyte would be in continuous contraction.

Physiological levels of end-diastolic cytosolic Ca^{2+} are maintained by removing cytosolic Ca^{2+} via two main pathways: Ca^{2+} extrusion from the cell via the $\text{Na}^+-\text{Ca}^{2+}$ exchanger NCX and via the plasma membrane Ca^{2+} ATP-ase (PMCA), and Ca^{2+} reuptake into the SR via the sarco/endoplasmic reticulum Ca^{2+} ATP-ase (SERCA) pump. The NCX exchanges 1 Ca^{2+} ion for 3 Na^+ ions, and hence it uses the energy of the dissipation of the Na^+ electrochemical gradient, which favors Na^+ entry, to extrude Ca^{2+} from the cell. PMCA, in turn, uses energy from ATP hydrolysis to pump Ca^{2+} into the extracellular medium. The i pumps are active transporters located at the non-junctional portions of SR membrane. The additional Na^+ entry in the myocyte promoted by NCX is extruded back through the Na^+-K^+ pump (NaK). This is the main efflux pathway of Na^+ and thus is the primary mechanism of intracellular Na^+ regulation. Because NaK regulates intracellular Na^+ levels, it also affects NCX function, and studies have shown that NKA subunits are collocated with NCX [29].

The set of processes in the cell that regulate transient intracellular calcium elevation is referred to as the calcium cycling. Figure 1.5 depicts a summarized description of the Ca^{2+} cycle in cardiac cells. References [16], [30], [31] provide a more comprehensive read on calcium handling in atrial myocytes.

Ventricular and some atrial myocytes possess T-tubules (TTs), which consists of invaginations of the sarcolemma inside the cell forming a 3D network. These structures provide a ‘highway’ for Ca^{2+} to reach the inner locations of the cell. TTs in atrial myocytes are less dense and well-organized than in ventricular myocytes, as illustrated in Figure 1.6, and can also be altogether absent in atrial cells of small animal species. The presence or lack of TTs results in substantial differences in the kinetics of the CaT. In atrial myocytes without a substantial TT network, EC-coupling initiates at the sarcolemma with calcium entering the cell via the LTCC and triggering junctional RyRs. Since the only a small fraction of the CRUs are located in close proximity to the membrane, direct

1. Introduction

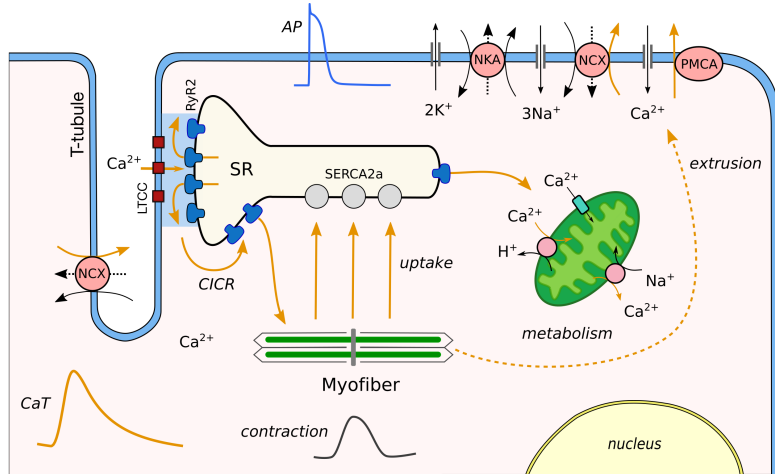


Figure 1.5: Schematic representation of the calcium handling system in a cardiac myocyte.

inflow of Ca^{2+} cannot trigger RyRs in non-junctional portions of the SR. Instead, calcium diffuses from the membrane vicinity towards neighbouring CRUs, where it activates RyRs, and the process is repeated until Ca^{2+} reaches the central regions of the cell and engages the contractile machinery.

It has been shown that this process of regenerative calcium release has a high level of spatio-temporal organization, and can give rise to calcium waves that propagate from the periphery towards the center (Figure 1.7). Intracellular calcium waves are driven by Ca^{2+} diffusion in the cytosol between neighbouring regions with differences in Ca^{2+} concentrations. This process has been appropriately termed ‘fire-diffuse-fire’ response. As a consequence of Ca^{2+} propagating from periphery to the center, a damping of the calcium signal can be observed in some myocytes, as shown by the recorded traces in Figure 1.7. This damping of the calcium signal is mainly a consequence of calcium being buffered by cytosolic proteins and the myofilaments [16], [32].

However, this advancing wave front of elevated Ca^{2+} concentration is not a continuous process, but rather it is saltatory, with calcium release passing from discrete CRU to CRU. Even in atrial myocytes with TTs, the central CaT is still mainly dependent on this mechanism. Figure 1.8 illustrates the commonly accepted model of calcium wave propagation. Furthermore, since calcium waves propagate with a finite velocity, CaTs elicited at the innermost regions of the cell are lagged in time compared to the CaTs originate at the membrane. This results in ‘u-shaped’ wave front when visualized in line scans (1.9Bii)), in contrast to ventricular cells where CaTs are elicited simultaneously at the membrane and center (Figure 1.9Bi).

Another important aspect of cardiac calcium handling is buffering. Buffers are macromolecules that have high affinity for a certain ligand. Calcium buffering

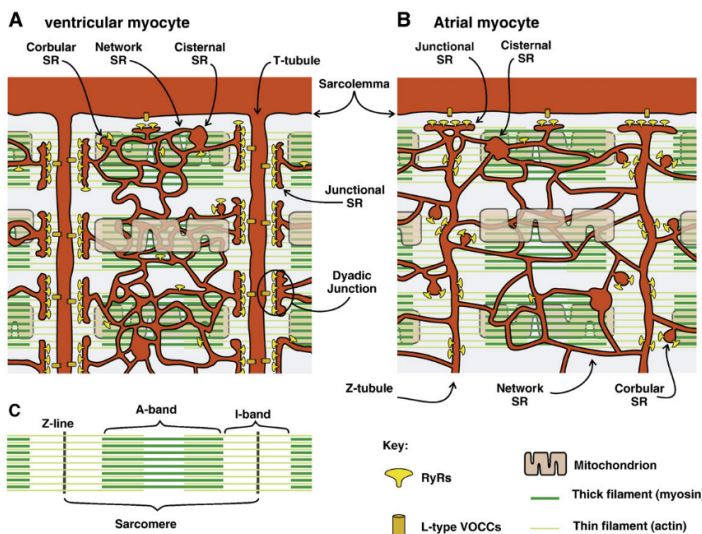


Figure 1.6: Structural differences between a ventricular (B) and an atrial (B) myocyte. While ventricular myocytes possess and extensive and well-developed T-tubule network, in atrial myocytes this is less extensive and less organized [16].

plays an important role on intracellular Ca^{2+} regulation by modulating Ca^{2+} diffusion and stabilizing spatio-temporal fluctuations of Ca^{2+} concentration. It has been estimated that only about 1% of Ca^{2+} ions entering the cell remain as free Ca^{2+} , and about 99% of the calcium entering via ion channels is bound to buffers [34]. Thus, buffers act as Ca^{2+} reservoirs which effectively regulates local Ca^{2+} availability and maximum systolic levels, affecting the strength and duration of contraction. Some buffers are mobile (diffusible within the cell compartment) and other stationary (anchored to large cell structures). The main stationary buffers in the cell are the sarcolemma, Troponin-C, myosin and SERCA, while the main diffusible buffers are ATP, calmodulin (in the cytosol), and calsequestrin (in the SR). The amount and affinity of calcium buffers, that is the buffer power, is controlled by several factors, such as the nature and distribution of buffers in the cell, diastolic calcium levels, pacing rate, as well as phosphorylation levels of SERCA and Troponin-C [34].

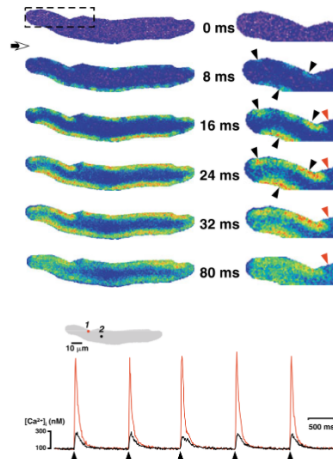


Figure 1.7: *Upper:* Ca^{2+} rise in rat atrial myocytes lacking T-tubules occurs first at the membrane regions of the cell, and propagated towards the center with a time delay. Ca^{2+} release in this type of atrial myocyte is rather heterogeneous, with visible regions of localized elevated Ca^{2+} concentration. *Lower:* membrane (red) and center of cell (black) Ca^{2+} transients, showing that calcium transients at the center are significantly damped compared to the membrane. Adapted from [31].

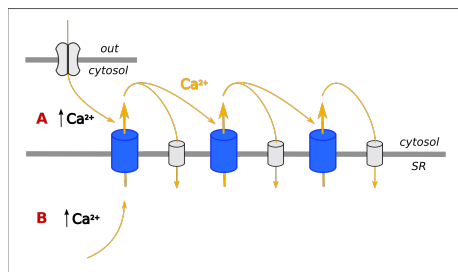


Figure 1.8: Schematic representation of the commonly accepted mechanism underlying Ca^{2+} wave propagation along non-junctional SR. According to this model, Ca^{2+} release from the RyRs is triggered by the local increase in cytosolic Ca^{2+} due to the opening on L-type calcium channels (A), or alternatively by an overload of SR Ca^{2+} , which sensitizes RyRs (B). Opening of RyRs causes Ca^{2+} to locally accumulate in a ‘micro-domain’ adjacent to the CRU, from which Ca^{2+} spreads diffusively into adjacent CRUs and triggers their activation. This process is repeated along neighbouring sites causing a Ca^{2+} wave to propagate towards to inner regions of the myocyte. Adapted from [33].

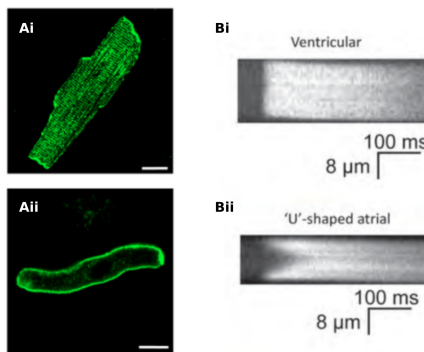


Figure 1.9: Rat ventricular myocytes have a well-developed T-tubule structure (Ai), while T-tubules are virtually absent from atrial myocytes (Aii). Adapted from [31]. These structural differences result in distinct intracellular calcium transients. An almost synchronous release of calcium is visible in a ventricular myocyte (Bi), while in the atrial myocyte calcium propagates in a wave with a characteristic U-shaped pattern. Adapted from [32].

1.5 AF pathophysiology

Under pathological conditions, electrical activity can be generated in regions other than the SA node (ectopic beats), and can ultimately become chaotic leading to atrial flutter and AF. ECG signals from healthy patients show three characteristic waves, the P, QRS, and T waves, at regular intervals. In contrast, the ECG of an AF patient shows an irregular and noisy wave between QRS and T waves, which also appear at irregular intervals, as depicted in Figure 1.1.

In disease, the atria undergo an array of changes which profoundly alter their electrical activity and contractile response. The collection of these processes is termed ‘atrial remodeling’, which can occur at cellular and sub-cellular level (functional remodeling), and at the tissue level (structural remodeling) [35], [36]. Remodeling is progressive, and may vary depending on the underlying causes as well as on previously existing heart conditions. At the cellular level, remodeling mainly includes changes in the expression levels of ion channels and transporters, and their regulatory proteins, alterations in calcium handling and signalling proteins, cellular volume, as well as in metabolism. At the tissue level, remodeling may include alterations in the expression of gap junction proteins, which affect cell-cell connectivity and conduction velocity, the proliferation of fibroblasts and the deposition of collagen, which also affects electrical conduction.

Remodeling ultimately results in changes in the AP and CaT morphologies. Typically, AP duration shortens, primarily as a consequence of decreased I_{CaL} magnitude, membrane becomes hyperpolarized due to increased I_{K1} , and CaT amplitude is reduced. These changes are illustrated in Figure 1.10. Other common hallmarks of AF include reduced conduction velocity and impaired rate

1. Introduction

adaptation (covered in more detail in section 1.6). These induced changes underlie both the cause and the outcome of AF, that is, the remodeling processes feedback on themselves in a closed loop, thus resulting in a progressive exacerbation of the arrhythmic alterations. This process has been appropriately described as ‘AF begets AFs’ by Allessie and colleagues [37].

Importantly, AF is also associated with major changes in the calcium handling system [38]. Most remarkably, increased RyR open probability as a result of increased protein kinase A phosphorylation, leading to exacerbated diastolic SR Ca^{2+} leak [39], increased SR Ca^{2+} load [40], as well as increased I_{NCX} function have all been associated with AF-induced remodeling [41]–[44]. Spontaneous Ca^{2+} release events from the SR have also been linked to AF remodeling [45], and associated with AP instabilities, such as afterdepolarizations, and ectopic beats (localized sources of electrical signals outside the SA node), and thus are thought to play an important role in the generation of arrhythmias.

Given the importance of disrupted calcium handling in AF initiation and maintenance, the mechanisms of impaired Ca^{2+} currents, RyRs, SERCA and their regulatory proteins have been widely investigated as potential targets for novel AF treatments [46]. These investigations have been paralleled with a substantial effort in developing models with a more detailed description of calcium handling system [47], and in particular incorporating atria-specific structural and electrophysiological characteristics [28], [48], [49]. Modeling of calcium handling will be addressed in more detail in section 1.8.3.

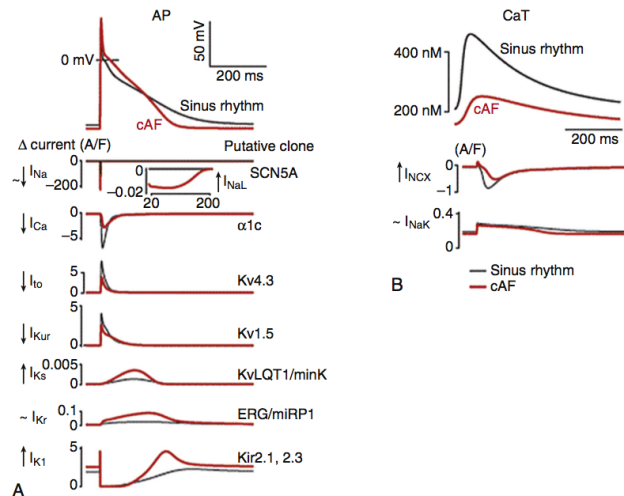


Figure 1.10: Comparison between AP, CaT and ionic currents in normal rhythm versus AF remodeling using a model of the human atrial myocyte [50].

1.6 Cardiac alternans

As discussed in the previous section, the stability of the electrical activity in cardiac cells is tightly linked to the calcium handling system. Disturbances in intracellular calcium regulation can greatly affect the normal functioning of the cardiac cell, potentially leading to instabilities in membrane repolarization, and ultimately to arrhythmic activity and contractile dysfunction. One particularly relevant condition associated with calcium deregulation is the so-called ‘cardiac alternans’.

Alternans was first detected in 1872 as periodic alternations in arterial pressure, and were at the time identified as ‘pulsus alternans’ [51]. Posteriorly, alternans were also observed in ECG signals as oscillations in T-wave amplitude (repolarization alternans). Alternans were eventually identified in isolated myocytes [52], whereby cells display beat-to-beat alternations in the AP duration (APD or electrical alternans), strength of contraction (mechanical alternans), and amplitude of the CaT (Ca^{2+} alternans) at constant pacing frequency.

APD alternans are normally accompanied by CaT amplitude alternans (high-low), which can be either concordant (short-long AP \rightarrow small-large CaT) or discordant (short-long AP \rightarrow large-small CaT), as illustrated in Figure 1.11. Alternans originate at the single cell level, but can eventually manifest at the tissue level as a consequence of cell-cell coupling, thus resulting in a patch of the tissue displays cyclic alternations in electrical and contractile activity. These are often referred to as spatial alternans [53] (Figure 1.12).

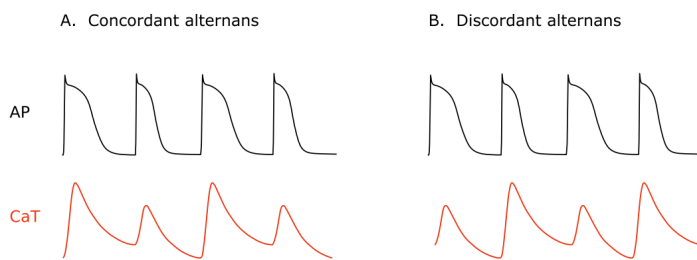


Figure 1.11: In concordant alternans the long AP is in phase with the small CaT (A), while in discordant alternans they are out of phase (B).

1.6.1 Clinical relevance

The occurrence of alternans has been associated with an increased risk of a number of cardiac conditions, in particular atrial and ventricular arrhythmias [55]–[59], as well as sudden cardiac death [60], [61]. Because of their correlation with ventricular arrhythmias, diagnosis of alternans has been proposed as a prognostic tool for ventricular arrhythmia risk stratification [62], [63]. Additionally, electrical alternans have been observed to precede episodes of atrial fibrillation in patients

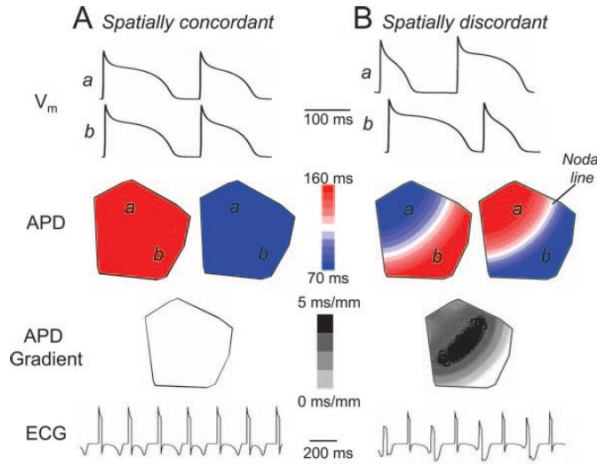


Figure 1.12: (A) Spatially concordant (A): the two regions a and b alternate in the same phase. (B) Spatially discordant alternans: a and b alternate at different phases, and are separated by nodal line with no alternans [54].

[64], [65], and thus it has been implicated as an effector of AF initiation and as an indicator of susceptibility to arrhythmias.

Alternans can be induced with increasing pacing rates upon reaching a certain pacing threshold, and is typically amplified at progressively faster rates, as shown in Figure 1.13. However, alternans threshold is not a set value, but rather a property specific of the tissue which depends on the subject, species, pre-existing heart conditions, and pharmacological treatment. Therefore, the pro-arrhythmic risk associated with alternans depends on existing pathologies, such as pre-existing heart conditions, diabetes, and metabolic disorders [66], which evinces the multi-factorial nature of cardiac alternans.

Repolarization alternans have also been observed in healthy patients when paced at high frequencies; however, in these cases alternans are initiated at much higher frequencies. This indicates that alternans are not solely the consequence of electrical remodeling, but rather an emergent behavior of the cardiac tissue when driven to instability. However, as discussed atrial remodeling can lead to electrical instabilities and this can exacerbate the pre-disposition to alternans [64].

Cellular alternans and arrhythmias are related through the formation of spatial alternans in the cardiac tissue. Spatially discordant alternans can generate a vulnerable substrate by promoting dispersion of repolarization and by giving rise to regional differences in APD. The discordant regions are separated by nodal lines (Figure 1.12B) which act as barriers for electrical conduction, which can potentially trigger reentrant circuits [54], [56], [59], [67]–[69] (see Figure 1.14). Reentrance refers to the formation of spiral waves of electrical propagation, which can subsequently break down into smaller wavelets and degenerate into

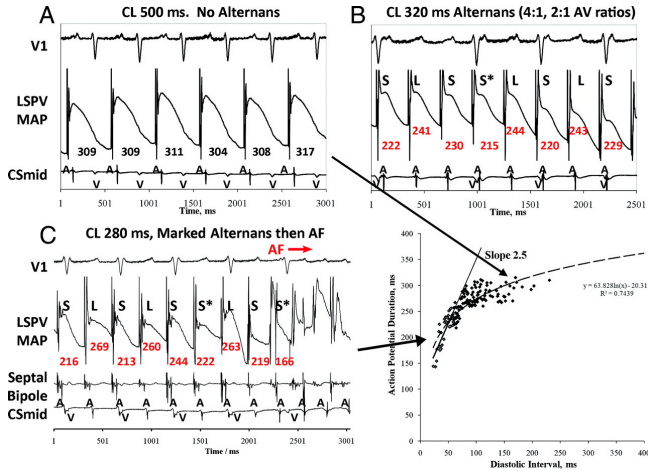


Figure 1.13: V1 lead EGC and MAP recordings of a paroxysmal patient at normal rhythm (A), showing repolarization alternans (B), and complex oscillations preceding an AF episode (C) [58].

fibrillatory activity [70].

It is clear then that alternans is a complex emergent phenomenon whose understanding requires the study of the cardiac system as whole. Given the evident clinical relevance of cardiac alternans, a considerable effort has been devoted towards a better understanding of alternans mechanisms. Although decades of studies have been able to shed light on a multitude of potential mechanisms underlying alternans, much still remains poorly understood regarding the source of cellular instability, and the role of the different states of the cell in maintaining alternans. The next section provides an overview of the main theories and hypothesis that have been proposed, as well as the most commonly accepted mechanisms.

1.6.2 Physiological mechanisms

Cell level mechanisms underlying cardiac alternans are rather complex, and several different mechanisms and theories have been proposed to explain the occurrence of this emergent behavior. Here I provide only a brief overview on this vast topic. However a comprehensive review of these mechanisms is outside the scope of this thesis, for a detailed read on the subject see [53], [54], [66], [71], [72].

As explained in the previous section, action potentials trigger the opening of Ca^{2+} channels which cause intracellular calcium to rise. Ca^{2+} in turn modulates the activity of Ca^{2+} -dependent currents, especially LTCC and NCX, which feeds back on the membrane voltage. Hence, V_m and CaT are intrinsically coupled, whereby intracellular Ca^{2+} acts as the mediating agent between the two systems. Disturbances in the bi-directional $V_m \leftrightarrow \text{Ca}^{2+}$ coupling have been implicated

1. Introduction

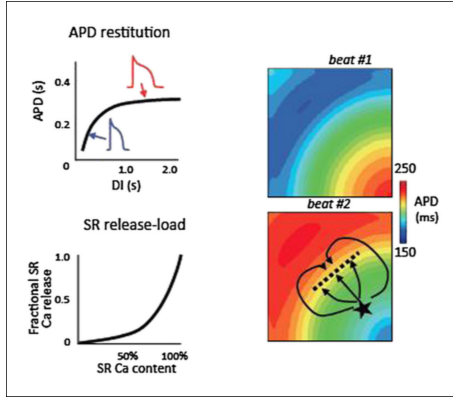


Figure 1.14: Spatially discordant alternans with a short-long pattern in one region (upper left corner), and long-short pattern in another (lower right corner), separated by a nodal line (yellow) with no alternans. Spatially discordant alternans may arise from a steep fractional SR Ca release coupled with steep APD restitution. The pattern in beat #1 is reversed in beat #2. An ectopic beat (star) arising in the short APD region can trigger reentry due to unidirectional block (dashed line) which forms a circular propagating circuit around (solid lines). Adapted from [69].

in the initiation of calcium alternans, with Ca^{2+} alternans can induce APD alternans, and vice-versa.

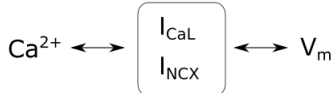
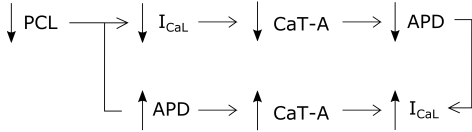


Figure 1.15: Coupling between the voltage and Ca^{2+} systems is mediated by Ca^{2+} -dependent currents.

There are two main proposed schools of thought on the generation of cardiac alternans. One stems from the observation that steep restitution (see section 1.7) is associated with APD alternans, which led to the hypothesis that alternans are driven by instabilities in repolarization dynamics [73], [74]. These are referred to as voltage-driven alternans [75]. The proposed mechanism is related to the coupling between I_{CaL} and Ca^{2+} release, whereby oscillations in LTCC refractoriness, ie. the time during which the channel is inactive and unresponsive to a new stimulus, causes variations in SR Ca^{2+} release [76], [77]. When pacing interval is shortened to the point where LTCCs cannot fully recover from inactivation before the onset of the next beat, less Ca^{2+} enters the cell resulting in a shorter AP and in a smaller CaT. Consequently, a short AP allows enough

time for Ca^{2+} channels to completely recover from inactivation in the next beat, resulting in an enhanced I_{CaL} , and a longer AP and a larger CaT. This V–Ca coupling is typically positive, meaning that a long AP corresponds to a strong CaT (concordant alternans) and is illustrated in Figure 1.16A. This frequency-dependent behavior of membrane repolarization, and in particular in APD, is referred to as ‘APD restitution’ (discussed in more detail in section 1.7).

A. V– Ca^{2+} coupling (+)



B. Ca^{2+} -V coupling

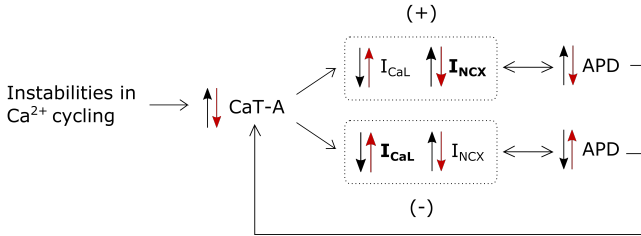


Figure 1.16: Diagrams of V–Ca and Ca–V coupling.

However, Ca^{2+} alternans have also been observed to occur in the absence of APD alternans, for instance in myocytes stimulated with clamped APs while I_{CaL} remains constant from beat to beat [78]–[81]. Therefore, the realization that Ca^{2+} alternans are independent of APD alternans has provided a strong argument for the second school of thought, whereby alternans are primarily driven by instabilities in Ca^{2+} handling cycling. These lead to CaT alternations, and secondary APD alternans can then arise through the bi-directional Ca–V coupling, in particular through modulation of LTCC and NCX currents (Ca–V coupling) [82]. In contrast to voltage-driven alternans, Ca^{2+} -driven alternans can be either concordant or discordant. An increase in CaT produces a smaller I_{CaL} current, which tends to shorten APD, but a larger I_{NCX} current which prolongs the AP. Thus, this two opposing effects contra-balance each other, and the effect on APD depends on which of them dominates. This process is illustrated in Figure 1.16B.

It is now well accepted that Ca^{2+} instabilities are the primary driver of cardiac alternans. However, the bidirectionally coupling between the voltage and calcium systems still lends a strong argument that both mechanisms can contribute, which has been supported by modeling and experimental studies [71], [83]. It has also been shown that the relative contribution of voltage and

1. Introduction

calcium instabilities depends on the recovery kinetics of I_{CaL} , the SR Ca^{2+} load dependence, and varies with the pacing frequency [71]. In particular the interplay between SR Ca^{2+} load, SR Ca^{2+} fractional release, and Ca^{2+} sequestration plays a critical role [53], [66], [78]–[80], [84]–[87].

Several studies have suggested a number of putative mechanisms by which impaired cytosolic and SR Ca^{2+} regulation promotes Ca^{2+} instabilities in myocytes. While an exhaustive review is outside the scope of this thesis, below is a summary of the main mechanisms proposed.

LTCC and NCX

The magnitude of trigger I_{CaL} determines the amount of Ca^{2+} being released from the SR, and it has been found that reduction of I_{CaL} , accompanied by an SR Ca^{2+} content above a certain threshold, can induce the formation of Ca^{2+} sub-cellular waves (fragmented SR Ca^{2+} release). The resulting large CaT can subsequently degenerates into alternans [88]. Therefore, Ca^{2+} alternans can result from the interplay between SR Ca^{2+} content and magnitude of the L-type Ca^{2+} current. Furthermore, reduction of I_{CaL} can induce alternans [88], thus indicating that regulation of SR Ca^{2+} release is an important factor.

SR Ca^{2+} load

SR Ca^{2+} load is affected mainly by SERCA activity, SR buffering strength, and RyR open probability and leak. At higher pacing frequencies, the slow kinetics of Ca^{2+} uptake via SERCA precludes the complete refilling of the SR, resulting in a smaller CaT in the next beat. The subsequent smaller CaT allows for enough time for the complete refilling of the SR stores, thus producing a large CaT in the next beat, and triggering alternans.

It has been hypothesized that this instability in the feedback control of end-diastolic SR Ca^{2+} load is a necessary condition for alternans development [66], [84]. However, it has also been shown that alternans can occur with unchanged SR Ca^{2+} content [89], [90]. Despite that most studies indicate a critical role of SR Ca^{2+} content regulation in the initiation of alternans, and that restoring or enhancing SERCA function can effectively suppresses arrhythmias [91], [92].

SR Ca^{2+} release

The open probability of the RyR is sensitive to luminal Ca^{2+} , and thus SR Ca^{2+} buffering and SR Ca^{2+} load play a role in controlling channel activity. Additionally, the RyRs are regulated by a plethora of regulatory proteins and complex signalling networks, which renders the regulation of RyR activity quite prone to instabilities. Furthermore, restitution of RyR availability is time-dependent and the channels require several milliseconds to fully recover from inactivation. Refractoriness of RyRs also seems to be delayed when a large amount of Ca^{2+} is released [66]. Thus, the open probability and availability of RyRs dictate how much calcium is released during CICR, that is the fraction of SR Ca^{2+} transferred to the cytosol in each beat. The hypothesis that alternans

are promoted by beat-to-beat alternations in the refractory kinetics of SR Ca^{2+} release has been supported by experimental and modeling data [81], [93].

Another factor to consider is the fractional release of Ca^{2+} , i.e. the amount of Ca^{2+} released relative to SR load. The larger SR Ca^{2+} content the higher the fractional release of Ca^{2+} [94], and studies have shown that a steep SR load-release dependency promotes instabilities in SR release control through SR Ca^{2+} cycling refractoriness and a limited rate of junctional SR refilling [88], [95], [96]. Furthermore, increased RyR inactivation has been linked to the occurrence of Ca^{2+} alternans [84], [97], [98]. Therefore, increasing the kinetics of SR Ca^{2+} release and the amount of Ca^{2+} released can potential reduce alternans vulnerability,

Subcellular Ca^{2+} alternans

Ca^{2+} alternans have also been reported to be a sub-cellular phenomenon, whereby different regions within the cell alternate in CaT amplitude (Figure 1.17). This has been observed in both intact tissue [99], [100], and isolated myocytes [101]–[103]. Subcellular alternans have been shown to be related to local heterogeneities in SR Ca^{2+} release, giving rise to gradients of Ca^{2+} concentration which can alternate out-of-phase [97], [100]–[102]. The steep gradients between two adjacent alternating regions can also generate propagating Ca^{2+} waves, which predispose the cell to arrhythmogenic activity in the form of afterdepolarizations (depolarizing currents in phases 2-4 of the AP) [97], [104]. Subcellular Ca^{2+} alternans are, at least in part, promoted by decreased RyR open probability by promoting regional variability of Ca^{2+} release from non-junctional SR sites [97]. Although sub-cellular alternans have been observed in both atrial and ventricular myocytes, the absence of a TT network in atrial myocytes has been shown to exacerbate regional heterogeneity of sub-cellular calcium transients [80].

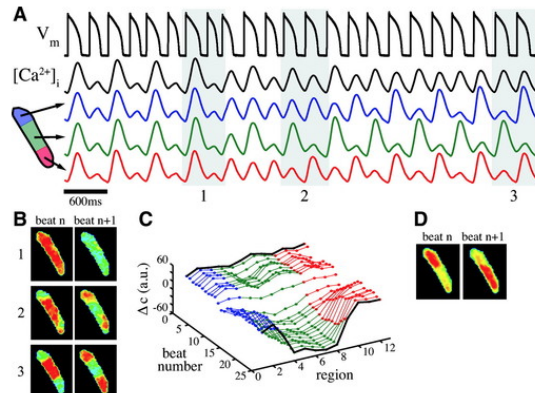


Figure 1.17: Subcellular alternans recorded in atrial myocytes [103].

Ca^{2+} sparks

Additionally, Ca^{2+} sparks and the subsequent generation subcellular calcium waves have also been postulated to be the fundamental mechanism of Ca^{2+} alternans [90]. Calcium sparks are dependent on the stochastic opening of the RyRs, but its open probability greatly increases with the local rise of calcium concentration. As previously discussed, saltatory Ca^{2+} waves can result from the amplification of local Ca^{2+} sparks [105], and these have been linked to alternans through a mechanism of collective recruitment of sparks determined by three properties of the Ca^{2+} of the CRUs (3R's):

- (1) randomness of spark activation,
- (2) refractoriness of a CRU after a release event, and
- (3) recruitment (CICR within one CRU) [90].

These three properties give rise to a steep relationship between fractional SR Ca^{2+} release and SR Ca^{2+} load without dependency on alternating SR load, providing the conditions for the initiation of Ca^{2+} alternans at high SR Ca^{2+} loads (higher spark probability).

1.7 APD restitution

As mentioned previously, the heart has the capacity to adapt its beating rate to accommodate changing needs in blood supply - rate adaptation. Changes in pacing cycle length (PCL), that is the interval between two consecutive beats, are accompanied by variations in APD and in the diastolic interval (DI). A decrease in PCL is accommodated by shortening of DI first and then APD (Figure 1.18), such that $\text{PCL} = \text{APD} + \text{DI}$ at all PCLs. The frequency dependency between APD and DI is often termed as 'APD restitution'.

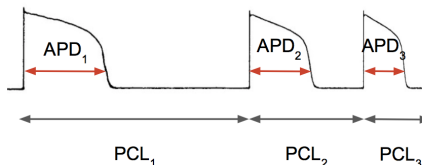


Figure 1.18: Representation of PCL-APD relation.

Because of the time-dependent recovery of the ion channels, and in particular the LTCC, there is a limit for how much the PCL can decrease without compromising repolarization. That is, PCL must be longer than the refractory period of the ion channels in order for repolarization to be complete before the onset of the following beat. APD typically varies inversely with PCL, with the rate dependence of APD being relatively stable at longer PCLs. At progressively higher frequencies, this relationship becomes steeper and can ultimately degenerate into repolarization instabilities in the transmembrane potential [73], [75]. These result in the development of voltage-driven alternans,

with the implications for the development of arrhythmias discussed in the previous section. The loss of rate adaptation in remodeled cells and tissue has been shown to increase the propensity to APD alternans [64]. Furthermore, AF remodeled tissue, APD is shortened due to electrical remodeling, and decreasing PCL has little effect on APD [106].

Although it is now well-established that voltage-driven alternans are not the primary route cause of pro-arrhythmic alternans, the value of APD restitution as a risk indicator continues to be included in the discussion on cardiac alternans, as evinced by recent reviews [65], [107], [108]. Curves of APD plotted as function of PCL allow to visualize APD rate adaptation, as shown in Figure 1.19A, with APD alternations visible as bifurcations in restitution curve (Figure 1.19B). Such APD restitution curves have been useful tools in assessing alternans behavior [109].

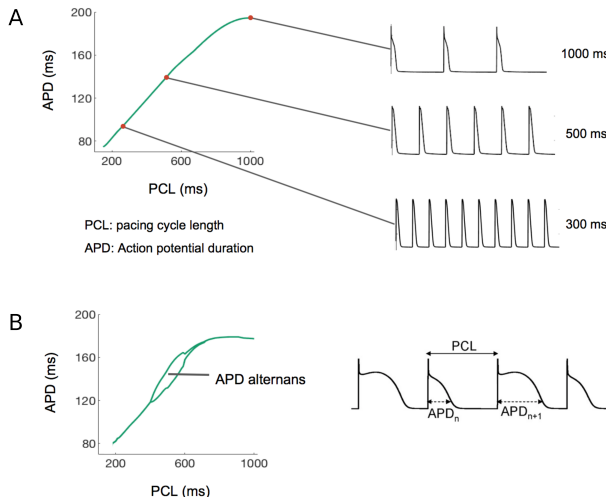


Figure 1.19: (A) PCL×APD restitution curve and AP traces corresponding to three PCLs. Decreasing PCLs results in shorter APD and DI. (B) Restitution curve with alternans shown by the bifurcation in the curve, where the upper branch corresponds to the long AP, and the lower branch to the short AP.

1.8 Models of cardiac electrophysiology

The first model of a cardiac cell was introduced by Denis Noble in 1962 [110], and was largely based on the formalism developed by Hodgkin and Huxley in their seminal work on electrophysiology of the giant squid axon [111]. Since then, models for cardiac cell electrophysiology have continuously been extended and improved, with the repertoire of single cardiac cell models now counting

1. Introduction

with hundreds of models representing different animal species, heart regions, signalling processes, and genotypes [112]. The first atria-specific EP, the rabbit atrial myocyte, model was developed by Hilgemann and Noble in 1987 [113]; since then more than a dozen atrial models have been published. The first human atrial myocyte model published was the Courtemanche model, schematically represented in Figure 1.20.

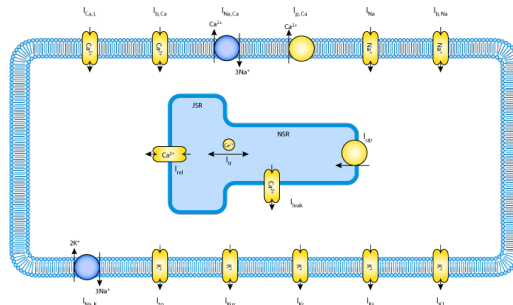


Figure 1.20: Schematic representation of the Courtemanche model [114].

A cardiac cell model consists in essence of a compilation of mathematical formulations that are solved by to calculate the kinetics of closing and opening of ion channels, transient ionic concentration, and the transmembrane potential. These include ion channels and transporters, transmembrane voltage, ionic fluxes across cell compartments, calcium regulation, and the contractile proteins. The models typically contain hundreds of mathematical equations, and hundreds to thousands of fixed model parameters and state variables. Fixed model parameters, such as cell geometry, capacitance, ion channel conductances, and diffusion coefficients, are typically obtained by fitting models to experimental data such as patch-clamp data. The state variables are dynamic in that they vary over time during a simulation, and characterize state of the cell, such as the transmembrane voltage, ionic concentrations, and gating variables of ion channels. Typically, the mathematical formulations in single cell models are either constitutive equations or ordinary differential equations (time dependent). The general framework used in computational modeling of cardiac myocytes is illustrated in Figure 1.21.

Figure 1.22 also shows the APs and CaTs produced by four commonly used human atrial myocyte models, to illustrate the considerable differences among different models.

A more extensive review on computational modeling of atrial pathophysiology and pharmacological treatment strategies is given in Chapter I.

1.8.1 Hodgkin-Huxley type of models

The Hodgkin-Huxley (HH) type of models borrows its formalism from electrical circuit theory (Figure 1.23). In these models the cell membrane is represented

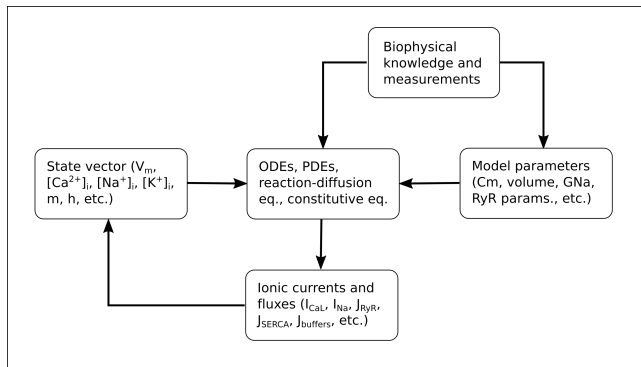


Figure 1.21: Basic components of a cardiac single cell model.

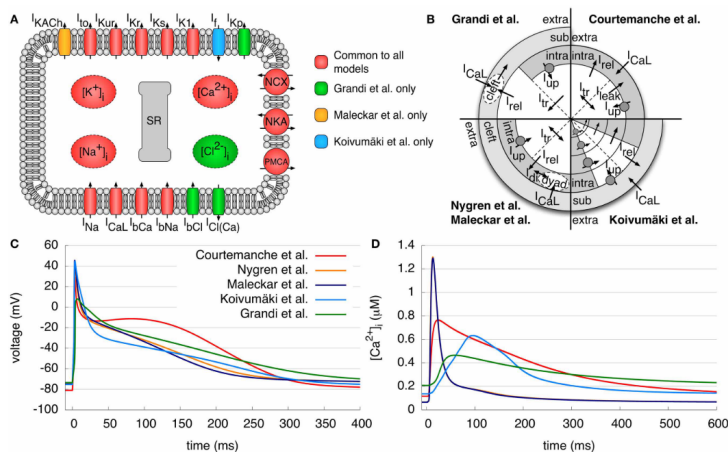


Figure 1.22: Four commonly used human atrial myocyte models: Courtemanche, Nygren, Maleckar, and Koivumäki. (A) Schematic representation of the cell membrane with the ionic currents specific from each model. (B) Differences in cellular compartmentalization of the calcium handling systems in the four models. Action potentials (C) and calcium transients (D) resultant from the four models also show considerable differences in their morphologies [115].

1. Introduction

as a simple electrical circuit with a capacitor (C) in parallel with an ohmic resistor (g), and in series with a battery (E). C and R can be viewed as the summation of the capacitances and resistances of all the individual ion channels and transporters.

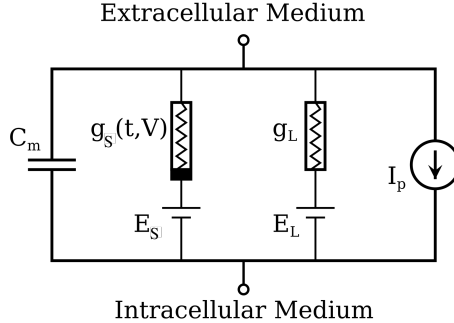


Figure 1.23: Equivalent electrical circuit of the membrane of an excitable cell [116].

The transmembrane potential in this circuit is calculated as:

$$\frac{dV}{dt} = -\frac{1}{C_m} I_{tot} \quad (1.1)$$

where C_m is the cell capacitance, and I_{tot} is the total current through the membrane. In the original HH model I_{tot} is the sum of the sodium current (I_{Na}), the potassium current (I_K), and a leakage current (I_l). The latter is commonly found in ionic models and represents the passive flow of ions out of the cell.

Furthermore, the voltage across the membrane (V_m) can be seen as having two components: the voltage drop due to different ionic concentrations inside and outside the membrane (E_S), and a voltage drop due to a current I_S flowing through the channel with conductance g . Thus, it follows that:

$$V_m = \frac{1}{g} I_S + E_S \quad (1.2)$$

$$I_S = g(V_m - E_S) \quad (1.3)$$

where E_S is the reversal potential, given by the Nernst equation:

$$E_S = \frac{RT}{zF} \ln \left(\frac{[S]_o}{[S]_i} \right) \quad (1.4)$$

where $[S]_i$ and $[S]_o$ are the concentrations of species S inside and outside the membrane. The Nernst potential, E_S , describes how a difference in ionic concentration across the membrane results in an electrical potential drop. Thus, $(V_m - E_S)$ is the driving force for ionic movement across the membrane. Note that the equilibrium potential at rest is the result of the interplay of the equilibrium

potentials of the three ionic currents. Because in this model the I_K is the dominant current, the equilibrium potential is close to $E_K = -12$ V. However, in cardiac cells the resting membrane potential is usually close to -80 V.

The proportion of channels in the open and closed states, and thus the maximum current flow through the channels, are governed by gating variables. In HH type models ion channel gating is defined from dynamic state variables in that they are both voltage and time dependent, which mathematically take the form of ordinary differential equations:

$$\frac{dg}{dt} = f(V, t) \quad (1.5)$$

By convenience, this can be expressed as an exponential function of some arbitrary variable:

$$g = G \cdot n(V, t) \quad (1.6)$$

where G is the maximum channel conductance, and n is a generic voltage- and time-dependent gating variable that defines the open probability of the channel. The fraction of open channels, n , can be represented as a simple two-state model having α_k and β_k probabilities of being in the open and closed state, respectively. Thus, n can be determined by the following differential equation:

$$\frac{dn}{dt} = \alpha_n(v)(1 - n) - \beta_n n \quad (1.7)$$

α_k and β_k are also called the activation and inactivation variables, respectively, and can be determined from the steady state fraction (n_∞) and time constant (τ_n) of activation and inactivation of the system:

$$\alpha_n(V) = \frac{n_\infty(V)}{\tau_n} \quad (1.8)$$

$$\beta_n(V) = \frac{(1 - n_\infty(V))}{\tau_n} \quad (1.9)$$

Rearranged these equations as a function of the steady state variables, it follows that:

$$n_\infty(V) = \frac{\alpha_n(V)}{\alpha_n(V) + \beta_n(V)} \quad (1.10)$$

$$\tau_n(V) = \frac{1}{\alpha_n(V) + \beta_n(V)} \quad (1.11)$$

The total ionic current (I_{tot}) is defined as the sum of the individual contributions of the individual sarcolemmal currents. In the example of the HH model, which contains three ionic currents, I_{Na} , I_{Na} , and a leak current I_l , the total ionic currents is given by:

1. Introduction

$$\begin{aligned} I &= C_m \cdot \frac{dV_m}{dt} + I_{Na} + I_K + I_l \\ &= C_m \cdot \frac{dV_m}{dt} + G_{Na}m^3h(V_m - E_{Na}) + g_Kn^4(V_m - E_K) + G_l(V_m - E_l) \end{aligned}$$

where the gating variables n , m , and h are given by the differential equation 1.7. The functions $n_\infty(V)$ and $\tau_n(V)$ are empirical and thus must be determined from experimental data. For the case of the HH model, these take the form:

$$\alpha_m = 0.1 \frac{25 - V}{e^{\frac{25-V}{10}} - 1}, \quad \beta_m = 4e^{\frac{-V}{18}} \quad (1.12)$$

$$\alpha_h = 0.07e^{\frac{-V}{20}}, \quad \beta_h = 1e^{\frac{30-V}{10}} + 1 \quad (1.13)$$

$$\alpha_n = 0.01 \frac{10 - V}{E^{\frac{10-V}{10}} - 1}, \quad \beta_n = 0.125e^{\frac{-V}{80}} \quad (1.14)$$

The resulting AP, time activation, inactivation, and conductance from the HH are represented in Figure 1.24. The remarkable differences between the HH AP and a cardiac AP are remarkable. However, the formalism introduced with the HH model laid the foundations for all cardiac ionic models that followed.

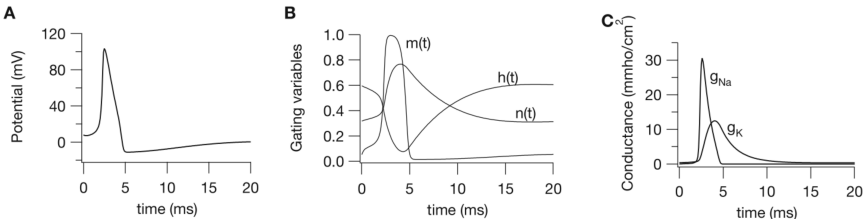


Figure 1.24: Action potential (A), gating variables (B), and conductances (C) in the Hodgkin-Huxley model [117].

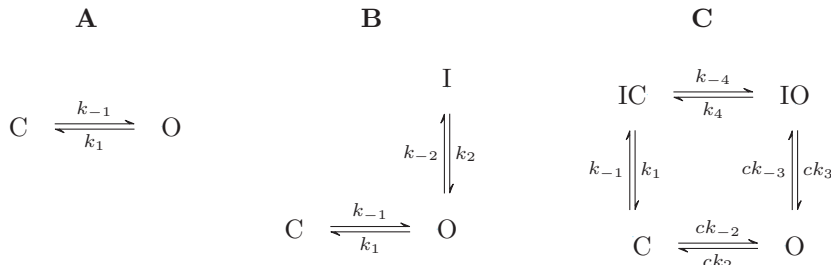
Although useful to represent the overall dynamic behavior of ion channels, HH models are intrinsically limited by their inability to reproduce various aspects of channel kinetics, such as state-dependent conformational changes and cooperativity. For instance, the I_{Na} current from the HH model presented above assumes that probabilities of the channel being active and inactive are independent. However, such is not the case; inactivation is more likely when the channel is in the open state, and therefore the kinetics given by m^3h is an over-simplification. To address these issues, Markov chain models (MCM) of ion channel gating were introduced in cardiac models.

1.8.2 Markov chain models

Markov models are an alternative way to model ion channels by representing channel gating as a chain of discrete states. In many instances MCM models of ion channels have shown to be more adequate than HH type of models, since they allow to formulate additional states of the channel in an easier and more convenient way, such as states where the channel is bound to a ligand, such as a signalling molecule or a drug, and channel mutations. The great advantage of MCM models is that they allow to explicitly represent single channel states as stochastic processes whose present state depends on the previous state of the system, ie., state-dependent transitions.

Markov models essentially compute the occupancy, ie. the probability, of the channel being in each discrete state, with state transitions determined by kinetic transition rates k_x . The transition rates k_x determine the dynamic behavior of the system, that is, the rate of transition from one state to another.

So, a state could, eg., transition between two states, closed (C) and open (O), as shown below in model A. However, it is widely known that this assumption is rather simplistic, and that most ion channels in fact undergo several different conformational changes. More elaborate models can take into also one or more inactivated states (I), as in models B and C.



In the example of model C, the channel has two inactivated states, open inactivated (IO) and closed inactivated (IC), and transitions $C \rightleftharpoons O$ and $O \rightleftharpoons IO$ are allosterically regulated by a ligand c . O, C, IO, and IC represent fractions of channels in each state, such that $O + C + IO + IC = 1$. Dynamical changes in state occupancies are then given by ordinary differential equations:

$$\begin{aligned}
 \frac{dIC}{dt} &= k_{-1}C + k_4IO - (k_1 + k_{-4})IC \\
 \frac{dC}{dt} &= k_1IC - k_{-1}C + (k_2O - k_{-2}C)c \\
 \frac{dO}{dt} &= (k_{-2}C + k_3IO)c - (k_2 + k_{-3})Oc \\
 \frac{dIO}{dt} &= k_{-4}IC - k_4IO + (k_{-3}O - k_3IO)c
 \end{aligned} \tag{1.15}$$

The current flow through the channel with single channel conductance g_{sc} ,

1. Introduction

membrane channel density n , and open probability O can be determined in an analogous way as in HH models:

$$I = g_{sc} \cdot n \cdot O \cdot (V_m - E) \quad (1.16)$$

1.8.3 Modelling calcium cycling

Calcium handling constitutes an essential part of cardiac models that aim to realistically reproduce calcium-dependent regulation of membrane potential and the generation of intracellular calcium transients. Because of the complexity of the calcium handling system, which involves a multitude of cellular processes and model components, several different models have been developed which aim at representing various aspects of the calcium system. These models vary considerably in size and complexity, with the simplest models providing only a basic mechanistic representation of calcium release and uptake into the SR, and with the more intricate models including models of the RyR with several states, calcium buffering, calcium diffusion, and spatial calcium compartmentalization.

This is a vast topic, and therefore this section will only give an overview of the basic components present in most models of calcium handling. Here I will give as example the the Shannon model ventricular model [47], which is schematically represented in Figure 1.25. This is one of the most commonly used models of calcium handling, but note that there exists several other relevant models of calcium handling.

The calcium model contains four different compartments, each with its own Ca^{2+} concentration: the cytosol (*cyt*), the SR, the sarcolemmal (SL) space, and the junctional (*j*) space. The *j* compartment corresponds to the narrow space between the RyRs and the Ca^{2+} channels in the CRU where Ca^{2+} is initially released into before diffusing out into adjacent compartments. The arrows in the Figure indicate the diffusional fluxes of Ca^{2+} between compartments, and the dots represent the buffer fluxes (J_{B_x}).

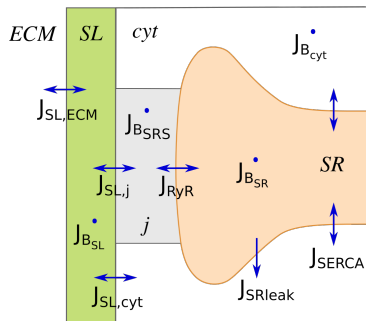


Figure 1.25: A schematic representation of the structure of the Shannon model of calcium handling.

SERCA pump

SERCA transports Ca^{2+} from the cytosol back into the SR at the expense of ATP (Figure 1.26). The flux through the SERCA pump in this model is formulated as a Hill equation:

$$J_{\text{SERCA}} = V_{\max} \cdot \frac{\left(\frac{C_{a_i}}{K_{mf}}\right)^H - \left(\frac{C_{a_{SR}}}{K_{mr}}\right)^H}{1 + \left(\frac{C_{a_i}}{K_{mf}}\right)^H + \left(\frac{C_{a_{SR}}}{K_{mr}}\right)^H} \quad (1.17)$$

where K_{mf} and K_{mr} are the forward mode and reverse mode pump constants, respectively, and H is the Hill coefficient. The larger the value of H , the more ‘sensitive’ SERCA is to Ca^{2+} . These three parameters modulate the flux of Ca^{2+} through SERCA; thus, they can be manipulated to emulate the effect of functional changes in SERCA, eg. up- or down-regulation, phosphorylation of the two regulatory proteins, phospholamban (PLB) and sarcolipin (SLP), or blockage. Changes in the expression levels or in the phosphorylation state of the regulatory proteins is often observed in remodeled cells, and these can be incorporated in the model by tuning the equation parameters. PLB in the dephosphorylated state suppresses SERCA activity, and changes in its expression levels can result in a shift in SERCA activity [118]. When phosphorylated, PLB dissociates from SERCA and enhances SR Ca^{2+} uptake. Increased phosphorylation of PLB may be present in AF [119]; however, there is no concluding evidence that this may play a role in AF pathophysiology [120].

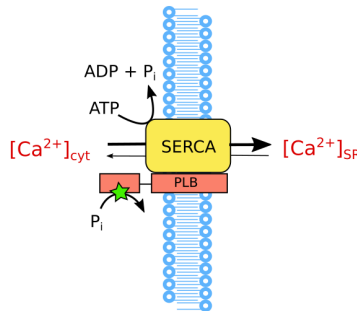


Figure 1.26: Schematic representation of the SERCA pump, showing the transport of Ca^{2+} from the cytosol into the SR at the expense of ATP hydrolysis into ADP. Phospholamban (PLB) inhibits SERCA activity when phosphorylated, hence decrease Ca^{2+} uptake.

RyR

The RyRs can be modeled as a Markovian 4-state Markov model, as shown in Figure 1.27. This model has an open (O), a closed (C), an inactivate (I), and

1. Introduction

a refractory (R) state. The transition rates k_x determine the dynamic behavior of the system, that is, the rate of transition from one state to another. This model is similar to the model discussed in section 1.8.2, and the state equations are thus analogous to equation 1.15.

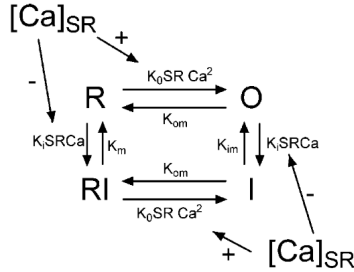


Figure 1.27: A 4-state Markov model of the RyR [47].

The Ca^{2+} flux through the RyRs depends on the fraction of open channels only, since RyRs in any of the other states cannot transport calcium. It also depends on the total number of RyRs, and on the gradient of Ca^{2+} concentration between the SR and the junctional space. Thus, the flux through the RyRs is given by:

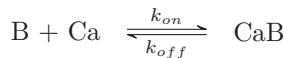
$$J_{\text{RyR}} = N_{\text{RyR}} \cdot O \cdot (C_{\text{aSR}} - C_{\text{aj}}) \quad (1.18)$$

And similarly, the constant passive leakage of Ca^{2+} from the RyRs is given by:

$$J_{\text{SRleak}} = D_{\text{SRleak}} \cdot (C_{\text{aSR}} - C_{\text{aj}}) \quad (1.19)$$

Calcium buffering

A buffer can be modeled as a simple two state model:



with the dynamic buffer concentrations being given as a differential equation:

$$\frac{d\text{Ca}_B}{dt} = k_{on}\text{Ca}(\text{B}_{\max} - \text{Ca}_B) - k_{off}\text{Ca}_B \quad (1.20)$$

where B_{\max} is the maximum buffer capacity, Ca and Ca_B represent the concentration of free and bound Ca^{2+} , and k_{on} and k_{off} are the rate coefficients of ion-buffer complex formation and dissociation, respectively.

The buffer fluxes $J_{\text{B}_{\text{cyt}}}$, $J_{\text{B}_{\text{SR}}}$, $J_{\text{B}_{\text{SL}}}$, and J_{B_j} , thus correspond the net flux of free Ca^{2+} being bound/unbound to each buffer. J_{B_x} in cell compartment x

can then be estimated as the sum of the buffered Ca^{2+} concentration changes, $d\text{Ca}_{\text{Bi}}/dt$, of each individual buffer i (Tropomeric-C, calmodulin, myosin, SR, etc.).

Calcium diffusion

Calcium diffuses inside the cell from regions of high to low concentrations, which allows Ca^{2+} to interact with transporters, signalling proteins and engage myofilament contraction. Thus, the level of Ca^{2+} diffusion detail in the model can greatly affect resulting Ca^{2+} dynamics [33]. Diffusion is usually modeled through reaction-diffusion equations, which for the model example in Figure 1.25 take the form:

$$J_{\text{SL,cyt}} = \frac{D_{\text{SL,cyt}}}{V_{\text{cyt}}} (C_{a\text{SL}} - C_{a_i}) \quad (1.21)$$

$$J_{\text{SL,cyt}} = \frac{D_{\text{SL,cyt}}}{V_{\text{SL}}} (C_{a_j} - C_{a\text{SL}}) \quad (1.22)$$

$$J_{\text{SL,j}} = \frac{D_{\text{SL,j}}}{V_{\text{SL}}} (C_{a_j} - C_{a\text{SL}}) \quad (1.23)$$

$$J_{\text{SL,j}} = \frac{D_{\text{SL,j}}}{V_j} (C_{a\text{SL}} - C_{a_j}) \quad (1.24)$$

Calcium balance

Finally, the mass calcium balance for this model is determined by the following system of differential equations:

$$\frac{dC_{a_i}}{dt} = -J_{\text{SERCA}} \frac{V_{\text{SR}}}{V_{\text{cyt}}} + \frac{J_{\text{SL,cyt}}}{V_{\text{cyt}}} - J_{\text{B}_{\text{cyt}}} \quad (1.25)$$

$$\frac{dC_{a\text{SR}}}{dt} = J_{\text{SERCA}} - J_{\text{RyR}} - J_{\text{SRleak}} \frac{V_{\text{cyt}}}{V_{\text{SR}}} + \frac{J_{\text{SL,cyt}}}{V_{\text{cyt}}} - J_{\text{B}_{\text{SR}}} \quad (1.26)$$

$$\frac{dC_{a\text{SL}}}{dt} = J_{\text{SL,ECM}} \frac{C_m}{2FV_{\text{SL}}} + \frac{J_{\text{SL,j}}}{V_{\text{SL}}} + \frac{J_{\text{SL,cyt}}}{V_{\text{SL}}} - J_{\text{B}_{\text{SL}}} \quad (1.27)$$

$$\frac{dC_{a_j}}{dt} = J_{\text{SL,ECM}} \frac{C_m}{2FV_j} + j_{\text{SL,j}} + J_{\text{RyR}} \frac{V_{\text{SR}}}{V_j} + J_{\text{SRleak}} \frac{V_{\text{SR}}}{V_j} - J_{\text{B}_j} \quad (1.28)$$

1.9 Sensitivity Analysis

Computational modeling and simulation offers a fast and cheap way to new research test hypotheses, and thus it has become widespread method in both scientific research and industrial practice. However, for computational models to be useful, they have to be able to reproduce certain phenomena or behaviors or to be able to make accurate predictions of quantities of interest and their evolution over time. In order for computational models to accurately and reliably reproduce a physical system, they must be parameterized with the ‘correct’ set of values

1. Introduction

and initial conditions. However, quite often these are ill-defined, or altogether unknown.

Furthermore, known parameters are typically affected by uncertainties that arise from a variety of sources, such as error in the experimental measurement setup, intrinsic stochasticity and variability of the quantities, and unknown model structure. Therefore, it can be extremely difficult to determine the appropriate values of certain model parameters. Hence, a critical part of the model development pipeline is to acknowledge model uncertainties, to incorporate variability into the simulations to allowed for more robust and realistic estimations. In this context, it becomes important to address methods of parameter identifiability. and how the sensitive model is by the particular choice of parameters. That is achieved by a class of methods referred to as ‘sensitivity analysis’ (SA).

SA enables the assessment of how much the outputs of the model (the physical quantities of interest) change when the input parameters are varied. SA can be valuable tools in assisting model development and parametrization, since these frameworks provide additional knowledge of the functioning of the model and of the relationship between multiple model parameters.

In the context of cardiac myocyte models, the output quantities of interest are typically AP properties (such as APD, RMP, upstroke velocity and APA), CaT properties (eg., CaT amplitude and duration), ionic current magnitudes, or ionic concentrations. There are a multitude of SA methods (a comprehensive review can be found in [121]), and a few of such methods have applied to cardiac myocyte models to constraining model parameters [122]–[124], to infer parameter importance on particular model outcomes [125]–[129], and to perform model optimization [130]. Some examples are multivariate linear regression [125], Gaussian processes [124], a genetic algorithms [131] and polynomial chaos [132], to name a few examples. Here, I will briefly cover a family of statistical methods called Linear Regression, since this method has more often been applied in the cardiac simulations.

Linear regression provides an algebraic representation of the linear relationship between one or more independent variables \mathbf{X}_p (predictors), and one or more dependent variables \mathbf{y} (responses) (equation 1.29). This method approximates a set of observations to a linear model by finding the ‘best-fit’ of a set of data points to a straight line, less of an error ϵ . This is typically using a Least Squares algorithm. When more than one independent and dependent variables are used, the method is called multivariate linear regression (MVLR). Non-linear regression methods can also be used, whereby the data is approximated by a polynomial, logarithmic, exponential, or other non-linear function. However, this considerably increases the complexity of the statistical model.

The coefficients (β) of the linear regression model measure the strength of the association between a given predictor and the response. Thus, they can then be used as relative measures of parameter importance, that is, sensitivity indices. Therefore, this method is adequate for sensitivity analysis of multi-parameter models, provided that a set of conditions are met, such as the sample size being larger than the number of unknowns, and independence between predictors (that

$$\begin{array}{c}
 \text{Model instance} \longrightarrow \left[\begin{array}{c} \text{Input parameter} \\ \downarrow \\ \begin{matrix} x_{11} & \dots & x_{1p} \\ \vdots & & \vdots \\ x_{m1} & \dots & x_{mp} \end{matrix} \\ (m \times p) \end{array} \right] \times \left[\begin{array}{c} \text{Regression coefficients} \\ \downarrow \\ \begin{matrix} \beta_{11} & \dots & \beta_{1k} \\ \vdots & & \vdots \\ \beta_{p1} & \dots & \beta_{pk} \end{matrix} \\ (p \times k) \end{array} \right] = \left[\begin{array}{c} \text{Output parameter} \\ \downarrow \\ \begin{matrix} y_{11} & \dots & y_{1k} \\ \vdots & & \vdots \\ y_{m1} & \dots & y_{mk} \end{matrix} \\ (m \times k) \end{array} \right]
 \end{array}$$

Figure 1.28: Matrix representation of the a MVLR system.

is, their variances are uncorrelated).

This method is often employed in combination with the so-called ‘populations-of-models’ (PoM) approach (further discussed in Chapters I and II). PoM are usually constructed by randomly sampling parameter values from prior distributions (\mathbf{X} matrix of input parameters), and then executing a large number of model simulations with different random parameter samples. Several AP and CaT features are then extracted from the simulated traces, which constitute the responses (y_{mk}) in the MVLR algorithm (Figure 1.28). Hence, β_{pk} represents a relative measure of the sensitivity of feature y_k to parameter x_p .

$$\mathbf{y} = \mathbf{X} \cdot \boldsymbol{\beta} + \boldsymbol{\epsilon} \quad (1.29)$$

For large datasets without considerable non-linear effects among model parameters the MVLR can be a powerful method. Although more precise and quantitative methods for SA exist, the useful of this method is in its simplicity and easy implementation. It can provide a reasonable qualitative estimation of sensitivity ‘scores’ of the model to input parameters, thus allowing to rank parameter importance.

1.10 Summary of Papers

Paper I reviews the state-of-the-art in computational models of AF pathophysiology and available pharmacological treatments. The paper provides and chronological overview of the development of atrial models at different scales, from single cell models to three-dimensional whole organ models. A focus is given on how these models contributed to providing new insight into the both the normal function of the atria, and into the mechanisms of AF initiation and maintenance. The paper also describes multiple research efforts made towards employing computational models in *in silico* testing of drug effects, as well as catheter ablation procedures. Finally, the paper reviews recent trends in using populations of models to incorporate biolog-

1. Introduction

ical variability into computer simulations, and in performing sensitivity analysis to evaluate the role of parameters of interest in model outcomes.

Paper II presents a framework to assess the mechanisms of action potential duration alternans in a model of the human atrial myocyte. We employed a populations-of-models approach to incorporate variability into model parameters, including the maximum conductances of the ionic currents, ryanodine receptor variables, and SERCA density. We then used multivariate linear regression to assess the relative role of the changed parameters on several biomarkers extracted from action potentials, calcium transients, and alternans characteristics measured from APD restitution curves. We also compared populations of models in normal and in AF remodeled conditions, and We observed significant differences in the two populations in terms of action potential, calcium transients, and APD alternans morphologies. Furthermore, the sensitivity analysis results indicated different parameter importance rankings in the normal as compared to the AF populations, indicating that different cellular mechanisms give rise to action potential duration alternans in these two conditions.

Paper III presents the development of a novel computational model of the rabbit atrial myocyte. We developed the model by combining a rabbit-specific ionic currents with a spatial model of calcium handling. Given the uncertainty in the magnitudes of the ionic current, we parameterized the maximum conductances using a populations-of-models approach, and calibrating the population against published experimental data on various action potential and calcium transient metrics. We also used correlation analysis to evaluate the role of the maximum conductances on differences observed in the calcium wave propagations patterns in sub-population.

Paper IV presents a computational study of the role of rapid pacing-induced remodelling in rabbit atrial myocytes. We used a previously developed population of healthy rabbit atrial myocytes on which we incorporated changes in several parameters representing experimentally observed alterations in remodeled myocytes. We assigned each model in the remodeled populations to one of five different categories of calcium propagation pattern observed, and compared the effects of the each remodeled parameter.

References

- [1] European Heart Rhythm Association (EHRA), D. with the special contribution of the, European Association for Cardio-Thoracic Surgery (EACTS), E. by the, Members, A. F., Camm, A. J., Kirchhof, P., Lip, G. Y., Schotten, U., and al., et, “Guidelines for the management of atrial fibrillation: The task force for the management of atrial fibrillation of the

- european society of cardiology (esc)”, *European Heart Journal*, vol. 31, no. 19, pp. 2369–2429, Oct. 2010.
- [2] Kannel, W. B., Abbott, R. D., Savage, D. D., and McNamara, P. M., “Epidemiologic features of chronic atrial fibrillation: The framingham study.”, eng, *N Engl J Med*, vol. 306, no. 17, pp. 1018–1022, Apr. 1982.
- [3] Wolf, P. A., Dawber, T. R., Thomas, H. E. J., and Kannel, W. B., “Epidemiologic assessment of chronic atrial fibrillation and risk of stroke: The framingham study.”, eng, *Neurology*, vol. 28, no. 10, pp. 973–977, Oct. 1978.
- [4] Vos, C. B. de, Pisters, R., Nieuwlaat, R., Prins, M. H., Tielemans, R. G., Coelen, R.-J. S., Heijkant, A. C. van den, Allessie, M. A., and Crijns, H. J., “Progression from paroxysmal to persistent atrial fibrillation: Clinical correlates and prognosis”, *Journal of the American College of Cardiology*, vol. 55, no. 8, pp. 725–731, 2010.
- [5] Calkins, H., Kuck, K. H., Cappato, R., Brugada, J., Camm, A. J., Chen, S.-A., and al., et, “2012 hrs/ehra/ecas expert consensus statement on catheter and surgical ablation of atrial fibrillation: Recommendations for patient selection, procedural techniques, patient management and follow-up, definitions, endpoints, and research trial design: A report of the heart rhythm society (hrs) task force on catheter and surgical ablation of atrial fibrillation. developed in partnership with the european heart rhythm association (ehra), a registered branch of the european society of cardiology (esc) and the european cardiac arrhythmia society (ecas); and in collaboration with the american college of cardiology (acc), american heart association (aha), the asia pacific heart rhythm society (aphrs), and the society of thoracic surgeons (sts). endorsed by the governing bodies of the american college of cardiology foundation, the american heart association, the european cardiac arrhythmia society, the european heart rhythm association, the society of thoracic surgeons, the asia pacific heart rhythm society, and the heart rhythm society”, *EP Europace*, vol. 14, no. 4, pp. 528–606, Mar. 2012.
- [6] Zoni-Berisso, M., Lercari, F., Carazza, T., and Domenicucci, S., “Epidemiology of atrial fibrillation: European perspective.”, *Clin Epidemiol*, vol. 6, pp. 213–220, 2014.
- [7] Cairns, J. A. and Connolly, S. J., “Nonrheumatic atrial fibrillation. risk of stroke and role of antithrombotic therapy.”, eng, *Circulation*, vol. 84, no. 2, pp. 469–481, Aug. 1991.
- [8] Krahn, A. D., Manfreda, J., Tate, R. B., Mathewson, F. A., and Cuddy, T. E., “The natural history of atrial fibrillation: Incidence, risk factors, and prognosis in the manitoba follow-up study.”, eng, *Am J Med*, vol. 98, no. 5, pp. 476–484, May 1995.

1. Introduction

- [9] Lip, G. Y., Laroche, C., Ioachim, P. M., Rasmussen, L. H., Vitali-Serdoz, L., Petrescu, L., Darabantiu, D., Crijns, H. J., Kirchhof, P., Vardas, P., Tavazzi, L., Maggioni, A. P., and Boriani, G., “Prognosis and treatment of atrial fibrillation patients by european cardiologists: One year follow-up of the eurobservational research programme-atrial fibrillation general registry pilot phase (eorp-af pilot registry)”, *European Heart Journal*, vol. 35, no. 47, pp. 3365–3376, Aug. 2014.
- [10] Schotten, U., Verheule, S., Kirchhof, P., and Goette, A., “Pathophysiological mechanisms of atrial fibrillation: A translational appraisal.”, *Physiol Rev*, vol. 91, no. 1, pp. 265–325, 2011.
- [11] Trayanova, N. A., “Mathematical approaches to understanding and imaging atrial fibrillation: Significance for mechanisms and management”, *Circulation research*, vol. 114, no. 9, pp. 1516–1531, Apr. 2014.
- [12] Heijman, J., Erfanian Abdoust, P., Voigt, N., Nattel, S., and Dobrev, D., “Computational models of atrial cellular electrophysiology and calcium handling, and their role in atrial fibrillation”, *The Journal of physiology*, vol. 594, no. 3, pp. 537–553, Feb. 2016.
- [13] Grandi, E. and Maleckar, M. M., “Anti-arrhythmic strategies for atrial fibrillation: The role of computational modeling in discovery, development, and optimization.”, *Pharmacol Ther*, vol. 168, pp. 126–142, Dec. 2016.
- [14] Vagos, M., Herck, I. G. M. van, Sundnes, J., Arevalo, H. J., Edwards, A. G., and Koivumäki, J. T., “Computational modeling of electrophysiology and pharmacotherapy of atrial fibrillation: Recent advances and future challenges”, *Frontiers in Physiology*, vol. 9, p. 1221, 2018.
- [15] (2019). The Comprehensive in Vitro Proarrhythmia Assay (CiPA) Initiative, [Online]. Available: <https://cipaproject.org>.
- [16] Bootman, M. D., Smyrnias, I., Rúdiger, Coombes, S., and Roderick, H. L., “Atrial cardiomyocyte calcium signalling”, *Biochimica et Biophysica Acta (BBA) - Molecular Cell Research*, vol. 1813, no. 5, pp. 922–934, 2011, Including the Special Section: 11th European Symposium on Calcium.
- [17] Betts, J. G., Young, K. A., Wise, J. A., Johnson, E., Poe, B., Kruse, D. H., Korol, O., Johnson, J. E., Womble, M., and DeSaix, P., *Anatomy and Physiology*. 2013.
- [18] Decker, M. L., Behnke-Barclay, M., Cook, M. G., Lesch, M., and Decker, R. S., “Morphometric evaluation of the contractile apparatus in primary cultures of rabbit cardiac myocytes.”, *Circ Res*, vol. 69, no. 1, pp. 86–94, 1991.
- [19] Bers, D. M. and Shannon, T. R., “Calcium movements inside the sarcoplasmic reticulum of cardiac myocytes.”, *J Mol Cell Cardiol*, vol. 58, pp. 59–66, 2013.

- [20] Diaz, M. E., Trafford, A. W., O'Neill, S. C., and Eisner, D. A., “Measurement of sarcoplasmic reticulum Ca^{2+} content and sarcolemmal Ca^{2+} fluxes in isolated rat ventricular myocytes during spontaneous Ca^{2+} release.”, *J Physiol*, vol. 501 (Pt 1), pp. 3–16, 1997.
- [21] Stern, M. D., Song, L.-S., Cheng, H., Sham, J. S., Yang, H. T., Boheler, K. R., and Rios, E., “Local Control Models of Cardiac Excitation–Contraction Coupling : A Possible Role for Allosteric Interactions between Ryanodine Receptors”, *Journal of General Physiology*, vol. 113, no. 3, pp. 469–489, Mar. 1999.
- [22] Eisner, D. A., Caldwell, J. L., Kistamás, K., and Trafford, A. W., “Calcium and excitation-contraction coupling in the heart.”, *Circ Res*, vol. 121, no. 2, pp. 181–195, 2017.
- [23] Woo, S.-H., Soldatov, N. M., and Morad, M., “Modulation of Ca^{2+} signalling in rat atrial myocytes: Possible role of the alpha1c carboxyl terminal.”, *J Physiol*, vol. 552, no. Pt 2, pp. 437–447, 2003.
- [24] Stern, M. D., “Theory of excitation-contraction coupling in cardiac muscle.”, *Biophys J*, vol. 63, no. 2, pp. 497–517, Aug. 1992.
- [25] Cheng, H., Lederer, W., and Cannell, M., “Calcium sparks: Elementary events underlying excitation-contraction coupling in heart muscle”, *Science*, vol. 262, no. 5134, pp. 740–744, 1993.
- [26] Lipp, P. and Niggli, E., “Modulation of Ca^{2+} release in cultured neonatal rat cardiac myocytes. insight from subcellular release patterns revealed by confocal microscopy.”, *Circulation Research*, vol. 74, no. 5, pp. 979–990, 1994.
- [27] Lopez-Lopez, J. R., Shacklock, P. S., Balke, C. W., and Wier, W. G., “Local, stochastic release of Ca^{2+} in voltage-clamped rat heart cells: Visualization with confocal microscopy.”, *J Physiol*, vol. 480 (Pt 1), pp. 21–29, 1994.
- [28] Voigt, N., Heijman, J., Qiongling, Chiang, D. Y., Li, N., Karck, M., Wehrens, X. H., Nattel, S., and Dobrev, D., “Cellular and molecular mechanisms of atrial arrhythmogenesis in patients with paroxysmal atrial fibrillation”, *Circulation*, vol. 129, no. 2, pp. 145–156, 2014.
- [29] Pavlovic, D., Fuller, W., and Shattock, M. J., “Novel regulation of cardiac na pump via phospholemman.”, *J Mol Cell Cardiol*, vol. 61, pp. 83–93, 2013.
- [30] Mackenzie, L., Roderick, H. L., Berridge, M. J., Conway, S. J., and Bootman, M. D., “The spatial pattern of atrial cardiomyocyte calcium signalling modulates contraction”, *Journal of Cell Science*, vol. 117, no. 26, pp. 6327–6337, 2004.
- [31] Bootman, M. D., Higazi, D. R., Coombes, S., and Roderick, H. L., “Calcium signalling during excitation-contraction coupling in mammalian atrial myocytes”, *Journal of Cell Science*, vol. 119, no. 19, pp. 3915–3925, 2006.

1. Introduction

- [32] Trafford, A. W., Clarke, J. D., Richards, M. A., Eisner, D. A., and Dibb, K. M., “Calcium signalling microdomains and the t-tubular system in atrial myocytes: Potential roles in cardiac disease and arrhythmias.”, *Cardiovasc Res*, vol. 98, no. 2, pp. 192–203, May 2013.
- [33] Swietach, P., Spitzer, K. W., and Vaughan-Jones, R. D., “Modeling calcium waves in cardiac myocytes: Importance of calcium diffusion.”, *Front Biosci (Landmark Ed)*, vol. 15, pp. 661–680, Jan. 2010.
- [34] Smith, G. L. and Eisner, D. A., “Calcium buffering in the heart in health and disease.”, *Circulation*, vol. 139, no. 20, pp. 2358–2371, May 2019.
- [35] Allessie, M., Ausma, J., and Schotten, U., “Electrical, contractile and structural remodeling during atrial fibrillation.”, *Cardiovasc Res*, vol. 54, no. 2, pp. 230–246, May 2002.
- [36] Eckstein, J., Verheule, S., Groot, N. de, Allessie, M., and Schotten, U., “Mechanisms of perpetuation of atrial fibrillation in chronically dilated atria”, *Progress in Biophysics and Molecular Biology*, vol. 97, no. 2, pp. 435–451, 2008, Life and Mechanosensitivity.
- [37] Wijffels, M. C., Kirchhof, C. J., Dorland, R., and Allessie, M. A., “Atrial fibrillation begets atrial fibrillation”, *Circulation*, vol. 92, no. 7, pp. 1954–1968, 1995.
- [38] Voigt, N., Nattel, S., and Dobrev, D., “Proarrhythmic atrial calcium cycling in the diseased heart.”, *Adv Exp Med Biol*, vol. 740, pp. 1175–1191, 2012.
- [39] Vest, J. A., Wehrens, X. H. T., Reiken, S. R., Lehnart, S. E., Dobrev, D., Chandra, P., Danilo, P., Ravens, U., Rosen, M. R., and Marks, A. R., “Defective cardiac ryanodine receptor regulation during atrial fibrillation.”, *Circulation*, vol. 111, no. 16, pp. 2025–2032, Apr. 2005.
- [40] Liu, T., Xiong, F., Qi, X.-Y., Xiao, J., Villeneuve, L., Abu-Taha, I., Dobrev, D., Huang, C., and Nattel, S., “Altered calcium handling produces reentry-promoting action potential alternans in atrial fibrillation-remodeled hearts”, *JCI Insight*, vol. 5, no. 8, Apr. 2020.
- [41] Dobrev, D. and Nattel, S., “New insights into the molecular basis of atrial fibrillation: Mechanistic and therapeutic implications.”, *Cardiovasc Res*, vol. 89, no. 4, pp. 689–691, Mar. 2011.
- [42] Heijman, J., Schirmer, I., and Dobrev, D., “The multiple proarrhythmic roles of cardiac calcium-handling abnormalities: Triggered activity, conduction abnormalities, beat-to-beat variability, and adverse remodelling.”, *Europace*, vol. 18, no. 10, pp. 1452–1454, Oct. 2016.
- [43] Heijman, J., Voigt, N., Nattel, S., and Dobrev, D., “Calcium handling and atrial fibrillation.”, *Wien Med Wochenschr*, vol. 162, no. 13-14, pp. 287–291, 2012.

- [44] Voigt, N., Li, N., Wang, Q., Wang, W., Trafford, A. W., Abu-Taha, I., Sun, Q., Wieland, T., Ravens, U., Nattel, S., Wehrens, X. H., and Dobrev, D., “Enhanced sarcoplasmic reticulum Ca^{2+} leak and increased $\text{Na}^+ \cdot \text{Ca}^{2+}$ exchanger function underlie delayed afterdepolarizations in patients with chronic atrial fibrillation”, *Circulation*, vol. 125, no. 17, pp. 2059–2070, 2012.
- [45] Hove-Madsen, L., Llach, A., Bayes-Genis, A., Roura, S., Rodriguez Font, E., Aris, A., and Cinca, J., “Atrial fibrillation is associated with increased spontaneous calcium release from the sarcoplasmic reticulum in human atrial myocytes.”, eng, *Circulation*, vol. 110, no. 11, pp. 1358–1363, Sep. 2004.
- [46] Dobrev, D. and Nattel, S., “Calcium handling abnormalities in atrial fibrillation as a target for innovative therapeutics.”, *J Cardiovasc Pharmacol*, vol. 52, no. 4, pp. 293–299, Oct. 2008.
- [47] Shannon, T. R., Wang, F., Puglisi, J., Weber, C., and Bers, D. M., “A mathematical treatment of integrated Ca dynamics within the ventricular myocyte.”, *Biophys J*, vol. 87, no. 5, pp. 3351–3371, Nov. 2004.
- [48] Grandi, E., Pandit, S. V., Voigt, N., Workman, A. J., Dobrev, D., Jalife, J., and Bers, D. M., “Human atrial action potential and Ca^{2+} model: Sinus rhythm and chronic atrial fibrillation.”, *Circ Res*, vol. 109, no. 9, pp. 1055–1066, 2011.
- [49] Koivumäki, J. T., Seemann, G., Maleckar, M. M., and Tavi, P., “In silico screening of the key cellular remodeling targets in chronic atrial fibrillation”, *PLOS Computational Biology*, vol. 10, no. 5, pp. 1–15, May 2014.
- [50] Pandit, S. V., “Ionic Mechanisms of Atrial Action Potentials”, in *Cardiac Electrophysiology: From Cell to Bedside (Seventh Edition)*, Zipes, D. P., Jalife, J., and Stevenson, W. G., Eds., Seventh Edition, Elsevier, 2018, pp. 293–303.
- [51] Traube, L., “Ein fall von pulsus bigeminus nebst bemerkungen über die leberschwellungen bei klappenfehlern und über acute leberatrophie.”, *Berliner Klinische Wochenschrift*, vol. 9, no. 16, pp. 185–188, 1872.
- [52] Lu, H.-H., Lange, G., and Brooks, C. M., “Comparative studies of electrical and mechanical alternation in heart cells”, *Journal of Electrocardiology*, vol. 1, no. 1, pp. 7–17, 1968.
- [53] Sato, D., Shiferaw, Y., Garfinkel, A., Weiss, J. N., Qu, Z., and Karma, A., “Spatially Discordant Alternans in Cardiac Tissue: Role of calcium cycling.”, *Circ Res*, vol. 99, no. 5, pp. 520–527, 2006.
- [54] Weiss, J. N., Karma, A., Shiferaw, Y., Chen, P.-S., Garfinkel, A., and Qu, Z., “From pulsus to pulseless: The saga of cardiac alternans.”, *Circ Res*, vol. 98, no. 10, pp. 1244–1253, 2006.

1. Introduction

- [55] Verrier, R. L. and Nearing, B. D., “Electrophysiologic basis for t wave alternans as an index of vulnerability to ventricular fibrillation.”, *J Cardiovasc Electrophysiol*, vol. 5, no. 5, pp. 445–461, May 1994.
- [56] Rosenbaum, D. S., Jackson, L. E., Smith, J. M., Garan, H., Ruskin, J. N., and Cohen, R. J., “Electrical Alternans and Vulnerability to Ventricular Arrhythmias”, *New England Journal of Medicine*, vol. 330, no. 4, pp. 235–241, 1994, PMID: 8272084.
- [57] Franz, M. R., Jamal, S. M., and Narayan, S. M., “The role of action potential alternans in the initiation of atrial fibrillation in humans: A review and future directions”, *Europace*, vol. 14, no. Suppl 5, pp. v58–v64, Nov. 2012.
- [58] Narayan, S. M., Franz, M. R., Clopton, P., Pruvot, E. J., and Krummen, D. E., “Repolarization alternans reveals vulnerability to human atrial fibrillation”, *Circulation*, vol. 123, no. 25, pp. 2922–2930, Jun. 2011.
- [59] Narayan, S. M., “T-wave alternans and the susceptibility to ventricular arrhythmias”, *Journal of the American College of Cardiology*, vol. 47, no. 2, pp. 269–281, 2006.
- [60] Verrier, R. L., Kumar, K., and Nearing, B. D., “Basis for sudden cardiac death prediction by t-wave alternans from an integrative physiology perspective”, *Heart rhythm*, vol. 6, no. 3, pp. 416–422, Mar. 2009.
- [61] Rosenbaum, D. S., “T-Wave Alternans in the Sudden Cardiac Death in Heart Failure Trial Population”, *Circulation*, vol. 118, no. 20, pp. 2015–2018, 2008.
- [62] Verrier, R. L. and Nieminen, T., “T-wave alternans as a therapeutic marker for antiarrhythmic agents.”, *J Cardiovasc Pharmacol*, vol. 55, no. 6, pp. 544–554, Jun. 2010.
- [63] Verrier, R. L., Klingenberg, T., Malik, M., El-Sherif, N., Exner, D. V., Hohnloser, S. H., Ikeda, T., Martinez, J. P., Narayan, S. M., Nieminen, T., and Rosenbaum, D. S., “Microvolt T-wave alternans testing has a role in arrhythmia risk stratification”, *Journal of the American College of Cardiology*, vol. 59, no. 17, pp. 1572–1573, 2012.
- [64] Narayan, S. M., Bode, F., Karasik, P. L., and Franz, M. R., “Alternans of Atrial Action Potentials During Atrial Flutter as a Precursor to Atrial Fibrillation”, *Circulation*, vol. 106, no. 15, pp. 1968–1973, 2002.
- [65] Kanaporis, G. and Blatter, L. A., “Alternans in atria: Mechanisms and clinical relevance”, *Medicina (Kaunas, Lithuania)*, vol. 53, no. 3, pp. 139–149, 2017.
- [66] Edwards, J. N. and Blatter, L. A., “Cardiac alternans and intracellular calcium cycling”, *Clinical and experimental pharmacology & physiology*, vol. 41, no. 7, pp. 524–532, Jul. 2014.
- [67] Pastore, J. M., Girouard, S. D., Laurita, K. R., Akar, F. G., and Rosenbaum, D. S., “Mechanism linking t-wave alternans to the genesis of cardiac fibrillation”, *Circulation*, vol. 99, no. 10, pp. 1385–1394, 1999.

- [68] Rubenstein, D. S. and Lipsius, S. L., “Premature beats elicit a phase reversal of mechanoelectrical alternans in cat ventricular myocytes. a possible mechanism for reentrant arrhythmias.”, *Circulation*, vol. 91, no. 1, pp. 201–214, 1995.
- [69] Weiss, J. N., Garfinkel, A., Karagueuzian, H. S., Nguyen, T. P., Olcese, R., Chen, P.-S., and Qu, Z., “Perspective: A dynamics-based classification of ventricular arrhythmias.”, *J Mol Cell Cardiol*, vol. 82, pp. 136–152, 2015.
- [70] Qu, Z., Garfinkel, A., Chen, P.-S., and Weiss, J. N., “Mechanisms of discordant alternans and induction of reentry in simulated cardiac tissue”, *Circulation*, vol. 102, no. 14, pp. 1664–1670, 2000.
- [71] Groenendaal, W., Ortega, F. A., Krogh-Madsen, T., and Christini, D. J., “Voltage and calcium dynamics both underlie cellular alternans in cardiac myocytes”, *Biophysical journal*, vol. 106, no. 10, pp. 2222–2232, May 2014.
- [72] Gaeta, S. A. and Christini, D. J., “Non-Linear Dynamics of Cardiac Alternans: Subcellular to Tissue-Level Mechanisms of Arrhythmia”, *Frontiers in Physiology*, vol. 3, p. 157, 2012.
- [73] Nolasco, J. B. and Dahlen, R. W., “A graphic method for the study of alternation in cardiac action potentials.”, *J Appl Physiol*, vol. 25, no. 2, pp. 191–196, Aug. 1968.
- [74] Riccio, M. L., Koller, M. L., and Gilmour, R. F., “Electrical restitution and spatiotemporal organization during ventricular fibrillation”, *Circulation Research*, vol. 84, no. 8, pp. 955–963, 1999.
- [75] Koller, M. L., Riccio, M. L., and Jr., R. F. G., “Dynamic restitution of action potential duration during electrical alternans and ventricular fibrillation”, *American Journal of Physiology-Heart and Circulatory Physiology*, vol. 275, no. 5, H1635–H1642, 1998, PMID: 9815071.
- [76] Fox, J. J., McHarg, J. L., and Gilmour, R. F., “Ionic mechanism of electrical alternans”, *American Journal of Physiology-Heart and Circulatory Physiology*, vol. 282, no. 2, H516–H530, 2002, PMID: 11788399.
- [77] Zhou, X., Bueno-Orovio, A., Orini, M., Hanson, B., Hayward, M., Taggart, P., Lambiase, P. D., Burrage, K., and Rodriguez, B., “In vivo and in silico investigation into mechanisms of frequency dependence of repolarization alternans in human ventricular cardiomyocytes”, *Circulation research*, vol. 118, no. 2, pp. 266–278, Jan. 2016.
- [78] Chudin, E., Goldhaber, J., Garfinkel, A., Weiss, J., and Kogan, B., “Intracellular Ca^{2+} dynamics and the stability of ventricular tachycardia.”, *Biophys J*, vol. 77, no. 6, pp. 2930–2941, 1999.
- [79] Wan, X., Laurita, K. R., Pruvot, E. J., and Rosenbaum, D. S., “Molecular correlates of repolarization alternans in cardiac myocytes.”, *J Mol Cell Cardiol*, vol. 39, no. 3, pp. 419–428, 2005.

1. Introduction

- [80] Huser, J., Wang, Y. G., Sheehan, K. A., Cifuentes, F., Lipsius, S. L., and Blatter, L. A., “Functional coupling between glycolysis and excitation-contraction coupling underlies alternans in cat heart cells.”, *J Physiol*, vol. 524 Pt 3, pp. 795–806, 2000.
- [81] Shkryl, V. M., Maxwell, J. T., Domeier, T. L., and Blatter, L. A., “Refractoriness of sarcoplasmic reticulum Ca^{2+} release determines Ca^{2+} alternans in atrial myocytes.”, *Am J Physiol Heart Circ Physiol*, vol. 302, no. 11, H2310–20, 2012.
- [82] Wan, X., Cutler, M., Song, Z., Karma, A., Matsuda, T., Baba, A., and Rosenbaum, D. S., “New experimental evidence for mechanism of arrhythrogenic membrane potential alternans based on balance of electrogenic I(NCX)/I(Ca) currents”, *Heart rhythm*, vol. 9, no. 10, pp. 1698–1705, Oct. 2012.
- [83] Jordan, P. N. and Christini, D. J., “Characterizing the contribution of voltage- and calcium-dependent coupling to action potential stability: Implications for repolarization alternans”, *American Journal of Physiology-Heart and Circulatory Physiology*, vol. 293, no. 4, H2109–H2118, 2007, PMID: 17586611.
- [84] Diaz, M. E., O'Neill, S. C., and Eisner, D. A., “Sarcoplasmic reticulum calcium content fluctuation is the key to cardiac alternans.”, *Circ Res*, vol. 94, no. 5, pp. 650–656, 2004.
- [85] Pruvot, E. J., Katra, R. P., Rosenbaum, D. S., and Laurita, K. R., “Role of calcium cycling versus restitution in the mechanism of repolarization alternans.”, *Circ Res*, vol. 94, no. 8, pp. 1083–1090, 2004.
- [86] Goldhaber, J. I., Xie, L.-H., Duong, T., Motter, C., Khuu, K., and Weiss, J. N., “Action potential duration restitution and alternans in rabbit ventricular myocytes: The key role of intracellular calcium cycling.”, *Circ Res*, vol. 96, no. 4, pp. 459–466, 2005.
- [87] Eisner, D. A., Li, Y., and O'Neill, S. C., “Alternans of intracellular calcium: Mechanism and significance”, *Heart Rhythm*, vol. 3, no. 6, pp. 743–745, 2006.
- [88] Li, Y., Diaz, M. E., Eisner, D. A., and O'Neill, S., “The effects of membrane potential, sr Ca^{2+} content and ryr responsiveness on systolic Ca^{2+} alternans in rat ventricular myocytes.”, *J Physiol*, vol. 587, no. Pt 6, pp. 1283–1292, 2009.
- [89] Picht, E., DeSantiago, J., Blatter, L. A., and Bers, D. M., “Cardiac alternans do not rely on diastolic sarcoplasmic reticulum calcium content fluctuations”, *Circulation Research*, vol. 99, no. 7, pp. 740–748, 2006.
- [90] Rovetti, R., Cui, X., Garfinkel, A., Weiss, J. N., and Qu, Z., “Spark-induced sparks as a mechanism of intracellular calcium alternans in cardiac myocytes.”, *Circ Res*, vol. 106, no. 10, pp. 1582–1591, 2010.

- [91] Lyon, A. R., Bannister, M. L., Collins, T., Pearce, E., Sepehripour, A. H., Dubb, S. S., Garcia, E., O'Gara, P., Liang, L., Kohlbrenner, E., Hajjar, R. J., Peters, N. S., Poole-Wilson, P. A., Macleod, K. T., and Harding, S. E., "Serca2a gene transfer decreases sarcoplasmic reticulum calcium leak and reduces ventricular arrhythmias in a model of chronic heart failure", *Circulation: Arrhythmia and Electrophysiology*, vol. 4, no. 3, pp. 362–372, 2011.
- [92] Cutler, M. J., Wan, X., Plummer, B. N., Liu, H., Deschenes, I., Laurita, K. R., Hajjar, R. J., and Rosenbaum, D. S., "Targeted sarcoplasmic reticulum Ca^{2+} ATPase 2a gene delivery to restore electrical stability in the failing heart.", *Circulation*, vol. 126, no. 17, pp. 2095–2104, 2012.
- [93] Alvarez-Lacalle, E., Cantalapiedra, I. R., Peñaranda, A., Cinca, J., Hove-Madsen, L., and Echebarria, B., "Dependency of calcium alternans on ryanodine receptor refractoriness", *PLOS ONE*, vol. 8, no. 2, pp. 1–11, Feb. 2013.
- [94] Bassani, J. W., Yuan, W., and Bers, D. M., "Fractional sr ca release is regulated by trigger ca and sr ca content in cardiac myocytes", *American Journal of Physiology-Cell Physiology*, vol. 268, no. 5, pp. C1313–C1319, 1995, PMID: 7762626.
- [95] Tao, T., O'Neill, S. C., Diaz, M. E., Li, Y. T., Eisner, D. A., and Zhang, H., "Alternans of cardiac calcium cycling in a cluster of ryanodine receptors: A simulation study", *American journal of physiology. Heart and circulatory physiology*, vol. 295, no. 2, H598–H609, Aug. 2008.
- [96] Tomek, J., Tomková, M., Zhou, X., Bub, G., and Rodriguez, B., "Modulation of cardiac alternans by altered sarcoplasmic reticulum calcium release: A simulation study", *Frontiers in Physiology*, vol. 9, p. 1306, 2018.
- [97] Diaz, M., Eisner, D., and O'Neill, S., "Depressed ryanodine receptor activity increases variability and duration of the systolic Ca^{2+} transient in rat ventricular myocytes", *Circulation Research*, vol. 91, no. 7, pp. 585–593, 2002.
- [98] Chang, K. C., Bayer, J. D., and Trayanova, N. A., "Disrupted calcium release as a mechanism for atrial alternans associated with human atrial fibrillation", *PLOS Computational Biology*, vol. 10, no. 12, pp. 1–16, Dec. 2014.
- [99] Aistrup, G. L., Kelly, J. E., Kapur, S., Kowalczyk, M., Sysman-Wolpin, I., Kadish, A. H., and Wasserstrom, J. A., "Pacing-induced heterogeneities in intracellular Ca^{2+} signaling, cardiac alternans, and ventricular arrhythmias in intact rat heart.", *Circ Res*, vol. 99, no. 7, e65–73, 2006.

1. Introduction

- [100] Aistrup, G. L., Shiferaw, Y., Kapur, S., Kadish, A. H., and Wasserstrom, J. A., “Mechanisms underlying the formation and dynamics of subcellular calcium alternans in the intact rat heart”, *Circulation Research*, vol. 104, no. 5, pp. 639–649, 2009.
- [101] Kockskämper, J. and Blatter, L. A., “Subcellular Ca^{2+} alternans represents a novel mechanism for the generation of arrhythmogenic Ca^{2+} waves in cat atrial myocytes.”, *J Physiol*, vol. 545, no. 1, pp. 65–79, 2002.
- [102] Blatter, L. A., Kockskamper, J., Sheehan, K. A., Zima, A. V., Huser, J., and Lipsius, S. L., “Local calcium gradients during excitation-contraction coupling and alternans in atrial myocytes.”, *J Physiol*, vol. 546, no. Pt 1, pp. 19–31, 2003.
- [103] Gaeta, S. A., Bub, G., Abbott, G. W., and Christini, D. J., “Dynamical mechanism for subcellular alternans in cardiac myocytes”, *Circulation Research*, vol. 105, no. 4, pp. 335–342, 2009.
- [104] Miura, M., Ishide, N., Oda, H., Sakurai, M., Shinozaki, T., and Takishima, T., “Spatial features of calcium transients during early and delayed afterdepolarizations.”, *Am J Physiol*, vol. 265, no. 2 Pt 2, H439–44, 1993.
- [105] Keizer, J., Smith, G. D., Ponce-Dawson, S., and Pearson, J. E., “Saltatory propagation of Ca^{2+} waves by Ca^{2+} sparks.”, *Biophys J*, vol. 75, no. 2, pp. 595–600, 1998.
- [106] Bosch, R. F., Zeng, X., Grammer, J. B., Popovic, K., Mewis, C., and Kuhlkamp, V., “Ionic mechanisms of electrical remodeling in human atrial fibrillation.”, eng, *Cardiovasc Res*, vol. 44, no. 1, pp. 121–131, Oct. 1999.
- [107] Franz, M. R., Jamal, S. M., and Narayan, S. M., “The role of action potential alternans in the initiation of atrial fibrillation in humans: A review and future directions.”, *Europace*, vol. 14 Suppl 5, no. Suppl 5, pp. v58–v64, 2012.
- [108] Tse, G., Wong, S. T., Tse, V., Lee, Y. T., Lin, H. Y., and Yeo, J. M., “Cardiac dynamics: Alternans and arrhythmogenesis.”, *J Arrhythm*, vol. 32, no. 5, pp. 411–417, 2016.
- [109] Kalb, S., Dobrovolny, H., Tolkacheva, E., Idriss, S., Krassowska, W., and Gauthier, D., “The restitution portrait: a new method for investigating rate-dependent restitution”, *Journal of cardiovascular electrophysiology*, vol. 15, pp. 698–709, Jul. 2004.
- [110] Noble, D., “A modification of the Hodgkin-Huxley equations applicable to Purkinje fibre action and pace-maker potentials”, *The Journal of physiology*, vol. 160, no. 2, pp. 317–352, Feb. 1962.
- [111] Hodgkin, A. L. and Huxley, A. F., “A quantitative description of membrane current and its application to conduction and excitation in nerve”, *The Journal of physiology*, vol. 117, no. 4, pp. 500–544, Aug. 1952.
- [112] (2020). Physiome Repository, [Online]. Available: <https://models.physiomeproject.org>.

- [113] Hilgemann, D. W. and Noble, D., “Excitation-contraction coupling and extracellular calcium transients in rabbit atrium: Reconstruction of basic cellular mechanisms”, *Proceedings of the Royal Society of London. Series B. Biological Sciences*, vol. 230, no. 1259, pp. 163–205, 1987.
- [114] (2020). Courtemanche, ramirez, nattel model, 1998, [Online]. Available: https://models.physiomeproject.org/exposure/0e03bbe01606be5811691f9d5de10b65/courtemanche_ramirez_nattel_1998.cellml/view.
- [115] Wilhelms, M., Hettmann, H., Maleckar, M. M., Koivumäki, J. T., Dossel, O., and Seemann, G., “Benchmarking electrophysiological models of human atrial myocytes.”, *Front Physiol*, vol. 3, p. 487, 2012.
- [116] Wikipedia. (2018). Hodgkin-Huxley, [Online]. Available: <https://commons.wikimedia.org/wiki/File:Hodgkin-Huxley.jpg>.
- [117] Keener, J. and Sneyd, J., *Mathematical Physiology*. 1998.
- [118] Periasamy, M., Bhupathy, P., and Babu, G. J., “Regulation of sarcoplasmic reticulum Ca^{2+} ATPase pump expression and its relevance to cardiac muscle physiology and pathology.”, *Cardiovasc Res*, vol. 77, no. 2, pp. 265–273, 2008.
- [119] El-Armouche, A., Boknik, P., Eschenhagen, T., Carrier, L., Knaut, M., Ravens, U., and Dobrev, D., “Molecular determinants of altered Ca^{2+} handling in human chronic atrial fibrillation.”, *Circulation*, vol. 114, no. 7, pp. 670–680, 2006.
- [120] Schotten, U., Greiser, M., Benke, D., Buerkel, K., Ehrenteidt, B., Stellbrink, C., Vazquez-Jimenez, J. F., Schoendube, F., Hanrath, P., and Allessie, M., “Atrial fibrillation-induced atrial contractile dysfunction: A tachycardiomyopathy of a different sort.”, *Cardiovasc Res*, vol. 53, no. 1, pp. 192–201, 2002.
- [121] Vagos, M. R., “Uncertainty quantification and sensitivity analysis of multi-parameter models”, Simula Research Laboratory, 2019.
- [122] Sarkar, A. X., Christini, D. J., and Sobie, E. A., “Exploiting mathematical models to illuminate electrophysiological variability between individuals.”, *J Physiol*, vol. 590, no. 11, pp. 2555–2567, 2012.
- [123] Muszkiewicz, A., Liu, X., Bueno-Orovio, A., Lawson, B., Burrage, K., Casadei, B., and Rodriguez, B., “From ionic to cellular variability in human atrial myocytes: An integrative computational and experimental study”, *American Journal of Physiology-Heart and Circulatory Physiology*, vol. 314, H895–H916, May 2018.
- [124] Chang, E. T. Y., Strong, M., and Clayton, R. H., “Bayesian sensitivity analysis of a cardiac cell model using a gaussian process emulator”, *PLOS ONE*, vol. 10, no. 6, pp. 1–20, Jun. 2015.
- [125] Sobie, E. A., “Parameter sensitivity analysis in electrophysiological models using multivariable regression.”, *Biophys J*, vol. 96, no. 4, pp. 1264–1274, 2009.

1. Introduction

- [126] Sarkar, A. X. and Sobie, E. A., “Regression Analysis for Constraining Free Parameters in Electrophysiological Models of Cardiac Cells”, *PLOS Computational Biology*, vol. 6, no. 9, pp. 1–11, Sep. 2010.
- [127] Lee, Y.-S., Liu, O. Z., Hwang, H. S., Knollmann, B. C., and Sobie, E. A., “Parameter sensitivity analysis of stochastic models provides insights into cardiac calcium sparks.”, *Biophys J*, vol. 104, no. 5, pp. 1142–1150, 2013.
- [128] Sánchez, C., Bueno-Orovio, A., Wettwer, E., Loose, S., Simon, J., Ravens, U., Pueyo, E., and Rodriguez, B., “Inter-Subject Variability in Human Atrial Action Potential in Sinus Rhythm versus Chronic Atrial Fibrillation”, *PLOS ONE*, vol. 9, no. 8, pp. 1–14, Aug. 2014.
- [129] Morotti, S. and Grandi, E., “Logistic regression analysis of populations of electrophysiological models to assess proarrythmic risk.”, *MethodsX*, vol. 4, pp. 25–34, 2017.
- [130] Krogh-Madsen, T., Sobie, E. A., and Christini, D. J., “Improving cardiomyocyte model fidelity and utility via dynamic electrophysiology protocols and optimization algorithms.”, *J Physiol*, vol. 594, no. 9, pp. 2525–2536, 2016.
- [131] Kherlopian, A. R., Ortega, F. A., and Christini, D. J., “Cardiac myocyte model parameter sensitivity analysis and model transformation using a genetic algorithm”, in *Proceedings of the 13th annual conference companion on Genetic and evolutionary computation - GECCO '11*, ser. the 13th annual conference companion, ACM Press, p. 755.
- [132] Geneser, S., Kirby, R., and Sachse, F., “Sensitivity analysis of cardiac electrophysiological models using polynomial chaos.”, *Conf Proc IEEE Eng Med Biol Soc*, vol. 2005, pp. 4042–4045, 2005.

Papers

Paper I

Computational Modeling of Electrophysiology and Pharmacotherapy of Atrial Fibrillation: Recent Advances and Future Challenges

Márcia R. Vagos, Ilsebeth G. M. van Herck, Joakim Sundnes,
Hermenegild J. Arevalo, Andrew G. Edwards, Jussi T.
Koivumäki

Computational modeling in pharmacotherapy of atrial fibrillation: recent advances and future challenges

Márcia R. Vagos^{1,2*}, Ilsebeth G.M. van Herck^{1,2*}, Joakim Sundnes^{1,3}, Hermenegild J. Arevalo^{1,3}, Andrew G. Edwards^{1,3#}, Jussi T. Koivumäki^{4,5#}

(* Joint first authors, # Joint senior authors)

¹ Computational Physiology Department, Simula Research Laboratory, Norway

² Department of Informatics, University of Oslo, Norway

³ Center for Cardiological Innovation (CCI), Norway

⁴ BioMediTech Institute and Faculty of Biomedical Sciences and Engineering, Tampere University of Technology, Tampere, Finland

⁵ A.I. Virtanen Institute for Molecular Sciences, University of Eastern Finland, Kuopio, Finland

Abstract

The pathophysiology of atrial fibrillation (AF) is broad, with components related to the unique and diverse cellular electrophysiology of atrial myocytes, structural complexity, and heterogeneity of atrial tissue, and pronounced disease-associated remodeling of both cells and tissue. A major challenge for rational design of AF therapy, particularly pharmacotherapy, is integrating these multiscale characteristics to identify approaches that are both efficacious and independent of ventricular contraindications. Computational modeling has long been touted as a basis for achieving such integration in a rapid, economical, and scalable manner. However, computational pipelines for AF specific drug screening are in their infancy, and while the field is progressing quite rapidly, major challenges remain before computational approaches can fill the role of workhorse in rational design of AF pharmacotherapies. In this review, we briefly detail the unique aspects of AF pathophysiology that determine requirements for compounds targeting AF rhythm control, with emphasis on delimiting mechanisms that promote AF triggers from those providing substrate or supporting reentry. We then describe modeling approaches that have been used to assess the outcomes of drugs acting on established AF targets, as well as on novel promising targets including the ultra-rapidly activating delayed rectifier potassium current, the acetylcholine-activated potassium current and the small conductance calcium-activated potassium channel. Finally, we describe how heterogeneity and variability are being incorporated into AF-specific models, and how these approaches are yielding novel insights into the basic physiology of disease, as well as aiding identification of the important molecular players in the complex AF etiology.

I.1 Introduction

Atrial fibrillation (AF) is a complex and multifactorial disease and the most common sustained cardiac arrhythmia, afflicting about 2% of the population. Age is the most powerful predictor of risk: approximately 5% of 65-year-olds and 10% of 75-year-olds suffer from AF (Heeringa et al., 2006).

AF is already a pervasive disease carrying an immense socioeconomic burden, and with increasing life expectancy both the human and economic costs are growing rapidly: AF prevalence in the European population is projected to increase to 3% by 2030 (Zoni-Berisso et al., 2014). Although rhythm control strategies are available, these are inadequate and there is at present an unmet need for safe and effective antiarrhythmic therapy for AF (Ehrlich and Nattel, 2009). Since 2010, the European Medicines Agency has not authorized any new drugs for treatment of AF. The most prominent explanations for this lack of new medicine are the limited understanding of this multi-etiological and progressive disease, as well as the challenge of designing compounds that are strongly specific for atrial rather than ventricular targets. As a result, the development of novel pharmacological therapies is necessarily coupled to a thorough understanding of the basic etiology and physiological mechanisms of AF.

Unlike most episodes of ventricular arrhythmia, which must either be terminated or are lethal, AF does not have immediate catastrophic consequences, and short episodes of self-terminating AF are often asymptomatic and go undetected. This allows prolonged AF episodes to drive pro arrhythmic remodeling across all levels of physiology (Schotten et al., 2011), as is succinctly captured by the phrase “AF begets AF” (Wijffels et al., 1995). In turn, this remodeling allows the mechanisms and complexity of AF to be richer than ventricular arrhythmia and causes treatment to be a moving target as the disease progresses from paroxysmal (pAF) to chronic (cAF) stages.

Both ectopic activity and the generation of a vulnerable substrate are accepted contributors to AF initiation and maintenance, although their respective contributions are thought to change as disease progresses. Triggering events are generally thought to play a more prominent role in pAF than at later stages when gross tissue-level remodeling is widespread. A range of evidence has led to this general perspective, but some key observations include: (1) prominent focal initiation of spontaneous episodes of pAF near the pulmonary vein (PV) junctions in patients (Haïssaguerre et al., 1998), (2) the absence of major alterations to action potential (AP) morphology and the excitable tissue gap in pAF (Diker et al., 1998; Voigt et al., 2013b), (3) elevated frequency of cellular triggering events (Voigt et al., 2012, 2013b).

As AF progresses, electrical and structural remodeling becomes pronounced, and characteristic changes to conduction and refractoriness leave the atrial myocardium more vulnerable to reentrant circuit formation (Nattel and Harada, 2014). AP duration (APD) and the effective refractory period (ERP) are consistently shortened in cAF (Iwasaki et al., 2011; Skibsbye et al., 2016), conduction is slowed (Lalani et al., 2012; Zheng et al., 2016), and the threshold for alternans induction, a key component of vulnerable substrate generation, is reduced (Narayan et al., 2011). Electrical remodeling exacerbates regional heterogeneities and promotes dispersion of refractoriness. Additionally, formation

I. Computational modeling in pharmacotherapy of atrial fibrillation: recent advances and future challenges

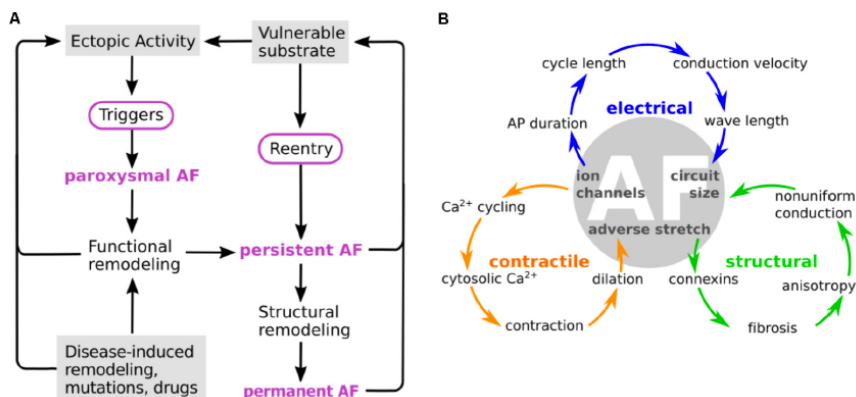


Figure 1: Characteristic processes and causalities at the different stages of atrial fibrillation (AF). A) AF is usually triggered by ectopic activity that act as “drivers” of electrical activation and override the normal sinus node pacemaking activity. The fast pacing induced by the ectopic activity initiates electrical and structural remodeling in the atria, which enhances cellular excitability of the atria, reduces conduction velocity, increases tissue heterogeneities, and creates fibrotic regions that act as reentry anchor points. All these changes contribute to creating a vulnerable substrate that render the atria more prone to arrhythmias, as AF progresses from paroxysmal to permanent, in a process commonly termed as “AF begets AF”.

of fibrotic regions, collagen patches, and fibroblast differentiation, as part of structural remodeling, enhances tissue anisotropy and is non-uniform throughout the atria, thus further promoting the development of a reentrant substrate. Moreover, contractile remodeling (atrial dilatation and increased wall compliance) is both a consequence and effector of AF (Schotten et al., 2003). All these identified mechanisms of progressive remodeling, resulting from recurrent rapid pacing or paroxysms of AF, generate positive feedback loops that ultimately set the conditions for sustained AF. These processes are likely to be important in determining the dynamic characteristics of reentrant circuit formation, and in certain cases may be important for understanding drug action. For example, the efficacy of class Ic antiarrhythmics depends on the dynamics inherent to spiral wave propagation (Comtois et al., 2005; Kneller et al., 2005). However, currently, we do not have sufficient understanding of the tissue-level dynamics driving AF at various stages, to focus pharmacologic design efforts on correcting specific tissue-level dynamical characteristics. For this reason, our discussion below focuses on remodeling occurring at subcellular and cellular levels and their implications in AF progression, and acknowledge that the sustaining effect of tissue-level electrical and structural remodeling causes antiarrhythmic targeting in cAF to be extremely challenging. The major components, interactions, and contributions of the characteristic processes at the various stages of disease progression are summarized in Figure 1.

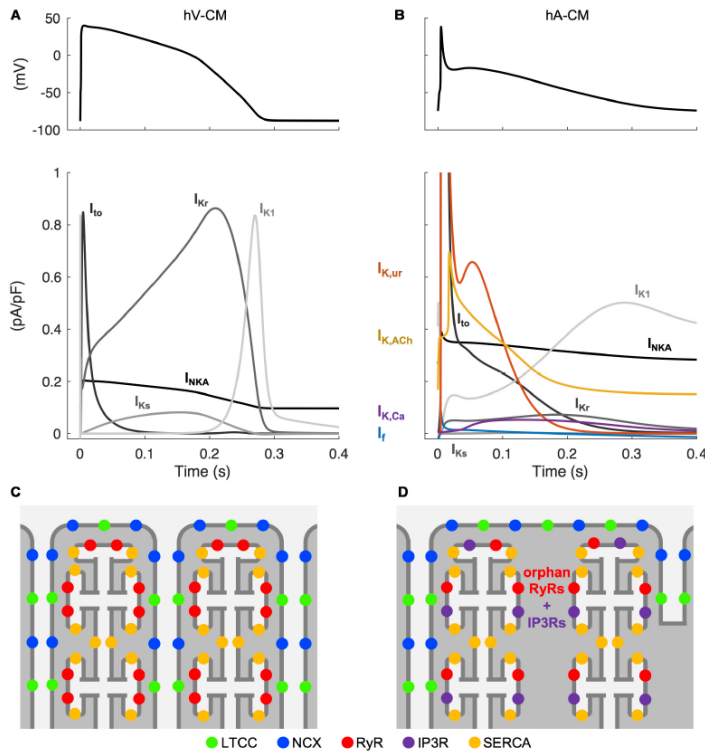


Figure 2: Unique electrophysiological and structural characteristics of atrial cardiomyocytes. Simulated AP in human ventricular (A) and atrial (B) CMs, as well the differences in underlying repolarizing ion potassium currents. Please, note that in order to visualize the weaker currents, the peaks of atrial transient outward potassium current (I_{to}) ($\sim 11 \text{ pA/pF}$) and the ultra rapidly activating delayed rectifier potassium current (I_{Kur}) ($\sim 4.6 \text{ pA/pF}$) are cut off. The atria-specific ion currents funny current (I_f), I_{Kur} , the acetylcholine-activated potassium current ($I_{K,ACh}$), and the small conductance calcium-activated potassium current ($I_{K,Ca}$) are

In the following four sections, we first briefly introduce the basic aspects of AF mechanisms and their related experimental findings (see the section “Arrhythmogenic Mechanisms of AF”). We then review current computational approaches for modeling atrial physiology and AF pathophysiology (see the section “In silico Atrial Modeling”). We present an overview of how drug–target interactions and their outcomes have been simulated in the heart, followed by current efforts to explore novel strategies for AF drug targeting (see the section “Computational Pharmacology in AF”). Finally, in the section “Modeling Variability and Uncertainty at the Cell Level,” we describe how variability and stochasticity can be incorporated into computational models to increase their robustness and predictive power in AF drug therapy.

I.2 Arrhythmogenic mechanisms of AF

I.2.1 Remodeling of cellular electrophysiology, ultrastructure, and calcium handling

I.2.1.1 Pathological changes to sarcolemmal current carriers

Human atrial cardiomyocytes (hA-CMs) exhibit a range of AP morphologies that differ markedly from those apparent in the ventricle. This is primarily due to differing expression levels of ion channel subunits, and concurrently ion current densities. The atrial AP exhibits a less pronounced plateau phase, largely due to the prominent expression of the fast-activating potassium

currents, particularly the ultra rapidly activating delayed rectifier current (I_{Kur}), which is virtually absent in the ventricle. Atrial APs also exhibit relatively slow late repolarization (phase 3), elevated resting potential, and slower AP upstroke, all of which are strongly-influenced by a reduced density of the inward-rectified potassium current (I_{K1}) relative to human ventricular CMs (hV-CMs). Like I_{Kur} , the small conductance calcium-activated potassium current ($I_{K,Ca}$) is only present in hA-CMs, and it is thought to assist hA-CM repolarization, although its relative contribution remains contentious. The major differences in atrial and ventricular AP morphology and underlying ion currents are summarized in Figure 2A-B.

The pathophysiology of cAF is characterized by several prototypical changes in current expression that result in both marked deceleration of early repolarization, and acceleration of late repolarization (Schotten et al., 2011). The two most prominent molecular changes that drive these outcomes are: (1) augmentation of inward-rectified potassium currents (increase of I_{K1} expression and constitutive activity of the acetylcholine-activated inward rectifier current; $I_{K,ACh}$), and (2) simultaneous decrease in the L-type calcium current (I_{CaL}). The major counteractive changes are carried by increased sodium-calcium exchanger (NCX) expression, and reductions in the major rapidly activating outward currents, namely I_{Kur} and the fast component of the transient outward potassium current (herein simply referred to as I_{to}). Together, these five alterations (I_{K1} , I_{CaL} , NCX, I_{Kur} , and I_{to}) constitute the majority of the known modulators of repolarization trajectory in cAF (Figure 3). Overall these effects result in the shortening of ERP, and a slightly more negative resting membrane potential (Ravens et al., 2014; Skibbsbye et al., 2014, 2016), both of which expand the window for reentrant excitation. However, as discussed further below, they are accompanied by a range of changes to cellular ultrastructure and to the function of major calcium- and sodium-handling proteins, such that predicting the integrated outcomes from any subset of changes is non-trivial and necessitates quantitative approaches.

I.2.1.2. Ultrastructural contributions to AF pathogenesis

Although there is important species-specificity of hA-CM ultrastructure, it has been generally observed that healthy hA-CMs exhibit a varied and relatively sparse membrane ultrastructure compared to ventricular CMs. This results in important baseline differences in excitation-contraction coupling. Most prominently, hA-CMs have a less developed T-tubule network (Dibb et al., 2013), particularly in rodents, as illustrated in Figure 2C-D. This morphological difference has implications for intracellular calcium diffusion. In the absence of T-tubules, Ca^{2+} enters the cells largely from the periphery, and thus must diffuse centripetally to engage the contractile machinery. Correspondingly, the localization of Ca^{2+} handling proteins is very different in ventricular and atrial CMs. In hA-CMs, as in hV-CMs, L-type Ca^{2+} channels interact with clusters of

sarcoplasmic reticulum (SR) Ca^{2+} release channels (RyRs; Ryanodine receptors) located in the junctional SR to trigger Ca^{2+} -induced Ca^{2+} release (CICR). However, in hA-CMs, a higher proportion of RyR clusters are concentrated in non-junctional SR, and this is a distinguishing structural characteristic. These orphan or non-junctional RyRs contribute to the fire-diffuse-fire propagation of Ca^{2+} , which is augmented by inositol 1,4,5- trisphosphate receptors (IP3Rs) that are also embedded in the SR membrane (Li et al., 2005; Lipp et al., 2000;

Wullschleger et al., 2017; Yamada et al., 2001; Zima and Blatter, 2004). The importance of IP3Rs is generally greater in atrial than ventricular CMs – in ventricle, they are generally only observed in disease states, such as heart failure (Go et al., 1995). These features of the calcium signaling system fundamentally alter the essential structure-function relationships governing calcium handling in atrial versus ventricular CMs, where the extensive and highly organized T-tubule network shortens the diffusion distances so that fast and uniform CICR is possible. The physiological outcome for the atrial CM is a slower rise phase of the intracellular Ca^{2+} transient (CaT) and contractile force (Frisk et al., 2014), and a delayed CaT at the center of the CM comparatively to the periphery, resulting from spatial (particularly centripetal) propagation of intracellular Ca^{2+} during atrial systole.

This unique membrane ultrastructure of atrial CMs is now also thought to contribute to AF pathogenesis. Recently, it has been shown that T-tubule density in atrial cells is reduced in animal models of AF (Frisk et al., 2014; Lenaerts et al., 2009; Wakili et al., 2010) ; however, supporting human atrial data is lacking. The putative loss of T-tubules may lead to contractile dysfunction, but is also strongly implicated in arrhythmogenesis. In particular, the increased spatial heterogeneity in subcellular Ca^{2+} signaling has been shown to promote CaT and APD alternans (Gaeta et al., 2009; Li et al., 2012), and incomplete excitation-contraction (E-C) coupling (Greiser et al., 2014).

I. Computational modeling in pharmacotherapy of atrial fibrillation: recent advances and future challenges

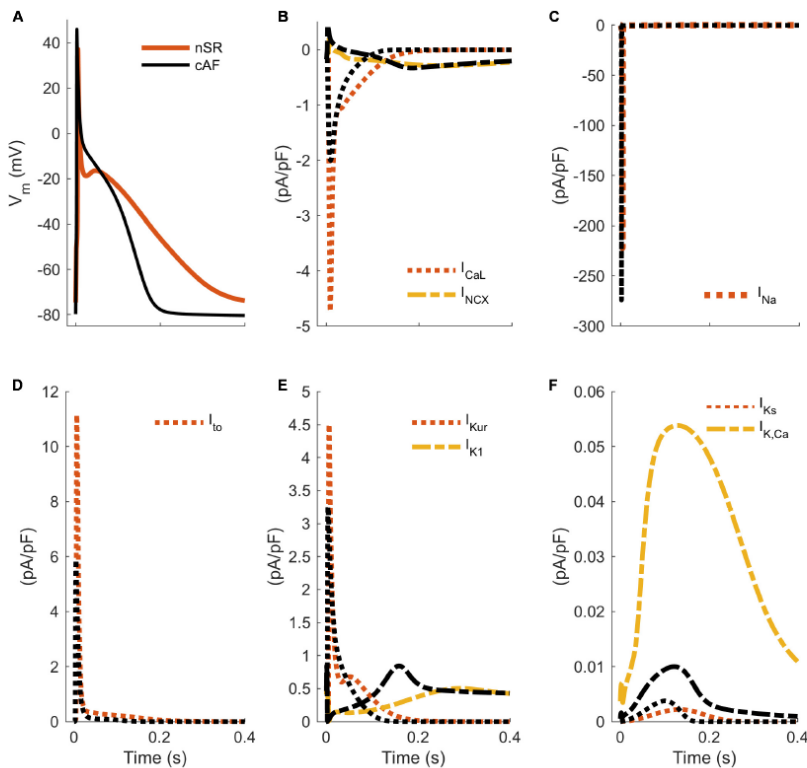


Figure 3: Hallmarks of altered electrophysiology of human atrial myocytes in AF. APs (A) and underlying ion currents (B-F) in normal sinus rhythm (solid lines) and chronic AF (dashed lines) variants of a hA-CM model (Skibsbye et al., 2016).

Reorganization of RyR clusters adds a further dimension to AF-related ultrastructural remodeling. It has been shown to be associated with more frequent Ca^{2+} sparks in a sheep model of cAF, and is thought to increase the probability of the propagating Ca^{2+} release underlying arrhythmogenic calcium waves (Macquaide et al., 2015). However, there are no human data available to corroborate the possible change in organization of RyRs in AF patients. Thus, additional structural and functional data from patients would be valuable for understanding the functional role of structural degradation in this disease.

Cell dilation/hypertrophy is also a common finding in cAF patient samples, where increases of 12% (Neef et al., 2010) and 16% to 54% (Corradi et al., 2012; Neef et al., 2010; Schotten et al., 2001) have been reported for length and diameter, respectively. In line with these findings, cell surface area in

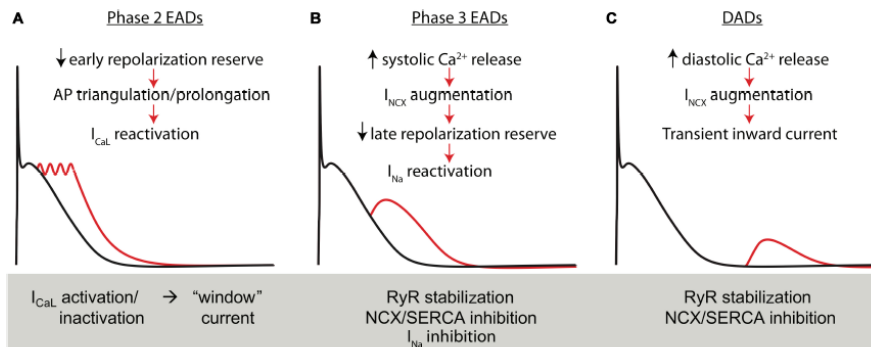


Figure 4: Electrophysiologic instabilities in atrial myocytes. Early afterdepolarizations in hA-CMs exhibit the same essential mechanisms as occur in ventricular cells. (A) Phase-2 EADs result from the kinetic interaction of I_{CaL} and the compound outward potassium current involving multiple K^+ channel species. In general, these events are uncovered during reduced repolarization reserve through I_{CaL} potentiation or K^+ channel antagonists, particularly I_{Kr} inhibitors. (B) A second class of EADs occurs when repolarization is disrupted during phase 3 by forward mode Na^+-Ca^{2+} exchange. This additional I_{NCX} is a secondary effect of dis-coordinated or simply exaggerated I_{CaL} -triggered SR Ca^{2+} release. Importantly these EADs

patients with cAF was reported be ~40% larger (Wouters et al., 2000). The increased cell volume and diameter reduce CaT amplitude and slow centripetal Ca^{2+} diffusion, respectively (Koivumäki et al., 2014). As hA-CMs are likely to have very few (if any) T-tubules in cAF, slower Ca^{2+} diffusion is thought to exacerbate dyssynchrony of the AP and CaT, thus potentially contributing to alternans.

As mentioned above, tissue-level remodeling also makes a major contribution to AF pathology, particularly in the advanced stages of disease. Reduced I_{CaL} in cAF promotes contractile dysfunction and atrial dilatation (atrial stretch). These mechanical perturbations are thought to be a major contributor to the widespread deposition of interstitial collagen, lateralization of gap junctions (connexin remodeling), and proliferation of myofibroblasts and potentially adipocyte infiltration observed in many animal models of chronic disease (Lau et al., 2017; Ravelli and Allessie, 1997; Schotten et al., 2003). While these characteristics are widely thought to be similarly prominent in humans, corroborating data remain relatively sparse because in vivo measures are technically challenging. Functional indicators (e.g. complex fractionated atrial electrograms) have often been used as primary measures of fibrosis, although gadolinium-enhanced MRI protocols have also been shown capable of quantifying in vivo differences between paroxysmal and more advanced disease (Daccarett et al., 2011). These changes in atrial tissue structure have profound consequences for tissue conductivity, wave propagation, and potential for reentry, and are thus likely to pose an insurmountable challenge to pharmacotherapy in later disease

I. Computational modeling in pharmacotherapy of atrial fibrillation: recent advances and future challenges

stages. For this reason, interventions targeting the suppression of the signaling pathways that results in these gross changes to atrial structure, have recently become an area of substantial interest (Nattel and Harada, 2014).

I.2.1.3 Role of remodeled calcium homeostasis in AF

Alterations to calcium handling are intrinsically linked to the ultrastructural changes described above, but further remodeling of expression or regulation of the major intracellular transporters is also likely to contribute. In general, the role for these mechanisms in AF, particularly pAF, has become well supported

in recent years, and ion transporters involved in calcium handling and their regulatory proteins seem to be promising targets for drug therapy of AF. As mentioned above, cAF is associated with increased NCX expression in patients (El-Armouche et al., 2006; Gaborit et al., 2005; Neef et al., 2010). There is also strong evidence of an increased coupling gain between intracellular Ca^{2+} load and INCX in cAF (Grandi et al., 2011; Voigt et al., 2012) and larger INCX amplitudes have also been reported in cAF patient samples (Christ et al., 2016). The data on altered RyR function in AF is less conclusive. Increased RyR activity has been reported in cAF patients (Neef et al., 2010; Voigt et al., 2012), whereas, RyR expression has been reported to be both reduced (Oh et al., 2010; Ohkusa et al., 1999) and unchanged (Shanmugam et al., 2011; Voigt et al., 2012) in cAF patients. Hyperphosphorylation of RyRs has been reported to increase their Ca^{2+} sensitivity and open probability, increasing Ca^{2+} leak from the SR into the cytosol (Neef et al., 2010; Vest et al., 2005; Voigt et al., 2012). One further player in the game of calcium remodeling is the SR Ca^{2+} -ATPase (SERCA), which pumps Ca^{2+} back into the SR from the cytosol. SERCA function is regulated by two inhibitory proteins: phospholamban and sarcolipin, and the phosphorylation levels of these regulatory proteins has an impact on the amplitude of the CaT and SR Ca^{2+} load. Reduced SERCA protein expression accompanied by increased activity was found in both pAF patients (Voigt et al., 2013b), while a rabbit model of rapid atrial pacing has shown remodeling-induced reduction in expression levels of SERCA with unchanged activity (Greiser et al., 2014). Although SERCA plays an important role in the modulation of SR Ca^{2+} load and, indirectly, in the extent of arrhythmogenic Ca^{2+} leak, there is currently no published in vitro human data on the AF-related change in function of SERCA, and the protein expression data is not conclusive.

I.2.2 Cellular electrophysiology instability in AF

As described above, one of the proposed mechanisms of AF initiation is the generation of triggered activity in the atria in early stages of AF. These triggering events are classified as they are in the ventricle. That is, instabilities in AP repolarization are named early afterdepolarizations (EADs), and diastolic

instabilities initiating from resting potential are delayed afterdepolarizations (DADs). Several of the established mechanisms of EADs and DADs are described in Figure 4. Because repolarization is hastened and I_{CaL} is reduced in cAF, AP triangulation is also reduced and the conditions for EAD generation via conventional I_{CaL} reactivation are generally impaired (Burashnikov and Antzelevitch, 2006; Ming et al., 1994). However, a body of literature supports that EADs initiating late in phase 3 of the AP may be important in some atrial regions and contexts, particularly focal arrhythmia initiating in the pulmonary vein sleeves (Burashnikov and Antzelevitch, 2003; Morotti et al., 2014, 2016; Patterson et al., 2006). These EADs are driven by enhanced Ca^{2+} signaling, which in turn exaggerates I_{NCX} , slows late repolarization, and thereby promotes I_{Na} reactivation (Morotti et al., 2014, 2016).

The decreased Ca^{2+} influx via I_{CaL} , enhanced calcium extrusion due to increased NCX expression, and a leaky population of RyR, has generally been observed to result in marked depletion of the intracellular Ca^{2+} in cAF. In and of itself, this would be expected to reduce the incidence of spontaneous Ca^{2+} waves and DADs, and the ability of these diastolic events to drive focal arrhythmia. Indeed, the majority of studies support silencing of Ca^{2+} signaling as a cardioprotective mechanism and a reduced role for spontaneous Ca^{2+} release in cAF (Christ et al., 2014; Greiser et al., 2014; Koivumäki et al., 2014; Schotten et al., 2007). However, opposite findings have also been reported in hA-CMs from cAF patients (Voigt et al., 2012). Importantly, rather than being reduced, SR Ca^{2+} load was maintained in that study, and thus the elevated RyR activity and NCX expression readily translated to increased Ca^{2+} waves and DADs. Data from patients in pAF suggest that SR Ca^{2+} load is either not depleted (Hove-Madsen et al., 2004), or may in fact be exacerbated at these early stages of disease (Voigt et al., 2013b). Thus, the conditions explaining the observed increases in magnitude and frequency of spontaneous Ca^{2+} waves are more obvious and consistent. Viewing this collection of studies together, the most parsimonious interpretation is that the molecular drivers of increased Ca^{2+} wave frequency (RyR hyperphosphorylation, possibly increased SERCA activity) may precede those that strongly deplete intracellular Ca^{2+} (NCX expression). Thus, the increase in spontaneous Ca^{2+} release observed early in AF may be lost as the delayed molecular adaptations, particularly increased NCX expression, act to shift Ca^{2+} flux balance towards extrusion, thus depleting the Ca^{2+} store and silencing Ca^{2+} signaling, even during tachycardia (Greiser et al., 2014). This conceptual model of how Ca^{2+} -driven diastolic instability develops during AF is largely hypothetical, and further characterization of the specific temporal development of these molecular and functional maladaptations during disease is highly desirable.

Another proposed mechanism of triggered diastolic activity in the atria has stemmed from the discovery of expression of hyperpolarization-activated cation

I. Computational modeling in pharmacotherapy of atrial fibrillation: recent advances and future challenges

channels (HCN), carriers of the pacemaker current (I_f), in the left atrial appendage (Scheruebel et al., 2014; Zorn-Pauly et al., 2004). Furthermore, If properties are altered in cAF (Stillitano et al., 2013), lending weight to the hypothesis of abnormal cell automaticity as an additional mechanism of diastolic triggered activity in the remodeled myocardium. HCN channels could, therefore, constitute a novel potential target for anti-arrhythmic drug therapy. However, the lack of conclusive experimental human data thus far has rendered this mechanism a less attractive option for pharmacotherapy discovery.

Finally, the role of APD alternans in driving AF initiation is increasingly becoming appreciated after the observation that it immediately precedes AF in patients (Narayan et al., 2011). While the mechanisms capable of driving APD alternans are diverse, dynamic, and interactive, a growing body of evidence suggests that the proximal driver at the cellular level is a period 2 instability in Ca^{2+} cycling (Gaeta et al., 2009). In ventricular CMs this form of instability

was initially thought to be driven by a kinetic mismatch in SR Ca^{2+} reuptake leading to variable refractoriness of Ca^{2+} release at high pacing frequencies (Diaz et al., 2004). However, more recently the role of subcellular heterogeneities in Ca^{2+} dynamics has emerged as a central aspect to the link between APD and Ca^{2+} transient alternans (Gaeta et al., 2009, 2010; Gaeta and Christini, 2012; Shiferaw and Karma, 2006). The intrinsic variability in atrial CM ultrastructure would be expected to promote these behaviors, particularly in AF, and this relationship between structure and dysfunction in AF requires stronger investigation by computational approaches.

I.3 *In silico* atrial modeling

I.3.1 Existing hA-CM models and AF model variants

Models for cardiac cellular electrophysiology and ion dynamics have been developed for more than five decades (Noble, 1962), and the first atria-specific hA-CM models were published by Courtemanche et al. (Courtemanche et al., 1998) and Nygren et al. (Nygren et al., 1998). These model lineages have been retroactively extended with novel features, and new models have also been introduced as shown in Figure 5. The Courtemanche, Nygren-Maleckar-Koivumäki and Grandi model lineages, were benchmarked in detail (Wilhelms et al., 2013), and shown to be based on varying datasets and assumptions. As Wilhelms et al. reported, there are substantial differences in AP and CaT morphology, and rate adaptation properties among these models. For example, the AP repolarization in the Courtemanche model depends more on I_{Kr} and less on I_{Kur} compared to the other models. The Nygren model has a substantially larger contribution of the I_{Ks} current. Furthermore, several models include ion

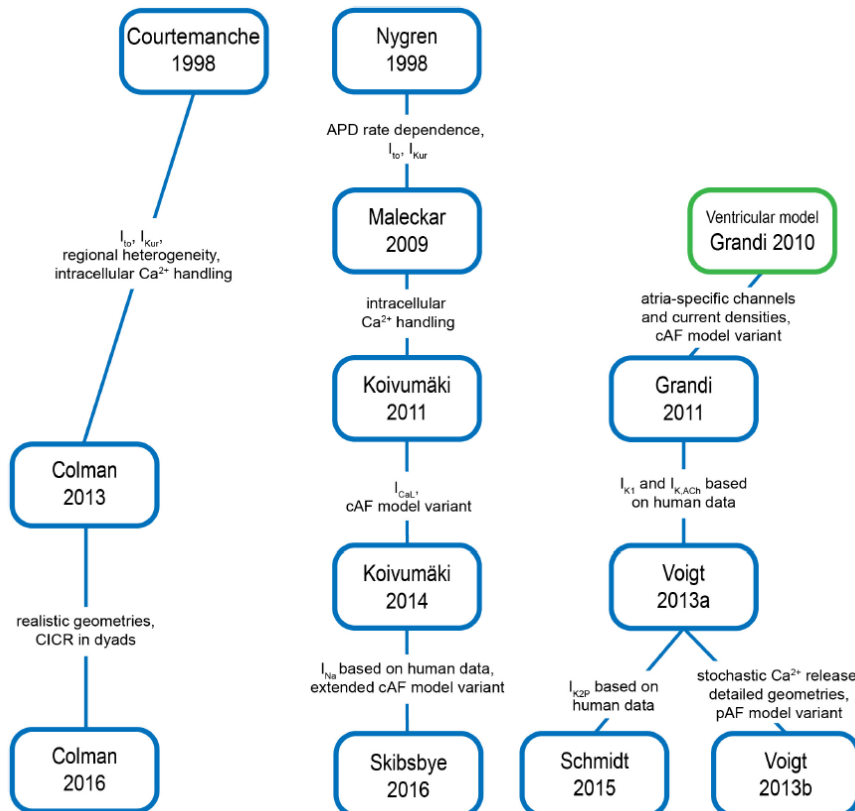


Figure 5: Overview of hA-CM model lineages and most important changes implemented in model iterations. References: (Courtemanche et al., 1998), (Nygren et al., 1998), (Maleckar et al., 2009b), (Grandi et al., 2010, 2011), (Koivumäki et al., 2011, 2014), (Colman et al., 2013, 2016), (Voigt et al., 2013a, 2013b), (Skibsbye et al., 2016).

currents not incorporated in the others. For example, $I_{K,ACh}$ (Maleckar and Grandi models); I_f (Koivumäki model); plateau potassium current, the Ca^{2+} -dependent chloride current and background chloride current (Grandi model).

With accumulating experimental (human) data supporting the unique characteristics of atrial Ca^{2+} handling and its role in AF pathophysiology and arrhythmogenesis, the foundational hA-CM models have been updated to particularly include more complex intracellular Ca^{2+} signaling and ion channel localization. To account for the centripetal diffusion of calcium due to the lack of T-tubules in hA-CMs, Voigt et al. (Voigt et al., 2013b) extended the Grandi model with a spatial representation of Ca^{2+} handling based on longitudinal and transverse division of the intracellular space, and included stochastic RyR gating. Colman et al. (Colman et al., 2016) also presented an atrial model with

I. Computational modeling in pharmacotherapy of atrial fibrillation: recent advances and future challenges

spatial representation of the calcium handling system to assess the role of variable T-tubule density on intracellular calcium waves and alternans. These efforts have generally attempted to approach more realistic Ca^{2+} handling representations by drawing on data describing the T-tubule structure in particular. For instance, it may be possible to replicate the approach now being

taken in ventricular CMs, where realistic SR and T-tubule geometries resolved by serial scanning electron microscopy have made it possible to reconstruct large sections of the cell directly from data (Colman et al., 2017). When applied to atrial CMs, this approach may provide a more realistic basis for simulating the effects of subcellular structure on macroscopic E-C coupling and arrhythmogenesis.

In addition to recapitulating physiology of healthy hA-CMs, all the above-mentioned cell models have variants to mimic cellular remodeling related to AF. The principle of ‘AF begets AF’ (Wijffels et al., 1995) emphasizes the need to represent the pathophysiological changes at different stages of AF progression with dedicated models. So far, the only pAF model variant has been published by Voigt et al. (Voigt et al., 2013b), accounting for early dysregulation of SR

Ca^{2+} release and enhanced uptake, with no significant changes to sarcolemmal current carriers, and AP morphology. Conversely, cAF involves a much more advanced and complex remodeling (Schotten et al., 2011), which has been implemented in the in silico models to varying degrees of detail. The vast majority of cAF model variants have focused on electrical remodeling as distinct from remodeling of subcellular structure and Ca^{2+} handling machinery. These efforts have generally included the decreased I_{to} , I_{CaL} and I_{Kur} , and increased I_{K1} , as described in section 2. More recently, cAF models that also account for the remodeling of intracellular Ca^{2+} handling have been developed (Colman et al., 2013; Grandi et al., 2011; Koivumäki et al., 2014; Voigt et al., 2013a). Furthermore, AF-related structural remodeling, specifically cell dilation, has been represented in one hA-CM model (Koivumäki et al., 2014). First steps in accounting for the role of changes to regulatory signaling have also been taken by Grandi et al. (Grandi et al., 2011), who showed dramatic APD shortening as a result of parasympathetic activation of $I_{\text{K,ACh}}$. However, the overly simplified $I_{\text{to}} - I_{\text{CaL}} - I_{\text{Kur}} - I_{\text{K1}}$ approach of cAF modeling is still commonly used. As the accumulating experimental evidence suggests a central role for altered E-C coupling and intracellular Ca^{2+} handling in AF pathophysiology, a greater emphasis should be put on these components in future modeling studies.

In silico hA-CM models are comprehensive tools, complementing the in vitro experiments, for increasing the understanding of AF mechanisms and discovering potential pharmacological targets. The diversity of hA-CM models

adds a layer of complexity to modeling of pharmacodynamics, as the outcome of pharmacological interventions in silico will vary between different models. This will be discussed in detail in section 4. As the physiological accuracy and robustness of atrial CM models have improved over the years, and continues to progress, so do their utility in higher dimensional and organ scale simulations, as discussed further below.

I.3.2 3D models of the atria

Single cell models of atrial electrophysiology have significantly contributed to increase our understanding of the cellular mechanisms of arrhythmia and underpinning novel pharmacotherapeutic targets (Heijman et al., 2015). However, multiscale models of the atria are necessary to understand the complexity of atrial arrhythmias and capture the essential dynamics of this disease. This need is accentuated by challenges associated with obtaining reliable AF activation maps, especially in patients, which has pressed the need for more elaborate in silico whole atrial models. Three-dimensional (3D) models of atrial electroconduction have been developed to enable simulation of normal atrial function and arrhythmogenesis in the context of full structural complexity of the atrial geometry, and incorporating many of the regional electrical heterogeneities present in the intact organ.

Electrical heterogeneities in the atria are mainly characterized by regional variations of ion current and connexin expression. However, as human data are sparse, these regional differences are generally incorporated from studies conducted in other species, mostly canine. The complex structural heterogeneities in the atria are also challenging to accurately represent in computational models, but are believed to be important for the understanding of AF dynamics. Thus, in recent years a considerable amount of effort has been devoted to the incorporation of detailed anatomic, structural and electrophysiological information in the modeling pipeline.

I.3.2.1 Incorporating heterogeneity into 3D models of the atria

The first attempts to develop 3D models of the atria relied on simplistic geometries with limited anatomical detail, such as spherical surfaces (Blanc et al., 2001), or geometrical surfaces designed to resemble the atria (Harrild and Henriquez, 2000; Ruiz-Villa et al., 2009; Vigmond et al., 2003). Additionally, most of these first models did not consider regional differences in electrophysiology (Blanc et al., 2001; Harrild and Henriquez, 2000; Virag et al., 2002). In their first stage of development, 3D models of the atria were mostly focused on the role of atrial geometry and structural heterogeneity on the development of a proarrhythmic substrate (Blanc et al., 2001; Harrild and Henriquez, 2000; Virag et al., 2002). Although useful in discerning the basic mechanisms underlying atrial arrhythmias, these studies recognized the importa-

I. Computational modeling in pharmacotherapy of atrial fibrillation: recent advances and future challenges

-nse of incorporating electrical and more detailed structural heterogeneity into the models in order to faithfully reproduce complex arrhythmogenic patterns. Vigmond et al. (Vigmond et al., 2003) presented the first atrial model, a canine model, containing all the major structural features of the atria, electrical propagation according to fiber orientation (constructed with a series of interconnected cables), AP heterogeneity, and electrical remodeling. The study provided new insight into the role of structural and electrical heterogeneity of atrial tissue on reentry and fibrillation maintenance, and confirmed the importance of including electrophysiological variations in atrial tissue models.

Since these earlier efforts, regional differences in AP morphology have typically been incorporated by varying ion channel maximum conductances and gating variables of the Courtemanche hA-CM model. Figure 6 shows an example of different AP morphologies in the different regions of the atria modeled in this way (Colman et al., 2013). These are mainly due to differences in expression of I_{Kr} , I_{Ks} , I_{to} , I_{Kur} , I_{K1} , and I_{CaL} . We will not describe these regional characteristics in detail, but a comprehensive overview of current densities and APD in the different atrial regions, and of the original experimental data sources, can be found in (Krueger et al., 2013). With these model variants as a baseline for electrical variation throughout the atria, it has been possible to begin understanding the role of electrophysiological heterogeneity both in normal atrial activation, and in AF arrhythmogenesis. During normal activation, the gradient in APD from the sino-atrial node (SAN) towards the atrio-ventricular node (AVN) and the left atrium (LA) (Ridler et al., 2006), is thought to facilitate conduction from the SAN towards the AVN and impede uni-directional conduction block during normal sinus rhythm. However, the role of these APD gradients in atrial arrhythmias is not fully understood, and the manner in which change associated with AF electrical remodeling contribute to arrhythmia is very complex (Colman et al., 2013). Patchy tissue heterogeneities in left versus right

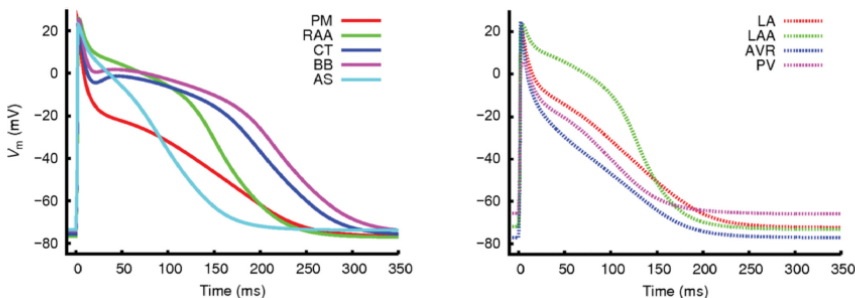


Figure 6: Regional differences in AP morphologies in the different atrial regions obtained with a hA-CM model. From (Colman et al., 2013). Creative Commons Attribution License BY.

atria are known to promote AF initiation (Luca et al., 2015), and it has often been suggested that left-right gradients in ion current expression increase dispersion of refractoriness and thereby promote reentrant substrate (Voigt et al., 2010). However, computational studies of the effect of right-left APD gradients in a canine model has found these gradients to be a protective mechanism against reentry, while increasing the complexity of arrhythmia patterns (Ridler et al., 2006, 2011). These studies highlight the complex effect of atrial heterogeneities and the need for a systematic characterization of the role of spatial variation of cell and tissue properties in AF.

In addition to the varying AP morphology, the atria present significant regional differences in conduction velocity and fiber orientation. These differences can be represented in models by spatially varying tissue conductivities according to tensor vectors obtained from fiber direction information. Fiber direction can be obtained with rule based methods (Aslanidi et al., 2011; Colman et al., 2013; Seemann et al., 2006), based on anatomical data obtained from ex vivo diffusion-tensor imaging (Pashakhanloo et al., 2016), or histological slices (Butters et al., 2013; Tobón et al., 2013).

Seemann et al. (Seemann et al., 2006) published the first model implementing realistic full 3D atrial geometries with regional heterogeneity. This model incorporated heterogeneity based on both human and animal experimental data of several atrial structures: Crista terminalis (CT), pectinate muscles (PM), Bachmann's bundle, atrial working myocardium, atrial appendage, and SAN.

More recently, Krueger et al. (Krueger et al., 2013) developed an extended model with patient-specific anatomical data and additional segmentation of atrial regions: the pulmonary veins (PVs), atrial septum, the tricuspid valve ring, the mitral valve ring, and the fossa ovalis. Colman et al. (Colman et al., 2013) have also published a similarly comprehensive model of the whole human atria incorporating both local heterogeneities and AF remodeling. Figure 7 shows examples of 3D atrial models constructed via regional segmentation and incorporating heterogeneous AP morphologies (Figure 7A). Segmentation into different regions is often carried out manually based on known anatomical features.

Given the relative abundance of animal data sources, computational models of animal atria anatomy and electrophysiology are an important tool for studying arrhythmia mechanisms. Therefore, models of other animal species have also been developed, such as the rabbit atrial model from Aslanidi et al. (Aslanidi et al., 2009), the canine models from Colman et al. (Colman et al., 2014) and Varela et al. (Varela et al., 2016), and the sheep model from Butters et al. (Butters et al., 2013). All these models have contributed to further elucidating of the mechanisms underlying atrial arrhythmogenesis, and exemplify the

I. Computational modeling in pharmacotherapy of atrial fibrillation: recent advances and future challenges

importance of considering models of other animal species, integrating available experimental data, in studies of AF mechanisms and in the discovery of novel therapeutic approaches (Nishida et al., 2010). Other 3D models of human atria developed in recent years have been reviewed in (Dössel et al., 2012).

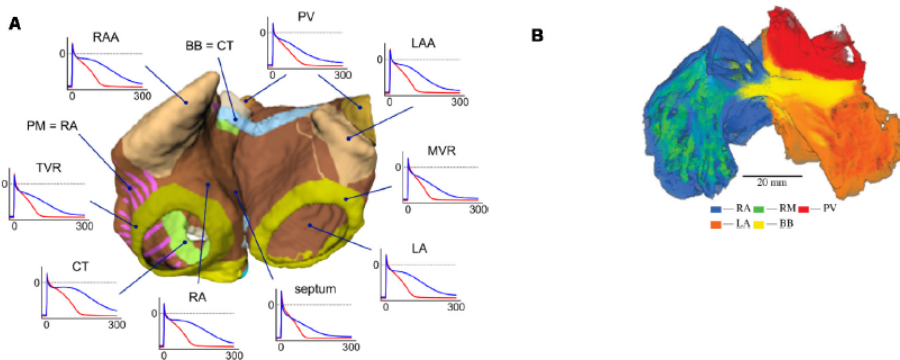


Figure 7: A) Three-dimensional atrial model with segmented regions and corresponding APs in physiological (blue) and AF-remodeled conditions (red), obtained with the Courtemanche model. From (Krueger, 2013). Creative Commons Attribution License BY-NC-ND. B) Regional segmentation of an atrial sheep model into Right Atrium (RA), Left Atrium (LA), Pectinate (PV), and Bachmann's bundle (BB).

I.3.2.2 Importance of modeling heterogeneities in AF studies

Several modeling studies have shown the importance of considering realistic anatomical structures, fiber orientation, and AP heterogeneity in the initiation and maintenance of reentry in both human (Colman et al., 2013; Krueger et al., 2013; Luca et al., 2015; Seemann et al., 2006; Zhao et al., 2017) and animal models (Aslanidi et al., 2009; Butters et al., 2013; Varela et al., 2016). Studies have shown the role of anisotropy, mainly due to fiber orientation, in maintenance of AF, and the role of electrical heterogeneity in the initiation of AF (Butters et al., 2013). In particular, it has been shown that the abrupt anisotropy in fiber orientation between the posterior LA and the PVs is critical for wave break leading to reentry (Klos et al., 2008).

Butters et al. (Butters et al., 2013) were the first to investigate computationally the mechanisms of initiation and maintenance of AF by describing the individual contributions of electrical heterogeneity and anisotropy, employing an anatomically detailed model of the sheep atria with regional AP variation. This study confirmed that the abrupt changes in tissue anisotropy between the LA and PVs provide an important AF substrate. This was primarily due to the complexity of the fiber structure of the PV region and the RA (in particular, the

CT and PMs), as compared to the LA, which is relatively homogeneous. More recently, Zhao et al. (Zhao et al., 2017) extended human 3D models by incorporating transmural fibrosis, atrial wall thickness, and 3D myofiber architecture, based on ex vivo functional and structural imaging of the atria. This study found that the structural characteristics of regions driving AF were characterized by intermediate wall thickness and fibrotic density, as well as twisted myofiber structure.

Although data supports the involvement of atrial fibrosis in the development of AF, whether this is a cause or consequence of AF is still an open question (Schotten et al., 2016). A study on post-mortem human samples from several locations of the atria supported the existence of a correlation between the extent of atrial fibrosis and fatty tissue infiltrations, and the development and severity of AF (Platonov et al., 2011). Simulation studies have contributed with some insight into the role of fibrosis in AF development. For example, Maleckar et al. (Maleckar et al., 2009a), showed that CM excitability, repolarization, and rate-adaptation properties are strongly modulated by CM-myofibroblast electrotonic coupling, in particular the strength of coupling, number of coupled myofibroblasts, and the pacing rate. These findings suggest that myofibroblast proliferation during structural remodeling may exacerbate repolarization heterogeneities and decrease tissue excitability, thus facilitating abnormal conduction patterns (e.g. conduction block) and the development of a reentrant substrate.

McDowell et al. (McDowell et al., 2013) included the effect of fibrotic lesions on the initiation and progression of AF in a whole atrial model, finding that atrial fibrosis contributes to dispersion of APD due to gap-junction remodeling, as well as to the proliferation of myofibroblasts. The study showed that the latter was a sufficient condition for unidirectional conduction block following an ectopic beat from the PV region, while myofibroblast proliferation in the fibrotic region was sufficient to trigger reentry. In agreement with the previous study by Maleckar et al. (Maleckar et al., 2009a) they found that the presence of myofibroblasts in the fibrotic region caused alterations of the transmembrane potential, in particular, shortening of APD and elevation of RMP, and these changes were exacerbated by the presence of collagen deposition. However, their proposed mechanism by which myofibroblasts cause inhomogeneous conduction slowing was through the remodeling of the potassium currents responsible for the repolarization phase of the AP, rather than by electrotonic effects resulting from the formation of direct connections between the myofibroblasts and CMs. Another computational study from the same group including the effects of atrial fibrosis, concluded that initiation of AF is independent of pacing location, and instead depends on the distance between the pacing location and the closest fibrotic region (McDowell et al., 2015).

I. Computational modeling in pharmacotherapy of atrial fibrillation: recent advances and future challenges

Although much is still unknown about the role of structural and electrophysiological heterogeneities in AF, computational studies have contributed to the systematic characterization of the mechanisms of arrhythmogenesis. In some cases, these have highlighted the importance of patient-specific aspects for clinical therapy, as, for instance, the role of patient-specific fibrosis patterns for guiding catheter ablation procedures (McDowell et al., 2015).

I.4 Computational pharmacology in AF

I.4.1 Lessons from existing rhythm control strategies in AF

The available compounds and therapeutic guidelines for AF cardioversion provide important context for AF drug design, and highlight key points of lacking knowledge that may be aided by computational approaches. Effective compounds include class III agents predominantly modulating potassium channels (amiodarone/dronedarone, intravenous ibutilide, vernakalant [in Europe], dofetilide, and sotalol), and class Ic antiarrhythmics primarily targeting sodium channels (flecainide, propafenone). Most often these compounds are administered intravenously in the early stages of AF to achieve cardioversion, but flecainide and propafenone are also used orally as pill-in-the-pocket strategies. A critical consideration for choosing among these options is whether structural disease is present. Flecainide and propafenone are contraindicated for all NYHA heart failure classes, while ibutilide and vernakalant are inappropriate for patients with class III-IV disease. These specific characteristics of therapy

and contraindications provide an important general hierarchy for understanding the links between the mechanisms of drug action and their clinical utility in AF.

First, agents with QT prolonging actions are broadly contraindicated, as even relatively subtle effects on ventricular APD limit their use in AF treatment due to high comorbidity with structural disease. Additionally, Na^+ channel antagonists may be effective if they do not simultaneously reduce the atrial ERP or increase QT (thus eliminating both classes Ia and Ib). It is likely that the efficacy of class Ic agents is largely due to prolonged ERP accompanying their slow dissociation kinetics, which promotes termination of spiral wave reentry (Comtois et al., 2005; Kneller et al., 2005), but they may also limit triggering ectopy particularly early in disease development (Liu et al., 2011; Watanabe et al., 2009). Lastly, non-cardiac contraindications and drug interactions are a significant consideration, particularly for anticoagulant therapy, a core prophylactic for AF-induced thrombosis.

Given these core characteristics of drugs with established efficacy, major current AF strategies can be classified into two broad groups: (1) those that focus on extending the atrial ERP through atria-specific K^+ channel targeting, (2)

Table 1. Summary of AF drugs, ionic targets, and related computational work.

Drug	Class	Target	Computational work
Flecainide	Ic	I_{Na} (Roden and Woosley, 1986) I_{to} , I_{kur} , I_K (Tamargo et al., 2004)	<u>Functional:</u> - Flecainide and lidocaine state specific binding models incorporating detailed voltage- and pH-dependence (Moreno et al., 2011) <u>Structural:</u> Gómez et al. (2014) and Melgari et al. (2015)
Propafenone	Ic	I_{Na} , I_{to} , I_{K1} , I_K (Duan et al., 1993) I_{to} , I_{kur} , I_K , I_{Na} (Tamargo et al., 2004) $I_{K,2P}$ (Schmidt et al., 2013)	<u>Functional:</u> - State-specificity and kinetics of binding via genetic algorithm search (Pásek and Simurda, 2004) <u>Structural:</u> Gómez et al. (2014) and Ngo et al. (2016)
Amiodarone	III	I_K , I_{KS} , I_{to} , I_{kur} (Tamargo et al., 2004) I_{Na} , I_{Ca} (Nattel et al., 1992) $I_{K,2P}$ (Gierten et al., 2010)	<u>Functional:</u> - Multi-target modeling of drug action in AF via Hill-type conductance-only block (Loewe et al., 2014) - Pharmacodynamic modeling of drug-drug interactions (Chen et al., 2015) - Effect of pharmacologically altered I_{Na} kinetics on post-repolarization refractoriness and APD prolongation (Franz et al., 2014) - Mechanistic understanding of amiodarone effects in 1D and 3D, focus on QT prolongation (Wilhelms et al., 2012) - Amiodarone targeting I_{NaL} in failing human myocardium simulations (Maltsev et al., 2001) <u>Structural:</u> Zhang et al. (2016)
Dronedarone	III	I_K , I_{KS} , I_{K1} , I_{Na} , I_{CaL} (Gautier et al., 2003) I_K , I_{KS} (Tamargo et al., 2004)	<u>Functional:</u> - Frequency and concentration dependent effects in cAF remodeled hearts (Loewe et al., 2014) - Drug-drug interaction dronedarone (Denisov et al., 2018)
Ibutilide	III	I_K (Tamargo et al., 2004)	<u>Functional:</u> - Clinical intervention with ibutilide linked with simulated phase synchrony between tissue regions (Vidmar et al., 2015)
Vernakalant	III	I_{to} , I_K , I_{kur} , $I_{K,ACh}$, I_{Na} (Fedida, 2007) $I_{K,2P}$ (Seyler et al., 2014)	<u>Functional:</u> - Multi-target, cellular mode of action (Loewe et al., 2015) - AF termination simulated by I_{Na} block with rapid dissociation through decreased wavebreak and blocked rotor generation (Comtois et al., 2008) <u>Structural:</u> Eldstrom and Fedida (2009)
Dofetilide	III	I_K (Tamargo et al., 2004)	<u>Functional:</u> - Multiscale cardiac toxicity (TdP risk) predictor (Costabal et al., 2018) - Contribution of fibroblasts to cardiac safety pharmacology (Gao et al., 2017) - Interaction of hERG channel kinetics and putative inhibition schemes in long QT syndrome (Romero et al., 2014) - New hERG Markov model including drug-binding dynamics for early drug safety assessment (Di Veroli et al., 2012) - Gender and age on dofetilide induced QT prolongation (Gonzalez et al., 2010) <u>Structural:</u> Dux-Santoy et al. (2011), Saiz et al. (2011) and Varkevisser et al. (2013)
Sotalol	III	I_K (Kpaeyeh and Wharton, 2016) I_K (Carmeliet, 1985)	<u>Functional:</u> - Prediction of drug effects at therapeutic doses in controlled clinical trials and real-life conditions (Chain et al., 2013) - Identifying total area of the ECG T-wave as a biomarker for drug toxicity (Jie et al., 2010) <u>Structural:</u> DeMarco et al. (2018)
Ranolazine	I, anti- anginal drug	I_{NaL} , late I_{Ca} , peak I_{Ca} , I_{NCX} , I_K , I_{KS} (Antzelevitch et al., 2004)	<u>Functional:</u> - Antiarrhythmic drug effect specifically in inherited long-QT syndrome and heart failure-induced remodeling (Moreno et al., 2013) - Prevention of late phase-3 EADs (Morotti et al., 2016) - Combined antiarrhythmic and torsadogenic effect of I_{NaL} and I_K block on hV-CMs (Trenor et al., 2013) <u>Structural:</u> Du et al. (2014)
Cardiac glycosides (digitalis compounds)	V	NKA (Vivo et al., 2008; Schmidt et al., 2018) Vagal stimulation (Falk, 1991)	<u>Functional:</u> - Effect NKA on cell and tissue refractoriness and rotor dynamics (Sánchez et al., 2012) - Physiologically based PK model (Neuhoff et al., 2013) - Two compartment PK-PD model for clinical dosage effect (Jelliffe et al., 2014) <u>Structural:</u> Weiss (2007)

combined therapies that leverage multi-target outcomes and minimize contraindications. In the case of ERP modulators, the key challenge is to improve atrial selectivity and reduce non-cardiac contraindications. For this reason channels that contribute to atrial repolarization but have little role in

I. Computational modeling in pharmacotherapy of atrial fibrillation: recent advances and future challenges

the ventricle (e.g. I_{Kur} , $I_{K,Ca}$, $I_{K,Ach}$) are the most attractive targets. Approaches targeting Ca^{2+} -handling are largely mechanism-driven, and address disturbances to calcium homeostasis, particularly via RyR hyperactivity and calcium overload secondary to dysregulated Na^+ homeostasis and CaMKII signaling (Heijman et al., 2015). Finally, recently developed multi-target therapies particularly seek to combine the efficacy of Na^+ channel blockade with repolarization modulators to generate ideal compound profiles (Ni et al., 2017).

Computational approaches are being applied to all of these avenues. Below we briefly review major computational methods applied to rational drug design, and then highlight approaches where simulations may be crucial in integrating information taken from high-throughput screening, and traditional *in vitro* and *in vivo* electrophysiology.

I.4.2 Pharmacological modeling approaches

Modeling drug interactions can start at the molecular level with molecular docking or dynamic simulations to test small molecule binding sites and structural protein changes. These approaches are attractive because they permit estimation of binding affinities (and kinetics in some cases) based on available 3D-structures. However, the availability of these structures has traditionally been quite limited for ion channel targets, largely due to difficulties in crystallizing transmembrane proteins. With recent advances in cryoelectron microscopy, structure-based drug discovery for integral membrane targets is quickly gaining traction (Lengauer and Rarey, 1996; Meng et al., 2011; Shoichet et al., 2002; Yarov-Yarovoy et al., 2014), and is thought to hold great promise as a support for drug development in the future.

Besides modeling molecular binding sites, one may focus on functionally-driven drug-ion channel interactions, based on the classical Hodgkin and Huxley (HH) formalism or more recent Markov modeling formulations. These approaches are largely independent of protein structure, and instead focus on measurable and assumed functional states of the ion channel or transporter, based on *in vitro* patch clamp data. Functional inhibition or enhancement of the target due to disease-related alterations or drug binding is represented in computational models by changes in ion channel conductance, gating, and state dependent kinetics. Markov models of ion channels have the advantage of being able to more accurately represent inter-dependence of state transitions which can considerably impact the outcome of drug binding simulations. However, Markov models of many ion channels require further development, and are often subject to insufficient data or contradictory parameterization requirements when trying to fit multiple experimental data sets.

I.4.3 Modelling specific ion channels as drug targets

As mentioned above, various potassium channels are remodeled during AF and several of them are almost only expressed in the atria (I_{Kur} , $I_{K,ACh}$ and $I_{K,Ca}$) (Hancox et al., 2016; Ravens and Christ, 2010). Pharmacological inhibition of these channels prolongs the AP and therefore extends the atrial ERP. Below, we focus on computational approaches to understanding the pharmacology of the range of potassium channels that are still considered viable targets for AF rhythm control.

I.4.3.1 I_{Kr}

I_{Kr} is expressed in both human atria and ventricles, and its inhibition prolongs APD in both regions. While I_{Kr} block remains a viable strategy for AF targeting, it presents many challenges of ventricular contra-indication. Dofetilide, is an example of a drug that specifically blocks I_{Kr} , and was approved for AF treatment (Elming et al., 2003), but for which safety remains a significant concern (Abraham et al., 2015; Cho et al., 2017; Mounsey and DiMarco, 2000). For this reason, computational approaches are an attractive means for screening compounds with atrial-selective of targeting of I_{Kr} , but so far this goal has not been addressed convincingly. Below we highlight, several aspects that should be considered when applying computational approaches to address the role of I_{Kr} antagonists in AF.

The manner in which I_{Kr} targeting compounds promote ventricular AP and QT interval prolongation is a topic of major interest in toxicology screening, and we will not cover it comprehensively here. However, it is worthwhile noting that a classical parameter for characterizing the ventricular arrhythmogenicity of I_{Kr} -targeting compounds, reverse-rate-dependence, is also important in atrial drug design. Strong frequency-dependence is highly desirable for AF cardioversion due to very high frequencies of tissue activation during AF. As such, modeling approaches that do not permit accurate assessment of this characteristic are of limited value. To this end, the commonly used Courtemanche model does not reproduce the reverse-frequency-dependency of I_{Kr} block on atrial APD (Tsujimae et al., 2007). By adding a slow activation parameter to the Hodgkin-Huxley model formulation, Tsujimae et al. (Tsujimae et al., 2007) reproduced the inhibition dynamics and the frequency dependence of known I_{Kr} blockers (Quinidine, Vesnarinone and Dofetilide). More recent models have attempted to define I_{Kr} pharmacology in a more detailed manner. For example, Li et al. first developed a detailed Markov model (Li et al., 2016) of I_{Kr} gating, and then embedded it in the O'Hara-Rudy hV-CM model to provide a basis for characterizing compounds with known and varying TdP risk (Li et al., 2017). As a result they found that a mechanism of trapping in the hERG pore (carrier of the I_{Kr} current) created a better predictability of TdP risk by I_{Kr} inhibitors.

I. Computational modeling in pharmacotherapy of atrial fibrillation: recent advances and future challenges

Applying models of this detail in atrial and ventricular CM models may provide a basis for better establishing the potential of I_{Kr} blockade for targeting of AF. We are not aware that such an approach has been pursued to date.

I.4.3.2 I_{Kur}

Due to atria-specific expression, pharmacological inhibition of I_{Kur} allows for atrial selective APD prolongation with minimal adverse effects in the ventricles(Nattel and Carlsson, 2006). Experimental investigation of I_{Kur} and pharmacological properties is complicated by the lack of drug selectivity and overlap of I_{Kur} block with other currents, such as I_{to} (Ravens and Wettwer, 2011). Furthermore, first clinical trials have controversially shown no decrease in AF burden in patients upon treatment with an I_{Kur} blocker (Shunmugam et al., 2018).

Experimental complications can be overcome by using in silico models to assess I_{Kur} involvement in AF and AF treatment. Tsujimae et al. (Tsujimae et al., 2008) computationally investigated the voltage- and time-dependent block of I_{Kur} to mimic experimental drug inhibition and effects on AP characteristics. In simulations incorporating AF remodeling, they showed overall APD prolongation for a blocker with fast association kinetics and frequency-dependent APD prolongation when association kinetics were slow, particularly when dissociation was also slow.

Computational approaches have also been used to define the kinetic properties of the ideal I_{Kur} antagonist: maximum effect in disease, minimum effect in healthy cells and no (non-cardiac) adverse effects. Ellinwood et al. (Ellinwood et al., 2017b) used a 6 state Markov model of I_{Kur} fitted with voltage clamp data from hA-CMs and expanded the model with drug-bound states. Incorporating the detailed channel model and drug interactions in the Grandi hA-CM model enabled in silico assessment of necessary drug characteristics, showing that drug binding to both open and inactive states yields the largest prolongation of APD

and ERP. This inhibition was most efficient at intermediate rates of association, and exhibited similar positive-frequency-dependence independent of binding mode (Ellinwood et al., 2017a, 2017b). These simulations have largely supported the perspective that I_{Kur} is an attractive AF target, and future simulations are likely to be useful for assessing whether the specific binding characteristics and multi-target effects of specific I_{Kur} blockers are capable of realizing this potential.

I.4.3.3 $I_{K,Ach}$

$I_{K,Ach}$ is selectively present in the atria and thus may hold potential as an AF treatment target (Ehrlich et al., 2008). Its response to acetylcholine is decreased in cAF (Dobrev et al., 2001), exhibiting constitutive activity (Dobrev et al., 2005;

Ehrlich et al., 2004). Single channel patch clamp experiments of $I_{K,ACh}$ expressed in canine atrial CMs suggest an increase in opening frequency and open probability after tachycardia-induced remodeling, while open-time, channel conductance, and membrane density were unchanged (Voigt et al., 2007). Bingen et al. (Bingen et al., 2013) showed that $I_{K,ACh}$ blockade decreased restitution-driven alternans, reduced AF inducibility, and promoted AF termination in rat atrial CM cultures and intact atria. These findings agree with tertiapin block of $I_{K,ACh}$ prolonging ERP and terminating AF in a canine model (Hashimoto et al., 2006).

The importance and involvement of $I_{K,ACh}$ in human atrial electro-physiology and fibrillation is well established, but computational models of this channel are still limited. The models of $I_{K,ACh}$ in human atria are based on various data sources, but show a similar and prototypical involvement in the atrial AP: activation of $I_{K,ACh}$ results in hyper-polarization and pronounced AP abbreviation. Maleckar et al. (Maleckar et al., 2009b) implemented the $I_{K,ACh}$ based on patch clamp experiments in canine atria (Kneller et al., 2002) and extended it with dose dependency. The first model of incorporating $I_{K,ACh}$ based on human data was the Grandi model (Grandi et al., 2011), yielding the expected dose-dependent reduction in APD and CaT amplitude with increasing concentration of acetylcholine.

Pharmacological block of $I_{K,ACh}$ in in vitro and ex vivo experiments showed promising anti-arrhythmic effects. However, recent studies have found $I_{K,ACh}$ block to be ineffective both in increasing the left-atrial ERP in vivo (Walfridsson et al., 2015) and reducing AF burden in clinical trials (Podd et al., 2016). Pharmacological effects and pathways activated by acetylcholine that are currently not implemented in the existing computational models (e.g. crosstalk with CaMKII and β -adrenergic stimulation) might explain the disagreement between in vitro, in silico, and clinical studies. In silico investigation may help to resolve these discrepancies, and confirm whether this ion channel holds potential as an AF target. Future computational work should address these possibilities, and better describe the effects of regional heterogeneity in $I_{K,ACh}$ expression and acetylcholine release in the atria, as the role of these ion channels in spatial aspects of parasympathetically driven AF remains poorly understood.

I.4.3.4 $I_{K,Ca}$

All subtypes of SK (SK1-3), carrying $I_{K,Ca}$, have been found in the atria, with SK2 and SK3 exhibiting the most atria-specific expression in human cells (Skibbsye et al., 2014; Tuteja et al., 2005; Xu et al., 2003). SK3 encoded by KCNN3 has also been genetically associated with AF (Ellinor et al., 2010; Olesen et al., 2011). The role of SK channels in AF progression appears especia-

I. Computational modeling in pharmacotherapy of atrial fibrillation: recent advances and future challenges

Table 2. Summary of ion currents included in the hA-CM models.

Model (reference)	$I_{K,Ach}$	I_{bCl}	$I_{Cl,Ca}$	I_f	$I_{K,2P}$	$I_{K,Ca}$	cAF variant
Courtemanche et al., 1998							
Colman et al., 2013							X
Colman et al., 2016							
Nygren et al., 1998							
Maleckar et al., 2009b				X			
Koivumäki et al., 2011						X	
Koivumäki et al., 2014b					X		X
Skibbsbye et al., 2016	X				X	X	
Grandi et al., 2011	X	X	X				X
Voigt et al., 2013a	X	X	X				X
Schmidt et al., 2015	X	X	X		X		X
Voigt et al., 2013b	X	X	X				X

Ion currents that are common to all models include: I_{Na} , I_{CaL} , I_{to} , I_{kur} , I_K , I_S , I_{NaP} , I_{NCX} , I_{PMCA} , I_{NaPi} , and I_{bCl} . Those models that have a comprehensive cAF variant are marked in the right most column.

-lly interesting since recent in vivo animal studies have showed that their inhibition can reduce the duration of, or even protect against, pacing-induced AF (Diness et al., 2010, 2011, 2017; Haugaard et al., 2015; Skibbsbye et al., 2011). However, some studies have also suggested a proarrhythmic effect of SK current inhibition (Hsueh et al., 2013). At the cellular level, SK inhibitors NS8593 and ICAGEN induce APD prolongation in hA-CMs (Skibbsbye et al., 2014), supporting a role for SK channels in atrial repolarization and encouraging the development of SK-antagonists as an anti-arrhythmic strategy. Indeed, the first clinical trial with an SK inhibitor for AF treatment has recently been announced [www.acesionpharma.com/news.php].

Inhibitors NS8593 and ICAGEN induced APD prolongation in hA-CMs, showing the involvement of SK channels in atrial repolarization and encouraging its use as an anti-arrhythmic drug target. Indeed, the first clinical trial with an SK inhibitor for AF treatment has recently been announced [www.acesionpharma.com/news.php].

At the pharmacodynamic level, drug-dependent regulation of SK function has been established for several different drugs, but the mechanisms and binding sites are still being examined (Dilly et al., 2011; Weatherall et al., 2010, 2011). In canine atria, inhibition of the SK channels by UCL1684 or apamin prolonged APD (Rosa et al., 1998). Even though the SK channel is a promising target for AF treatment, most drugs targeting SK channels have been shown to have significant affinity for other ion channels (particularly I_K), and as such have often fallen victim to toxicological exclusion.

The most detailed computational modeling effort of SK channels to date has focused on incorporating dynamics from single channel patch clamp experiments in rat SK2 (Hirschberg et al., 1998). This study established two Markov gating binding schemes, each consisting of four closed and two open states, which differ-

-entiated two modes of channel gating associated with different mean open probabilities. These models recapitulate observed kinetic components of Ca^{2+} -dependent activation and the varied macroscopic open probabilities of single channels, and thus provide a mechanistic basis for interrogating state-dependent drug interaction with SK. However, a comprehensive understanding of SK channel gating is still lacking, particularly

as it relates to heteromeric channels, signaling-dependent effects, and to explain the apparent modal gating observed by Hirschberg et al. Additionally, in the context of the intact atrial CM, subcellular localization and possible colocalization with calcium sources or regulatory proteins remains largely unknown, and is surely important for constructing realistic whole cell models incorporating SK function (Dolga et al., 2013; Ren et al., 2006; Zhang et al., 2018).

There is currently no cardiac-specific computational model that represents both the complex kinetics and pharmacology of SK channels, and their interaction with cardiac Ca^{2+} dynamics. A detailed computational model of the SK channel would enhance our ability to interrogate both the pharmacologic targeting of SK, and the fundamental physiology of SK currents in the atria and in AF. In combination with a hA-CM model with realistic definition of subcellular Ca^{2+} gradients in healthy and AF CMs, the antiarrhythmic effect of SK channels can be probed and drug development optimized.

I.4.4 Multi target drug modeling

The strategies described in the previous section focused on specific potassium channels. While these approaches provide simplicity of interpretation, it is well known that virtually all drugs in clinical use have multiple targets in the therapeutic dose range. In some contexts, these effects are thought to be counterproductive, and in others they appear advantageous. AF is a disease that has been particularly well targeted by the so-called ‘dirty drugs’, namely amiodarone, dronedarone, and most recently in Europe, vernakalant. Various research fields take advantage of multi-target drug design to discover new treatment options or targets (Koutsoukas et al., 2011; Ma et al., 2010). In AF and other cardiac diseases, existing knowledge has been largely incorporated in computational models, and provides a strong basis for guiding these multi-target therapies.

In general, amiodarone, dronedarone and vernakalant are thought to be effective in AF for their ability to prolong the atrial ERP through multiple modes of action (Ni et al., 2017), and also to a lesser extent through inhibiting triggered activity via I_{Na} inhibition. Using these drugs as a base, an effort is

I. Computational modeling in pharmacotherapy of atrial fibrillation: recent advances and future challenges

now being made both computationally and experimentally to define idealized compounds (or personalized multi-therapy approaches), where dual I_{Na} and I_K targeting may yield the best therapies. In the case of vernakalant, the primary potassium current target is I_{Kur} , while for amiodarone/dronedarone it is I_{Kr} (Heijman et al., 2016). To this end, recent efforts have established a useful line of computational work to describe what idealized versions of these multi-target schemes may be. First, a key requirement was to understand how to limit adverse effects of Na^+ channel block by optimizing state-dependent block, as shown by (Aguilar-Shardonofsky et al., 2012). Following this, the same group showed improved theoretical AF selectivity by combining Na^+ current inhibition with I_{Kr} or putative I_{Kur} inhibition (Aguilar et al., 2015)). Combined I_{Na}/I_{Kr} block improved atrial selectivity over I_{Na} alone, but still exhibited ventricular outcomes (Aguilar et al., 2015). Both that study, and a subsequent investigation only concerning combined I_{Na}/I_{Kur} inhibition (Ni et al., 2017), established that selective I_{Kur} blockade could be combined with idealized I_{Na} block to provide more atria-selective antiarrhythmic properties than is achievable via dual I_{Na}/I_{Kr} targeting. Adding some complexity to the clinical interpretation of these approaches, Morotti et al. (Morotti et al., 2016) applied a detailed Markov model to assess the ability of ranolazine to prevent AF re-initiation by blocking I_{Na} reactivation. Like amiodarone, ranolazine is a known antagonist of both I_{Na} and I_{Kr} , and while only the I_{Na} interaction was modelled in that study, their results suggest that multiple types of I_{Na} antagonism should be considered for permitting atrial-selectivity.

Additional novel targets, including those described above, as well as calcium handling targets, such as RyR, are likely to offer additional potential through multi-target approaches, particularly once disease-stage specific aspects of AF pathophysiology are better understood. It is already known that the class 1c compounds flecainide and propafenone have RyR blocking activity, which is thought to contribute to their ventricular efficacy (Galimberti and Knollmann, 2011; Watanabe et al., 2009, 2011). In silico models will surely be necessary for integrating and further characterizing these multi-target outcomes, and thereby find the most suitable treatment option and guide drug development for various stages of AF.

I.5 Modeling variability and uncertainty at the cell level

In silico drug-screening studies have typically been based on a mechanistic approach where the effect of drug binding is simulated by altering the conductance or the gating kinetics of the target ion channel, as detailed in the previous section. More recently, studies of the mechanistic effects of drug binding on CM electrophysiology have been combined with approaches that allow incorporating natural variability into CM models. This methodology is based on the previously proposed so-called ‘Population of Models’ (PoMs)

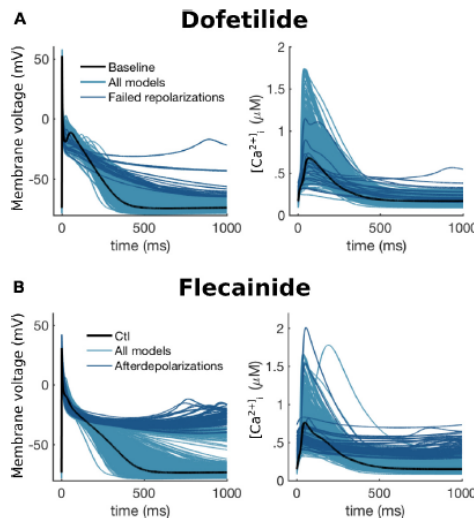


Figure 8: Population of models approach to modelling drug binding effects of Dofetilide and Flecainide on repolarization abnormalities with an atrial myocyte model. APs (left) and calcium transient (right) traces of Dofetilide (A) and Flecainide (B) at 10-fold free plasma concentration are shown. Black lines represent the baseline (control) model, light blue traces represent all models in the populations, and dark blue lines show the models that presented repolarization abnormalities. Simulation results were published in preliminary form in abstract at the Cardiac

approach for the study of arrhythmia mechanisms. Simulation studies incorporating the effect of drugs in populations of ventricle myocyte (Passini et

al., 2017) and induced pluripotent stem cell-derived CM models (Gong and Sobie, 2018) have shown that incorporating variability into the modeling pipeline allows for a more robust analysis of model predictions. For instance, the proarrhythmic effects of disease-related remodeling, and drug binding in cardiotoxicity studies of anti-arrhythmic drugs. Although similar studies with atrial myocyte models are still lacking, *in silico* AF pharmacotherapies can substantially benefit from these approaches.

I.5.1 Sources of variability

As discussed in the section 3.2, atrial tissue has natural regional heterogeneity both at the cell and tissue (structural) levels. Furthermore, experimental findings have revealed a wide variability in measured APs and ionic current densities that cannot be attributed to regional variations. This intrinsic variability has been demonstrated in numerous reports of experimental data on atrial electrophysiology, both in healthy and pathological conditions, and spanning from the single cell to organ levels. Variability in experimental data has been observed in electrophysiological measurements of both different individuals (inter-subject), and CMs of the same individual (intra-subject). This

I. Computational modeling in pharmacotherapy of atrial fibrillation: recent advances and future challenges

arises from several sources, in particular, varying expression levels and post-transcriptional changes of ion channels, leading to variable ionic current densities, and of calcium handling proteins in CMs. Additional variability arises from local differences in cellular morphology and shape, and even from circadian rhythms. For a more detailed overview of sources of variability and uncertainty in experimental measurements and models of cardiac electrophysiology see (Johnstone et al., 2016; Muszkiewicz et al., 2016).

I.5.2 Population of models approach

Single cell models are typically constructed by fitting the model to average values of experimental measurements, with the aim of deriving a single representative model. The available experimental data have permitted the development of increasingly detailed and refined mathematical hA-CM models. However, the fact that these models are matched to specific data sources, obtained under different experimental settings, often results in families of models that are overfitted to a single source of experimental data. As mentioned above, electrophysiological properties, such as APD, RMP, and repolarization reserve, may vary substantially between the different model lineages, which raises questions about their applicability in a general setting. The degree of reported variability differs between different ion channels and cellular components, with values as high as 200% for certain parameters (Johnstone et al., 2016).

In order to capture the variability observed in experimental data, the PoM approach has been proposed for the study of cellular electrophysiological mechanisms. This approach, first introduced by Prinz et al. (Prinz et al., 2003) to model neurons, generally refers to a set of models sharing the same ionic and molecular formulations, but with variable parameters to reflect uncertainty and observed variability in experimental measurements of the biomarkers. Allowing multiple parameters to vary within large ranges can easily lead to unphysiological models, and thus the PoMs typically need to be calibrated. The calibration step can be experimentally-driven, by using experimental data to set the boundaries of maximum and minimum values of APD (or other biomarkers) allowed in the population. An alternative approach, when experimental data is not available, consists of using the distributions of chosen AP characteristics to select models.

The PoM approach may uncover new emergent phenomena that are not observed in the traditionally single “averaged” model (Lee et al., 2013; Sánchez et al., 2014; Sobie, 2009). Another application is to use PoMs in combination with sensitivity analysis to uncover the ‘global’ effect of model parameters on arrhythmogenic behavior, such as ectopic activity, and reentry.

I.5.3 Extending PoM to incorporate drug effects

One major advantage of using PoMs is that it allows to study the effect of drugs on a wide range of cellular phenotypes and thus provides a better prediction tool of the effect of drugs on the ionic currents. This can be done both in control conditions, and incorporating drug binding effects.

The PoM approach has become part of the routine when assessing drug risk with computational models. It has also been adopted by the CiPA initiative as part of the framework for assessing the risk of TdP development in ventricular CMs under antiarrhythmic drug treatment (Colatsky et al., 2016). The combination of PoM approach and drug binding offers a tool for systematically assessing pro-arrhythmic risk of drugs including inter- and intra-subject variability and tissue heterogeneities. Studies have suggested that comprehensive CM models incorporating variability and uncertainty can provide more robust and reliable arrhythmia risk markers and metrics (Johnstone et al., 2016; Passini et al., 2017; Pathmanathan et al., 2015; Vagos et al., 2017). Figure 8 illustrates the use of the PoM approach in the assessment of the effects of two commonly used drugs in AF rhythm control, Dofetilide and Flecainide, on repolarization instabilities (here considered as either failed repolarization or afterdepolarizations). The PoM was constructed by varying the density of the major ionic currents in a hA-CM model (Skibsbye et al., 2016). This study indicated an increased incidence (or probability) of repolarization abnormalities in the populations with both drugs (dark blue to light blue traces ratio), with a 10-fold free plasma concentration, while the baseline (black traces) was mostly unaffected. This example showcases the advantage of using a PoM approach instead of a single averaged model in predicting drug binding outcomes.

Thus, PoMs provide a useful platform for the systematic study of arrhythmia mechanisms at both the single cell and tissue levels, and to obtain a more robust mechanistic insight into, and prediction of drug action on repolarization instabilities, triggered activity, and reentry.

I.6 Concluding remarks and future perspectives

- Computational modeling of AF has progressed rapidly in the past two decades and has yielded a body of knowledge surrounding AF disease complexity that could not have been achieved with experimental approaches alone. Although current models are generally oversimplified and computational approaches are not yet truly multiscale with respect to pharmacology, aspects of current approaches, such as idealized drug modeling, are critically involved in the cycle of hypothesis generation and testing.

I. Computational modeling in pharmacotherapy of atrial fibrillation: recent advances and future challenges

- As described in section 4, much work still needs to be done in order to develop functionally detailed models of the ion channels thought to offer therapeutic potential in AF. These models, and the cell models in which they are tested, will rely upon new experimental data, not just of the drug-channel interaction but also key aspects of AF pathophysiology, particularly the time course of mechanistic changes during disease progression. New experimental data on the metabolic pathways, such as signaling cascades and phosphorylation of regulatory proteins, involved in remodeling processes and calcium homeostasis dysfunction could be a meaningful addition to hA-CM models. This is especially relevant to models of advanced stages of AF, where pathological phenotype is largely an interplay of several concurrent mechanisms.
- Methods that permit a more direct path from experimental characterization to model generation will improve efficiency and constrain uncertainty in the drug-target models. Structure-based approaches may eventually be very useful in this way. Integrated activities of experimentalists and computational scientists will also be essential to determine the most important knowledge for future modeling efforts, particularly as it relates to the stages of AF progression, and personalization. These efforts should be fostered, and cross the boundary between academic and commercial pharmacology.
- Personalized approaches will eventually be the ultimate goal of model-based treatment, although in the short-term, applications outside ablation therapy are still relatively distant. Using models as a foundation for developing general rules about the interaction of pharmacologic targeting with geometric characteristics and disease-stage will provide an important intermediate step to the clinic, and one that can be approached in the short to medium term.

Conflict of interest

The authors declare that the research was conducted in the absence of any commercial or financial relationships that could be construed as a potential conflict of interest.

Author contributions

All authors contributed to drafting the article and reviewing it critically for important intellectual content, as well as, approved the final version of the manuscript.

Funding

M.R.S.S.V and I.v.H were supported by funding from the European Union's Horizon 2020 MSCA ITN AFib-TrainNet, under grant agreement No 675351. J.S. was funded by the SysAFib project (ERACoSysMed program, Call JTC-1,

proposal number 82). H.J.A. was funded by the Novo Nordisk Foundation. A.G.E. was supported through the SUURPh program, an initiative of the Norwegian Department of Research and Education. J.T.K. was supported by the Paavo Nurmi Foundation, the Finnish Foundation for Cardiovascular Research, and the Academy of Finland, Centre of Excellence in Body-on Chip Research (grant No 312412).

Acknowledgements

The authors acknowledge the contribution of Bernardo Lino de Oliveira to the simulation results presented in Figure 8.

References

- Abraham, J. M., Saliba, W. I., Vekstein, C., Lawrence, D., Bhargava, M., Bassiouny, M., et al. (2015). Safety of Oral Dofetilide for Rhythm Control of Atrial Fibrillation and Atrial Flutter. *Circulation: Arrhythmia and Electrophysiology* 8, 772–776. doi:10.1161/CIRCEP.114.002339.
- Aguilar, M., Xiong, F., Qi, X. Y., Comtois, P., and Nattel, S. (2015). Potassium Channel Blockade Enhances Atrial Fibrillation—Selective Antiarrhythmic Effects of Optimized State-Dependent Sodium Channel BlockadeCLINICAL PERSPECTIVE. *Circulation* 132, 2203–2211. doi:10.1161/CIRCULATIONAHA.115.018016.
- Aguilar-Shardonofsky, M., Vigmond, E. J., Nattel, S., and Comtois, P. (2012). In Silico Optimization of Atrial Fibrillation-Selective Sodium Channel Blocker Pharmacodynamics. *Biophysical Journal* 102, 951–960. doi:10.1016/j.bpj.2012.01.032.
- Allessie, M., Ausma, J., and Schotten, U. (2002). Electrical, contractile and structural remodeling during atrial fibrillation. *Cardiovasc Res* 54, 230–246.
- Aslanidi, O. V., Boyett, M. R., Dobrzynski, H., Li, J., and Zhang, H. (2009). Mechanisms of Transition from Normal to Reentrant Electrical Activity in a Model of Rabbit Atrial Tissue: Interaction of Tissue Heterogeneity and Anisotropy. *Biophysical Journal* 96, 798–817. doi:10.1016/j.bpj.2008.09.057.
- Aslanidi, O. V., Colman, M. A., Stott, J., Dobrzynski, H., Boyett, M. R., Holden, A. V., et al. (2011). 3D virtual human atria: A computational platform for studying clinical atrial fibrillation. *Progress in Biophysics and Molecular Biology* 107, 156–168. doi:10.1016/j.pbiomolbio.2011.06.011.
- Bingen, B. O., Neshati, Z., Askar, S. F. A., Kazbanov, I. V., Ypey, D. L., Panfilov, A. V., et al. (2013). Atrium-Specific Kir3.x Determines Inducibility, Dynamics, and Termination of Fibrillation by Regulating Restitution-Driven

I. Computational modeling in pharmacotherapy of atrial fibrillation: recent advances and future challenges

Alternans - Clinical Perspective. *Circulation* 128, 2732–2744. doi:10.1161/CIRCULATIONAHA.113.005019.

Blanc, O., Virag, N., Vesin, J. M., and Kappenberger, L. (2001). A computer model of human atria with reasonable computation load and realistic anatomical properties. *IEEE Transactions on Biomedical Engineering* 48, 1229–1237. doi:10.1109/10.959315.

Burashnikov, A., and Antzelevitch, C. (2003). Reinduction of Atrial Fibrillation Immediately After Termination of the Arrhythmia Is Mediated by Late Phase 3 Early Afterdepolarization-Induced Triggered Activity. *Circulation* 107, 2355–2360.

Burashnikov, A., and Antzelevitch, C. (2006). Late-Phase 3 EAD. A Unique Mechanism Contributing to Initiation of Atrial Fibrillation. *Pacing and Clinical Electrophysiology* 29, 290–295. doi:10.1111/j.1540-8159.2006.00336.x.

Butters, T. D., Aslanidi, O. V., Zhao, J., Smaill, B., and Zhang, H. (2013). A novel computational sheep atria model for the study of atrial fibrillation. *Interface Focus* 3, 20120067. doi:10.1098/rsfs.2012.0067.

Cho, J. H., Youn, S. J., Moore, J. C., Kyriakakis, R., Vekstein, C., Militello, M., et al. (2017). Safety of Oral Dofetilide Reloading for Treatment of Atrial Arrhythmias. *Circulation: Arrhythmia and Electrophysiology* 10, e005333. doi:10.1161/CIRCEP.117.005333.

Christ, T., Kovács, P. P., Acsai, K., Knaut, M., Eschenhagen, T., Jost, N., et al. (2016). Block of Na⁺/Ca²⁺ exchanger by SEA0400 in human right atrial preparations from patients in sinus rhythm and in atrial fibrillation. *Eur J Pharmacol* 788, 286–293. doi:10.1016/j.ejphar.2016.06.050.

Christ, T., Rozmaritsa, N., Engel, A., Berk, E., Knaut, M., Metzner, K., et al. (2014). Arrhythmias, elicited by catecholamines and serotonin, vanish in human chronic atrial fibrillation. *PNAS* 111, 11193–11198. doi:10.1073/pnas.1324132111.

Colatsky, T., Fermini, B., Gintant, G., Pierson, J. B., Sager, P., Sekino, Y., et al. (2016). The Comprehensive in Vitro Proarrhythmia Assay (CiPA) initiative — Update on progress. *Journal of Pharmacological and Toxicological Methods* 81, 15–20. doi:10.1016/j.vascn.2016.06.002.

Colman, M. A., Aslanidi, O. V., Kharche, S., Boyett, M. R., Garratt, C. J., Hancock, J. C., et al. (2013). Pro-arrhythmogenic Effects of Atrial Fibrillation Induced Electrical Remodelling- Insights from 3D Virtual Human Atria. *J Physiol.* doi:10.1113/jphysiol.2013.254987.

- Colman, M. A., Pinali, C., Trafford, A. W., Zhang, H., and Kitmitto, A. (2017). A computational model of spatio-temporal cardiac intracellular calcium handling with realistic structure and spatial flux distribution from sarcoplasmic reticulum and t-tubule reconstructions. *PLOS Computational Biology* 13, e1005714. doi:10.1371/journal.pcbi.1005714.
- Colman, M. A., Sarathy, P. P., MacQuaide, N., and Workman, A. J. (2016). A new model of the human atrial myocyte with variable T-tubule organization for the study of atrial fibrillation. in 2016 Computing in Cardiology Conference (CinC), 221–224. doi:10.23919/CIC.2016.7868719.
- Colman, M. A., Varela, M., Hancox, J. C., Zhang, H., and Aslanidi, O. V. (2014). Evolution and pharmacological modulation of the arrhythmogenic wave dynamics in canine pulmonary vein model. *Europace* 16, 416–423. doi:10.1093/europace/eut349.
- Comtois, P., Kneller, J., and Nattel, S. (2005). Of circles and spirals: Bridging the gap between the leading circle and spiral wave concepts of cardiac reentry. *Europace* 7, S10–S20. doi:10.1016/j.eupc.2005.05.011.
- Corradi, D., Callegari, S., Maestri, R., Ferrara, D., Mangieri, D., Alinovi, R., et al. (2012). Differential Structural Remodeling of the Left-Atrial Posterior Wall in Patients Affected by Mitral Regurgitation with or Without Persistent Atrial Fibrillation: A Morphological and Molecular Study. *Journal of Cardiovascular Electrophysiology* 23, 271–279. doi:10.1111/j.1540-8167.2011.02187.x.
- Courtemanche, M., Ramirez, R. J., and Nattel, S. (1998). Ionic mechanisms underlying human atrial action potential properties: insights from a mathematical model. *Am.J.Physiol.Heart Circ.Physiol.* 275, H301–321.
- Daccarett, M., Badger, T. J., Akoum, N., Burgon, N. S., Mahnkopf, C., Vergara, G., et al. (2011). Association of Left Atrial Fibrosis Detected by Delayed-Enhancement Magnetic Resonance Imaging and the Risk of Stroke in Patients With Atrial Fibrillation. *Journal of the American College of Cardiology* 57, 831–838. doi:10.1016/j.jacc.2010.09.049.
- Diaz, M. E., O'Neill, S. C., and Eisner, D. A. (2004). Sarcoplasmic reticulum calcium content fluctuation is the key to cardiac alternans. *Circ. Res.* 94, 650–656.
- Diker, E., Özdemir, M., Aydoğdu, S., Tezcan, U. K., Korkmaz, Ş., Küük, E., et al. (1998). Dispersion of repolarization in paroxysmal atrial fibrillation. *International Journal of Cardiology* 63, 281–286. doi:10.1016/S0167-5273(97)00327-6.

I. Computational modeling in pharmacotherapy of atrial fibrillation: recent advances and future challenges

Dilly, S., Lamy, C., Marrion, N. V., Liégeois, J.-F., and Seutin, V. (2011). Ion-Channel Modulators: More Diversity Than Previously Thought. *ChemBioChem* 12, 1808–1812. doi:10.1002/cbic.201100236.

Diness, J. G., Skibsbye, L., Jespersen, T., Bartels, E. D., Sørensen, U. S., Hansen, R. S., et al. (2011). Effects on Atrial Fibrillation in Aged Hypertensive Rats by Ca²⁺-Activated K⁺ Channel Inhibition. *Hypertension* 57, 1129–1135. doi:10.1161/HYPERTENSIONAHA.111.170613.

Diness, J. G., Skibsbye, L., Simó-Vicens, R., Santos, J. L., Lundsgaard, P., Citterni, C., et al. (2017). Termination of Vernakalant-Resistant Atrial Fibrillation by Inhibition of Small-Conductance Ca²⁺-Activated K⁺ Channels in Pigs. *Circulation: Arrhythmia and Electrophysiology* 10, e005125. doi:10.1161/CIRCEP.117.005125.

Diness, J. G., Sørensen, U. S., Nissen, J. D., Al-Shahib, B., Jespersen, T., Grunnet, M., et al. (2010). Inhibition of small-conductance Ca²⁺-activated K⁺ channels terminates and protects against atrial fibrillation. *Circ Arrhythm Electrophysiol* 3, 380–390. doi:10.1161/CIRCEP.110.957407.

Dobrev, D., Friedrich, A., Voigt, N., Jost, N., Wettwer, E., Christ, T., et al. (2005). The G Protein-Gated Potassium Current IK,ACh Is Constitutively Active in Patients With Chronic Atrial Fibrillation. *Circulation* 112, 3697–3706.

Dobrev, D., Graf, E., Wettwer, E., Himmel, H. M., Hala, O., Doerfel, C., et al. (2001). Molecular Basis of Downregulation of G-Protein-Coupled Inward Rectifying K⁺ Current (IK,ACh) in Chronic Human Atrial Fibrillation: Decrease in GIRK4 mRNA Correlates With Reduced IK,ACh and Muscarinic Receptor-Mediated Shortening of Action Potentials. *Circulation* 104, 2551–2557.

Dolga, A. M., Netter, M. F., Perocchi, F., Doti, N., Meissner, L., Tobaben, S., et al. (2013). Mitochondrial Small Conductance SK2 Channels Prevent Glutamate-induced Oxytosis and Mitochondrial Dysfunction. *J. Biol. Chem.* 288, 10792–10804. doi:10.1074/jbc.M113.453522.

Dössel, O., Krueger, M., Weber, F., Wilhelms, M., and Seemann, G. (2012). Computational modeling of the human atrial anatomy and electrophysiology. *Medical and Biological Engineering and Computing* 50, 773–799. doi:10.1007/s11517-012-0924-6.

- Ehrlich, J. R., Biliczki, P., Hohnloser, S. H., and Nattel, S. (2008). Atrial-Selective Approaches for the Treatment of Atrial Fibrillation. *Journal of the American College of Cardiology* 51, 787–792. doi:10.1016/j.jacc.2007.08.067.
- Ehrlich, J. R., Cha Tae-Joon, Zhang Liming, Chartier Denis, Villeneuve Louis, Hébert Terence E., et al. (2004). Characterization of a hyperpolarization-activated time-dependent potassium current in canine cardiomyocytes from pulmonary vein myocardial sleeves and left atrium. *The Journal of Physiology* 557, 583–597. doi:10.1113/jphysiol.2004.061119.
- Ehrlich, J. R., and Nattel, S. (2009). Novel approaches for pharmacological management of atrial fibrillation. *Drugs* 69, 757–774.
- El-Armouche, A., Boknik, P., Eschenhagen, T., Carrier, L., Knaut, M., Ravens, U., et al. (2006). Molecular Determinants of Altered Ca²⁺ Handling in Human Chronic Atrial Fibrillation. *Circulation* 114, 670–680.
- Ellinor, P. T., Lunetta, K. L., Glazer, N. L., Pfeufer, A., Alonso, A., Chung, M. K., et al. (2010). Common variants in KCNN3 are associated with lone atrial fibrillation. *Nat Genet* 42, 240–244. doi:10.1038/ng.537.
- Ellinwood, N., Dobrev, D., Morotti, S., and Grandi, E. (2017a). In Silico Assessment of Efficacy and Safety of IKur Inhibitors in Chronic Atrial Fibrillation: Role of Kinetics and State-Dependence of Drug Binding. *Front. Pharmacol.* 8. doi:10.3389/fphar.2017.00799.
- Ellinwood, N., Dobrev, D., Morotti, S., and Grandi, E. (2017b). Revealing kinetics and state-dependent binding properties of IKur-targeting drugs that maximize atrial fibrillation selectivity. *Chaos* 27, 093918. doi:10.1063/1.5000226.
- Elming, H., Brendorp, B., Pedersen, O. D., Køber, L., and Torp-Petersen, C. (2003). Dofetilide: a new drug to control cardiac arrhythmia. *Expert Opinion on Pharmacotherapy* 4, 973–985. doi:10.1517/14656566.4.6.973.
- Frisk, M., Koivumäki, J. T., Norseng, P. A., Maleckar, M. M., Sejersted, O. M., and Louch, W. E. (2014). Variable t-tubule organization and Ca²⁺ homeostasis across the atria. *Am J Physiol Heart Circ Physiol* 307, H609–H620. doi:10.1152/ajpheart.00295.2014.
- Gaborit, N., Steenman, M., Lamirault, G., Le Meur, N., Le Bouter, S., Lande, G., et al. (2005). Human Atrial Ion Channel and Transporter Subunit Gene-Expression Remodeling Associated With Valvular Heart Disease and Atrial Fibrillation. *Circulation* 112, 471–481.

I. Computational modeling in pharmacotherapy of atrial fibrillation: recent advances and future challenges

Gaeta, S. A., Bub, G., Abbott, G. W., and Christini, D. J. (2009). Dynamical Mechanism for Subcellular Alternans in Cardiac Myocytes. *Circulation Research* 105, 335–342. doi:10.1161/CIRCRESAHA.109.197590.

Gaeta, S. A., Krogh-Madsen, T., and Christini, D. J. (2010). Feedback-control induced pattern formation in cardiac myocytes: A mathematical modeling study. *Journal of Theoretical Biology* 266, 408–418. doi:10.1016/j.jtbi.2010.06.041.

Gaeta, S., and Christini, D. J. (2012). Non-Linear Dynamics of Cardiac Alternans: Subcellular to Tissue-Level Mechanisms of Arrhythmia. *Front. Physiol.* 3. doi:10.3389/fphys.2012.00157.

Galimberti, E. S., and Knollmann, B. C. (2011). Efficacy and potency of class I antiarrhythmic drugs for suppression of Ca^{2+} waves in permeabilized myocytes lacking calsequestrin. *J. Mol. Cell. Cardiol.* 51, 760–768. doi:10.1016/j.yjmcc.2011.07.002.

Go, L. O., Moschella, M. C., Watras, J., Handa, K. K., Fyfe, B. S., and Marks, A. R. (1995). Differential regulation of two types of intracellular calcium release channels during end-stage heart failure. *J Clin Invest* 95, 888–894. doi:10.1172/JCI117739.

Gong, J. Q. X., and Sobie, E. A. (2018). Population-based mechanistic modeling allows for quantitative predictions of drug responses across cell types. *npj Systems Biology and Applications* 4, 11. doi:10.1038/s41540-018-0047-2.

Grandi, E., Pandit, S. V., Voigt, N., Workman, A. J., Dobrev, D., Jalife, J., et al. (2011). Human Atrial Action Potential and Ca^{2+} Model: Sinus Rhythm and Chronic Atrial Fibrillation. *Circ Res* 109, 1055–1066. doi:10.1161/CIRCRESAHA.111.253955.

Grandi, E., Pasqualini, F. S., and Bers, D. M. (2010). A novel computational model of the human ventricular action potential and Ca transient. *J Mol Cell Cardiol* 48, 112–121. doi:10.1016/j.yjmcc.2009.09.019.

Greiser, M., Kerfant, B.-G., Williams, G. S. B., Voigt, N., Harks, E., Dibb, K. M., et al. (2014). Tachycardia-induced silencing of subcellular Ca^{2+} signaling in atrial myocytes. *Journal of Clinical Investigation* 124, 4759–4772. doi:10.1172/JCI70102.

Haïssaguerre, M., Jaïs, P., Shah, D. C., Takahashi, A., Hocini, M., Quiniou, G., et al. (1998). Spontaneous Initiation of Atrial Fibrillation by Ectopic Beats Originating in the Pulmonary Veins. *N Engl J Med.* 339, 659–666.

- Hancox, J. C., James, A. F., Marrion, N. V., Zhang, H., and Thomas, D. (2016). Novel ion channel targets in atrial fibrillation. *Expert Opinion on Therapeutic Targets* 20, 947–958. doi:10.1517/14728222.2016.1159300.
- Harrild, D., and Henriquez, C. (2000). A computer model of normal conduction in the human atria. *Circ. Res.* 87, E25-36.
- Hashimoto, N., Yamashita, T., and Tsuruzoe, N. (2006). Tertiapin, a selective IKACh blocker, terminates atrial fibrillation with selective atrial effective refractory period prolongation. *Pharmacological Research* 54, 136–141. doi:10.1016/j.phrs.2006.03.021.
- Haugaard, M. M., Hesselkilde, E. Z., Pehrson, S., Carstensen, H., Flethøj, M., Præstegaard, K. F., et al. (2015). Pharmacologic inhibition of small-conductance calcium-activated potassium (SK) channels by NS8593 reveals atrial antiarrhythmic potential in horses. *Heart Rhythm* 12, 825–835. doi:10.1016/j.hrthm.2014.12.028.
- Heeringa, J., Kuip, D. A. M. van der, Hofman, A., Kors, J. A., Herpen, G. van, Stricker, B. H. C., et al. (2006). Prevalence, incidence and lifetime risk of atrial fibrillation: the Rotterdam study. *Eur Heart J* 27, 949–953. doi:10.1093/eurheartj/ehi825.
- Heijman, J., Algalarrondo, V., Voigt, N., Melka, J., Wehrens, X. H. T., Dobrev, D., et al. (2015). The value of basic research insights into atrial fibrillation mechanisms as a guide to therapeutic innovation: A critical analysis. *Cardiovascular Research*, cvv275. doi:10.1093/cvr/cvv275.
- Heijman, J., Algalarrondo, V., Voigt, N., Melka, J., Wehrens, X. H. T., Dobrev, D., et al. (2016). The value of basic research insights into atrial fibrillation mechanisms as a guide to therapeutic innovation: a critical analysis. *Cardiovasc Res* 109, 467–479. doi:10.1093/cvr/cvv275.
- Hirschberg, B., Maylie, J., Adelman, J. P., and Marrion, N. V. (1998). Gating of Recombinant Small-Conductance Ca-activated K⁺ Channels by Calcium. *J Gen Physiol* 111, 565–581. doi:10.1085/jgp.111.4.565.
- Hove-Madsen, L., Llach, A., Bayes-Genis, A., Roura, S., Font, E. R., Aris, A., et al. (2004). Atrial Fibrillation is Associated with Increased Spontaneous Calcium Release from the Sarcoplasmic Reticulum in Human Atrial Myocytes. *Circulation* 110, 1358–1363.
- Hsueh, C.-H., Chang, P.-C., Hsieh, Y.-C., Reher, T., Chen, P.-S., and Lin, S.-F. (2013). Proarrhythmic effect of blocking the small conductance calcium activated

I. Computational modeling in pharmacotherapy of atrial fibrillation: recent advances and future challenges

potassium channel in isolated canine left atrium. Heart Rhythm 10, 891–898. doi:10.1016/j.hrthm.2013.01.033.

Iwasaki, Y., Nishida, K., Kato, T., and Nattel, S. (2011). Atrial Fibrillation Pathophysiology: Implications for Management. Circulation 124, 2264–2274. doi:10.1161/CIRCULATIONAHA.111.019893.

Johnstone, R. H., Chang, E. T. Y., Bardenet, R., de Boer, T. P., Gavaghan, D. J., Pathmanathan, P., et al. (2016). Uncertainty and variability in models of the cardiac action potential: Can we build trustworthy models? Journal of Molecular and Cellular Cardiology 96, 49–62. doi:10.1016/j.yjmcc.2015.11.018.

Klos, M., Calvo, D., Yamazaki, M., Zlochiver, S., Mironov, S., Cabrera, J.-A., et al. (2008). Atrial Septopulmonary Bundle of the Posterior Left Atrium Provides a Substrate for Atrial Fibrillation Initiation in a Model of Vagally Mediated Pulmonary Vein Tachycardia of the Structurally Normal HeartCLINICAL PERSPECTIVE. Circulation: Arrhythmia and Electrophysiology 1, 175–183. doi:10.1161/CIRCEP.107.760447.

Kneller, J., Kalifa, J., Zou, R., Zaitsev, A. V., Warren, M., Berenfeld, O., et al. (2005). Mechanisms of Atrial Fibrillation Termination by Pure Sodium Channel Blockade in an Ionically-Realistic Mathematical Model. Circulation Research 96, e35–e47. doi:10.1161/01.RES.0000160709.49633.2b.

Kneller, J., Zou, R., Vigmond, E. J., Wang, Z., Leon, L. J., and Nattel, S. (2002). Cholinergic atrial fibrillation in a computer model of a two-dimensional sheet of canine atrial cells with realistic ionic properties. Circ.Res. 90, E73-87.

Koivumäki, J. T., Korhonen, T., and Tavi, P. (2011). Impact of sarcoplasmic reticulum calcium release on calcium dynamics and action potential morphology in human atrial myocytes: a computational study. PLoS Comput Biol 7, e1001067. doi:10.1371/journal.pcbi.1001067.

Koivumäki, J. T., Seemann, G., Maleckar, M. M., and Tavi, P. (2014). In Silico Screening of the Key Cellular Remodeling Targets in Chronic Atrial Fibrillation. PLoS Comput Biol 10, e1003620. doi:10.1371/journal.pcbi.1003620.

Koutsoukas, A., Simms, B., Kirchmair, J., Bond, P. J., Whitmore, A. V., Zimmer, S., et al. (2011). From in silico target prediction to multi-target drug design: Current databases, methods and applications. Journal of Proteomics 74, 2554–2574. doi:10.1016/j.jprot.2011.05.011.

Krueger, M. W. (2013). Personalized Multi-Scale Modeling of the Atria : Heterogeneities, Fiber Architecture, Hemodialysis and Ablation Therapy. doi:10.5445/KSP/1000031226.

- Krueger, M. W., Dorn, A., Keller, D. U. J., Holmqvist, F., Carlson, J., Platonov, P. G., et al. (2013). In-silico modeling of atrial repolarization in normal and atrial fibrillation remodeled state. *Med Biol Eng Comput* 51, 1105–1119. doi:10.1007/s11517-013-1090-1.
- Lalani, G. G., Schricker, A., Gibson, M., Rostamian, A., Krummen, D. E., and Narayan, S. M. (2012). Atrial Conduction Slows Immediately Before the Onset of Human Atrial Fibrillation: A Bi-Atrial Contact Mapping Study of Transitions to Atrial Fibrillation. *Journal of the American College of Cardiology* 59, 595–606. doi:10.1016/j.jacc.2011.10.879.
- Lau, D. H., Linz, D., Schotten, U., Mahajan, R., Sanders, P., and Kalman, J. M. (2017). Pathophysiology of Paroxysmal and Persistent Atrial Fibrillation: Rotors, Foci and Fibrosis. *Heart, Lung and Circulation* 26, 887–893. doi:10.1016/j.hlc.2017.05.119.
- Lee, Y.-S., Liu, O. Z., Hwang, H. S., Knollmann, B. C., and Sobie, E. A. (2013). Parameter Sensitivity Analysis of Stochastic Models Provides Insights into Cardiac Calcium Sparks. *Biophysical Journal* 104, 1142–1150. doi:10.1016/j.bpj.2012.12.055.
- Lenaerts, I., Bito, V., Heinzel, F. R., Driesen, R. B., Holemans, P., D'hooge, J., et al. (2009). Ultrastructural and Functional Remodeling of the Coupling Between Ca²⁺ Influx and Sarcoplasmic Reticulum Ca²⁺ Release in Right Atrial Myocytes From Experimental Persistent Atrial Fibrillation. *Circ.Res.* 105, 876–885.
- Lengauer, T., and Rarey, M. (1996). Computational methods for biomolecular docking. *Current Opinion in Structural Biology* 6, 402–406. doi:10.1016/S0959-440X(96)80061-3.
- Li, Q., O'Neill, S. C., Tao, T., Li, Y., Eisner, D., and Zhang, H. (2012). Mechanisms by which Cytoplasmic Calcium Wave Propagation and Alternans Are Generated in Cardiac Atrial Myocytes Lacking T-Tubules—Insights from a Simulation Study. *Biophys J* 102, 1471–1482. doi:10.1016/j.bpj.2012.03.007.
- Li, X., Zima, A. V., Sheikh, F., Blatter, L. A., and Chen, J. (2005). Endothelin-1-Induced Arrhythmogenic Ca²⁺ Signaling Is Abolished in Atrial Myocytes of Inositol-1,4,5-Trisphosphate(IP3)-Receptor Type 2-Deficient Mice. *Circ Res* 96, 1274–1281.
- Li, Z., Dutta, S., Sheng, J., Tran, P. N., Wu, W., Chang, K., et al. (2017). Improving the In Silico Assessment of Proarrhythmia Risk by Combining hERG (Human Ether-à-go-go-Related Gene) Channel–Drug Binding Kinetics and Multi channel Pharmacology. *Circulation: Arrhythmia and Electrophysiology* 10,

I. Computational modeling in pharmacotherapy of atrial fibrillation: recent advances and future challenges

e004628. doi:10.1161/CIRCEP.116.004628.

Li, Z., Dutta, S., Sheng, J., Tran, P. N., Wu, W., and Colatsky, T. (2016). A temperature-dependent in silico model of the human ether-à-go-go-related (hERG) gene channel. *Journal of Pharmacological and Toxicological Methods* 81, 233–239. doi:10.1016/j.vascn.2016.05.005.

Lipp, P., Laine, M., Tovey, S. C., Burrell, K. M., Berridge, M. J., Li, W., et al. (2000). Functional InsP₃ receptors that may modulate excitation-contraction coupling in the heart. *Current Biology* 10, S1. doi:10.1016/S0960-9822(00)00624-2.

Liu, N., Denegri, M., Ruan, Y., Avelino-Cruz, J. E., Perissi, A., Negri, S., et al. (2011). Short Communication: Flecainide Exerts an Antiarrhythmic Effect in a Mouse Model of Catecholaminergic Polymorphic Ventricular Tachycardia by Increasing the Threshold for Triggered Activity Novelty and Significance. *Circulation Research* 109, 291–295. doi:10.1161/CIRCRESAHA.111.247338.

Luca, A., Jacquemet, V., Virag, N., and Vesin, J. M. (2015). Influence of right and left atrial tissue heterogeneity on atrial fibrillation perpetuation. in 2015 Computing in Cardiology Conference (CinC), 449–452. doi:10.1109/CIC.2015.7408683.

Ma, X. H., Shi, Z., Tan, C., Jiang, Y., Go, M. L., Low, B. C., et al. (2010). In Silico Approaches to Multi-target Drug Discovery. *Pharm Res* 27, 739–749. doi:10.1007/s11095-010-0065-2.

Macquaide, N., Tuan, H.-T. M., Hotta, J., Sempels, W., Lenaerts, I., Holemans, P., et al. (2015). Ryanodine receptor cluster fragmentation and redistribution in persistent atrial fibrillation enhance calcium release. *Cardiovascular Research* 108, 387–398. doi:10.1093/cvr/cvv231.

Maleckar, M. M., Greenstein, J. L., Giles, W. R., and Trayanova, N. A. (2009a). Electrotonic Coupling between Human Atrial Myocytes and Fibroblasts Alters Myocyte Excitability and Repolarization. *Biophysical Journal* 97, 2179–2190. doi:10.1016/j.bpj.2009.07.054.

Maleckar, M. M., Greenstein, J. L., Giles, W. R., and Trayanova, N. A. (2009b). K⁺ current changes account for the rate dependence of the action potential in the human atrial myocyte. *Am.J.Physiol.Heart Circ.Physiol.* 297, H1398–1410.

McDowell, K. S., Vadakkumpadan, F., Blake, R., Blauer, J., Plank, G., MacLeod, R. S., et al. (2013). Mechanistic Inquiry into the Role of Tissue

- Remodeling in Fibrotic Lesions in Human Atrial Fibrillation. *Biophysical Journal* 104, 2764–2773. doi:10.1016/j.bpj.2013.05.025.
- McDowell, K. S., Zahid, S., Vadakkumpadan, F., Blauer, J., MacLeod, R. S., and Trayanova, N. A. (2015). Virtual Electrophysiological Study of Atrial Fibrillation in Fibrotic Remodeling. *PLOS ONE* 10, e0117110. doi:10.1371/journal.pone.0117110.
- Meng, X.-Y., Zhang, H.-X., and Cui, M. M. and M. (2011). Molecular Docking: A Powerful Approach for Structure-Based Drug Discovery. *Current Computer-Aided Drug Design*. Available at: <http://www.eurekaselect.com/74117/article> [Accessed May 7, 2018].
- Ming, Z., Nordin, C., and Aronson, R. S. (1994). Role of L-Type Calcium Channel Window Current in Generating Current-Induced Early Afterdepolarizations. *Journal of Cardiovascular Electrophysiology* 5, 323–334. doi:10.1111/j.1540-8167.1994.tb01169.x.
- Morotti, S., Edwards, A. G., McCulloch, A. D., Bers, D. M., and Grandi, E. (2014). A novel computational model of mouse myocyte electrophysiology to assess the synergy between Na⁺ loading and CaMKII. *J Physiol* 592, 1181–97. doi:10.1113/jphysiol.2013.266676.
- Morotti, S., McCulloch, A. D., Bers, D. M., Edwards, A. G., and Grandi, E. (2016). Atrial-selective targeting of arrhythmogenic phase-3 early afterdepolarizations in human myocytes. *J Mol Cell Cardiol* 96, 63–71. doi:10.1016/j.yjmcc.2015.07.030.
- Mounsey, J. P., and DiMarco, J. P. (2000). Dofetilide. *Circulation* 102, 2665–2670. doi:10.1161/01.CIR.102.21.2665.
- Muszkiewicz, A., Britton, O. J., Gemmell, P., Passini, E., Sánchez, C., Zhou, X., et al. (2016). Variability in cardiac electrophysiology: Using experimentally-calibrated populations of models to move beyond the single virtual physiological human paradigm. *Progress in Biophysics and Molecular Biology* 120, 115–27. doi:10.1016/j.pbiomolbio.2015.12.002.
- Narayan, S. M., Franz, M. R., Clopton, P., Pruvot, E. J., and Krummen, D. E. (2011). Repolarization Alternans Reveals Vulnerability to Human Atrial Fibrillation. *Circulation* 123, 2922–2930. doi:10.1161/CIRCULATIONAHA.110.977827.
- Nattel, S., and Carlsson, L. (2006). Innovative approaches to anti-arrhythmic drug therapy. *Nature Reviews Drug Discovery* 5, 1034–1049. doi:10.1038/nrd2112.

I. Computational modeling in pharmacotherapy of atrial fibrillation: recent advances and future challenges

- Nattel, S., and Harada, M. (2014). Atrial Remodeling and Atrial Fibrillation: Recent Advances and Translational Perspectives. *Journal of the American College of Cardiology* 63, 2335–2345. doi:10.1016/j.jacc.2014.02.555.
- Neef, S., Dybkova, N., Sossalla, S., Ort, K. R., Fluschnik, N., Neumann, K., et al. (2010). CaMKII-Dependent Diastolic SR Ca₂₊ Leak and Elevated Diastolic Ca₂₊ Levels in Right Atrial Myocardium of Patients With Atrial Fibrillation. *Circ. Res.* 106, 1134–1144.
- Ni, H., Whittaker, D. G., Wang, W., Giles, W. R., Narayan, S. M., and Zhang, H. (2017). Synergistic Anti-arrhythmic Effects in Human Atria with Combined Use of Sodium Blockers and Acacetin. *Front. Physiol.* 8. doi:10.3389/fphys.2017.00946.
- Nishida, K., Michael, G., Dobrev, D., and Nattel, S. (2010). Animal models for atrial fibrillation: clinical insights and scientific opportunities. *Europace* 12, 160–172. doi:10.1093/europace/eup328.
- Noble, D. (1962). A modification of the Hodgkin-Huxley equations applicable to Purkinje fibre action and pace-maker potentials. *J.Physiol.* 160, 317–352.
- Nygren, A., Fiset, C., Firek, L., Clark, J. W., Lindblad, D. S., Clark, R. B., et al. (1998). Mathematical model of an adult human atrial cell: the role of K⁺ currents in repolarization. *Circ.Res.* 82, 63–81.
- Oh, S., Kim, K.-B., Ahn, H., Cho, H.-J., and Choi, Y.-S. (2010). Remodeling of Ion Channel Expression in Patients with Chronic Atrial Fibrillation and Mitral Valvular Heart Disease. *Korean J Intern Med* 25, 377. doi:10.3904/kjim.2010.25.4.377.
- Ohkusa, T., Ueyama, T., Yamada, J., Yano, M., Fujumura, Y., Esato, K., et al. (1999). Alterations in cardiac sarcoplasmic reticulum Ca₂₊ regulatory proteins in the atrial tissue of patients with chronic atrial fibrillation. *J.Am.Coll.Cardiol.* 34, 255–263.
- Olesen, M. S., Jabbari, J., Holst, A. G., Nielsen, J. B., Steinbrüchel, D. A., Jespersen, T., et al. (2011). Screening of KCNN3 in patients with early-onset lone atrial fibrillation. *Europace* 13, 963–967. doi:10.1093/europace/eur007.
- Pashakhanloo, F., Herzka, D. A., Ashikaga, H., Mori, S., Gai, N., Bluemke, D. A., et al. (2016). Myofiber Architecture of the Human Atria as Revealed by Submillimeter Diffusion Tensor Imaging. *Circulation: Arrhythmia and Electrophysiology* 9, e004133. doi:10.1161/CIRCEP.116.004133.
- Passini, E., Britton, O. J., Lu, H. R., Rohrbacher, J., Hermans, A. N., Gallacher, D. J., et al. (2017). Human In Silico Drug Trials Demonstrate Higher

- Accuracy than Animal Models in Predicting Clinical Pro-Arrhythmic Cardiotoxicity. *Front. Physiol.* 8. doi:10.3389/fphys.2017.00668.
- Pathmanathan, P., Shotwell, M. S., Gavaghan, D. J., Cordeiro, J. M., and Gray, R. A. (2015). Uncertainty quantification of fast sodium current steady-state inactivation for multi-scale models of cardiac electrophysiology. *Progress in Biophysics and Molecular Biology* 117, 4–18. doi:10.1016/j.pbiomolbio.2015.01.008.
- Patterson, E., Lazzara, R., Szabo, B., Liu, H., Tang, D., Li, Y.-H., et al. (2006). Sodium-Calcium Exchange Initiated by the Ca²⁺Transient: An Arrhythmia Trigger Within Pulmonary Veins. *Journal of the American College of Cardiology* 47, 1196–1206. doi:10.1016/j.jacc.2005.12.023.
- Platonov, P. G., Mitrofanova, L. B., Orshanskaya, V., and Ho, S. Y. (2011). Structural Abnormalities in Atrial Walls Are Associated With Presence and Persistency of Atrial Fibrillation But Not With Age. *Journal of the American College of Cardiology* 58, 2225–2232. doi:10.1016/j.jacc.2011.05.061.
- Podd, S. J., Freemantle, N., Furniss, S. S., and Sulke, N. (2016). First clinical trial of specific IKACh blocker shows no reduction in atrial fibrillation burden in patients with paroxysmal atrial fibrillation: pacemaker assessment of BMS 914392 in patients with paroxysmal atrial fibrillation. *Europace* 18, 340–346. doi:10.1093/europace/euv263.
- Prinz, A. A., Billimoria, C. P., and Marder, E. (2003). Alternative to Hand-Tuning Conductance-Based Models: Construction and Analysis of Databases of Model Neurons. *J.Neurophysiol.* 90, 3998–4015.
- Ravelli, F., and Allessie, M. (1997). Effects of Atrial Dilatation on Refractory Period and Vulnerability to Atrial Fibrillation in the Isolated Langendorff-Perfused Rabbit Heart. *Circulation* 96, 1686–1695. doi:10.1161/01.CIR.96.5.1686.
- Ravens, U., and Christ, T. (2010). Atrial-selective drugs for treatment of atrial fibrillation. *Herzschriftmacherther Elektrophysiolog* 21, 217–221. doi:10.1007/s00399-010-0088-8.
- Ravens, U., Katircioglu-Öztürk, D., Wettwer, E., Christ, T., Dobrev, D., Voigt, N., et al. (2014). Application of the RIMARC algorithm to a large data set of action potentials and clinical parameters for risk prediction of atrial fibrillation. *Med Biol Eng Comput* 53, 263–273. doi:10.1007/s11517-014-1232-0.
- Ravens, U., and Wettwer, E. (2011). Ultra-rapid delayed rectifier channels: molecular basis and therapeutic implications. *Cardiovascular Research* 89, 776–785. doi:10.1093/cvr/cvq398.

I. Computational modeling in pharmacotherapy of atrial fibrillation: recent advances and future challenges

Ren, Y., Barnwell, L. F., Alexander, J. C., Lubin, F. D., Adelman, J. P., Pfaffinger, P. J., et al. (2006). Regulation of Surface Localization of the Small Conductance Ca²⁺-activated Potassium Channel, Sk2, through Direct Phosphorylation by cAMP-dependent Protein Kinase. *J. Biol. Chem.* 281, 11769–11779. doi:10.1074/jbc.M513125200.

Ridler, M., McQueen, D. M., Peskin, C. S., and Vigmond, E. (2006). Action Potential Duration Gradient Protects the Right Atrium from Fibrillating. in 2006 International Conference of the IEEE Engineering in Medicine and Biology Society, 3978–3981. doi:10.1109/IEMBS.2006.260522.

Ridler, M.-E., Lee, M., McQueen, D., Peskin, C., and Vigmond, E. (2011). Arrhythmic consequences of action potential duration gradients in the atria. *Can J Cardiol* 27, 112–119. doi:10.1016/j.cjca.2010.12.002.

Rosa, J. C., Galanakis, D., Ganellin, C. R., Dunn, P. M., and Jenkinson, D. H. (1998). Bis-Quinolinium Cyclophanes: 6,10-Diaza-3(1,3),8(1,4)-dibenzena-1,5(1,4)- diquinolinacyclodecaphane (UCL 1684), the First Nanomolar, Non-Peptidic Blocker of the Apamin-Sensitive Ca²⁺-Activated K⁺ Channel. *J. Med. Chem.* 41, 2–5. doi:10.1021/jm970571a.

Ruiz-Villa, C., Tobón, C., Rodríguez, J., Ferrero, J., Hornero, F., and Saíz, J. (2009). Influence of atrial dilatation in the generation of re-entries caused by ectopic activity in the left atrium. in 2009 36th Annual Computers in Cardiology Conference (CinC), 457–460.

Sánchez, C., Bueno-Orovio, A., Wettwer, E., Loose, S., Simon, J., Ravens, U., et al. (2014). Inter-Subject Variability in Human Atrial Action Potential in Sinus Rhythm versus Chronic Atrial Fibrillation. *PLoS ONE* 9, e105897. doi:10.1371/journal.pone.0105897.

Scheruebel, S., Koyani, C. N., Hallström, S., Lang, P., Platzer, D., Mächler, H., et al. (2014). If blocking potency of ivabradine is preserved under elevated endotoxin levels in human atrial myocytes. *Journal of Molecular and Cellular Cardiology* 72, 64–73. doi:10.1016/j.yjmcc.2014.02.010.

Schotten, U., Ausma, J., Stellbrink, C., Sabatschus, I., Vogel, M., Frechen, D., et al. (2001). Cellular Mechanisms of Depressed Atrial Contractility in Patients With Chronic Atrial Fibrillation. *Circulation* 103, 691–698.

Schotten, U., de Haan, S., Verheule, S., Harks, E. G. A., Frechen, D., Bodewig, E., et al. (2007). Blockade of atrial-specific K⁺-currents increases atrial but not ventricular contractility by enhancing reverse mode Na⁺/Ca²⁺-exchange. *Cardiovasc Res* 73, 37–47.

- Schotten, U., Dobrev, D., Platonov, P. G., Kottkamp, H., and Hindricks, G. (2016). Current controversies in determining the main mechanisms of atrial fibrillation. *J Intern Med* 279, 428–438. doi:10.1111/joim.12492.
- Schotten, U., Neuberger, H.-R., and Allessie, M. A. (2003). The role of atrial dilatation in the domestication of atrial fibrillation. *Progress in Biophysics and Molecular Biology* 82, 151–162. doi:10.1016/S0079-6107(03)00012-9.
- Schotten, U., Verheule, S., Kirchhof, P., and Goette, A. (2011). Pathophysiological mechanisms of atrial fibrillation: a translational appraisal. *Physiol. Rev.* 91, 265–325. doi:10.1152/physrev.00031.2009.
- Seemann, G., Hoper, C., Sachse, F. B., Dossel, O., Holden, A. V., and Zhang, H. (2006). Heterogeneous three-dimensional anatomical and electrophysiological model of human atria. *Phil Trans Roy Soc A* 364, 1465–1481.
- Shanmugam, M., Molina, C. E., Gao, S., Severac-Bastide, R., Fischmeister, R., and Babu, G. J. (2011). Decreased sarcolipin protein expression and enhanced sarco(endo)plasmic reticulum Ca²⁺ uptake in human atrial fibrillation. *Biochem.Biophys.Res.Commun.* 410, 97–101.
- Shiferaw, Y., and Karma, A. (2006). Turing instability mediated by voltage and calcium diffusion in paced cardiac cells. *PNAS* 103, 5670–5675. doi:10.1073/pnas.0511061103.
- Shoichet, B. K., McGovern, S. L., Wei, B., and Irwin, J. J. (2002). Lead discovery using molecular docking. *Current Opinion in Chemical Biology* 6, 439–446. doi:10.1016/S1367-5931(02)00339-3.
- Shummugam, S. R., Sugihara, C., Freemantle, N., Round, P., Furniss, S., and Sulke, N. (2018). A double-blind, randomised, placebo-controlled, cross-over study assessing the use of XEN-D0103 in patients with paroxysmal atrial fibrillation and implanted pacemakers allowing continuous beat-to-beat monitoring of drug efficacy. *J Interv Card Electrophysiol*, 1–7. doi:10.1007/s10840-018-0318-2.
- Skibsbye, L., Diness, J. G., Sørensen, U. S., Hansen, R. S., and Grunnet, M. (2011). The Duration of Pacing-induced Atrial Fibrillation Is Reduced in Vivo by Inhibition of Small Conductance Ca²⁺-activated K⁺ Channels. *Journal of Cardiovascular Pharmacology* 57, 672–681. doi:10.1097/FJC.0b013e318217943d.
- Skibsbye, L., Jespersen, T., Christ, T., Maleckar, M. M., van den Brink, J., Tavi, P., et al. (2016). Refractoriness in human atria: Time and voltage dependence of sodium channel availability. *J Mol Cell Cardiol* 101, 26–34. doi:10.1016/j.yjmcc.2016.10.009.

I. Computational modeling in pharmacotherapy of atrial fibrillation: recent advances and future challenges

- Skibsbye, L., Poulet, C., Diness, J. G., Bentzen, B. H., Yuan, L., Kappert, U., et al. (2014). Small conductance calcium activated potassium (SK) channels contribute to action potential repolarisation in human atria. *Cardiovasc Res* 103, 156–167. doi:10.1093/cvr/cvu121.
- Sobie, E. A. (2009). Parameter Sensitivity Analysis in Electrophysiological Models Using Multivariable Regression. *Biophys.J.* 96, 1264–1274.
- Stillitano, F., Lonardo, G., Giunti, G., Del Lungo, M., Coppini, R., Spinelli, V., et al. (2013). Chronic Atrial Fibrillation Alters the Functional Properties of If in the Human Atrium. *J Cardiovasc Electrophysiol* 24, 1391–1400. doi:10.1111/jce.12212.
- Tobón, C., Ruiz-Villa, C. A., Heidenreich, E., Romero, L., Hornero, F., and Saiz, J. (2013). A Three-Dimensional Human Atrial Model with Fiber Orientation. Electrograms and Arrhythmic Activation Patterns Relationship. *PLoS ONE* 8, e50883. doi:10.1371/journal.pone.0050883.
- Tsujimae, K., Murakami, S., and Kurachi, Y. (2008). In silico study on the effects of IKur block kinetics on prolongation of human action potential after atrial fibrillation-induced electrical remodeling. *Am.J.Physiol.Heart Circ.Physiol.* 294, H793-800.
- Tsujimae, K., Suzuki, S., Murakami, S., and Kurachi, Y. (2007). Frequency-dependent effects of various IKr blockers on cardiac action potential duration in a human atrial model. *Am.J.Physiol.Heart Circ.Physiol.* 293, H660-669.
- Tuteja, D., Xu, D., Timofeyev, V., Lu, L., Sharma, D., Zhang, Z., et al. (2005). Differential expression of small-conductance Ca^{2+} -activated K^+ channels SK1, SK2, and SK3 in mouse atrial and ventricular myocytes. *American Journal of Physiology-Heart and Circulatory Physiology* 289, H2714–H2723. doi:10.1152/ajpheart.00534.2005.
- Vagos, M. R., Arevalo, H., de Oliveira, B. L., Sundnes, J., and Maleckar, M. M. (2017). A computational framework for testing arrhythmia marker sensitivities to model parameters in functionally calibrated populations of atrial cells. *Chaos* 27, 093941. doi:10.1063/1.4999476.
- Varela, M., Colman, M. A., Hancox, J. C., and Aslanidi, O. V. (2016). Atrial Heterogeneity Generates Re-entrant Substrate during Atrial Fibrillation and Anti-arrhythmic Drug Action: Mechanistic Insights from Canine Atrial Models. *PLOS Computational Biology* 12, e1005245. doi:10.1371/journal.pcbi.1005245.

- Vest, J. A., Wehrens, X. H. T., Reiken, S. R., Lehnart, S. E., Dobrev, D., Chandra, P., et al. (2005). Defective Cardiac Ryanodine Receptor Regulation During Atrial Fibrillation. *Circulation* 111, 2025–2032.
- Vigmond, E. J., Ruckdeschel, R., and Trayanova, N. (2003). Reentry in a Morphologically Realistic Atrial Model. *Journal of Cardiovascular Electrophysiology* 12, 1046–1054. doi:10.1046/j.1540-8167.2001.01046.x.
- Virag, N., Jacquemet, V., Henriquez, C. S., Zozor, S., Blanc, O., Vesin, J.-M., et al. (2002). Study of atrial arrhythmias in a computer model based on magnetic resonance images of human atria. *Chaos* 12, 754–763. doi:10.1063/1.1483935.
- Voigt, N., Friedrich, A., Bock, M., Wettwer, E., Christ, T., Knaut, M., et al. (2007). Differential phosphorylation-dependent regulation of constitutively active and muscarinic receptor-activated IK,ACh channels in patients with chronic atrial fibrillation. *Cardiovasc Res* 74, 426–437.
- Voigt, N., Heijman, J., Trausch, A., Mintert-Jancke, E., Pott, L., Ravens, U., et al. (2013a). Impaired Na⁺-dependent regulation of acetylcholine-activated inward-rectifier K⁺ current modulates action potential rate dependence in patients with chronic atrial fibrillation. *Journal of Molecular and Cellular Cardiology* 61, 142–152. doi:10.1016/j.yjmcc.2013.03.011.
- Voigt, N., Heijman, J., Wang, Q., Chiang, D. Y., Li, N., Karck, M., et al. (2013b). Cellular and Molecular Mechanisms of Atrial Arrhythmogenesis in Patients With Paroxysmal Atrial Fibrillation. *Circulation* 129, 145–56. doi:10.1161/CIRCULATIONAHA.113.006641.
- Voigt, N., Li, N., Wang, Q., Wang, W., Trafford, A. W., Abu-Taha, I., et al. (2012). Enhanced Sarcoplasmic Reticulum Ca²⁺ Leak and Increased Na⁺-Ca²⁺ Exchanger Function Underlie Delayed Afterdepolarizations in Patients With Chronic Atrial Fibrillation. *Circulation* 125, 2059–2070. doi:10.1161/CIRCULATIONAHA.111.067306.
- Voigt, N., Trausch, A., Knaut, M., Matschke, K., Varr \tilde{A} ³, A., Van Wagoner, D. R., et al. (2010). Left-to-Right Atrial Inward Rectifier Potassium Current Gradients in Patients With Paroxysmal Versus Chronic Atrial Fibrillation. *Circ Arrhythm Electrophysiol* 3, 472–480.
- Wakili, R., Yeh, Y.-H., Yan Qi, X., Greiser, M., Chartier, D., Nishida, K., et al. (2010). Multiple Potential Molecular Contributors to Atrial Hypocontractility Caused by Atrial Tachycardia Remodeling in Dogs / Clinical Perspective. *Circ Arrhythm Electrophysiol* 3, 530–541.

I. Computational modeling in pharmacotherapy of atrial fibrillation: recent advances and future challenges

- Walfridsson, H., Anfinsen, O.-G., Berggren, A., Frison, L., Jensen, S., Linhardt, G., et al. (2015). Is the acetylcholine-regulated inwardly rectifying potassium current a viable antiarrhythmic target? Translational discrepancies of AZD2927 and A7071 in dogs and humans. *Europace* 17, 473–482. doi:10.1093/europace/euu192.
- Watanabe, H., Chopra, N., Laver, D., Hwang, H. S., Davies, S. S., Roach, D. E., et al. (2009). Flecainide prevents catecholaminergic polymorphic ventricular tachycardia in mice and humans. *Nature Medicine* 15, 380–383. doi:10.1038/nm.1942.
- Watanabe, H., Steele, D. S., and Knollmann, B. C. (2011). Mechanism of Antiarrhythmic Effects of Flecainide in Catecholaminergic Polymorphic Ventricular Tachycardia. *Circulation Research* 109, 712–713. doi:10.1161/CIRCRESAHA.111.251322.
- Weatherall, K. L., Goodchild, S. J., Jane, D. E., and Marrion, N. V. (2010). Small conductance calcium-activated potassium channels: From structure to function. *Progress in Neurobiology* 91, 242–255. doi:10.1016/j.pneurobio.2010.03.002.
- Weatherall, K. L., Seutin, V., Liégeois, J.-F., and Marrion, N. V. (2011). Crucial role of a shared extracellular loop in apamin sensitivity and maintenance of pore shape of small-conductance calcium-activated potassium (SK) channels. *PNAS* 108, 18494–18499. doi:10.1073/pnas.1110724108.
- Wijffels, M. C. E. F., Kirchhof, C. J. H. J., Dorland, R., and Allessie, M. A. (1995). Atrial Fibrillation Begets Atrial Fibrillation : A Study in Awake Chronically Instrumented Goats. *Circulation* 92, 1954–1968.
- Wilhelms, M., Hettman, H., Maleckar, M. M., Koivumäki, J. T., Dössel, O., and Seemann, G. (2013). Benchmarking electrophysiological models of human atrial myocytes. *Front. Physio* 3, 487. doi:10.3389/fphys.2012.00487.
- Wouters, L., Guo-Shu, L., Flameng, W., Thijssen, V. L. J. L., Thone, F., and Borgers, M. (2000). Structural remodelling of atrial myocardium in patients with cardiac valve disease and atrial fibrillation. *Exp Clin Cardiol* 5, 158–163.
- Wullschleger, M., Blanch, J., and Egger, M. (2017). Functional local crosstalk of inositol 1,4,5-trisphosphate receptor- and ryanodine receptor-dependent Ca²⁺ release in atrial cardiomyocytes. *Cardiovasc Res* 113, 542–552. doi:10.1093/cvr/cvx020.
- Xu, Y., Tuteja, D., Zhang, Z., Xu, D., Zhang, Y., Rodriguez, J., et al. (2003). Molecular identification and functional roles of a Ca(2+)-activated K⁺ channel

- in human and mouse hearts. *J. Biol. Chem.* 278, 49085–49094. doi:10.1074/jbc.M307508200.
- Yamada, J., Ohkusa, T., Nao, T., Ueyama, T., Yano, M., Kobayashi, S., et al. (2001). Up-regulation of inositol 1,4,5 trisphosphate receptor expression in atrial tissue in patients with chronic atrial fibrillation. *Journal of the American College of Cardiology* 37, 1111–1119. doi:10.1016/S0735-1097(01)01144-5.
- Yarov-Yarovoy, V., Allen, T. W., and Clancy, C. E. (2014). Computational models for predictive cardiac ion channel pharmacology. *Drug Discovery Today: Disease Models* 14, 3–10. doi:10.1016/j.ddmod.2014.04.001.
- Zhang, X.-D., Coulibaly, Z. A., Chen, W. C., Ledford, H. A., Lee, J. H., Sirish, P., et al. (2018). Coupling of SK channels, L-type Ca²⁺ channels, and ryanodine receptors in cardiomyocytes. *Scientific Reports* 8, 4670. doi:10.1038/s41598-018-22843-3.
- Zhao, J., Hansen, B. J., Wang, Y., Csepe, T. A., Sul, L. V., Tang, A., et al. (2017). Three-dimensional Integrated Functional, Structural, and Computational Mapping to Define the Structural “Fingerprints” of Heart-Specific Atrial Fibrillation Drivers in Human Heart Ex Vivo. *Journal of the American Heart Association* 6, e005922. doi:10.1161/JAHA.117.005922.
- Zheng, Y., Xia, Y., Carlson, J., Kongstad, O., and Yuan, S. (2016). Atrial average conduction velocity in patients with and without paroxysmal atrial fibrillation. *Clinical Physiology and Functional Imaging* 37, 596–601. doi:10.1111/cpf.12342.
- Zima, A. V., and Blatter, L. A. (2004). Inositol-1,4,5-trisphosphate-dependent Ca²⁺ signalling in cat atrial excitation–contraction coupling and arrhythmias. *The Journal of Physiology* 555, 607–615. doi:10.1113/jphysiol.2003.058529.
- Zoni-Berisso, M., Lercari, F., Carazza, T., and Domenicucci, S. (2014). Epidemiology of atrial fibrillation: European perspective. *Clin Epidemiol* 6, 213–220. doi:10.2147/CLEP.S47385.
- Zorn-Pauly, K., Schaffer, P., Pelzmann, B., Lang, P., Machler, H., Rigler, B., et al. (2004). If in left human atrium: a potential contributor to atrial ectopy. *Cardiovasc.Res.* 64, 250–259.

Paper II

A computational framework for testing arrhythmia marker sensitivities to model parameters in functionally calibrated populations of atrial cells

Márcia R. Vagos, Hermenegild Arevalo, Bernardo Lino de Oliveira, Joakim Sundnes, Molly M. Maleckar

II

A computational framework for testing arrhythmia marker sensitivities to model parameters in functionally calibrated populations of atrial cells

Márcia R. Vagos^{1,2}, Hermenegild Arevalo^{1,3}, Bernardo Lino de Oliveira¹, Joakim Sundnes^{1,2,3}, Molly M. Maleckar^{1,4}

¹ Simula Research Laboratory, Computational Physiology Department, Martin Linges vei 25, 1325 Lysaker, Norway

² University of Oslo, Department of Informatics, Gaustadalléen 23B, 0373 Oslo, Norway

² Center for Cardiological Innovation (CCI), Rikshospitalet, 0372 Oslo, Norway

⁴ Modeling Division, Allen Institute for Cell Science, Seattle, WA, USA 98109

Abstract

Models of cardiac cell electrophysiology are complex non-linear systems which can be used to gain insight into mechanisms of cardiac dynamics in both healthy and pathological conditions. However, the complexity of cardiac models can make mechanistic insight difficult. Moreover, these are typically fitted to averaged experimental data which does not incorporate the variability in observations. Recently, building populations of models to incorporate inter- and intra-subject variability in simulations has been combined with sensitivity analysis (SA) to uncover novel ionic mechanisms and potentially clarify arrhythmogenic behaviors. We used the Koivumäki human atrial cell model to create two populations, representing normal Sinus Rhythm (nSR), and chronic Atrial Fibrillation (cAF), by varying 22 key model parameters. In each population, 14 biomarkers related to the action potential and dynamic restitution were extracted. Populations were calibrated based on distributions of biomarkers to obtain reasonable physiological behavior, and subjected to SA to quantify correlations between model parameters and pro-arrhythmia markers. The two populations showed distinct behaviors under steady state and dynamic pacing. The nSR population revealed greater variability, and more unstable dynamic restitution, as compared to the cAF population, suggesting that simulated cAF remodeling rendered cells more stable to parameter variation and rate adaptation. SA revealed that the biomarkers depended mainly on five ionic currents, with noted differences in sensitivities to these between nSR and cAF. Also, parameters could be selected to produce a model variant with no alternans and unaltered action potential morphology, highlighting that unstable dynamical behavior may be driven by specific cell parameters settings. These results ultimately suggest that arrhythmia maintenance in cAF may not be due to instability in cell membrane excitability, but rather due to tissue-level effects which promote initiation and maintenance of reentrant arrhythmia.

II.1 Introduction

Cardiac tissue has long been recognized to behave as a highly complex dynamical non-linear system. The non-linear nature of the interactions between cellular and tissue components give rise to characteristic pathological behaviors observed in the heart, such as cardiac alternans, spiral waves and spatiotemporal chaos, ultimately leading to arrhythmia and fibrillation. Atrial and ventricular arrhythmias, in particular, are linked to multiple mechanisms interacting in a

non-linear manner on a number of temporal and spatial scales, ranging from beat-to-beat to months and years, and from the subcellular to tissue levels[1]–[4]. On a subcellular and cellular scale, alterations of ion channel and pump distribution and function, intracellular ion dynamics, and metabolic pathways are the main causes of abnormal excitability.

One particular emergent behavior of interest for the study of cardiac arrhythmias is the adaptation of action potential (AP) to the pacing rate. This property is manifested at both cell and tissue levels and is often represented as the relationship between AP duration (APD) and the previous diastolic interval or the pacing cycle length (PCL). Due to the so-called cardiac memory of the excitable membrane, rate adaptation and restitution properties are highly dependent on the initial conditions of the system. Depending on the pacing protocol chosen and on the particular electrophysiology (EP) of the cell (i.e., ion channel density and distribution), the APD restitution properties can either be stable, i.e. decreasing monotonically with faster pacing, or multistable[5]. In the latter case, the cell can enter a period-doubling bifurcation, which is seen on the APD restitution curve as alternans, which are periodic alternations of long-short APs. The presence of APD alternans is generally seen as an indicator of cell instability, and has been shown to be often tightly linked to calcium transient alternans, i.e. beat-to-beat fluctuations of the calcium transient (CaT) amplitude from cycle to cycle[4], [6], [7].

Computational models constitute a powerful tool for studying the dynamics and underlying mechanisms of arrhythmia initiation and sustenance, by providing a quantitative framework to study the mechanisms underlying experimentally observed behaviors. Computer models have also been widely used to test new mechanistic hypotheses[8], [9] and to predict putative clinical outcomes of pharmacological treatments, thus paving the way for *in silico* drug screening and therapy planning[10].

Recent decades have shown numerous reports of experimental data on atrial EP, both in healthy and pathological conditions, and spanning from the single cell to organ. In parallel with the increasing amount of experimental data, a number of detailed and increasingly refined mathematical models have been developed for the atrial myocyte EP[11]–[15]. These models are typically constructed by fitting the model to averaged values of experimental measurements, with the aim of arriving at a single representative EP model. However, experimental findings have revealed a huge variability in the measured action potentials and ionic currents. These variations may result from different experimental conditions, i.e. "noise", but may also be representative of inherent intra-subject or inter-subject variability in the atria electrophysiology. The sources of the observed variability may in part be attributed to differences in ion channel expression and dynamics, in particular the ionic currents I_{CaL} , I_{to} , I_{Kur} , I_{K1} and I_{NaK} [16], which are among the most important currents in determining AP morphology.

In order to capture the variability observed in experimental data, an approach based on a so-called "population of models" has recently been proposed for the study of cellular electrophysiological mechanisms[17]. A population of models generally refers to a set of models sharing the same ionic and molecular

II. A computational framework for testing arrhythmia marker sensitivities to model parameters in functionally calibrated populations of atrial cells

formulations, but with variable parameters to reflect observed variability in experimental measurements of the biomarkers. Conducting *in silico* experiments on populations of models allows the inclusion of inter- and intra-subject variability in the model system, and may uncover new emergent phenomena that are not observed in the traditionally single “averaged” model[16], [18], [19].

Sensitivity analysis (SA) is a technique that has been widely used in cardiac cell models to assess which parameters in the model exert the most influence on certain properties, and thus is particularly useful for studying dynamics of populations of models. In cardiac cell models, these properties are usually well-established EP markers, such as APD, AP amplitude, resting membrane potential, upstroke velocity, and afterdepolarizations[16], [20]–[22].

A previous unpublished study using the Koivumäki model of the normal Sinus Rhythm (nSR) atrial cell[23] has shown evidence of unstable alternans behavior under dynamic pacing[24]. Simulations with the latest model version have shown the presence of APD alternans at unrealistic slow pacing rates compared to what has been observed experimentally. This bistable behavior is usually associated with chronic Atrial Fibrillation (cAF), as alternans in cAF-remodeled hearts are typically induced at much slower pacing rates as compared to nSR cells, and show impaired rate adaptation (i.e. flattened restitution)[25]–[27]. This study aims to correct the physiologically unrealistic APD alternans behavior during dynamic pacing in this version of the Koivumäki human atrial cell model by fine-tuning specific model parameters. Additionally, we aim to elucidate the possible cellular mechanisms underlying APD alternans in both nSR and cAF by using a combined populations of models and sensitivity analysis approach.

II.2 Methods

From the observation of the unstable behavior of the nSR model under dynamic pacing, we wanted to fine-tune the baseline model to mimic experimentally and clinically observed alternans behavior, while keeping the AP morphology observed in nSR. After fine-tuning the model to correct for the APD alternans behavior, we constructed and calibrated two populations of models representing both nSR and cAF, and performed sensitivity analyses on the populations to draw mechanistic conclusions regarding the influence of model parameters on pro-arrhythmia biomarkers.

II.2.1 Generation and calibration of populations of models

We constructed a population of 1000 models using the Koivumäki atrial cell model (2016) in nSR[23] by varying 22 parameter values using a Gaussian distribution to randomly sample values around within $\pm 30\%$ of the baseline ($\sigma=0.15$). The parameters that were varied and their baseline values are listed in Table II.1. The population of single cell models was implemented and solved using the single cell simulation environment BENCH (<http://www.cardiosolv.com>).

From the population, 14 single cell biomarkers were extracted, all based on properties of the AP morphology, and the APD alternans behavior. A list of the

Table II.1: List of varied model parameters and their definitions.

Varied parameters	Baseline	Definition
GCaL	0.13 nS/pF	Maximum conductance of L-type calcium current
GNa	11.52 nS/pF	Maximum conductance of sodium current
GK1	0.056 nS/pF	Maximum conductance of inward rectifier potassium current
GCab	0.00156 nS/pF	Maximum conductance of background calcium current
GKr	0.104 nS/pF	Maximum conductance of rapidly Activating delayed rectifier Potassium current
GKs	0.0035 nS/pF	Maximum conductance of slowly Activating delayed rectifier potassium current
GKur	0.045 nS/pF	Maximum conductance of ultra-rapid delayed rectifier current
Gto	0.22 nS/pF	Maximum conductance of transient outward potassium current
GNaL	0.00702 nS/pF	Maximum conductance of late sodium current
GKCa	0.072 nS/pF	Maximum conductances of ionic currents
kSRleak	6e-6 ms ⁻¹	Rate of SR Ca ²⁺ leak
ICaPmax	0.04 pA/pF	Maximum flux of plasmalemmal ATPase Ca ²⁺ pump
INaKmax	1.417 pA/pF	Maximum flux of Na ⁺ -K ⁺ -exchanger
INaCamax	0.02 pA/pF	Maximum flux of Na ⁺ -Ca ²⁺ -exchanger
RyRmax	0.0016 (ms·nL) ⁻¹	Maximum flux of ryanodine receptors (RyR)
RyRmaxss	0.9 (ms·nL) ⁻¹	Maximum flux of RyR in subsarcolemmal space
RyRtauadapt	850 ms	Adaptation variable of RyR
RyRtauact	16 ms	Activation time constant of RyR
RyRtauactss	4.3 ms	Activation time constant of RyR in subsarcolemmal space
RyRtauinact	74 ms	Inactivation time constant of RyR
RyRtauinactss	13 ms	Inactivation time constant of RyR in subsarcolemmal space
kCa	7e-4 mmol/L	Half-maximum binding concentration of I _{CaL}

14 biomarkers, and their definitions, is provided in Table II.2. All the chosen biomarkers are commonly used metrics to characterize single cell EP. The APD90, APD50, APD20, APtri and APA are common metrics of AP morphology, which change characteristically in many pathological conditions, including cAF. The RMP and dVdt_{max} are closely linked to the intracellular ion concentrations, and are important parameters of cell membrane repolarisation. The CaT amplitude, Δ CaT, was calculated as the difference between maximum and minimum (CaT₀) intracellular calcium concentration during one cycle. The time-to-peak of the CaT, CaT-tpeak, was determined from the onset of the CaT to the time of peak, and the time of decay, CaT-tdecay, was calculated as the interval from the peak to the point where CaT reached 10% of the CaT amplitude.

Biomarkers related to APD alternans were calculated from the APD (at 90%) restitution curve using a dynamic pacing protocol as follows: cells were first pre-paced at a PCL of 1000 ms for 30 seconds, and the PCL was decreased to 150 ms in steps of 10 ms. At each step the cell was stimulated for 15 beats, and the last 5 beats recorded for analysis. APD alternans were registered when the maximum and minimum APD values in the last 5 beats differed by more than 2%.

Following the definition of the single cell biomarkers, chosen biomarkers were constrained within an acceptable range. This calibration step prevents model outliers that do not represent physiological behavior from being included in the sensitivity analysis. Choosing this calibration step is non-trivial, since the purpose of the population models is to capture variability, even beyond that

II. A computational framework for testing arrhythmia marker sensitivities to model parameters in functionally calibrated populations of atrial cells

Table II.2: List of cellular biomarkers extracted from the populations of models and their definitions.

Cell biomarkers	Definition
APD90	Action potential duration at 90% of repolarization
APD50	Action potential duration at 50% of repolarization
APD20	Action potential duration at 20% of repolarization
APtri	Action potential triangulation, defined as APD90 - APD50
APA	Action potential amplitude
RMP	Resting membrane potential
dVdt _{max}	Maximum action potential upstroke velocity
ΔCaT	Amplitude of calcium transient (CaT) in subsarcolemmal space
CaT ₀	Diastolic calcium concentration in subsarcolemmal space
CaT-tpeak	Time to peak of the CaT in the subsarcolemmal space
CaT-tdecay	Time of decay of CaT in subsarcolemmal space
Alt-th	Highest PCL at which APD alternans occur in the dynamic restitution curve
Alt-range	Total range of APD alternans observed in the dynamic restitution curve
ΔAPD _{max}	Maximum difference between long and short AP in the alternans region

observed in experimental results, but we wanted to exclude models that are obviously non-physiological. We calibrated the nSR population so that all models would fall within one standard deviation of the median values of APD90, APD50, APD20, APtri, APA, RMP and dVdt_{max}. These biomarkers were chosen since they characterize AP morphology. Therefore, this type of calibration can be seen as 'functional calibration', in contrast to other calibration schemes employed.

In addition, we also excluded models with dynamic restitution curves exhibiting extreme maximum APD values. For the nSR population, the minimum and maximum APD accepted were 190 and 440 ms, respectively. These boundary values were taken from experimental reports of maximum and minimum APD90 values of nSR and cAF cells paced at 1000 ms PCL by Sanchez et al[16].

II.2.2 Modulation of APD alternans behavior in the nSR model

From the nSR population generated in section A, we selected models with alternans threshold no larger than 250 ms (Alt-th≤250). This particular value of alternans threshold was chosen for constraining the subpopulation since it is close to that reported by Narayan et al[26] for patients in nSR. Imposing this constraint on the functionally calibrated nSR population resulted in subpopulation of models with no alternans or with alternans occurring only below 250 ms, whose mean parameter values were used to construct a new fine-tuned nSR baseline variant. This fine-tuned model was then used to represent the baseline nSR model in the rest of the study.

II.2.3 Populations of nSR and cAF models

We constructed two new populations of models, one representing nSR (from the fine-tuned model created in section II.2.1 and another representing cAF remodeling. cAF remodeling was simulated by the making the following changes on ionic components: 65% decrease in I_{CaL}, 18% decrease in I_{Na}, 68% increase in I_{K1}, 145% increase in I_{Ks}, 38% decrease in I_{Kur}, 50% decrease in I_{KCa}, and 62% decrease in I_{to}. The remodeling also accounted for a two-fold upregulation of RyR,

16% decrease in SERCA expression, two-fold increase in SERCA phosphorylation, and 10% cell dilation.

The two populations of models were generated and calibrated following the procedure described in section II.2.1. For the cAF population the maximum and minimum accepted APD were 140 and 330 ms, respectively, as reported by Sánchez et al[16].

II.2.4 Sensitivity Analysis of nSR and cAF populations

Then we performed sensitivity analysis on the functionally calibrated nSR and cAF populations in order to find linear correlations between responses (biomarkers) and multiple model predictors (model parameters). Sensitivity analysis was implemented based on the method proposed by Sobie et al.[28], whereby chosen parameters from the model are simultaneously varied within a specified range to capture the ‘global’ effect of a certain parameter on the model behavior. Sensitivity analyses were performed using the Multivariate Linear Regression (MVR) method[17]. This method approximates non-linear dynamics to a linear model thus allowing to identify key parameters that define the behaviors observed in the non-linear model. For each population, the varied model parameters were compiled into a matrix X of predictors, and the measured markers into a matrix Y of single cell biomarkers. X and Y matrices were centered and normalised prior to regression. The output of the MVR algorithm is a matrix B of regression coefficients calculated by (II.1).

$$Y = X \cdot B + \epsilon \rightarrow \hat{Y} = X \cdot B \quad (\text{II.1})$$

Where \hat{Y} is an approximation of Y and ϵ is the regression error. The values b_{ij} in matrix B can be interpreted as surrogates of the sensitivity of marker y_j towards model parameter x_i . Larger values of b_{ij} indicate greater sensitivity, and positive b_{ij} means that an increase x_i is associated with an increase in y_j , while negative b_{ij} means that an increase in x_i results in a decrease in y_j . All analyses were implemented in Matlab2016a (<https://mathworks.com>).

In order to have a compact overview of the population sensitivities to the various parameters, we grouped the different cell biomarkers in AP- (APD90, APD50, APD20, APtri, APA, RMP and $dVdt_{max}$), CaT- (ΔCaT , CaT_0 , CaT-tpeak and CaT-tdecay) and alternans- (Alt-th, Alt-range, and ΔAPD_{max}) related makers. For each group of biomarkers we determined their overall sensitivity to the parameters by normalising the regression coefficients to the baseline and summing the contributions of the parameters to each marker in the group. We call these relative sensitivity values ‘global sensitivities’.

II.3 Results

II.3.1 Modulation of APD alternans behavior in the nSR model

Fig.II.1A and B show the AP and CaT traces of the original nSR population at 1000 ms PCL. Fig.II.1C shows the dynamic restitution curves of the original

II. A computational framework for testing arrhythmia marker sensitivities to model parameters in functionally calibrated populations of atrial cells

Table II.3: List of the actual fine-tuned values of the varied model parameters used to simulate the populations.

Parameter	New value	Parameter	New value
GCaL	0.13 nS/pF	iCaPmax	0.0374 pA/pF
GNa	11.28 nS/pF	iNaKmax	1.592 pA/pF
GK1	0.0535 nS/pF	iNaCamax	0.0203 pA/pF
GCab	0.00149 nS/pF	RyRmax	$0.00159 \text{ (ms}\cdot\text{nL})^{-1}$
GKr	0.1026 nS/pF	RyRmaxss	$0.85 \text{ (ms}\cdot\text{nL})^{-1}$
GKs	0.0036 nS/pF	RyRtauadapt	885.6 ms
GKur	0.0455 nS/pF	RyRtauact	15.95 ms
Gto	0.212 nS/pF	RyRtauactss	4.52 ms
GNaL	0.00708 nS/pF	RyRtauinact	70.9 ms
GKCa	0.0721 nS/pF	RyRtauinactss	10.83 ms
kSRleak	$5.9\text{e-}6 \text{ ms}^{-1}$	kCa	6.8e-4 mmol/L

nSR population before and after functional calibration, and Fig.II.1D shows a few representative restitution curves for better visualization. The calibration step reduced the total population of 1000 models to 202 models.

As can be seen in Fig.II.1C, the original nSR population displayed a rather dynamic restitution behavior, with APD alternans occurring at all PCLs. The original nSR baseline model presents a single alternans region between 460 and 650 ms, with maximum ΔAPD of 21 ms. Fig.II.2 shows APD and calcium alternans in the nSR baseline model at a PCL 600 ms during dynamic pacing. The AP traces show a slight alternation in APD90 between long and short pulses of 18 ms (11% of APD90 of the long beat), with pronounced alternation of ΔCaT of ca $0.3 \mu\text{M}$ (60% of maximum ΔCaT).

Models from the calibrated population were then selected into a subpopulation of models showing APD alternans at PCLs equal or lower than 250 ms (Fig.II.3). From this subpopulation, the mean parameter values were calculated in order to create a new baseline nSR model ($\text{nSR}_{\text{tuned}}$). This model did not exhibit APD alternans. However, the model did exhibit slight APD prolongation of 35ms. The percent difference in the mean parameters relative to the original nSR baseline are shown in Fig.II.4. The parameters that changed the most were iNaKmax and RyRtauinactss, and to a smaller extent, iCaPmax, RyRmaxss and RyRtauactss. These parameters are related to alternans dynamics through the calcium cycling system. This results shows that a smaller change in these parameters is sufficient to alter the alternans behavior at the single cell level.

II.3.2 Variability of nSR and cAF populations

The simulated nSR and cAF populations are presented in Fig.II.5. After functional calibration, the populations of 1000 models each were reduced to 213 models in the nSR and 357 models in the cAF population. The baseline, median, mean and standard deviation values of the functionally calibrated nSR and cAF populations are shown in Table II.4. The populations reproduced the AP morphologies characteristic of nSR and cAF cells. The nSR models presented a peak-and-dome shape, while the cAF models showed a more triangulated morphology, which is a known result of cAF ionic remodeling. Although the cAF

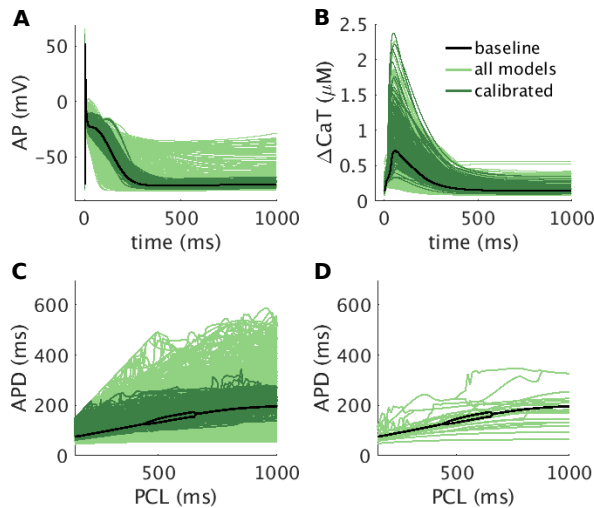


Figure II.1: Simulated nSR population using the original atrial cell model. AP (A) and CaT (B) traces of the original nSR population, before (1000 models) and after (202 models) functional calibration, at 1000 ms PCL. (C) Dynamic restitution curves of the original nSR population before and after calibration. (D) Representative APD restitution curves from the population. Black lines represent the nSR baseline model.

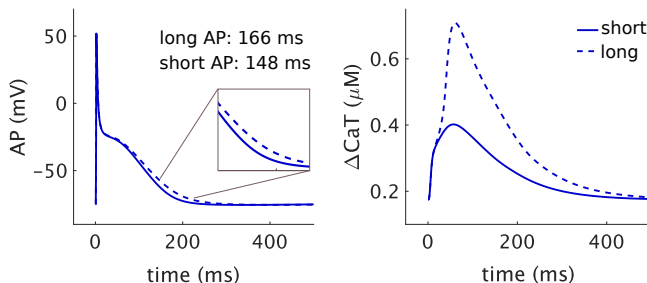


Figure II.2: AP and CaT at PCL=600 ms of the nSR baseline model during dynamic pacing. This model presents APD and calcium alternans at this pacing rate, with a difference in APD90 between long and short beats of 18 ms, and in ΔCaT of 0.3 μM . The cAF baseline model does not present alternans at the same PCL.

baseline model did not present significant APD90 shortening as compared to the nSR baseline, which is a characteristic trace of cAF remodeling, the median APD90 of the functionally calibrated cAF population was shortened by 30 ms,

II. A computational framework for testing arrhythmia marker sensitivities to model parameters in functionally calibrated populations of atrial cells

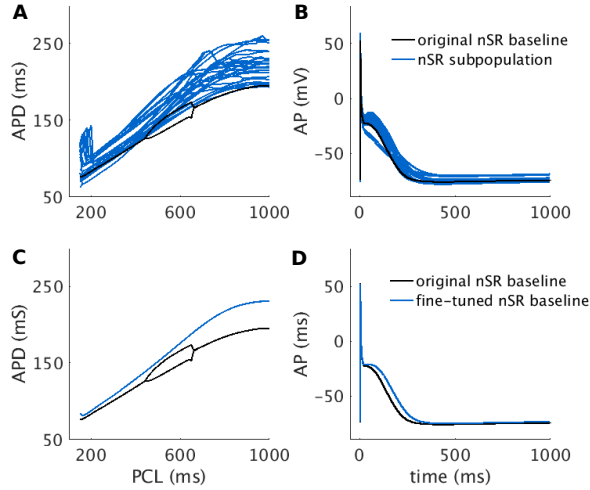


Figure II.3: (A) Dynamic restitution curves of the original nSR baseline and of the subpopulation of models, obtained by selecting models from the original nSR population with Alt-th \leq 250 ms. nSR baseline restitution curve is also shown for comparison. (B) AP traces of the original nSR baseline and of the subpopulation at a PCL of 1000 ms. (C) Dynamic restitution curves and AP traces (D) of the original nSR baseline and of the fine-tuned nSR model obtained with the mean parameter values of the selected subpopulation.

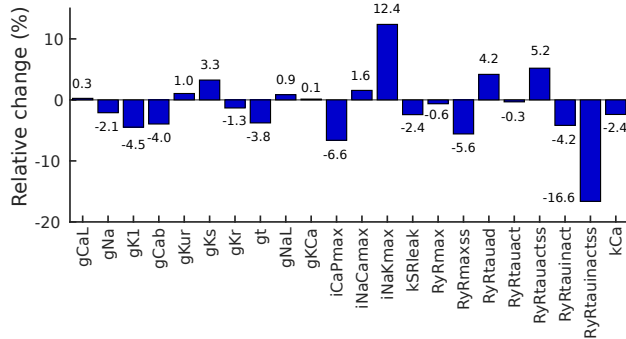


Figure II.4: Percent change of the parameters of the fine-tuned nSR baseline relative to the original nSR baseline.

and RMP hyperpolarized by 6 mV, as compared to nSR population. The CaT showed significant differences in nSR and cAF, with a 55% reduction of ΔCaT in cAF as compared to nSR, in agreement with previous studies[29]. Furthermore, while CaT-tpeak remained unchanged in cAF, CaT-tdecay was significantly longer in the cAF population as compared to the nSR population.

Fig.II.6 shows the distributions of APD90, APD50, APD20, APA, APtri, RMP, $dVdt_{max}$, ΔCaT , CaT_0 , $CaT-tpeak$, $CaT-tdecay$ and Alt-th of the functionally calibrated nSR and cAF populations. The distributions of the biomarkers in the two populations presented in general different morphologies, with different mean values and standard deviations.

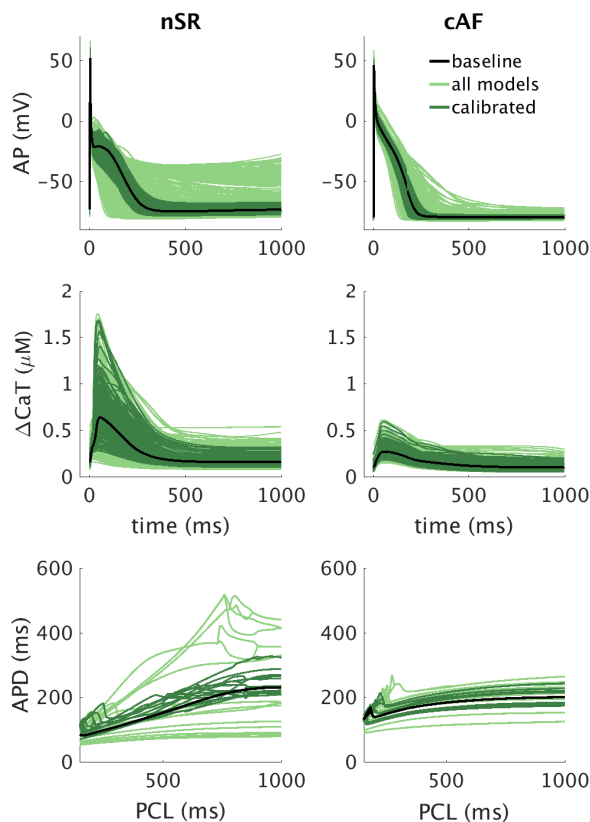


Figure II.5: Simulated nSR and cAF populations: steady-state AP (upper) and CaT (middle) traces at a PCL of 1000 ms, and a few representative dynamic restitution curves (lower). AP and CaT traces, as well as restitution curves of the nSR baseline are also shown for comparison. The populations (of 1000 models each) were functionally calibrated, resulting in 213 models in the nSR population, and in 357 in the cAF population.

II. A computational framework for testing arrhythmia marker sensitivities to model parameters in functionally calibrated populations of atrial cells

Table II.4: Baseline, median, mean, and standard deviation of biomarkers in the nSR and cAF populations.

Marker	nSR			cAF		
	baseline	median	mean \pm std	baseline	median	mean \pm std
APD (ms)	230	220	226 \pm 26	200	194	196 \pm 19
APD50 (ms)	8	9	10 \pm 5	72	71	71 \pm 10
APD20 (ms)	2	2	2 \pm 0.2	6	6	5 \pm 0.4
APA (mV)	126	124	124 \pm 8	125	125	125 \pm 3
RMP (mV)	-73	-73	-73 \pm 2	-79	-79	-79 \pm 0.8
dVdt _{max} (V/s)	265	268	273 \pm 37	247	250	251 \pm 13
Δ CaT (μ M)	0.48	0.52	0.53 \pm 0.2	0.17	0.17	0.18 \pm 0.04
CaT ₀ (μ M)	0.16	0.16	0.17 \pm 0.04	0.10	0.11	0.11 \pm 0.02
CaT-t _{peak} (ms)	56	54	56 \pm 12	63	63	63 \pm 4
CaT-t _{decay} (mS)	289	298	302 \pm 34	455	456	468 \pm 74

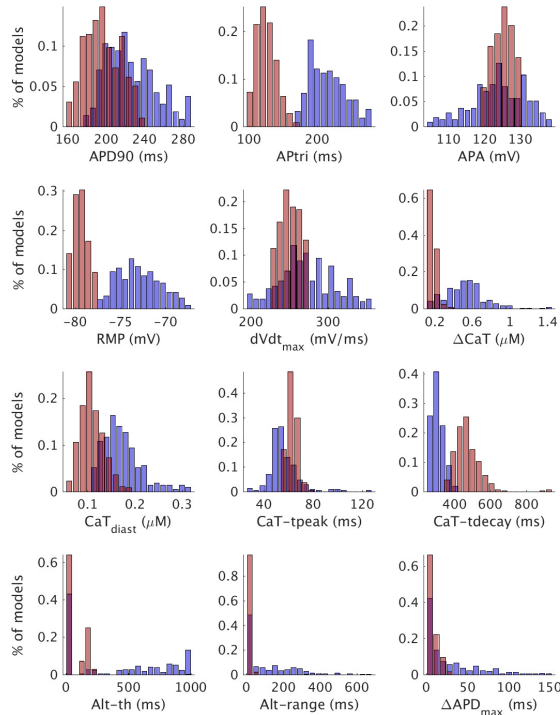


Figure II.6: Distribution of biomarkers of the functionally calibrated nSR (blue) and cAF (red) populations, presented as percentage of the total number of models in the calibrated populations to correct for population size.

II.3.3 Sensitivity analysis of nSR and cAF populations

The sensitivities of APD90, APA, RMP, $dVdt_{max}$, ΔCaT , CaT_{diast} , Alt-th and Alt-range are shown in Fig.II.7. In our analyses, APD90 depends mostly on GCaL, GCab, GNa, GK1 and GKur, in line with previous reports[15], [16], [21], [23], [28]. APD50 and APD20 showed different sensitivity trends in nSR and cAF. In nSR, APD50 is most dependent on GCaL, GKur, Gto and GNa, while in cAF, APD50 depends on GKur, GNa, GCaL and GNaL. APD20 in turn is most sensitive to Gto, GNa, GCab and GK1 in nSR, and to Gto, GKur, GNa and GCaL in cAF (not shown). Both APA and $dVdt_{max}$ are most sensitive to GK1, GCab, as well as GNa and INaKmax, with higher sensitivity in cAF. RMP is defined by GK1 and GCab in both nSR and cAF.

ΔCaT is primarily affected by GCaL, and to a smaller extent by Gto, RyRtauinactss and kCa. CaT_0 is sensitive to Gab, INaKmax and INaCamax. This is expected, since sarcolemmal calcium currents, in particular I_{CaL} , I_{NaK} and I_{NCX} , are associated with intracellular calcium cycling. $CaT-tpeak$ is also affected by GCaL, GCab and GKur, RyRtauinactss and RyRtauinact (not shown), while $CaT-tdecay$ is affected by INaCamax, INaKmax and GCab (not shown).

The alternans markers also revealed different sensitivities in the nSR and cAF populations. Alternans threshold and range in the nSR population is most related to GCaL, INaKmax, GCab and RyRtauinactss, while in the cAF population it is most related to GCab, GK1, GKur and INaKmax. ΔAPD_{max} , on the other hand, depends mostly on GCaL GK1, GCab and GKur (not shown).

Fig.II.8 shows the global sensitivities of the AP, CaT and alternans markers as percentages. This result highlights the relative importance of the various ionic currents on the overall AP morphology, with GNa, GK1, GKur and GCab having the most influence on AP properties. Both CaT morphology and alternans behavior displayed overall greatest sensitivity to GCaL, GCab, INaKmax and INaCamax. Our results also evince differences in sensitivities of the nSR and cAF populations towards some of the tested parameters, in particular towards INaKmax, INaCamax, GCaL and GCab.

II. A computational framework for testing arrhythmia marker sensitivities to model parameters in functionally calibrated populations of atrial cells

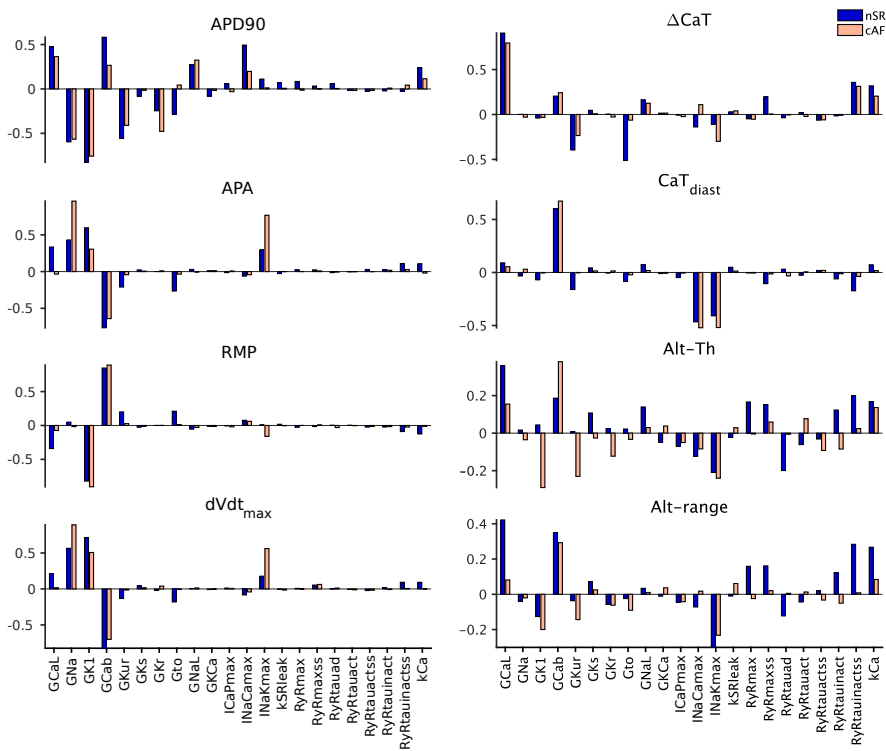


Figure II.7: Sensitivities of selected biomarkers to the varied model parameters, in both the functionally calibrated nSR and cAF populations.

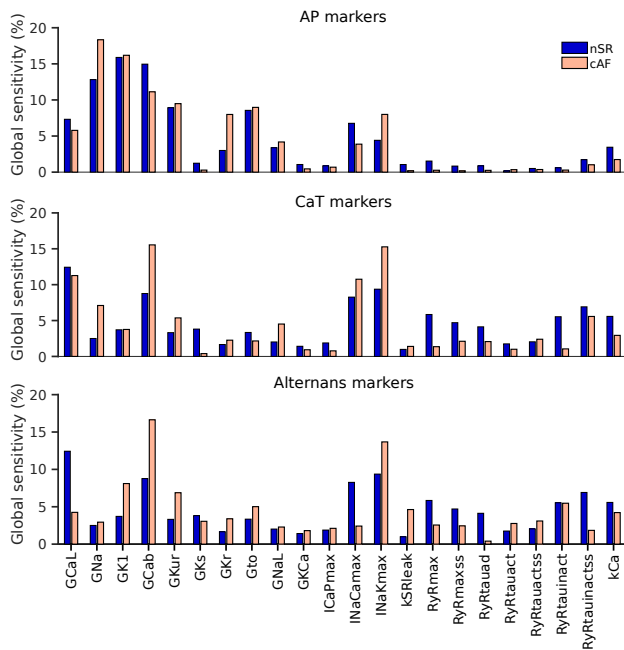


Figure II.8: Global sensitivities of the AP, CaT and alternans markers to the varied parameters. These sensitivities are relative percentages of the overall correlation between markers and parameters, and therefore are all positive values.

II.4 Discussion

II.4.1 Modulation of APD alternans behavior in the nSR model

The nSR_{tuned} baseline obtained from fine-tuning model parameters displays no APD alternans under dynamic pacing, as designed. AP traces obtained with steady-state pacing at 1000 ms PCL show similar AP morphology as the original nSR baseline, with a slight APD90 prolongation of 35 ms. This prolongation in APD90 is a consequence of the models selected into the new subpopulation all displaying a longer APD90 than the original baseline. However, it should be noted that the scheme chosen in this study for the modulation of parameters to produce a model variant with no alternans is not unique. Other parameter fine-tuning approaches we tested could also produce model variants with no APD alternans under dynamic pacing, these showing no prolongation and even slight shortening of APD90. This attests that model parameters can be fine-tuned within certain tight ranges to produce desired outcomes. However, this observation also seems to suggest that there exists no direct link between APD90 and suppression of APD alternans during dynamic pacing. This observation can be related to the fact that the model parameters changed most dramatically to produce model nSR_{tuned}, RyRtauinact, iNaKmax and iCaPmax, are more closely related to the calcium cycling system than to the AP duration. It can thus be inferred that APD alternans underpinned by Ca-cycling abnormalities will not be suppressed by modulation of APD in this context.

II.4.2 Variability in nSR and cAF populations

The nSR population presented greater variability in AP and CaT morphology as compared to the cAF population. In particular, APD90 showed the greatest difference in variability between nSR and cAF. The cause might be associated with the electrical remodeling in cAF, such as the 68% increase in I_{K1} . In a previous study[29], it was found that the hyperpolarization induced by the increased I_{K1} in cAF reduces cell excitability, resulting in the stabilization of RMP. Moreover, the authors found that the cAF model was less sensitive to changes in the model parameters than the nSR model, a result which is confirmed by our results.

II.4.3 Sensitivity analysis of nSR and cAF populations

Our SA showed that AP morphology was mostly affected by GK1, GNa, GCab, Gto, GKur, GCal and INaKmax, which are all conductances which scale major cell membrane currents. The collective importance of these major depolarizing and repolarizing currents in the modulation of AP morphology, in particular the five currents I_{K1} , I_{to} , I_{Cal} , I_{Kur} and I_{NaK} , has also been shown by other authors[16], [22], [30], [31].

Increased calcium (depolarizing) and decreased potassium (repolarizing) currents caused APD prolongation in both nSR and cAF, Fig.II.7, indicating the

dominant role of depolarization in extending the AP. Increased g_{Na} , however, resulted in APD shortening, which may be attributed to early activation of repolarizing currents. Increased g_{Na} also resulted in increased APA and $dVdt_{max}$, as expected (I_{Na} is the main depolarizing current of the AP). RMP showed a negative correlation with GK_1 ; I_{K1} is a repolarizing current and, therefore, when it increases, the membrane becomes more hyperpolarized. A more negative RMP allows more sodium channels to recover from inactivation earlier, and to be available at the onset of the next beat[23], resulting in a higher upstroke velocity. This is reflected by the positive correlation between $dVdt_{max}$ and I_{K1} .

In our analyses, larger I_{CaL} increased ΔCaT and prolonged APD. I_{CaL} stimulates Ca^{2+} release from the sarcoplasmic reticulum (SR) and is deactivated by the rise in intracellular Ca^{2+} . Therefore, a much larger ΔCaT could result in early inactivation of I_{CaL} . Additionally, increased Ca^{2+} content in the cytosol can activate I_{NCX} , which pumps Na^+ inside the cell and activates I_{NaK} , promoting repolarization and APD prolongation.

Our analyses also showed that an increase in I_{NaK} is correlated with larger APA and $dVdt_{max}$, possibly through intracellular Na^+ homeostasis. I_{NaK} has earlier been shown to be linked to calcium cycling and rate adaptation in a model of the atrial cell[15]. I_{NaK} and I_{NCX} have additionally been reported to be associated with altered calcium cycling[15], [29]. In these analyses, CaT_0 and CaT -tdecay decreased with increasing $INaCamax$, which reflects the normal function of NCX of extruding calcium from the cell. Decreases in both $INaCamax$ and $INaK$ also caused an increase in Alt-th (i.e., alternans occur at slower pacing rates) and Alt-range, with $INaCamax$ having a more pronounced effect and $INaKmax$ a less pronounced effect on nSR as compared to the cAF population (Fig.II.8). This highlights the importance of I_{NCX} and I_{NaK} in rate adaptation, in nSR and cAF populations, as previously reported[29].

In the nSR population, an increase in the inactivation time constant of the RyRs, implying less time occupying an open state, also resulted in increased Alt-th (increase in the PCL at which alternans occurred), Alt-range (range of PCL at which alternans occur) and ΔAPD_{max} (difference between short and long beats when alternans are present as a measure of degree of alternans). RyRs, as the primary intracellular Ca release channel, are one of the main components implicated in calcium cycling and alternans behavior: Chang et al[32] found that decreasing the inactivation rate constant of RyR resulted in the promotion of APD alternans. In our analyses, we found that an increase in the inactivated state of the RyRs may promote alternans, possibly by allowing more calcium to be released from the SR into the cytosol and prolonging the CaT. If calcium accumulates in the cytosol, the SR may not be fully repleted before the next beat, resulting in decreased CaT. A smaller amount of calcium in the cytosol, in turn, allows enough time for calcium to be re-uptaken into the SR by the SERCA pumps, thus restarting the cycle and leading to CaT alternans. As a result, APD alternans can occur through calcium-voltage coupling. This effect was not observed in the cAF population possibly due to the reduced I_{CaL} preventing cytosolic calcium overload. However, a more in-depth analysis is required to further investigate these observations.

II. A computational framework for testing arrhythmia marker sensitivities to model parameters in functionally calibrated populations of atrial cells

GCab also seems to have had a greater effect on AP properties than expected, as this is a background current not directly based on experimental measurements. The high sensitivity of the model to GCab across all biomarkers is somewhat surprising and requires further investigation. It is possible that the large dependency on GCab is an artifact resultant of an overestimation of the magnitude of I_{Cab} in the model.

Note the increased sensitivity of the cAF population to GNa as compared to the nSR population. This is likely related to increased GK1 in cAF which results in a slight hyperpolarization of the RMP in the cAF population. This slightly more negative RMP is sufficient to have a great impact on sodium channel availability, as demonstrated by Skibsbye et al[23].

II.4.4 Dynamic AP stability

The two simulated populations also displayed distinct dynamic behavior. The cAF population revealed enhanced stability of the restitution curves, showing the steady tendency for the APD90 to decrease as pacing frequency increased (PCL decreased), whereas the restitution curves of the nSR population showed more erratic behavior with increased pacing frequency. This was somewhat unexpected given the higher instability and impaired rate adaptation in cAF in clinical reports[25]–[27]. Note, however, that all referenced studies were conducted in whole hearts and not on single cells. It has been shown that the electrical restitution properties can change substantially in the presence of electrotonic effects (result of cell-cell coupling) and cardiac memory. Thus, it is expected that alternans behavior at the single cell level differs from that of the whole tissue, where cell-cell coupling can alter or even suppress alternans[33], [34]. Alternans at the tissue level are induced by additional effects such, as structural remodelling[35], dispersion of refractoriness and conduction velocity restitution[7], [34], which are not directly related to cell membrane stability. Therefore, these results lend weight to the hypothesis that the electrical remodeling associated with cAF at the cell level, which accounts only for alterations in membrane channels and calcium cycling transporters, may be “cardioprotective” in the sense that these alterations stabilize the cell membrane and thereby reduce alternans and dynamical instability at the level of the single cell.

On the other hand, due to cardiac memory, steady state is highly dependent on pacing duration and on the initial state of the system. In order to make a direct comparison between different models, the pacing duration at each PCL during the dynamic restitution protocol was kept constant. The consequence of using this protocol is that it is not possible to distinguish between steady state alternans and transient alternans. That is, this dynamic restitution experiment detects alternans, regardless of whether these alternans are transient or stable. Thus, a possible extension of the method could involve establishing a dynamic restitution protocol with an adaptive pacing duration to guarantee that only persistent alternans are included in the analysis.

II.5 Conclusions and future directions

In the present study, we refined a human atrial single cell model by selecting a subpopulation of models with an alternans threshold at higher pacing rates and longer APD90 from an nSR population, which resulted in a new, more physiologically relevant 'average' baseline model with no APD alternans. We also generated two populations of models based on the Koivumäki human atrial cell model[23], nSR and cAF, by varying parameters related to AP morphology and calcium cycling, such as maximum ion channel conductances, pump fluxes, RyR gating variables and SR calcium leak. A series of *in silico* experiments were then performed in order to measure AP and CaT markers, as well as dynamic restitution curves of each model. The populations were functionally calibrated to exclude outliers and several cell biomarkers related to AP and CaT morphology and APD alternans behavior were measured in order to characterize cell stability. The functionally calibrated populations were also subject to SA in order to quantify the sensitivity of different biomarkers to the varied parameters.

Sensitivity analysis with respect to 22 parameters showed that the nSR and cAF populations have high sensitivities with respect to similar parameters related to the calcium currents, I_{CaL} and I_{Cab} , I_{K1} , I_{Na} , I_{Kur} , I_{NaK} and I_{NCX} . We have also found that the nSR population exhibited larger variability of APD90 and dynamic restitution behavior than the cAF population, likely due to the stabilizing effect of electrical remodeling in cAF, as outlined in previous sections.

The method presented here could be extended to include other single-cell and tissue arrhythmia biomarkers, such as EADs/DADs, effective refractory period, conduction velocity restitution, tissue-level alternans and spiral wave inducibility. These phenomena have also been linked to arrhythmogenicity and atrial fibrillation initiation and maintenance, and therefore constitute logical extensions of the method. Furthermore, future work will include the definition of a dynamic stability score based on a comprehensive set of arrhythmia biomarkers to rate or classify models according to their stability and propensity to display arrhythmogenic behaviors. We have also observed that alternans threshold exhibits an interdependence with other cell biomarkers, resulting in two distinct clusters for the nSR and cAF populations, as shown in Fig.II.9. This suggests that Alt-th is a rather complex mechanism that results from an interplay of multiple cell behaviors, which in turn exhibit some level of interdependence among them. This highlights that more advanced classification via non-linear regression methods may provide additional insight into arrhythmogenic cellular mechanisms. The prospective dynamic stability score could also be combined with cluster analysis to classify or segment between populations or subpopulations with distinct biomarker targets. The resulting clustered population biomarkers would then represent, for instance, "arrhythmogenic" or "non-arrhythmogenic" models, thus generating a threshold score between the two clusters, which would allow to better classify models according to, e.g., arrhythmia risk based on specific known cell prescribed biomarkers.

II. A computational framework for testing arrhythmia marker sensitivities to model parameters in functionally calibrated populations of atrial cells

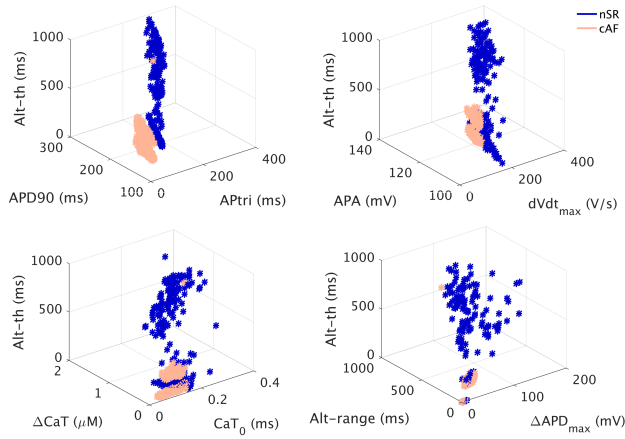


Figure II.9: Interdependence of alternans threshold with selected AP and CaT markers of the calibrated nSR and cAF populations.

Acknowledgments

This project has received funding from the European Union’s Horizon 2020 MSCA ITN under grant agreement No 675351. This project has received funding from the European Union’s Horizon 2020 MSCA ITN under grant agreement No 675351. We wish to thank the founder of the Allen Institute for Cell Science, Paul G. Allen, for his vision, encouragement and support. Thanks also to Valeriya Naumova for critical reading of the manuscript.

References

- [1] Christini, D. J., Stein, K. M., Markowitz, S. M., Mittal, S., Slotwiner, D. J., Scheiner, M. A., Iwai, S., and Lerman, B. B., “Nonlinear-dynamical arrhythmia control in humans”, *Proceedings of the National Academy of Sciences of the United States of America*, vol. 98, no. 10, pp. 5827–5832, May 2001.
- [2] Karma, A. and Gilmour, R., “Nonlinear dynamics of heart rhythm disorders”, *Physics Today*, vol. 30, p. 51, 3 2007.
- [3] Cherry, E. M., Fenton, F. H., and Gilmour, R. F., “Mechanisms of ventricular arrhythmias: A dynamical systems-based perspective”, *American Journal of Physiology - Heart and Circulatory Physiology*, vol. 302, no. 12, H2451–H2463, 2012.
- [4] Gaeta, S. A. and Christini, D. J., “Non-Linear Dynamics of Cardiac Alternans: Subcellular to Tissue-Level Mechanisms of Arrhythmia”, *Frontiers in Physiology*, vol. 3, p. 157, 2012.

- [5] Surovyatkina, E., Noble, D., Gavaghan, D., and Sher, A., “Multistability property in cardiac ionic models of mammalian and human ventricular cells”, *Progress in Biophysics and Molecular Biology*, vol. 103, no. 1, pp. 131–141, 2010, Ion channels: Growing evidence for the role in disease.
- [6] Weiss, J. N., Qu, Z., Chen, P.-S., Lin, S.-F., Karagueuzian, H. S., Hayashi, H., Garfinkel, A., and Karma, A., “The Dynamics of Cardiac Fibrillation”, *Circulation*, vol. 112, no. 8, pp. 1232–1240, 2005.
- [7] Weiss, J. N., Karma, A., Shiferaw, Y., Chen, P.-S., Garfinkel, A., and Qu, Z., “From pulsus to pulseless: The saga of cardiac alternans.”, *Circ Res*, vol. 98, no. 10, pp. 1244–1253, 2006.
- [8] Heijman, J., Erfanian Abdoust, P., Voigt, N., Nattel, S., and Dobrev, D., “Computational models of atrial cellular electrophysiology and calcium handling, and their role in atrial fibrillation”, *The Journal of physiology*, vol. 594, no. 3, pp. 537–553, Feb. 2016.
- [9] Grandi, E. and Maleckar, M. M., “Anti-arrhythmic strategies for atrial fibrillation: The role of computational modeling in discovery, development, and optimization.”, *Pharmacol Ther*, vol. 168, pp. 126–142, Dec. 2016.
- [10] Heijman, J., Voigt, N., Ghezelbash, S., Schirmer, I., and Dobrev, D., “Calcium Handling Abnormalities as a Target for Atrial Fibrillation Therapeutics: How Close to Clinical Implementation?”, *Journal of Cardiovascular Pharmacology*, vol. 66, no. 6, 2015.
- [11] Courtemanche, M., Ramirez, R. J., and Nattel, S., “Ionic mechanisms underlying human atrial action potential properties: Insights from a mathematical model”, *American Journal of Physiology-Heart and Circulatory Physiology*, vol. 275, no. 1, H301–H321, 1998, PMID: 29586616.
- [12] Nygren, A., Fiset, C., Firek, L., Clark, J. W., Lindblad, D. S., Clark, R. B., and Giles, W. R., “Mathematical Model of an Adult Human Atrial Cell”, *Circulation Research*, vol. 82, no. 1, pp. 63–81, 1998.
- [13] Maleckar, M. M., Greenstein, J. L., Giles, W. R., and Trayanova, N. A., “K⁺ current changes account for the rate dependence of the action potential in the human atrial myocyte”, *American Journal of Physiology - Heart and Circulatory Physiology*, vol. 297, no. 4, H1398–H1410, 2009.
- [14] Koivumäki, J. T., Korhonen, T., and Tavi, P., “Impact of Sarcoplasmic Reticulum Calcium Release on Calcium Dynamics and Action Potential Morphology in Human Atrial Myocytes: A Computational Study”, *PLOS Computational Biology*, vol. 7, no. 1, pp. 1–14, Jan. 2011.
- [15] Grandi, E., Pandit, S. V., Voigt, N., Workman, A. J., Dobrev, D., Jalife, J., and Bers, D. M., “Human atrial action potential and Ca²⁺ model: Sinus rhythm and chronic atrial fibrillation.”, *Circ Res*, vol. 109, no. 9, pp. 1055–1066, 2011.

II. A computational framework for testing arrhythmia marker sensitivities to model parameters in functionally calibrated populations of atrial cells

- [16] Sánchez, C., Bueno-Orovio, A., Wettwer, E., Loose, S., Simon, J., Ravens, U., Pueyo, E., and Rodriguez, B., “Inter-Subject Variability in Human Atrial Action Potential in Sinus Rhythm versus Chronic Atrial Fibrillation”, *PLOS ONE*, vol. 9, no. 8, pp. 1–14, Aug. 2014.
- [17] Sobie, E. A., “Parameter sensitivity analysis in electrophysiological models using multivariable regression.”, *Biophys J*, vol. 96, no. 4, pp. 1264–1274, 2009.
- [18] Lee, Y.-S., Liu, O. Z., Hwang, H. S., Knollmann, B. C., and Sobie, E. A., “Parameter sensitivity analysis of stochastic models provides insights into cardiac calcium sparks.”, *Biophys J*, vol. 104, no. 5, pp. 1142–1150, 2013.
- [19] Passini, E., Mincholé, A., Coppini, R., Cerbai, E., Rodriguez, B., Severi, S., and Bueno-Orovio, A., “Mechanisms of pro-arrhythmic abnormalities in ventricular repolarisation and anti-arrhythmic therapies in human hypertrophic cardiomyopathy”, *Journal of Molecular and Cellular Cardiology*, vol. 96, pp. 72–81, Jul. 2016.
- [20] Sarkar, A. X. and Sobie, E. A., “Regression Analysis for Constraining Free Parameters in Electrophysiological Models of Cardiac Cells”, *PLOS Computational Biology*, vol. 6, no. 9, pp. 1–11, Sep. 2010.
- [21] Britton, O. J., Bueno-Orovio, A., Van Ammel, K., Lu, H. R., Towart, R., Gallacher, D. J., and Rodriguez, B., “Experimentally calibrated population of models predicts and explains intersubject variability in cardiac cellular electrophysiology”, vol. 110, no. 23, E2098–E2105, 2013.
- [22] Chang, E. T. and Clayton, R. H., “Parameter sensitivity analysis of a human atrial cell model using multivariate regression”, in *Computing in Cardiology 2014*, 2014, pp. 521–524.
- [23] Skibsbye, L., Jespersen, T., Christ, T., Maleckar, M. M., Brink, J. van den, Tavi, P., and Koivumäki, J. T., “Refractoriness in human atria: Time and voltage dependence of sodium channel availability”, *Journal of Molecular and Cellular Cardiology*, vol. 101, pp. 26–34, 2016.
- [24] Brink, J. van den, “Modeling Atrial Fibrillation - Exploring the Koivumäki Human Atrial Cell Model”, Master thesis, University of Oslo, 2016.
- [25] Narayan, S. M., Bode, F., Karasik, P. L., and Franz, M. R., “Alternans of Atrial Action Potentials During Atrial Flutter as a Precursor to Atrial Fibrillation”, *Circulation*, vol. 106, no. 15, pp. 1968–1973, 2002.
- [26] Narayan, S. M., Franz, M. R., Clopton, P., Pruvot, E. J., and Krummen, D. E., “Repolarization alternans reveals vulnerability to human atrial fibrillation”, *Circulation*, vol. 123, no. 25, pp. 2922–2930, Jun. 2011.
- [27] Franz, M. R., Jamal, S. M., and Narayan, S. M., “The role of action potential alternans in the initiation of atrial fibrillation in humans: A review and future directions”, *Europace*, vol. 14, no. Suppl 5, pp. v58–v64, Nov. 2012.

-
- [28] Sarkar, A. X., Christini, D. J., and Sobie, E. A., “Exploiting mathematical models to illuminate electrophysiological variability between individuals.”, *J Physiol*, vol. 590, no. 11, pp. 2555–2567, 2012.
 - [29] Koivumäki, J. T., Seemann, G., Maleckar, M. M., and Tavi, P., “In Silico Screening of the Key Cellular Remodeling Targets in Chronic Atrial Fibrillation”, *PLOS Computational Biology*, vol. 10, no. 5, pp. 1–15, May 2014.
 - [30] Sánchez, C., Corrias, A., Bueno-Orovio, A., Davies, M., Swinton, J., Jacobson, I., Laguna, P., Pueyo, E., and Rodriguez, B., “The Na^+/K^+ pump is an important modulator of refractoriness and rotor dynamics in human atrial tissue”, *American Journal of Physiology - Heart and Circulatory Physiology*, vol. 302, no. 5, H1146–H1159, 2012.
 - [31] Morotti, S., Ellinwood, N., Koivumäki, J., Chiamvimonvat, N., and Grandi, E., “Small-conductance Ca^{2+} -activated K^+ current in atrial fibrillation: Both friend and foe”, in *Biophysics Society 60th Annual Meeting*, Los Angeles, 2016.
 - [32] Chang, K. C., Bayer, J. D., and Trayanova, N. A., “Disrupted calcium release as a mechanism for atrial alternans associated with human atrial fibrillation”, *PLOS Computational Biology*, vol. 10, no. 12, pp. 1–16, Dec. 2014.
 - [33] Cherry, E. M. and Fenton, F. H., “Suppression of alternans and conduction blocks despite steep APD restitution: Electrotonic, memory, and conduction velocity restitution effects”, *American Journal of Physiology - Heart and Circulatory Physiology*, vol. 286, no. 6, H2332–H2341, 2004.
 - [34] Sato, D., Shiferaw, Y., Garfinkel, A., Weiss, J. N., Qu, Z., and Karma, A., “Spatially Discordant Alternans in Cardiac Tissue: Role of calcium cycling.”, *Circ Res*, vol. 99, no. 5, pp. 520–527, 2006.
 - [35] Corradi, D., Callegari, S., Maestri, R., Benussi, S., and Alfieri, O., “Structural remodeling in atrial fibrillation”, *Nat Clin Pract Cardiovasc Med*, vol. 5, no. 12, pp. 782–796, Dec. 2008.

Paper III

A novel computational model of the rabbit atrial cardiomyocyte with spatial calcium dynamics

Márcia R. Vagos, Hermenegild Arevalo, Jordi Heijman, Ulrich Schotten, Joakim Sundnes

III

A novel computational model of the rabbit atrial cardiomyocyte with spatial calcium dynamics

Márcia R. Vagos^{1,2}, Hermenegild Arevalo^{1,3}, Jordi Heijman⁴, Ulrich Schotten⁴, Joakim Sundnes^{1,2,3}

¹ Simula Research Laboratory, Computational Physiology Department, Martin Linges vei 25, 1325 Lysaker, Norway

² University of Oslo, Department of Informatics, Gaustadalléen 23B, 0373 Oslo, Norway

² Center for Cardiological Innovation (CCI), Rikshospitalet, 0372 Oslo, Norway

² CARIM School for Cardiovascular Diseases, Faculty of Health, Medicine and Life Sciences, Maastricht University, Universiteitssingel 50, 6229 ER Maastricht, Netherlands

Abstract

Models of cardiac electrophysiology are widely used to supplement experimental results and to provide insight into mechanisms of cardiac function and pathology. The rabbit has been a particularly important animal model for studying mechanisms of atrial pathophysiology and atrial fibrillation, which has motivated the development of models for the rabbit atrial cardiomyocyte electrophysiology. Previously developed models include detailed representations of membrane currents and intracellular ionic concentrations, but these so-called “common-pool” models lack a spatially distributed description of the calcium handling system, which reflects the detailed ultrastructure likely found in cells *in vivo*. Because of the less well-developed T-tubular system in atrial compared to ventricular cardiomyocytes, spatial heterogeneities in intracellular calcium dynamics may play a more significant role in atrial myocyte pathophysiology, rendering common-pool models less suitable for investigating underlying electrophysiological mechanisms.

In this study, we developed a novel computational model of the rabbit atrial cardiomyocyte incorporating detailed compartmentalization of intracellular calcium dynamics, in addition to a description of membrane currents and intracellular processes. The spatial representation of calcium was based on dividing the intracellular space into eighteen different compartments in the transversal direction, each with separate systems for internal calcium storage and release, and tracking ionic fluxes between compartments in addition to the dynamics driven by membrane currents and calcium release. The model was parameterized employing a population-of-models approach using experimental data from different sources.

The parameterization of this novel model resulted in a calibrated population of models with inherent variability in calcium dynamics and electrophysiological properties, all of which fall within the range of observed experimental values. As such, the population of models may represent natural variability in myocyte electrophysiology or inherent uncertainty in the underlying experimental data. The ionic model population was also able to reproduce the U-shaped waveform observed in line scans of calcium dynamics in atrial myocytes, characteristic of spatial heterogeneity and subcellular calcium diffusion. This novel spatial model of the rabbit atrial cardiomyocyte can be used to integrate experimental findings, and thus offers the potential to enhance our understanding of the pathophysiological role of calcium-handling abnormalities under diseased conditions, such as atrial fibrillation.

III.1 Introduction

Mathematical models of cardiac electrophysiology (EP) have advanced significantly over the past decades, and are valuable tools for gaining physiological insight from the expanding pool of experimental data [1], [2]. While animal models remain the primary source of experimental data on ion channels and electrical activity in the heart, computational models of different animal species constitute an important tool for knowledge extraction and translation between species. The rabbit has been a particularly useful animal model to study different aspects of cardiac electrophysiology and arrhythmia, given the similarities of their electrophysiological properties to the human [3]–[9]. The wide application of the experimental rabbit model has motivated the development of rabbit-specific mathematical models of cardiomyocyte (CM) electrophysiology, see, e.g. [10]–[16], which incorporate rabbit-specific formulations of ionic currents.

One important characteristic of rabbit atrial CMs is the lack of a well-developed T-tubule system [17], [18], which leads to a characteristic U-shaped wave front in line-scans of intracellular Ca^{2+} , indicating asynchronous Ca^{2+} release [6], [19]. This shape results from the ‘fire-diffuse-fire’ response [20], in which a Ca^{2+} wave is initiated by L-type Ca^{2+} channels (LTCC) at the cell periphery and subsequently propagates towards the center of the cell in a saltatory manner through diffusion and Ca^{2+} -induced Ca^{2+} release [21], [22]. Similar U-shaped Ca^{2+} propagation patterns have been observed in atrial myocytes of other small animal species, such as cat [23], [24], and rat [21], [25]. However, it has also been observed in rat atrial myocytes that Ca^{2+} signals originating at the cell periphery typically did not fully propagate to the center [21]. This effective truncation of the Ca^{2+} wave was due to the lack of T-tubules, increased Ca^{2+} buffering capacity, and the so-called ‘diffusion barrier’ of the mitochondria and Serca2a in these cells. This lack of regeneration of the Ca^{2+} signal results in a progressive damping of the centripetal Ca^{2+} wave with a peak amplitude and rate of Ca^{2+} rise significantly lower at central regions as compared to the periphery [25], [26]. These observations have also been replicated in a model of Ca^{2+} propagation in a CM without T-tubules, demonstrating that Ca^{2+} propagation or lack thereof results from a complex interplay between different effectors of the Ca^{2+} handling system [27]. Non-uniform systolic Ca^{2+} transients (CaTs) associated with the lack of T-tubules in some atrial myocytes, or remodelling-induced detubulation, have been linked to arrhythmogenic activity. The spatial heterogeneities in Ca^{2+} distribution observed in these atrial myocytes can translate into fluctuations in membrane potential, exacerbating alterations in electrical activity resulting from atrial remodelling [26], [28], [29].

Despite the important role that spatial intracellular Ca^{2+} dynamics can play in the generation and maintenance of aberrant electrical activity in atrial cells and tissues, previously developed mathematical models of the rabbit atrial CM do not incorporate spatial description of Ca^{2+} movement within the cell. Therefore, although useful in reproducing whole-cell characteristics of rabbit EP, these models are not able to assess the sub-cellular mechanisms of altered Ca^{2+} propagation and their role in arrhythmic activity. In contrast, models with

III. A novel computational model of the rabbit atrial cardiomyocyte with spatial calcium dynamics

spatial Ca^{2+} description would permit assessment of the effect of sub-cellular structures on intracellular Ca^{2+} dynamics and Ca^{2+} wave propagation, but such models have not been developed for rabbit atrial physiology.

In this paper, we describe the development of a novel model of the rabbit atrial CM with spatial description of ionic species and the Ca^{2+} handling system. The structure of the model allows simulation of the spatial distribution of Ca^{2+} , as well as the propagation of intracellular Ca^{2+} over time. We parameterized the maximum conductances in the model using a ‘population of models’ (PoM) approach to reproduce the normal electrophysiological properties of the rabbit, as supported by experimental data reported in the literature. The result is a population of calibrated models that all closely approximate the experimental data, but with differences in the models that appropriately reflect individual variability or inherent uncertainty in the data. We are aware that the dynamics of Ca^{2+} wave propagation are most directly affected by parameters that modulate the SR content, and Ca^{2+} release and uptake kinetics. However, the aim of the present study was not to focus on the role of these parameters in modulating Ca^{2+} wave propagation, but instead to parameterize the maximum conductances of ionic currents and assess their effect on intracellular Ca^{2+} dynamics. We used this calibrated population to (1) assess if changes in current conductances have an effect on Ca^{2+} propagation dynamics; (2) to quantify possible correlations between Ca^{2+} properties at the membrane and at the center of cell; and (3) to query the underlying mechanisms of the differences observed in the Ca^{2+} propagation patterns across the calibrated population.

III.2 Methods

III.2.1 Model development

The rabbit atrial CM model was developed based on the previously published human atrial CM model by Voigt & Heijman [30], which is a spatial model with the Ca^{2+} handling system divided into discrete domains. We modified this model to incorporate ion current formulations from the non-spatial rabbit atrial CM models by Lindblad et al.[12], and Aslanidi et al.[15] to reflect the rabbit electrophysiology.

To capture radial flux and heterogeneities in Ca^{2+} concentrations, the model was constructed as a compartmentalized cross-section of the myocyte, as illustrated in Figure III.1. A total of 18 domains represent a one-dimensional cross-section of the cell, where the two outermost domains (1 and 18) correspond to the region close to the cell membrane. These domains therefore include the sarcolemmal currents, Ca^{2+} release units (CRU), and Ca^{2+} buffers. In contrast, the inner domains (2-17) are not in direct contact with the cell membrane and contain only the CRUs and Ca^{2+} buffers. The inner domains contain a cytosolic space, the sarcoplasmic reticulum (SR), and a sub-SR space (SRS), while the membrane domains also include a subsarcolemmal (SL) space. In domains 1 and 18, the SRS represents a junctional space in which LTCC and the ryanodine receptors (RyR) interact, which is indicated with “junc”. We used a cell volume of

16 pL based on an estimated cell length of 130 μm [12] and a radius of 6.3 μm [6]. The cytosolic, SR, SRS, and SL spaces occupy 65%, 3.5%, 0.1%, 2% of the domain volume, respectively. The domains and compartments, as well as the ionic fluxes between them, are schematically illustrated in Fig. III.1.

The membrane model includes Ca^{2+} currents I_{CaL} and I_{CaT} ; the fast Na^+ current I_{Na} ; repolarising K^+ currents I_{to1} , I_{Kr} , I_{Ks} , and I_{K1} , as well as three background currents I_{Cab} , I_{Nab} , and I_{Clb} . Additionally, the model includes the ionic currents of the Na^+ - Ca^{2+} exchanger (I_{NCX}); the Na^+ - K^+ pump (I_{NaK}); and the plasmalemmal Ca^{2+} pump (I_{CaP}). The total membrane current in the model is the sum of all these currents:

$$I_{\text{Ca}_{\text{tot}}} = (I_{\text{CaL}_{\text{junc}}} + I_{\text{CaL}_{\text{SL}}}) + (I_{\text{CaT}_{\text{junc}}} + I_{\text{CaT}_{\text{SL}}}) + (I_{\text{CaP}_{\text{junc}}} + I_{\text{CaP}_{\text{SL}}}) + (I_{\text{Cab}_{\text{junc}}} + I_{\text{Cab}_{\text{SL}}}) - 2(I_{\text{NCX}_{\text{junc}}} + I_{\text{NCX}_{\text{SL}}}).$$

$$I_{\text{Na}_{\text{tot}}} = (I_{\text{Na}_{\text{junc}}} + I_{\text{Na}_{\text{SL}}}) + 3(I_{\text{NCX}_{\text{junc}}} + I_{\text{NCX}_{\text{SL}}}) - 3 \times (I_{\text{NaK}_{\text{junc}}} + I_{\text{NaK}_{\text{SL}}}) + (I_{\text{Nab}_{\text{junc}}} + I_{\text{Nab}_{\text{SL}}}).$$

$$I_{\text{K}_{\text{tot}}} = I_{\text{to}} + I_{\text{Kr}} + I_{\text{Ks}} + I_{\text{K1}} - 2 \times (I_{\text{NaK}_{\text{junc}}} + I_{\text{NaK}_{\text{SL}}}) + I_{\text{stim}}.$$

$$I_{\text{tot}} = I_{\text{Ca}_{\text{tot}}} + I_{\text{Na}_{\text{tot}}} + I_{\text{K}_{\text{tot}}} + I_{\text{Clb}}$$

$$\frac{dV}{dt} = - \frac{1}{C_m} I_{\text{tot}}$$

Most of the formulations were adopted from Aslanidi et al. [15], which in turn are modifications of the formulations in Lindblad et al. [12]. We included the background chloride current (I_{Clb}) from the Lindblad et al. model, since a chloride current has been reported in rabbit atrial myocytes [31]. The formulation of I_{NCX} was taken from the Voigt & Heijman et al. model [30] (equations provided in the Supplement), originally described by Weber et al. [32], since we found this current to replicate more realistically the forward and reverse modes of the Na^+ - Ca^{2+} exchanger. We tested this model component specifically by simulating a caffeine-induced Ca^{2+} release protocol to assess Ca^{2+} extrusion rate through the NCX. As illustrated in Figure III.2, the normalized CaT and decay time of I_{NCX} closely matched experimental data [6].

The rabbit atrial CM model was implemented in C++, and the state equations were solved using a forward Euler scheme. All simulations were performed on the Abel computer cluster from the University of Oslo, running the Linux Operating system (64 bit CentOS 6). The source code of the model is available at https://github.com/marciavagos/Rabbit_model.git.

III. A novel computational model of the rabbit atrial cardiomyocyte with spatial calcium dynamics

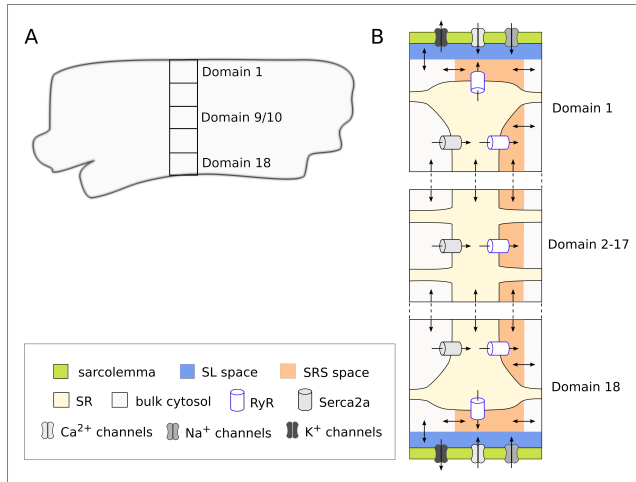


Figure III.1: Schematic representation of the rabbit CM model with the discrete cell domains and different intracellular compartments. One segment represents a cross section of the myocyte (A), and is composed of 18 domains. The membrane domains (domains 1 and 18), contain the sarcolemmal currents, and Ca²⁺ handling system; the inner domains (domains 2-17), contain only the Ca²⁺ handling system (B). Each membrane domain contains five different compartments: cytosolic space, sarcoplasmic reticulum (SR), sub-SR (SRS) space, and subsarcolemmal (SL) spaces, which together constitute the cleft space. Ca²⁺ diffuses between the different compartments in the model, and between adjacent domains. Because we use a deterministic RyR model, the model is symmetrical around the central domains.

III.2.2 Parametrization of ionic currents

We initially implemented the model using the original published parameters from Aslanidi et al., which resulted in an action potential (AP) that was morphologically similar to experimentally measured APs, but did not match in terms of quantifiable metrics. The action potential duration at 90% repolarization (APD₉₀) was 143 ms, which is longer than the reported 120 ms, and the resting membrane potential (RMP) was around -74 mV as compared to the -80 mV reported in literature. Additionally, the CaT amplitude (CaT-A) in the baseline model was only about 0.09 μM, compared to the ~1.0 μM amplitude in simulated CaTs by Lindblad et al.[12], and Aslanidi et al. [15]. The model also showed a suppression of the Ca²⁺ signal at the centre of cell, contrary to observations of a fully regenerative CaT in rabbit atrial myocytes [6].

In order to adjust the model parameters to match reported experimental CaT and AP data [6], [12], [15], [31], [33]–[36], we employed a PoM approach to scale the maximum conductances of the 13 ionic currents in the model. This approach is useful to perform parameter fitting, while at the same time allowing

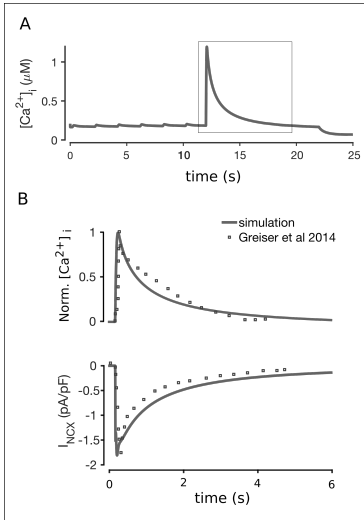


Figure III.2: Simulation of the caffeine-induced Ca^{2+} release protocol (A), and comparison of I_{NCX} and normalized CaT with experimental data from Greiser et al. [6] (B), after pacing at 0.5 Hz for 12 s, and 10 s quiescent period.

uncertainty and natural variability to be incorporated into the models [37], [38]. A PoM is constructed by randomly sampling the model parameters from specified probability distributions, thereby generating a population of several ‘baseline’ models. For the present PoM the 13 maximum conductances were varied over a range between 25% and 400% of their published values, and resampled from uniform distributions using Latin Hypercube sampling. Such a large degree of variation was chosen to incorporate as much variability as possible, allowing for the population to capture the natural variability and uncertainty in the data. The initial PoM consisted of 3000 models, which were all paced at 2 Hz pacing for 2 min to ensure approximation to steady state, and then the last 5 beats were recorded for analysis. The varied maximum conductances and their respective nominal (published) values are listed in Table III.1, and the initial ionic concentrations are listed in Table III.7.

The population was then calibrated with experimental data from measurements of rabbit APs and CaTs to select models whose APs and CaTs represent typical rabbit-like morphology [6], [12], [15], [31], [33]–[36].

Finally, uncertainties of output measures of APs and CaTs were defined through the mean and standard deviation (std).

III.2.3 Calibration of the population

Since we allowed a large degree of variation in the model parameters, the initial population included a number of non-physiological models. The second step of the PoM approach was to select a subset of models that matched previous

III. A novel computational model of the rabbit atrial cardiomyocyte with spatial calcium dynamics

Table III.1: List of the maximum conductances of the ionic currents in the model and their nominal values.

Parameter	Nominal value	Description
G_{CaL}	0.144 nS/pF	Maximum conductance of the L-type Ca^{2+} channel
G_{CaT}	0.120 nS/pF	Maximum conductance of the T-type Ca^{2+} channel
I_{NaCa}^{max}	4.41 pA/pF	Maximum flux of the Ca^{2+} - Na^+ exchanger
I_{NaK}^{max}	1.288×10^{-3} nA/pF	Maximum flux of the Na^+ - K^+ pump
I_{CaP}^{max}	0.190 nS/pF	Maximum flux of the plasmalemmal Ca^{2+} ATPase
G_Na	0.028×10^{-3} μ L/(spF)	Maximum conductance of the fast Na^+ channel
G_{to}	0.200 nS/pF	Maximum conductance of the transient outward K^+ channel
G_{Kr}	0.070 nS/pF	Maximum conductance of the rapidly activating delayed rectifier K^+ channel
G_{Ks}	0.050 nS/pF	Maximum conductance of the slowly activating delayed rectifier K^+ channel
G_{K1}	0.203 nS/pF	Maximum conductance of the inward rectifier K^+ channel
G_{Cab}	0.4×10^{-3} nS/pF	Maximum conductance of the background Ca^{2+} channels
G_{Nab}	0.4×10^{-3} nS/pF	Maximum conductance of the background Na^+ channels
G_{Clb}	2.4×10^{-3} nS/pF	Maximum conductance of the background K^+ channels

experimental recordings, to create a calibrated model population. Experimentally measured APs of rabbit atrial CMs reported in literature are rather inconsistent. For instance, Muraki et al. [34], Wang et al. [35] recorded APs with APD_{90} values of 93, and 103 ms, respectively, while Yamashita et al. [39] reported 70 ms. Lindblad et al. [12] reported a similar APD_{90} of 80 ms at 2 Hz, while more recent studies have reported higher values. Greiser et al. [6] measured APD_{90} in rabbit myocytes paced at 2 Hz between 100 and 140 ms, in agreement with the 130 ms Hou et al. [36] at 1 Hz. APD_{50} measured in Wang et al. [35] and Hou et al. [36] was 44 (at 2 Hz) and 55 ms (at 1 Hz), respectively, while in Yamashita et al. [39] this was about 18 ms in the crista terminalis, and 38 ms in pectinate muscle CMs. Additionally, APD_{40} in Qi te al. [33] was 30 ms in left atrium, and 51 ms in right atrium at 1 Hz. APD_{20} in [36] was also between 13 to 17 ms. Given this wide range of reported APD_{50} and APD_{40} values, we required APD_{40} to be between of 20 and 60 ms.

AP amplitude (APA) has been reported at around 100 mV [15], [33], [34], [36], and 120 mV [12], [31]. Reported values of RMP are more consistent across sources, with most reporting around -80 mV [6], [15], [33], [34], [36], [39], although Lindblad et al. reported an RMP of -71 mV [12]. Given this heterogeneity of measured electrophysiological properties of CMs, there is no single generic model of an atrial cell, which motivated our choice of a PoM approach to parameterize the model.

To our knowledge, absolute values of Ca^{2+} and CaT amplitude have not been measured in rabbit atrial myocytes. Lindblad et al. [12] assumed a resting Ca^{2+} of 50 nM, and peak Ca^{2+} levels in their model simulations were within ~ 0.1 and $\sim 1.0 \mu M$. CaTs measured from fluorescence imaging of rat [25], [40] and human [30], [41] atrial CMs also show amplitude values in this range. Therefore, we excluded models whose whole-cell CaT amplitude was outside this range. The rise time of the CaT was also constrained to be no larger than 100 ms at 2 Hz pacing [6]. Additionally, $[Na^+]_i$ was constrained to be between 6.5 and

12.5 mM, which corresponds to reported values in rabbit atrial cells [6], [10]. Finally, models showing early after-depolarisations (EAD), and alternans were also excluded. The output properties and corresponding value ranges considered in the calibration of the models are listed in Table III.2.

III.2.4 Analysis of Ca^{2+} wave propagation

The primary focus of this paper is on Ca^{2+} dynamics, and the Ca^{2+} signal and wave dynamics were subject to a more extensive analysis than the other output variables. Spatio-temporal plots of Ca^{2+} dynamics, resembling line-scan plots of Ca^{2+} fluorescence, were created to assess the radial propagation of calcium. More detailed analysis of spatial variations in Ca^{2+} signal morphology was analysed by comparing plots of the cytosolic CaTs in the membrane domains (CaT_m) to the central domains (CaT_c), and by extracting and analysing a number of relevant metrics that characterize CaT_m and CaT_c traces at steady state (20 min pacing). Specifically, we analyzed the rise time (measured from onset of the CaT to peak), duration at 50% decay (CD50), and amplitude, in addition to the time difference between peaks of CaT_c and CaT_m , as measured from AP onset ($\text{CaT}_{\text{delay}}$). The Ca^{2+} wave metrics and their definitions are represented schematically in Fig.III.3.

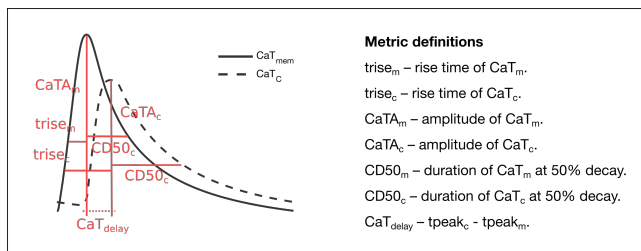


Figure III.3: Schematic representation of the defined Ca^{2+} metrics, and their definitions.

Finally, we performed correlation analysis to identify significant correlations between selected model parameters and output variables. We analysed the correlations between the maximum ion channel conductances and the Ca^{2+} metrics defined above, as well as correlations between the Ca^{2+} metrics in the membrane domains and in the central domains, and between Ca_{SR} and $[\text{Na}^+]_{\text{i}}$ and the central Ca^{2+} metrics. The correlations were determined using Kendall's tau (τ), since the variables followed discrete distributions. Significance was determined with 95% confidence, and all data analyses were performed in Matlab R2017a.

III. A novel computational model of the rabbit atrial cardiomyocyte with spatial calcium dynamics

Table III.2: Experimental values of parameters used for calibrating the population of models. (values were based on experimental data by [6], [12], [15], [31], [33]–[36]), and mean and standard deviation (std) values of the whole and calibrated PoMs.

Metric	Calibration criteria	Whole		Calibrated	
		Mean	Std	Mean	Std
APD ₉₀ (ms)	80 - 120	165	126	96	13
APD ₄₀ (ms)	20 - 60	98	91	57	6
APA (mV)	90 - 140	102	31	121	7
RMP (mV)	< -75	-57	37	-78	2
CaT-A (μ M)	0.1 - 1.0	1.0	2.9	0.30	0.05
[Na ⁺] _i (mM)	8 - 12	11.7	6.4	9.5	2.0
CaT rise time	< 100 ms	89	60	97	11
EAD	absent	38%		absent	
Alternans	absent	18%		absent	

III.3 Results

III.3.1 Population of models

Varying the maximum conductances between 25% and 400% resulted in an initial population of 3000 models with a large degree of variation in AP and CaT properties. Calibration of the population by constraining output values to the ranges in Table III.2 resulted in the selection of 16 out of 3000 models. Restricting values of APD₉₀, APD₄₀, and CaT-A was responsible for excluding the majority of models, with 175 models satisfying the requirements for these 3 parameters. Mean and standard deviation of APD₉₀, APD₄₀, APA, RMP, CaT-A, [Na⁺]_i, and CaT rise time for the whole and calibrated populations are shown in Table III.2. EAD and alternans in the whole PoM are shown as % of occurrence.

The APs and CaTs of the calibrated population are shown in Figure III.4A-B. Although the calibration step obviously reduced the variability in APs and CaTs, the maximum values of the ionic conductances retained a relatively large range of variation. Only six of the thirteen varied maximum conductances showed significantly reduced variation in the calibrated as compared to the whole population (G_{CaL}, I_{NaK}^{max}, G_{Na}, G_{Kr}, G_{Ks}, and G_{Clb}). The reduced variability in these six parameters was found to be significant (two-sample Kolmogorov-Smirnov test, $\alpha=0.05$), and the distributions are illustrated in Fig. III.5. This indicates that these ion currents affect the rabbit AP and CaT morphology to a larger extent than the other conductances, and also that these parameters are easier to constrain and identify using the considered metrics.

Fig. III.4B shows the CaT_m and CaT_c traces of the calibrated population. As expected, the Ca²⁺ signals at these two different locations showed differences in morphology, resulting from the differences in the underlying mechanisms driving the signal. The membrane signal CaT_m results from a combination of Ca²⁺ entering the cell via I_{CaL} and Ca²⁺ released from junctional CRUs, while the central signal CaT_c is the Ca²⁺ released from non-junctional CRUs via CICR as a result of Ca²⁺ diffusing from neighbouring domains. The CaT_c therefore showed a longer time to peak from onset of the AP than CaT_m, which

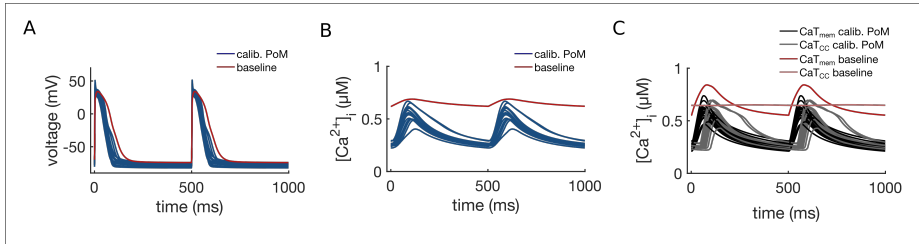


Figure III.4: Action potentials (A), whole-cell Ca^{2+} transients (B), and CaT_m and CaT_c (C) traces of the calibrated population, at 2 Hz steady pacing. The red traces represent the baseline model (unscaled maximum conductances).

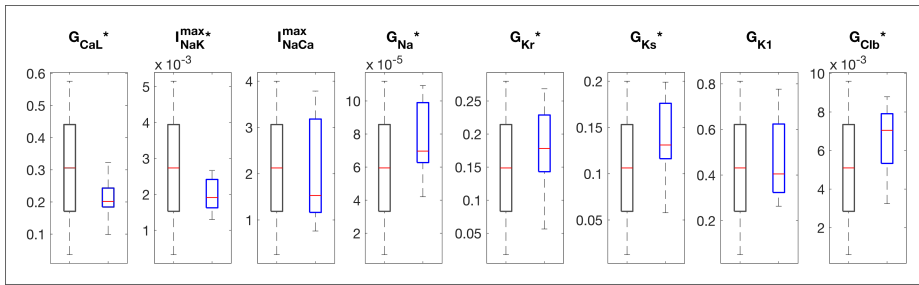


Figure III.5: Boxplots of eight of the maximum conductances. The '*' indicates distributions that were significantly altered (Kolmogorov-Smirnov test, $p\text{-val}<0.05$) after calibration of the population. Black boxes represent the whole population ($n=3000$), and blue boxes the calibrated population ($n=16$).

corresponds to the diffusion time of Ca^{2+} from the membrane to the centre of the cell.

III.3.2 Calcium dynamics and wave propagation

The values of the Ca^{2+} metrics for 16 models are shown in Table III.3. Both the rise time and CD_{50} were significantly different between the CaT_m and CaT_c traces (two-sample Kolmogorov-Smirnov test, $\alpha=0.05$), with no significant differences in the amplitudes of CaT_m and CaT_c , which is consistent with findings in control atrial CMs [6]. The CaT_c showed a shorter rise time and a longer CD_{50} than CaT_m . Furthermore, $\text{CaT}_{\text{delay}}$ in the population was 42 ± 12 ms, which matches the 52 ms time delay measured from line scans of rabbit atrial myocytes [6]. While Ca_{SR} was fairly consistent across the 16 models ($0.30\text{ }\mu\text{M}$), $[\text{Na}^+]_i$ showed a large degree of variation among models.

All 16 models of the calibrated population showed similar Ca^{2+} wave propagation patterns with physiological characteristics under normal conditions, including full regenerative propagation, delayed CaT_c , and steady Ca^{2+} transients over time. However, despite the similarities there were also measurable differences

III. A novel computational model of the rabbit atrial cardiomyocyte with spatial calcium dynamics

Table III.3: Values of the Ca^{2+} metrics for the calibrated population.

Model	trise_m (ms)	trise_c (ms)	$\text{CaT}_{\text{delay}}$ (ms)	CaTA_m (μM)	CaTA_c (μM)	CD50_m (ms)	CD50_c (ms)	$[\text{Na}^+]_i$	Ca_{SR} (μM)	
1	74	67	47	0.29	0.28	92	96	7.8	0.29	
2	88	67	40	0.24	0.28	110	96	7.8	0.29	
3	74	61	34	0.32	0.37	103	99	7.5	0.31	
4	60	62	41	0.37	0.34	9	84	98	12.5	0.30
5	72	63	38	0.35	0.32	92	98	6.9	0.30	
6	78	62	34	0.27	0.41	133	166	10.6	0.32	
7	63	67	51	0.39	0.27	71	96	10.9	0.29	
8	71	61	31	0.35	0.37	99	99	10.5	0.31	
9	72	67	50	0.29	0.28	86	96	8.9	0.29	
10	70	64	38	0.30	0.31	95	98	8.2	0.30	
11	67	63	38	0.39	0.32	85	99	11.1	0.30	
12	65	61	36	0.50	0.36	73	99	10.4	0.31	
13	89	67	48	0.25	0.27	108	96	7.6	0.28	
14	70	74	79	0.25	0.21	95	94	7.1	0.26	
15	65	63	36	0.41	0.41	99	192	12.3	0.32	
16	68	61	31	0.39	0.37	84	99	12.5	0.31	
Mean	72	64	42	0.33	0.32	94	109	9.5	0.30	
Std	8	4	12	0.07	0.06	15	28	2.0	0.02	

in the propagation patterns, as characterized by the Ca^{2+} metrics defined above and by plots of the spatio-temporal Ca^{2+} dynamics. Three representative Ca^{2+} wave propagation patterns (models 1, 15, and 7 in Table III.3) are also shown in Fig. III.6. Model #1 corresponds to a $\text{CaT}_{\text{delay}}$ very close to the average, and with similar CaTA_m and CaTA_c ; model #15 shows a shorter $\text{CaT}_{\text{delay}}$, and slowed CaT_c decay ; and model #7, in turn, showed a slightly longer $\text{CaT}_{\text{delay}}$, but a damping of CaT_c .

III.3.3 Correlation analysis

We next analyzed the correlations between the maximum conductances of individual currents and the Ca^{2+} metrics defined in Fig. III.3. The results are summarized in Table III.4, where significant correlation coefficients ($p\text{-value}<0.05$) are highlighted in bold. Our analyses reveal that the Ca^{2+} wave properties of these 16 models were primarily sensitive to G_{CaL} , I_{NaCa}^{\max} , and I_{NaK}^{\max} . The L-type Ca^{2+} channel conductance G_{CaL} showed a negative correlation with CD50_m , but not the amplitudes CaTA_m and CaTA_c . I_{NaCa}^{\max} showed significant correlation with trise_m , CaTA_m , and CD50_m , where a larger I_{NaCa}^{\max} negatively correlated with trise_m , which is expected given role of IN_{CX} in Ca^{2+} extrusion. However, I_{NaCa}^{\max} did not affect $\text{CaT}_{\text{delay}}$. Finally, we found I_{NaK}^{\max} to be negatively correlated with CaTA_c and CD50_c , indicating that a larger I_{NaK} current resulted in a smaller CaT_c signal.

The correlation among the seven Ca^{2+} metrics , $[\text{Na}^+]_i$, and Ca_{SR} are compiled in Table III.5, with significant correlation coefficients ($p\text{-value}<0.05$) highlighted in bold. We observe that $\text{CaT}_{\text{delay}}$ which was not sensitive to any of the ion current conductances, was strongly correlated with Ca_{SR} . We also found $[\text{Na}^+]_i$ to be correlated with trise_m , and CaTA_m . Furthermore, we observe that the individual Ca^{2+} metrics related to CaT_m and CaT_c were in general not correlated, except for CaTA_m which was correlated with trise_c , and CD50_c , while $\text{CaT}_{\text{delay}}$ was strongly correlated with all CaT_c properties, trise_c , CaTA_c ,

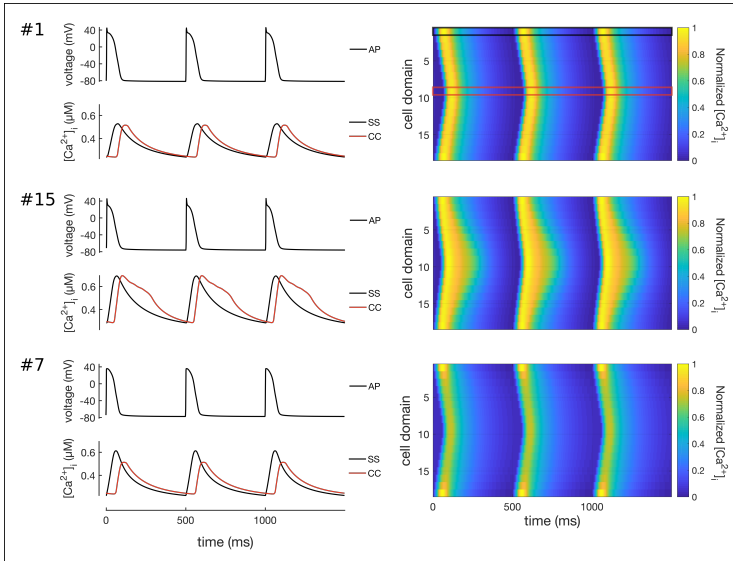


Figure III.6: Simulation of Ca^{2+} waves in three representative models of the selected population. Traces on left hand-side show the APs (top), and CaTs (bottom) at the membrane (black lines) and centre of cell (red lines). The right hand-side of the Figure shows line scans of propagating Ca^{2+} waves in three consecutive beats at 2 Hz pacing. The lines on the top-right panel show the locations where the CaT traces were recorded. Model #1 shows a propagating Ca^{2+} wave where CaT_m and CaT_c have rather similar morphologies; model #15 shows a Ca^{2+} wave with slightly larger $\text{CaT}_{\text{delay}}$; and model #7 shows a wave patterns with decreased CaTA_c as compared to CaTA_m .

and CD50_c . The three Ca^{2+} metrics t_{rise} , CD50 , and amplitude, were correlated for both CaT_m and CaT_c , as expected (data not shown).

III. A novel computational model of the rabbit atrial cardiomyocyte with spatial calcium dynamics

Table III.4: Kendall's τ and p-values between maximum conductances and CaT_m and CaT_c properties.

Parameters	trise _m		trise _c		CaT _{delay}		CaTA _m	
	τ	p-val	τ	p-val	τ	p-val	τ	p-val
G_{CaL}	-0.33	0.086	0.13	0.52	0.31	0.11	0.30	0.12
G_{CaT}	0.093	0.65	0.13	0.52	0.10	0.62	-0.25	0.19
G_{NaK}	0.14	0.47	0.27	0.17	0.31	0.11	-0.20	0.31
$I_{\text{NaCa}}^{\text{max}}$	-0.72	0.0001	-0.079	0.71	0.10	0.62	0.45	0.015
G_{Na}	-0.19	0.32	-0.044	0.85	-0.051	0.82	0.22	0.27
G_{to}	-0.11	0.59	0.13	0.52	0.10	0.62	0.10	0.63
G_{Kr}	-0.16	0.42	-0.11	0.58	0.017	0.96	0.13	0.51
G_{Ks}	-0.21	0.28	0.13	0.52	0.19	0.34	0.0	1.0
G_{K1}	-0.36	0.058	0.062	0.78	0.17	0.39	0.15	0.45
G_{CaP}	0.30	0.12	-0.027	0.93	-0.068	0.75	-0.30	0.12
G_{Cab}	-0.13	0.53	-0.22	0.27	-0.14	0.50	0.10	0.63
G_{Nab}	0.093	0.65	-0.34	0.082	-0.31	0.11	-0.083	0.69
G_{Clb}	-0.30	0.12	0.20	0.31	0.29	0.13	0.10	0.63
Parameters	CaTA _c		CD50 _m		CD50 _c			
	τ	p-val	τ	p-val	τ	p-val		
G_{CaL}	-0.23	0.23	-0.51	0.0076	-0.21	0.31		
G_{CaT}	-0.18	0.35	0.10	0.62	-0.25	0.23		
G_{NaK}	-0.43	0.020	-0.14	0.50	-0.54	0.007		
$I_{\text{NaCa}}^{\text{max}}$	-0.050	0.82	-0.75	0.0001	-0.045	0.85		
G_{Na}	0.017	0.97	-0.15	0.44	0.082	0.71		
G_{to}	-0.13	0.51	-0.12	0.56	-0.082	0.71		
G_{Kr}	-0.033	0.89	-0.22	0.26	-0.064	0.78		
G_{Ks}	-0.033	0.89	-0.17	0.39	-0.064	0.78		
G_{K1}	-0.083	0.69	-0.27	0.16	-0.12	0.58		
G_{CaP}	0.067	0.76	0.27	0.16	-0.10	0.64		
G_{Cab}	0.10	0.63	-0.24	0.22	0.064	0.78		
G_{Nab}	0.15	0.45	-0.017	0.96	0.12	0.58		
G_{Clb}	-0.20	0.31	-0.085	0.68	-0.17	0.40		

Table III.5: Kendall's τ and p-values for correlations between CaT_m properties, $[\text{Na}^+]_i$, and Ca_{SR} , and CaT_c properties.

Parameters	trise _c		CaTA _c		CD50 _c		CaT _{delay}	
	τ	p-val	τ	p-val	τ	p-val	τ	p-val
trise _m	0.18	0.38	-0.093	0.65	-0.15	0.49	0.0	1.0
CaTA _m	-0.41	0.035	0.33	0.08	0.43	0.03	-0.27	0.16
CD50 _m	0.081	0.71	0.10	0.62	0.10	0.64	-0.16	0.44
CaT _{delay}	0.79	0.0001	-0.77	0.0001	-0.77	0.0001	1	0
$[\text{Na}^+]_i$	-0.34	0.082	0.37	0.052	0.41	0.041	-0.26	0.19
Ca_{SR}	-0.79	0.0001	1.0	0.0	0.88	0.00	-0.77	0.0001

III.4 Discussion

We have developed a model of a healthy atrial CM with rabbit-specific EP and spatially distributed Ca^{2+} dynamics. The central motivation for developing the model was to be able to describe radial diffusion of calcium, which is important for the investigation of the effects of asynchronous Ca^{2+} release on arrhythmic activity in atrial myocytes lacking T-tubules. We used a PoM approach to parameterize the maximum conductances of sarcolemmal ion currents to match model outputs to reported experimental data from the rabbit atria. The result was a population of 16 models that were all consistent with observed experimental values, but still recapitulated observed variability in Ca^{2+} wave characteristics.

The small number of models selected by the experimental calibration shows that imposing a sufficiently large number of constraints in model outputs

(in this case, 8 parameters) can reduce the parameter space to discrete sets of parametrizations, each following a unique trajectory. We also show that significantly different parameter combinations can result in models with very similar behaviors (see Fig.III.4 and Table III.8, highlighting the non-uniqueness of CM models, a consequence of the compensatory effects of ionic currents [42]–[44]. Nonetheless, the calibration step significantly reduced the variability in six of the maximum conductances, as seen in Fig. III.5, indicating that the electrophysiology and Ca^{2+} metrics used in the experimental calibration were, in general, sensitive to these maximum conductances.

It is worth noting that the data used here to constrain the model were obtained from a large assortment of published experimental data. Therefore, the 16 models selected reflect not only the natural variability observed within different atrial regions, but also experimental uncertainties inherent to methodologies used by different research groups. The PoM-based approach we used here contrasts with the more standard approach, wherein a computational model is fitted to a small set of experimental observations, often obtained from a single atrial region, to yield a single model parametrization that captures the average behavior in the experimental data. Although useful for assessing the mechanisms underlying general characteristic behaviors of the model, the single-parameter approach lacks the ability to reproduce experimental observations from a range of data. In contrast, incorporating variability into the model via the PoM-based approach employed here allows a generalization of model results to a wider set of conditions and phenotypes.

III.4.1 Correlation analysis

The seven extracted Ca^{2+} metrics from CaT_m and CaT_c quantify differences in the Ca^{2+} wave properties across the 16 models. Correlation analysis showed that G_{CaL} and I_{NaCa}^{\max} and I_{NaK}^{\max} were the only maximum conductances significantly affecting Ca^{2+} wave propagation in the model. This result is consistent with the known role of these ionic currents in intracellular Ca^{2+} regulation. For instance, experimental observations have shown the role of increased sarcolemmal Ca^{2+} in modulating the regenerative propagation of the Ca^{2+} signal towards the inner locations of the cell [25].

The strong correlation between I_{NaCa}^{\max} and CaT_m metrics indicates a strong modulating effect of I_{NCX} on Ca^{2+} dynamics at the cell membrane. The importance of the role of I_{NCX} on modulation of Ca^{2+} dynamics during the AP is well documented both experimentally, and through computational simulations [45]–[47]. Furthermore, since I_{NaK} affects $[\text{Na}^+]_i$ homeostasis, which in turn affects I_{NCX} function, it is not surprising that I_{NaK} was correlated with CaTA_c and $CD50_c$. However, it is somewhat unexpected that I_{NaK} was more strongly correlated to the CaT_c than to CaT_m properties.

The observed correlations between CaTA_m and trise_c and $CD50_c$ indicates that the rate of Ca^{2+} release and uptake in the CRUs is modulated to some extent by the amount of Ca^{2+} that enters the membrane and initiates CICR. We also observed that $\text{CaT}_{\text{delay}}$ was correlated to trise_c , CaTA_c , and $CD50_c$, which

III. A novel computational model of the rabbit atrial cardiomyocyte with spatial calcium dynamics

indicates that the velocity of Ca^{2+} wave propagation was mostly modulated by the dynamics of the regenerative propagation of the Ca^{2+} signal along CRUs, and not by the amount of Ca^{2+} entering via the cell membrane. $\text{CaT}_{\text{delay}}$ measures the time for the Ca^{2+} wave to propagate to the innermost cell domains which depends on the strength and rate of the regenerative CICR. This also determines the shape of the local CaTs in each inner domains. Therefore, it is expected that $\text{CaT}_{\text{delay}}$ co-varies with the CaT_c properties, but not with the CaT_m properties.

The observation that $\text{CaT}_{\text{delay}}$ strongly correlated with Ca_{SR} is not unexpected, since a higher SR Ca^{2+} load would naturally promote a faster rise of the CaT at inner domains (smaller trise_c), and thus reduce $\text{CaT}_{\text{delay}}$, while simultaneously promoting a longer CaT duration (larger CD50_c). The observed correlation between Ca^{2+} metrics and $[\text{Na}^+]_i$ is also expected since $[\text{Na}^+]_i$ plays a significant role in the modulation of NCX function, and therefore in the regulation of the sub-sarcolemmal Ca^{2+} signal [45]–[47].

Overall the results of the correlation analyses presented here are in good agreement with our understanding of Ca^{2+} handling dynamics in atrial CMs, and provide additional insight into the mechanisms driving Ca^{2+} wave propagation in the newly developed model taking into account population variability.

III.4.2 Limitations and future directions

It is important to note that the conclusions derived from the analyses presented here are limited by the experimental data that was used in the calibration of the population. In particular, the lack of quantitative measurements of intracellular Ca^{2+} makes it difficult to validate the model predictions of the spatial characteristics of the Ca^{2+} dynamics. The correlation analysis used in this paper also has its own limitations and assumptions. For instance, simultaneously varying parameters to build the population can lead to interaction effects, which can mask the individual contributions of each varied parameter. The analysis presented here can be extended by, for example, determining multivariate correlations. Increasing sample size would allow to perform a more robust analysis of correlations in the population, and a way to achieve this would be by constructing new models by perturbing the parameters around the values that originated the 16 models.

Furthermore, the developed pool of normal rabbit atrial CM models can be used to study the effects of altered Ca^{2+} handling mechanisms, such as SR Ca^{2+} content, release and uptake on the dynamics of arrhythmogenic Ca^{2+} waves. The deterministic RyR model used in this study assumes homogeneous distribution and behavior of CRUs long the longitudinal axis of the cell, Therefore, this simplification does not allow to simulate stochastic Ca^{2+} release events and subcellular fluctuations in calcium-handling proteins, which may influence the results [48].

It would also be relevant to improve the model by including the calcium-dependent component of the chloride current, which has been shown to be involved in APD alternans in rabbit atria [31]. and could therefore potentially affect Ca^{2+} wave propagation dynamics. Future work could also address the

effects of AF-induced remodelling on Ca^{2+} wave propagation, and in particular look at the role of RyRs and Sercal2a parameters in abnormal behaviors such as failed Ca^{2+} propagation, Ca^{2+} alternans, and afterdepolarisations.

III.5 Conclusions

This paper presented a novel model of the rabbit atrial myocyte, and provides a framework for analysing cardiac cell models based on correlation analysis. We have shown that the model is able to reproduce experimentally observed physiological Ca^{2+} wave propagation patterns. These differences were directly linked to two Ca^{2+} currents, I_{CaL} , and I_{NCX} . However, the study also showed the Ca^{2+} wave patterns to be a complex interplay among different components, including Ca_{SR} and $[\text{Na}^+]_i$.

The spatial Ca^{2+} description in the model, along with the methodology presented here can be used as a tool to study sub-cellular mechanisms, and their implication in the arrhythmogenesis in diseased condition, such as atrial fibrillation. This work can therefore be extended to assess such mechanisms under altered conditions, such as electrical remodelling. In particular, the framework can be useful for querying the drivers of arrhythmogenic Ca^{2+} cycling, such as Ca^{2+} alternans, and to formulate hypothesis on new targets to restore normal cell function.

Acknowledgments

This project has received funding from the European Union's Horizon 2020 MSCA ITN under grant agreement No 675351.

Appendix III.A Na^+ - Ca^{2+} exchanger model

$$I_{NCX} = I_{NCX}^{max} \cdot \frac{1}{1 + \left(\frac{k_{dact}}{Ca_i}\right)^2} \cdot \frac{e^{\frac{\nu V_m F}{RT}} \cdot Ca_o \cdot Na_i^3 - e^{\frac{(\nu-1) V_m F}{RT}} \cdot Na_o^3 \cdot Ca_i}{Km_{Ca_i} \cdot Na_o^3 \left(1 + \left(\frac{Na_i}{Km_{Na_i}}\right)^3\right)} \cdot \frac{1}{1 + k_{sat} \cdot e^{\frac{(\nu-1) V_m F}{RT}}} \\ + Km_{Na_o}^3 \cdot Ca_i \cdot \left(1 + \frac{Ca_i}{Km_{Ca_i}}\right) \\ + (Km_{Ca_o} + Ca_o) \cdot Na_i^3 + Na_o^3 \cdot Ca_i$$

$$I_{NCX}^{max} = 4.41 \text{ pA/pF}$$

$$k_{dact} = 0.384 \times 10^{-3} \mu\text{M}$$

$$Km_{Ca_i} = 3.59 \times 10^{-3} \mu\text{M}$$

$$Km_{Ca_o} = 1.3 \text{ mM}$$

$$Km_{Na_i} = 12.29 \text{ mM}$$

$$Km_{Na_o} = 87.5 \text{ mM}$$

$$\nu = 0.35$$

$$k_{sat} = 0.27$$

III. A novel computational model of the rabbit atrial cardiomyocyte with spatial calcium dynamics

Appendix III.B Serca2a model

$$J_{Serc} = V_{max} \cdot \frac{\left(\frac{Ca_i}{Kmf}\right)^{nh} - \left(\frac{Ca_{SR}}{Kmr}\right)^{nh}}{1 + \left(\frac{Ca_i}{Kmf}\right)^{nh} + \left(\frac{Ca_{SR}}{Kmr}\right)^{nh}}$$

$$V_{max} = 5.3 \times 10^{-3} \text{ mM/s}$$

$$Kmf = 0.000625 \text{ mM}$$

$$Kmr = 1.0 \text{ mM}$$

$$nh = 1.787$$

Appendix III.C Ca²⁺ buffers

Buffers are modelled using a two-state model:

$$\frac{dC_B}{dt} = k_{on}C(B_{max} - C_B) - k_{off}C_B$$

where B_{max} is the maximum buffer capacity, C and Ca_B represent the concentration of free and bound ligand, and k_{on} and k_{off} are the rate coefficients of ion-buffer complex formation and dissociation, respectively.

Table III.6: Buffer parameters.

Buffer	Compartment	Bmax (μM)	kon (/s)	koff (/μMs)
Troponin C High (Ca ²⁺)	cytosol	140E-3	2.37	3.2E-5
Troponin C High (Mg ²⁻)	cytosol	140E-3	3E-3	3.33E-3
Troponin C Low	cytosol	70E-3	163.5	98E-3
Calmodulin	cytosol	2.4E-3	34	238E-3
Myosin (Ca)	cytosol	140E-3	13.8	4.6E-4
Myosin (Mg)	cytosol	140E-3	0.0157	5.7E-5
SR	cytosol	17.1E-3	100	6E-2
SLlow	SL	37.4E-3 · $\frac{v_{myo}}{v_{SL}}$	100	1.3
SLlow	junc	4.6E-4 · $\frac{v_{myo}}{v_{junc}}$	100	1.3
SLhigh	SL	13.4E-3 · $\frac{v_{myo}}{v_{SL}}$	100	3E-2
SLhigh	junc	1.65E-4 · $\frac{v_{myo}}{v_{junc}}$	100	3E-2
Calsequestrin	SR	140E-3 · $\frac{v_{myo}}{v_{SR}}$	100	65
Na ⁺	SL	7.561	1.0E-4	1.0E-3
Na ⁺	junc	1.65	1.0E-4	1.0E-3

Appendix III.D Initial conditions

Table III.7: Initial concentrations of the ionic species in the different compartments of the model.

Ionic traces	Initial concentration	Description
Ca _{cyt}	0.21 μM	Ca ²⁺ concentration in the cytosol.
Ca _{junc}	0.073 μM	Ca ²⁺ concentration in the junctional domain of the SS space.
Ca _{s1}	0.23 μM	Ca ²⁺ concentration in the sarcolemmal domain of the SS space.
Ca _{SR}	0.25 μM	Luminal Ca ²⁺ concentration in the sarcoplasmic reticulum.
Ca _{SRS}	0.073 μM	Ca ²⁺ concentration in the sub SR space.
Na _{cyt}	11.3 mM	Na ⁺ concentration in the cytosol (2Hz).
Na _{junc}	11.3 mM	Na ⁺ concentration in the junctional domain of the SS space.
Na _{sL}	11.3 mM	Na ⁺ concentration in the sarcolemmal domain of the SS space.
K _{cyt}	120 mM	K ⁺ concentration in the cytosol.
Cl _{cyt}	30 mM	Cl ⁻ concentration in the cytosol.
Ca _o	1.8 mM	Extracellular Ca ²⁺ concentration.
Na _o	140 mM	Extracellular Na ⁺ concentration.
K _o	5.4 mM	Extracellular K ⁺ concentration.
Cl _o	132 mM	Extracellular Cl ⁻ concentration.

Appendix III.E Selected population

Table III.8: Parameter values of the 16 models of the calibrated population.

G _{CaL}	G _{CaT}	I _{NaK} ^{ext}	I _{NaCa} ^{ext}	G _{Na}	G _{to}	G _{Kr}	G _{Ks}	G _{K1}	I _{CaP} ^{ext}	G _{Cab}	G _{Nab}	G _{C1b}
0.228	0.415	2.449 E-3	1.436	0.088 E-3	0.712	0.120	0.174	0.623	0.589	0.970 E-3	0.398 E-3	6.392 E-3
0.146	0.474	1.801 E-3	1.162	0.068 E-3	0.606	0.056	0.119	0.333	0.246	0.506 E-3	0.623 E-3	7.647 E-3
0.192	0.069	2.425 E-3	1.073	0.068 E-3	0.443	0.268	0.058	0.277	0.401	1.348 E-3	0.885 E-3	5.078 E-3
0.202	0.437	1.651 E-3	3.314	0.060 E-3	0.492	0.176	0.178	0.673	0.403	1.024 E-3	0.612 E-3	8.786 E-3
0.295	0.124	2.573 E-3	1.165	0.071 E-3	0.790	0.248	0.199	0.263	0.244	0.348 E-3	0.631 E-3	5.742 E-3
0.099	0.147	1.320 E-3	0.762	0.063 E-3	0.155	0.135	0.182	0.344	0.466	1.022 E-3	0.772 E-3	4.047 E-3
0.256	0.156	1.892 E-3	3.786	0.050 E-3	0.354	0.193	0.155	0.777	0.067	1.033 E-3	0.143 E-3	6.964 E-3
0.189	0.406	1.599 E-3	1.313	0.064 E-3	0.435	0.181	0.084	0.697	0.582	0.482 E-3	0.944 E-3	5.345 E-3
0.222	0.325	2.366 E-3	2.012	0.104 E-3	0.449	0.209	0.122	0.625	0.399	1.594 E-3	0.221 E-3	5.321 E-3
0.189	0.431	2.100 E-3	1.532	0.042 E-3	0.514	0.205	0.113	0.432	0.220	1.360 E-3	0.176 E-3	7.643 E-3
0.231	0.038	1.602 E-3	3.161	0.073 E-3	0.604	0.142	0.174	0.299	0.120	0.524 E-3	0.405 E-3	7.133 E-3
0.322	0.388	2.407 E-3	3.200	0.109 E-3	0.558	0.262	0.121	0.414	0.315	0.949 E-3	1.570 E-3	8.421 E-3
0.180	0.458	1.934 E-3	1.081	0.062 E-3	0.162	0.144	0.062	0.314	0.455	0.312 E-3	0.851 E-3	7.995 E-3
0.293	0.204	2.671 E-3	1.528	0.104 E-3	0.729	0.262	0.181	0.396	0.505	0.173 E-3	1.228 E-3	7.827 E-3
0.201	0.305	1.302 E-3	1.882	0.105 E-3	0.699	0.161	0.133	0.531	0.263	0.471 E-3	0.112 E-3	8.358 E-3
0.155	0.329	1.775 E-3	3.535	0.094 E-3	0.574	0.146	0.129	0.380	0.339	1.410 E-3	1.373 E-3	3.252 E-3

References

- [1] Heijman, J., Erfanian Abdoust, P., Voigt, N., Nattel, S., and Dobrev, D., “Computational models of atrial cellular electrophysiology and calcium handling, and their role in atrial fibrillation”, *The Journal of physiology*, vol. 594, no. 3, pp. 537–553, Feb. 2016.
- [2] Vagos, M., Herck, I. G. M. van, Sundnes, J., Arevalo, H. J., Edwards, A. G., and Koivumäki, J. T., “Computational modeling of electrophysiology and pharmacotherapy of atrial fibrillation: Recent advances and future challenges”, *Frontiers in Physiology*, vol. 9, p. 1221, 2018.

III. A novel computational model of the rabbit atrial cardiomyocyte with spatial calcium dynamics

- [3] Ravelli, F. and Allessie, M., “Effects of atrial dilatation on refractory period and vulnerability to atrial fibrillation in the isolated langendorff-perfused rabbit heart”, *Circulation*, vol. 96, no. 5, pp. 1686–1695, 1997.
- [4] Eijsbouts, S. C., Majidi, M., Zandvoort, M. v., and Allessie, M. A., “Effects of acute atrial dilation on heterogeneity in conduction in the isolated rabbit heart”, *Journal of Cardiovascular Electrophysiology*, vol. 14, no. 3, pp. 269–278, 2003.
- [5] Rouge, L., Yoho, J., Hayes, K., Herling, I., Gambert, S., Ostrander, G. K., and Mower, M. M., “47 ineffectiveness of acetylcholine for induction of atrial fibrillation in rabbits.”, *Journal of Investigative Medicine*, vol. 54, no. 1, S264–S264, 2006.
- [6] Greiser, M., Kerfant, B.-G., Williams, G. S., Voigt, N., Harks, E., Dibb, K. M., Giese, A., Meszaros, J., Verheule, S., Ravens, U., Allessie, M. A., Gammie, J. S., Velden, J. van der, Lederer, W. J., Dobrev, D., and Schotten, U., “Tachycardia-induced silencing of subcellular Ca^{2+} signaling in atrial myocytes”, *The Journal of Clinical Investigation*, vol. 124, no. 11, pp. 4759–4772, Nov. 2014.
- [7] Li, H., Scherlag, B. J., Kem, D. C., Zillner, C., Male, S., Thirunavukkarasu, S., Shen, X., Benbrook, A., Pitha, J. V., Lazzara, R., and Yu, X., “The propensity for inducing atrial fibrillation: A comparative study on old versus young rabbits”, *Journal of Aging Research*, vol. 2014, 2014.
- [8] Wang, H. L., Zhou, X. H., Li, Z. Q., Fan, P., Zhou, Q. N., Li, Y. D., Hou, Y. M., and Tang, B. P., “Prevention of atrial fibrillation by using sarcoplasmic reticulum calcium atpase pump overexpression in a rabbit model of rapid atrial pacing”, *Medical science monitor : international medical journal of experimental and clinical research*, vol. 23, pp. 3952–3960, Aug. 2017.
- [9] Frommeyer, G., Wolfes, J., Ellermann, C., Kochhäuser, S., Dechering, D. G., and Eckardt, L., “Acute electrophysiologic effects of the polyphenols resveratrol and piceatannol in rabbit atria”, *Clinical and Experimental Pharmacology and Physiology*, vol. 46, no. 1, pp. 94–98, 2019.
- [10] Hilgemann, D. W. and Noble, D., “Excitation-contraction coupling and extracellular calcium transients in rabbit atrium: Reconstruction of basic cellular mechanisms”, *Proceedings of the Royal Society of London. Series B. Biological Sciences*, vol. 230, no. 1259, pp. 163–205, 1987.
- [11] Demir, S. S., Clark, J. W., Murphey, C. R., and Giles, W. R., “A mathematical model of a rabbit sinoatrial node cell”, *American Journal of Physiology-Cell Physiology*, vol. 266, no. 3, pp. C832–C852, 1994, PMID: 8166247.
- [12] Lindblad, D., Murphey, C., Clark, J., and Giles, W., “A model of the action potential and underlying membrane currents in a rabbit atrial cell”, *The American journal of physiology*, vol. 271, H1666–96, Nov. 1996.

- [13] Demir, S. S., Clark, J. W., and Giles, W. R., “Parasympathetic modulation of sinoatrial node pacemaker activity in rabbit heart: A unifying model”, *American Journal of Physiology-Heart and Circulatory Physiology*, vol. 276, no. 6, H2221–H2244, 1999, PMID: 29592423.
- [14] Shannon, T. R., Wang, F., Puglisi, J., Weber, C., and Bers, D. M., “A Mathematical Treatment of Integrated Ca Dynamics within the Ventricular Myocyte”, *Biophysical Journal*, vol. 87, no. 5, pp. 3351–3371, 2004.
- [15] Aslanidi, O., Boyett, M., Dobrzynski, H., Li, J., and Zhang, H., “Mechanisms of transition from normal to reentrant electrical activity in a model of rabbit atrial tissue: Interaction of tissue heterogeneity and anisotropy”, *Biophysical journal*, vol. 96, pp. 798–817, Feb. 2009.
- [16] Mahajan, A., Shiferaw, Y., Sato, D., Baher, A., Olcese, R., Xie, L.-H., Yang, M.-J., Chen, P.-S., Restrepo, J. G., Karma, A., Garfinkel, A., Qu, Z., and Weiss, J. N., “A rabbit ventricular action potential model replicating cardiac dynamics at rapid heart rates”, *Biophysical Journal*, vol. 94, no. 2, pp. 392–410, 2008.
- [17] Tidball, J., Cederdahl, J., and Bers, D., “Quantitative analysis of regional variability in the distribution of transverse tubules in rabbit myocardium”, *Cell and tissue research*, vol. 264, pp. 293–8, Jun. 1991.
- [18] Blatter, L. A., “The intricacies of atrial calcium cycling during excitation-contraction coupling”, *The Journal of General Physiology*, vol. 149, no. 9, pp. 857–865, 2017.
- [19] Smyrnias, I., Mair, W., Harzheim, D., Walker, S. A., Roderick, H. L., and Bootman, M. D., “Comparison of the T-tubule system in adult rat ventricular and atrial myocytes, and its role in excitation–contraction coupling and inotropic stimulation”, *Cell Calcium*, vol. 47, no. 3, pp. 210–223, 2010.
- [20] Coombes, S. and Timofeeva, Y., “Sparks and waves in a stochastic fire-diffuse-fire model of Ca^{2+} release.”, *Phys Rev E Stat Nonlin Soft Matter Phys*, vol. 68, no. 2 Pt 1, p. 021915, Aug. 2003.
- [21] Bootman, M. D., Smyrnias, I., Rüdiger, Coombes, S., and Roderick, H. L., “Atrial cardiomyocyte calcium signalling”, *Biochimica et Biophysica Acta (BBA) - Molecular Cell Research*, vol. 1813, no. 5, pp. 922–934, 2011, Including the Special Section: 11th European Symposium on Calcium.
- [22] Bootman, M. D., Berridge, M. J., and Roderick, H., “Calcium signalling: More messengers, more channels, more complexity”, *Current Biology*, vol. 12, no. 16, R563–R565, 2002.
- [23] Hüser, J., Lipsius, S. L., and Blatter, L. A., “Calcium gradients during excitation-contraction coupling in cat atrial myocytes.”, *The Journal of Physiology*, vol. 494, no. 3, pp. 641–651, 1996.

III. A novel computational model of the rabbit atrial cardiomyocyte with spatial calcium dynamics

- [24] Blatter, L. A., Kockskamper, J., Sheehan, K. A., Zima, A. V., Huser, J., and Lipsius, S. L., “Local calcium gradients during excitation-contraction coupling and alternans in atrial myocytes.”, *J Physiol*, vol. 546, no. Pt 1, pp. 19–31, 2003.
- [25] Mackenzie, L., Roderick, H. L., Berridge, M. J., Conway, S. J., and Bootman, M. D., “The spatial pattern of atrial cardiomyocyte calcium signalling modulates contraction”, *Journal of Cell Science*, vol. 117, no. 26, pp. 6327–6337, 2004.
- [26] Trafford, A. W., Clarke, J. D., Richards, M. A., Eisner, D. A., and Dibb, K. M., “Calcium signalling microdomains and the t-tubular system in atrial myocytes: Potential roles in cardiac disease and arrhythmias.”, *Cardiovasc Res*, vol. 98, no. 2, pp. 192–203, May 2013.
- [27] Thul, R., Coombes, S., Roderick, H. L., and Bootman, M. D., “Subcellular calcium dynamics in a whole-cell model of an atrial myocyte”, *Proceedings of the National Academy of Sciences*, vol. 109, no. 6, pp. 2150–2155, 2012.
- [28] Shinohara, T., Joung, B., Kim, D., Maruyama, M., Luk, H.-N., Chen, P.-S., and Lin, S.-F., “Induction of atrial ectopic beats with calcium release inhibition: Local hierarchy of automaticity in the right atrium”, *Heart rhythm*, vol. 7, no. 1, pp. 110–116, Jan. 2010.
- [29] Campos, F. O., Shiferaw, Y., and Plank, G., “Tissue structure and Ca^{2+} -mediated ectopic beats”, *Biomedizinische Technik. Biomedical engineering*, vol. 58 Suppl 1, no. Suppl 1, Aug. 2013.
- [30] Voigt, N., Heijman, J., Qiongling, Chiang, D. Y., Li, N., Karck, M., Wehrens, X. H., Nattel, S., and Dobrev, D., “Cellular and molecular mechanisms of atrial arrhythmogenesis in patients with paroxysmal atrial fibrillation”, *Circulation*, vol. 129, no. 2, pp. 145–156, 2014.
- [31] Kanaporis, G. and Blatter, L. A., “Calcium-activated chloride current determines action potential morphology during calcium alternans in atrial myocytes”, *The Journal of Physiology*, vol. 594, no. 3, pp. 699–714, 2016.
- [32] Weber, C. R., Ginsburg, K. S., Philipson, K. D., Shannon, T. R., and Bers, D. M., “Allosteric regulation of Na/Ca exchange current by cytosolic Ca in intact cardiac myocytes”, *The Journal of general physiology*, vol. 117, no. 2, pp. 119–131, Feb. 2001.
- [33] Qi, A., Yeung-Lai-Wah, J. A., Xiao, J., and Kerr, C. R., “Regional differences in rabbit atrial repolarization: Importance of transient outward current”, *American Journal of Physiology-Heart and Circulatory Physiology*, vol. 266, no. 2, H643–H649, 1994, PMID: 8141365.
- [34] Muraki, K., Imaizumi, Y., Watanabe, M., Habuchi, Y., and Giles, W. R., “Delayed rectifier K^+ current in rabbit atrial myocytes”, *American Journal of Physiology-Heart and Circulatory Physiology*, vol. 269, no. 2, H524–H532, 1995, PMID: 7653616.

- [35] Wang, Z., Fermini, B., Feng, J., and Nattel, S., “Role of chloride currents in repolarizing rabbit atrial myocytes”, *American Journal of Physiology-Heart and Circulatory Physiology*, vol. 268, no. 5, H1992–H2002, 1995, PMID: 7771549.
- [36] Hou, J.-W., Li, W., Fei, Y.-D., Chen, Y.-H., Wang, Q., Wang, Y.-P., and Li, Y.-G., “ I_{CaL} and I_{to} mediate rate-dependent repolarization in rabbit atrial myocytes”, *Journal of Physiology and Biochemistry*, vol. 74, no. 1, pp. 57–67, 2018.
- [37] Amrita, X., Christini, D. J., and Sobie, E. A., “Exploiting mathematical models to illuminate electrophysiological variability between individuals.”, *J Physiol*, vol. 590, no. 11, pp. 2555–2567, 2012.
- [38] Sánchez, C., Bueno-Orovio, A., Wettwer, E., Loose, S., Simon, J., Ravens, U., Pueyo, E., and Rodriguez, B., “Inter-subject variability in human atrial action potential in sinus rhythm versus chronic atrial fibrillation”, *PLOS ONE*, vol. 9, no. 8, pp. 1–14, Aug. 2014.
- [39] Yamashita, T., Nakajima, T., Hazama, H., Hamada, E., Murakawa, Y., Sawada, K., and Omata, M., “Regional differences in transient outward current density and inhomogeneities of repolarization in rabbit right atrium”, *Circulation*, vol. 92, no. 10, pp. 3061–3069, 1995.
- [40] Mackenzie, L., Bootman, M. D., Berridge, M. J., and Lipp, P., “Predetermined recruitment of calcium release sites underlies excitation-contraction coupling in rat atrial myocytes.”, *J Physiol*, vol. 530, no. Pt 3, pp. 417–429, Feb. 2001.
- [41] Voigt, N., Li, N., Wang, Q., Wang, W., Trafford, A. W., Abu-Taha, I., Sun, Q., Wieland, T., Ravens, U., Nattel, S., Wehrens, X. H., and Dobrev, D., “Enhanced sarcoplasmic reticulum Ca^{2+} leak and increased Na^+-Ca^{2+} exchanger function underlie delayed afterdepolarizations in patients with chronic atrial fibrillation”, *Circulation*, vol. 125, no. 17, pp. 2059–2070, 2012.
- [42] Sarkar, A. X. and Sobie, E. A., “Regression Analysis for Constraining Free Parameters in Electrophysiological Models of Cardiac Cells”, *PLOS Computational Biology*, vol. 6, no. 9, pp. 1–11, Sep. 2010.
- [43] Zaniboni, M., “3D current-voltage-time surfaces unveil critical repolarization differences underlying similar cardiac action potentials: A model study”, *Mathematical Biosciences*, vol. 233, no. 2, pp. 98–110, 2011.
- [44] Muszkiewicz, A., Liu, X., Bueno-Orovio, A., Lawson, B. A. J., Burrage, K., Casadei, B., and Rodriguez, B., “From ionic to cellular variability in human atrial myocytes: An integrative computational and experimental study”, *American Journal of Physiology-Heart and Circulatory Physiology*, vol. 314, no. 5, H895–H916, 2018, PMID: 29351467.

III. A novel computational model of the rabbit atrial cardiomyocyte with spatial calcium dynamics

- [45] Hilgemann, D. W., Matsuoka, S., Nagel, G. A., and Collins, A., “Steady-state and dynamic properties of cardiac sodium-calcium exchange. sodium-dependent inactivation.”, *J Gen Physiol*, vol. 100, no. 6, pp. 905–932, Dec. 1992.
- [46] Sher, A. A., Noble, P. J., Hinch, R., Gavaghan, D. J., and Noble, D., “The role of the $\text{Na}^+/\text{Ca}^{2+}$ exchangers in Ca^{2+} dynamics in ventricular myocytes.”, *Prog Biophys Mol Biol*, vol. 96, no. 1-3, pp. 377–398, Jan. 2008.
- [47] Xie, Y., Liao, Z., Grandi, E., Shiferaw, Y., and Bers, D. M., “Slow $[\text{na}]_i$ changes and positive feedback between membrane potential and $[\text{ca}]_i$ underlie intermittent early afterdepolarizations and arrhythmias.”, *Circ Arrhythm Electrophysiol*, vol. 8, no. 6, pp. 1472–1480, Dec. 2015.
- [48] Sutanto, H., Sloun, B. van, Schonleitner, P., Zandvoort, M. A. M. J. van, Antoons, G., and Heijman, J., “The subcellular distribution of ryanodine receptors and L-Type Ca^{2+} channels modulates Ca^{2+} -transient properties and spontaneous Ca^{2+} -release events in atrial cardiomyocytes.”, *Front Physiol*, vol. 9, p. 1108, 2018.

Paper IV

A computational study of the effects of rapid atrial pacing-induced remodeling on calcium wave propagation in rabbit atrial cardiomyocytes

Márcia R. Vagos, Hermenegild Arevalo, Jordi Heijman, Ulrich Schotten, Joakim Sundnes

IV

A computational study of the effects of rapid atrial pacing remodeling on calcium wave propagation in rabbit atrial cardiomyocytes

Márcia R. Vagos^{1,2}, Hermenegild Arevalo^{1,3}, Jordi Heijman⁴, Ulrich Schotten⁴, Joakim Sundnes^{1,2,3}

¹ Simula Research Laboratory, Computational Physiology Department, Martin Linges vei 25, 1325 Lysaker, Norway

² University of Oslo, Department of Informatics, Gaustadalléen 23B, 0373 Oslo, Norway

² Center for Cardiological Innovation (CCI), Rikshospitalet, 0372 Oslo, Norway

² CARIM School for Cardiovascular Diseases, Faculty of Health, Medicine and Life Sciences, Maastricht University, Universiteitssingel 50, 6229 ER Maastricht, Netherlands

Abstract

In atrial cardiomyocytes without a well-developed T-tubule system, calcium diffuses from the periphery towards the center via centripetal calcium waves. Remodeling of the processes controlling calcium diffusion can result in a failure of calcium wave propagation towards the cell center, in what has been termed “calcium silencing”. This has been observed in rabbit atrial cardiomyocytes after exposure to prolonged rapid pacing. Although experimental studies have pointed to possible mechanisms underlying calcium silencing, their individual effects and relative importance remain largely unknown.

In this study we used computational modelling of the rabbit atrial cardiomyocyte to query the individual and combined determinants of calcium silencing and abnormal calcium wave propagation. We employed a population of models obtained from a newly developed model of the rabbit atrial cardiomyocyte with spatial calcium description of intracellular calcium handling. We selected parameters in the model that represent experimentally observed cellular remodeling which have been implicated in calcium silencing, and scaled their values in the population to match experimental observations. In particular, we changed the maximum conductances of L-type calcium (I_{CaL}), sodium-calcium exchanger (I_{NCX}), and sodium-potassium pump (I_{NaK}) currents, ryanodine receptor (RyR) open probability and density, Serca2a density, and calcium buffering strength. We incorporated remodeling in a population of 16 models by independently varying parameters that reproduce the experimentally observed remodeling. We then quantified resulting alterations in calcium wave propagation patterns, and classified models in different wave propagation categories.

Our results show a strong effect of I_{CaL} in driving calcium silencing, with I_{NaCa} , I_{NaK} , and RyR density also resulting in calcium silencing in some models. Potentially proarrhythmic calcium alternans were observed in some models where I_{NaCa} and Serca2a density had been changed. Simultaneously incorporating changes in all remodeled parameters resulted in calcium silencing in all models, indicating the dominant role of decreased I_{CaL} in the population phenotype.

This study provides insight into the underlying mechanisms of calcium silencing and altered wave propagation in rabbit atrial cardiomyocytes and motivates further investigations into the effects of altered calcium diffusion on wave-propagation abnormalities and arrhythmogenesis.

IV.1 Introduction

Computational models of cardiac electrophysiology are important tools for studying the mechanisms of heart disease and impaired cardiomyocyte (CM)

function, and have been particularly relevant in the study of arrhythmic events such as atrial fibrillation (AF) [1]–[3]. An important application of the computational models is the interpretation and translation of knowledge gained from animal experiments performed on a variety of different species. Atrial CMs have a less well-developed T-tubule system than their ventricular counterpart, and in many species this results in markedly different intracellular Ca^{2+} dynamics [4]. In both cell types Ca^{2+} enters via L-type Ca^{2+} channels, locally accumulates close to the membrane, and triggers Ca^{2+} -induced Ca^{2+} release from Ca^{2+} release units (CRU) in the junctional sarcoplasmic reticulum (SR) into the cytosol. The complex T-tubular system of ventricular cells effectively ensures that every CRU is in close proximity with the membrane, and therefore that this process occurs simultaneously throughout the cell. In atrial cells without well-developed T-tubules, only a small fraction of the CRU are close to the membrane and therefore activated by the initial L-type channel influx [5]. Activation of the remaining CRUs occurs as a Ca^{2+} wave that propagates from the membrane towards the center of the cell via a regenerative 'fire-diffuse-fire' response [6], [7]. As one CRU is activated, Ca^{2+} diffuses through the cytosol causing a local concentration rise at the neighboring CRUs, which then reaches the threshold level for activation and releases more Ca^{2+} , and the process repeats resulting in a centripetally propagating Ca^{2+} wave.

Given the heterogeneous nature of intracellular Ca^{2+} signalling in atrial CMs [7], they are prone to developing Ca^{2+} instabilities, such as local fluctuations in cytosolic Ca^{2+} levels, and intracellular Ca^{2+} waves, which can translate into arrhythmogenic activity [8]–[10]. Furthermore, sustained arrhythmic conditions such as AF can lead to severe electrophysiological remodeling of atrial CMs, including up- or down-regulation of numerous ion channels and other membrane transporters [11]. Furthermore, remodeling of the Ca^{2+} handling system, and in particular of the RyRs has been shown to be implicated in abnormal Ca^{2+} release which, including increased CaT refractoriness, and increased dispersion of Ca^{2+} release restitution [12]. This in turn has been associated with increased susceptibility to alternans [12], ectopic activity and arrhythmias [13], [14]. For instance, Ca^{2+} alternans have been extensively observed and implicated as precursors of AF episodes in patients [15]–[18].

It has also been shown in rat atrial CMs that under basal conditions, Ca^{2+} does not fully propagate towards the center of the cell, mainly due to extensive Ca^{2+} buffering, as well as the diffusion barrier of the mitochondria and Serca2a [19]. It is believed that this lack of a Ca^{2+} signal at the inner regions of the cell under normal conditions acts as a reserve to allow Ca^{2+} release to be increased under conditions of higher contraction demand, such as during β -adrenergic stimulation. Although atrial CMs of rabbit and rat species share similar morphological traits, such as size, and the lack of a well-developed T-tubule system, atrial CM from control rabbits do show a fully regenerative centripetal Ca^{2+} wave at baseline. However, there is a complete absence of Ca^{2+} propagation at the center of the cell in rapid atrial pacing (RAP)-remodeled CMs [20]. This phenomenon was termed ' Ca^{2+} silencing', and was suggested to be a cardio-protective mechanism of the cell to suppress arrhythmogenic after-

IV. A computational study of the effects of rapid atrial pacing-induced remodeling on calcium wave propagation in rabbit atrial cardiomyocytes

depolarizations [21]. Additionally, cytosolic Ca^{2+} buffering plays a significant role in regulating free Ca^{2+} availability [22], which is thought to modulate Ca^{2+} wave dynamics [20], [23], [24]. However, the exact mechanisms leading to Ca^{2+} silencing and their relative importances remains unclear.

In the present study we aim to elucidate the mechanisms Ca^{2+} silencing by comparing computational model results with experimental observations. We have previously developed a model of the rabbit atrial CM with spatial Ca^{2+} description [25], which was parameterized to match experimentally observed rabbit-specific electrophysiology using a population-of-models approach. The parameterization resulted in 16 different models of the rabbit atrial CM, each with a unique combination of ion channel maximum conductances, but all closely matching experimentally observed electrophysiology characteristics. All models showed rabbit-like action potential (AP) and Ca^{2+} transient (CaT) morphologies, as well as fully propagating Ca^{2+} waves. The purpose of the present study is to assess the role of different cellular parameters that are believed to change as a result of pacing-induced remodeling by changing their values in the model in a one-at-a-time fashion, and applying these changes to each of the 16 models obtained from our previous study [25]. Rabbit atrial CMs subject to RAP-dependent remodeling showed alterations in I_{CaL} , I_{NaCa} , and I_{NaK} current density or activity, as well as increased ryanodine receptor (RyR) open probability and density, increased Ca^{2+} buffering strength, and decreased Serca2a activity [20]. Therefore, we changed parameters in the model that modulate these cellular functions by scaling their values in accordance with experimental observations [20]. Thus, the changes introduced in the model to incorporate remodeling effects are based on direct measurements rather than indirect estimates from AP or CaT observations.

Furthermore, it has been extensively shown that cardiac CMs have a large degree of variability in ion channel expression levels, and electrophysiological properties. Therefore, the advantage of changing the parameters in 16 different models is that it allows to incorporate electrophysiological variability in the simulations, and provides a more comprehensive assessment of the effects of each individual parameter. Therefore, using a population of models, rather than a single ‘representative’ model, provides a more robust and insightful analysis of the model behavior under uncertainty, and by testing the effects of parameters in different model instances it is possible to obtain a more generalized response of the model, while identifying possible drivers of the observed responses.

IV.2 Methods

IV.2.1 Control population

We used the previously published model of the rabbit atrial CM with spatial description of the Ca^{2+} handling system. This model contains domain-specific Ca^{2+} dynamics and thus allows to simulate intracellular Ca^{2+} wave propagation. A complete description of the model development and structure is provided in Vagos et al. [25]. In brief, the model was based on the rabbit atrial CM

model by Aslanidi et al. [26], and the human atrial CM by Voigt&Heijman et al. [14]. Conceptually, the model is based on segmenting the CM into slices in the longitudinal direction, which are further sub-divided into domains in the radial direction. The domains are discrete units which contain ionic concentrations, ionic currents, and Ca^{2+} handling components. As described in detail in [25], the model distinguishes between the domains close to the membrane and the interior domains. The inner domains contain the cytosol, sarcoplasmic reticulum (SR), a sub-SR space (SRS), and Ca^{2+} release units (CRU), while the membrane domains also contain the sarcolemmal currents; I_{CaL} , I_{CaT} , I_{Na} , I_{K1} , I_{to} , I_{Kr} , I_{Ks} , I_{NCX} , I_{NaK} , I_{CaP} , I_{Cab} , I_{Nab} , and I_{Clb} . The membrane domains (1 and 18) also include a subsarcolemmal (SL) space. In these domains, the SRS represents a junctional space in which LTCC and the ryanodine receptors (RyR) interact, and thus this is indicated with “junc”. Each intracellular domain has a volume of 16 pL, which corresponds, with the cytosolic, SR, SRS/junc, and SL spaces occupying 65%, 3.5%, 0.1%, and 2% of the domain volume, respectively.

The calibrated population of models developed in [25] consists of 16 models with rabbit-like electrophysiological parameters: (1) fully regenerative Ca^{2+} wave propagation from periphery to center of the cell; (2) absence of alternans or afterdepolarizations; and (3) AP and whole-cell CaT morphologies within the physiological ranges experimentally observed in rabbit atrial CMs. The models differed only in the values of maximum conductances of the ionic currents, thus capturing the natural variability observed in atrial cells. Henceforth we will refer to these 16 models as the ‘control population’, and its main characteristics are illustrated in Figure IV.1. Panels A and B show the APs and the CaTs from the membrane domains, CaT_m , and from innermost domains, CaT_c . An exemplary Ca^{2+} wave from one of the models is also shown in panel C of Fig.IV.1.

IV.2.2 Incorporating RAP remodeling

An experimental study has shown that rabbit atrial CMs subjected to rapid atrial pacing (RAP), at 10 Hz for 5 days, developed an array of cellular remodeling at the structural and biochemical levels [20]. Most notably, a decrease in I_{CaL} and I_{NaK} currents, an increase in I_{NCX} , reduced Serca2a density, increased RyR open probability, decreased RyR cluster density, and increased Ca^{2+} buffering strength were observed. Cellular remodeling was incorporated by scaling the model parameters that modulate the affected cellular mechanisms to match experimental measurements. The alterations listed in Table IV.1 were applied to the control population, resulting in 8 different remodeled populations. By applying individual alterations to a calibrated control population, rather than a single representative model, we were able to assess their relative importance on Ca^{2+} wave dynamics, as well as to capture more of the natural variability and parameter uncertainty underlying the models.

IV. A computational study of the effects of rapid atrial pacing-induced remodeling on calcium wave propagation in rabbit atrial cardiomyocytes

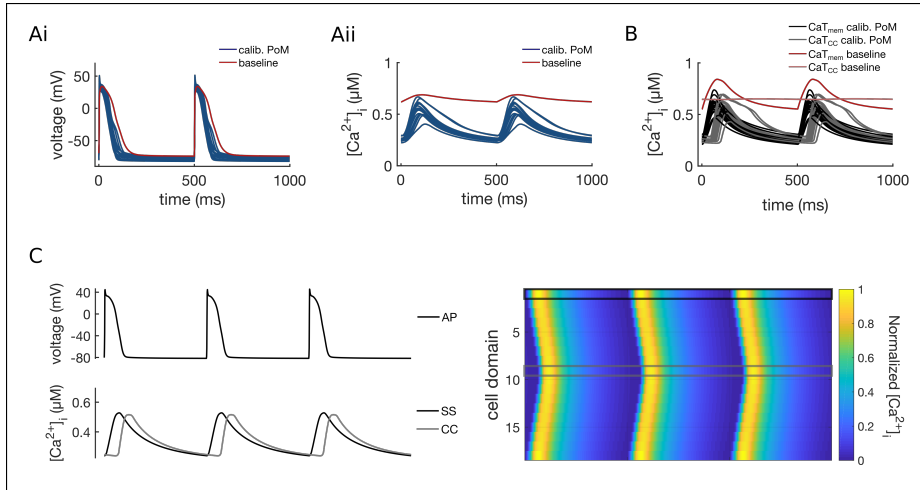


Figure IV.1: APs (A), and CaTs at the membrane domains (SS), and at the center of cell (CC) (B) of the control PoM ($n=16$). (C) AP and CaTs of model #1 of the control PoM (Table Table III.8 in Paper III), and corresponding simulated line scan. The black and red rectangles on the line scan indicate the domains from which CaT_m and CaT_c were extracted, respectively.

IV.2.3 Vizualization and analysis of calcium waves

Calcium wave propagation in the models was visualized in spatio-temporal plots of CaTs from each cell domain over time, equivalent to line-scan images of individual CMs. We characterized the individual remodeling effects by studying the occurrence of CaT amplitude alternans and the occurrence of Ca^{2+} silencing. Ca^{2+} alternans arise from instabilities in the Ca^{2+} handling system [27]–[29], and have also been clinically associated with arrhythmogenesis. We defined alternans as beat-to-beat differences in CaT amplitude larger than 5%, while Ca^{2+} silencing was defined as a ratio of central to membrane CaT amplitude (CaT_c amplitude/ CaT_m amplitude) ≤ 0.10 for all beats. Based on the presence of alternans and Ca^{2+} silencing, the individual models were classified into five different categories:

1. normal propagation;
2. Ca^{2+} alternans;
3. Ca^{2+} silencing;
4. alternans and Ca^{2+} silencing;
5. unphysiological wave patterns ('other').

Finally, we also report values of AP duration at 90% repolarization (APD90), and of resting membrane potential (RMP) of the remodeled populations, since APD90 shortening and RMP depolarization have been linked to arrhythmogenic activity in CMs [11], [30] and thus are important quantities to characterize pro-arrhythmic remodeling.

Table IV.1: List of the 8 different RAP-induced remodeled populations, and the parameters changed in the rabbit atrial CM model to represent remodeling in each case.

#	Remodeling	Parameters	Parameters definition
1	Down-regulation of I_{CaL}	G_{CaL}	Maximum conductance of the L-type Ca^{2+} channel
2	Up-regulation of I_{NCX}	I_{NaCa}^{max}	Maximum flux of the Ca^{2+} - Na^+ exchanger
3	Down-regulation of I_{NaK}	I_{NaK}^{max}	Maximum flux of the Na^+ - K^+ pump
4	Decreased Serca2a density	J_{up}^{max}	Maximum pump flux
5	Increased RyR open probability	RyR_P[0] RyR_P[1] RyR_P[5]	RyR property to balance open probability and SR Ca^{2+} leak RyR property to balance open probability and CaT amplitude RyR single-channel open probability
6	Decreased RyR density	RyR_P[11] NRyRs	RyR2 density in SR fractions Number of ryanodine receptors per cluster
7	Increased Ca^{2+} buffering strength	Buff_factor	Ca^{2+} buffering factor
8	Full remodeling	All	-
#	Baseline value	Scaling	
1	see [25]	0.4	
2	see [25]	2.5	
3	see [25]	0.5	
4	0.0053	0.7	
	0.2		
5	0.22	2	
	8E-5		
6	0.007		
	198000	0.25	
7	1.0	0.15	
8	-	-	

IV.3 Results

IV.3.1 Effects of changing RAP-remodeling parameters

In this section we list the effects of the remodeling alterations defined in Table IV.2, including both the individual mechanisms and the combined effect of all mechanisms.

IV.3.1.1 Down-regulation of I_{CaL}

Fig.IV.2-1 shows the population after reduction of G_{CaL} to 40%, which resulted in a consistent response of Ca^{2+} silencing across all models. An example of a Ca^{2+} wave from this population is shown in Fig.IV.3B. Additionally, CaT_m showed a considerably reduced amplitude as compared to the control population, as would be expected since the amplitude of the sarcolemmal CaT is directly linked to the magnitude of I_{CaL} . We also observed a significantly shortening of APD90 (Table IV.2) in this population, which is a well-documented effect of reduced I_{CaL} in CM models.

IV. A computational study of the effects of rapid atrial pacing-induced remodeling on calcium wave propagation in rabbit atrial cardiomyocytes

IV.3.1.2 Up-regulation of I_{NaCa}

The effects of increasing I_{NaCa}^{max} in the population resulted in a variety of Ca^{2+} wave propagation patterns, including Ca^{2+} alternans, silencing, and alternans and silencing, see Panel 3 of Fig.IV.2. Additionally, this modulation produced large variations in APD90 across the population, with a mean APD90 larger than in the control population, as well as large variations in CaT amplitudes and diastolic Ca^{2+} levels. Furthermore, one of the models failed to repolarize, as seen from the ripples in Fig.IV.2 Panel 2A, with corresponding rippled CaTs (not shown). This model corresponded to a $[Na^+]_i$ of 41 mM, quite far from physiological values, and a $[Ca^{2+}]_i$ of 5.8 μM . The perturbations in AP and CaTs observed in this population are not surprising given the known role of I_{NCX} in regulating both $[Ca^{2+}]_i$ and repolarization [31].

IV.3.1.3 Down-regulation of I_{NaK}

Decreasing I_{NaK}^{max} resulted in about 60% of the models developing Ca^{2+} silencing, while the remainder did not significantly change. This population showed significantly elevated $[Na^+]_i$ levels (22 ± 4 mM versus 9.5 ± 2 mM, (two-sample t -test, $\alpha=0.05$), as expected given the decreased outflow of Na^+ from the cell, which shifted the activity of I_{NCX} . As a consequence of reducing I_{NaK}^{max} , the magnitude of the forward mode and reverse mode components of I_{NCX} (measured as maximum and minimum current values during a complete AP) were significantly smaller and larger, respectively, in the I_{NaK}^{max} population as compared to the control (two-sample t -test, $\alpha=0.05$). Of note, the reverse mode component is typically relatively small as compared to the forward mode component of I_{NCX} . This resulted in an accumulation of Ca^{2+} in the cytosol and in the SR.

RMP was also significantly more depolarized, possibly due to a reduction in I_{K1} in this population (-74 mV in I_{NaK}^{max} -remodeled versus -80 mV in control PoM). Although we did not find any association between RMP and the magnitude of I_{NaK} or I_{K1} , we did find a significant correlation between RMP and I_{CaP}^{max} (Kendall's $\tau=-0.6$, $p\text{-val}=0.001$). However, the mechanism underlying this possible association in the model is not clear.

CaT_m amplitude and diastolic Ca^{2+} levels varied also considerably in this population (see Fig.IV.2 Panel 3B and TableIV.2). Although the maximum conductances of the models that either showed normal propagation or Ca^{2+} silencing did not show observable differences, we did find that models showing Ca^{2+} silencing mostly corresponded to higher values of both $[Na^+]_i$, and $[Ca_{SR}]$.

IV.3.1.4 Decreased Serca2a density

Decreasing Serca2a density to 70% of baseline value resulted in largely unchanged APs, and an overall small effect on CaT_m and CaT_c , with only about 20% of the models showing alternans and the others being mostly unaltered.

IV.3.1.5 Increased RyR open probability

Increasing RyR open probability resulted in about 40% of the models developing Ca^{2+} silencing. None of the models resulted in the development of alternans, as opposed to experimental observations of increased alternans threshold in AF-remodeled dog CMs [12]. Additionally, we did not observe any associations between the occurrence of Ca^{2+} silencing in this PoM and the values of the maximum conductances, nor $[\text{Na}^+]_i$ and $[\text{CasR}]$.

IV.3.1.6 Decreased RyR density

The effect of decreasing RyR density largely resulted in a variety of unphysiological Ca^{2+} propagation patterns. One such wave pattern is shown in Fig.IV.3F. This result indicates that the Ca^{2+} system in this model is quite sensitive to such large changes of the two target parameters, NRyRs and RyR_P[11].

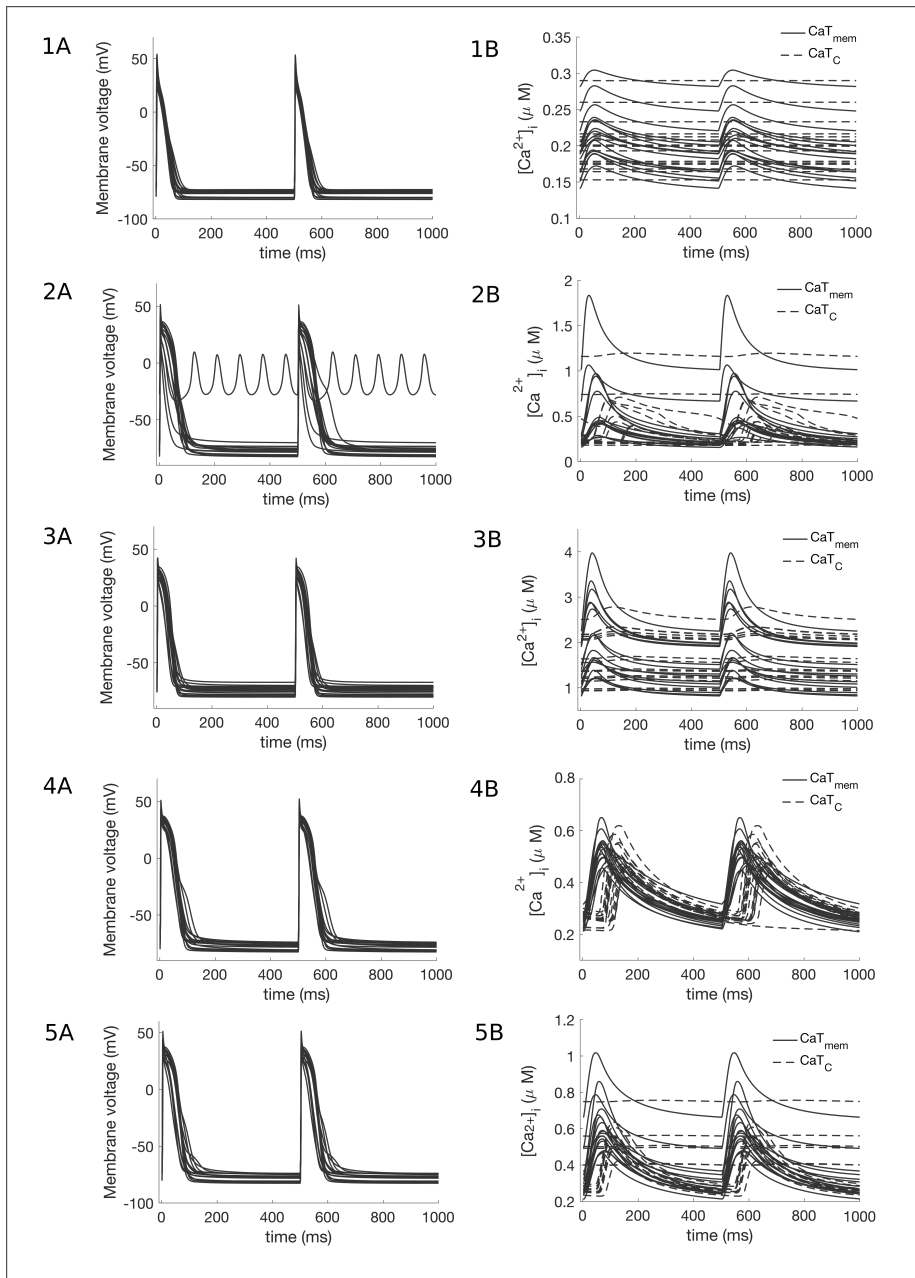
IV.3.1.7 Increased Ca^{2+} buffering strength

Increasing the Ca^{2+} buffering strength in the population did not result in any form of abnormal Ca^{2+} wave propagation, with all models showing a normal Ca^{2+} propagation pattern. This is in contrast with experimental observations from Greiser et al. [20] where the authors reported that an increased Ca^{2+} buffering strength in the cell was likely to be correlated with the observed Ca^{2+} silencing in the remodeled cells.

IV.3.1.8 Full RAP remodeling

Finally, we simultaneously incorporated all seven RAP remodeling mechanisms considered above. This change incorporating all 10 parameter changes listed in Table IV.1, resulted in a population with significantly shorter APD90, reduced CaT_m amplitude, and Ca^{2+} silencing. This result is in good agreement with experimental observations in [20], where the authors observed Ca^{2+} silencing in linescans of RAP remodeled cells, without the occurrence of alternans or other pathological Ca^{2+} propagation behaviors.

IV. A computational study of the effects of rapid atrial pacing-induced remodeling on calcium wave propagation in rabbit atrial cardiomyocytes



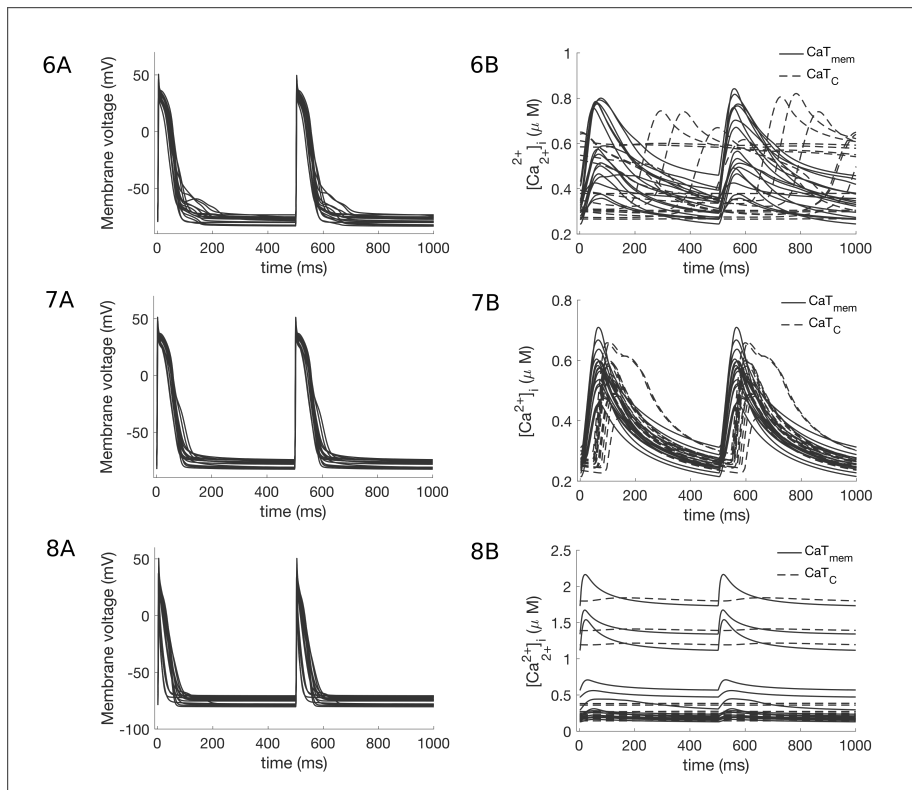


Figure IV.2: RAP remodeled populations (1-8): (A) action potentials, and (B) CaT_m and CaT_c traces.

Table IV.2: AP and CaT properties (mean \pm std) of the control and remodeled populations.

Population	APD90 (ms)	RMP (mV)	CaTA _m (μM)	CaTA _c (μM)	CaT _{ratio}
Control	96 \pm 13	-78 \pm 2	0.33 \pm 0.07	0.32 \pm 0.06	0.99 \pm 0.20
G _{CaL}	65 \pm 9	-76 \pm 3	0.033 \pm 0.006	0.0001 \pm 0.00	0.0040 \pm 0.0009
I _{NaCa} ^{max}	113 \pm 90	-73 \pm 17	0.32 \pm 0.23	0.15 \pm 0.13	0.47 \pm 0.38
I _{NaCa} ^{max}	69 \pm 10	-74 \pm 4	0.76 \pm 0.40	0.078 \pm 0.07	0.086 \pm 0.04
Serca2a density	92 \pm 13	-78 \pm 3	0.28 \pm 0.05	0.23 \pm 0.06	0.84 \pm 0.28
RyR Po	91 \pm 17	-77 \pm 3	0.32 \pm 0.08	0.17 \pm 0.14	0.57 \pm 0.45
RyR dens.	107 \pm 29	-78 \pm 3	0.26 \pm 0.13	0.064 \pm 0.07	0.18 \pm 0.20
Ca ²⁺ buff.	93 \pm 12	-78 \pm 3	0.31 \pm 0.06	0.28 \pm 0.05	0.92 \pm 0.19
full remodeling	57 \pm 19	-75 \pm 3	0.13 \pm 0.14	0.0061 \pm 0.013	0.019 \pm 0.030
Population	CD50 _m (ms)	CD50 _c (ms)			
Control	94 \pm 15	108 \pm 28			
G _{CaL}	114 \pm 10	71 \pm 33			
I _{NaCa} ^{max}	77 \pm 26	107 \pm 61			
I _{NaK} ^{max}	64 \pm 8	159 \pm 19			
Serca2a density	100 \pm 17	99 \pm 17			
RyR Po	90 \pm 14	119 \pm 36			
RyR density	119 \pm 33	76 \pm 56			
Ca ²⁺ buff.	96 \pm 15	110 \pm 20			
full remodeling	102 \pm 29	86 \pm 77			

IV. A computational study of the effects of rapid atrial pacing-induced remodeling on calcium wave propagation in rabbit atrial cardiomyocytes

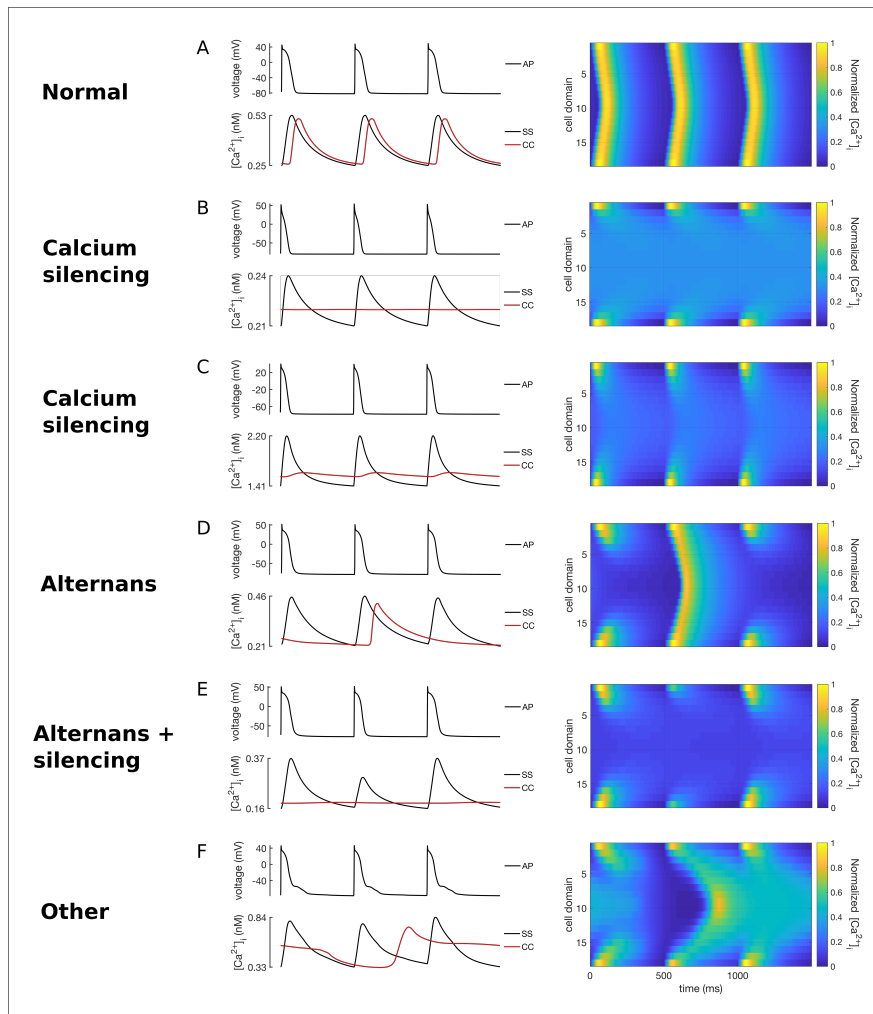


Figure IV.3: Exemplary Ca^{2+} waves from the RAP remodeled populations showing Ca^{2+} propagation patterns from the 5 wave categories.

Table IV.3: Effects of individually changing the RAP parameters in each of the 16 models of the control population. Values correspond to % incidence of each type of Ca^{2+} wave patterns in the population.

Population	Normal	Alternans	Silencing	Alt+Silenc	Other
Control	100	0	0	0	0
G_{CaL}	0	0	100	0	0
$I_{\text{NaCa}}^{\text{max}}$	37.5	31.25	18.75	6.25	6.25
$I_{\text{NaK}}^{\text{max}}$	37.5	0	62.5	0	0
Serca2a density	87.5	12.5	0	0	0
RyR Po	62.5	0	37.5	0	0
RyR density	0	0	31.25	0	68.75
Ca^{2+} buffering strength	100	0	0	0	0
Full RAP remodeling	0	0	100	0	0

IV.4 Discussion

We used a previously developed population of 16 models representing normal rabbit atrial electrophysiology, and incorporated known remodeling effects from rapid atrial pacing. We built 8 new populations, each incorporating one or a set of remodeled parameters representing a single physiological alteration, such as altered expression levels of an ionic current. One of the populations incorporated the changes in all parameters simultaneously to simulate full RAP remodeling, as has been observed experimentally [20].

In our simulations each remodeled population showed different phenotypes, especially in the CaT morphologies. More importantly, some parameter changes lead to similar outcomes across the population (I_{CaL} and Ca^{2+} buffering strength), while others resulted in myriad different phenotypes (especially $INCX$ and RyR density). The overall effects of changing RAP parameters in the 16 models are compiled in Table IV.3, and population APD90, RMP, and CaT characteristics are compiled in Table IV.2. Mean CaT_m amplitude was significantly reduced in the G_{CaL} , I_{NaCa}^{max} , I_{NaK}^{max} , and RyR_P [11] populations, while CaT_c amplitude was reduced in all populations, except the $Buff_factor$ population. These amplitude changes resulted in an overall reduced CaT_{ratio} in the G_{CaL} , $I_{NaCa}^{max}, I_{NaK}^{max}$, $Serca2a$ density, $RyR Po$, and RyR density populations.

In our simulations Ca^{2+} silencing was mainly driven by reduction of G_{CaL} and I_{NaK}^{max} , when these parameters are changed individually. The similarities between the G_{CaL} and full remodeling populations indicate that the 60% reduction of G_{CaL} was the dominant effector of changes in AP and CaT morphologies. Furthermore, despite significant differences in APD90 and RMP among the various remodeled populations, with one model showing an afterdepolarization and another showing failed repolarization, APs were mostly consistent across the population. Greater differences were observed in CaT_m and CaT_c morphologies, especially in the G_{CaL} , I_{NaCa}^{max} , $RyR Po$, RyR density, and full remodeling populations. Furthermore, changes in G_{CaL} , $Serca2a$ density, $Buff_factor$, and full remodeling resulted in consistent alterations in Ca^{2+} wave propagation patterns, while changes in the other parameters entailed a more complex response, despite considerable differences in the values of their maximum ionic conductances. In contrast, changes in the other parameters which resulted in a more varied set of responses indicate that those parameters play a more complex role in the Ca^{2+} handling system, where the values of maximum ionic conductances may also have had an impact.

Experimental observations from Greiser et al. [20] suggested that the main driver of Ca^{2+} silencing in rabbit atrial cells could be increased Ca^{2+} buffering strength, whereas the reduction in I_{ICaL} was unlikely to play a significant role. Our computer simulations of the full remodeling case, which aims to emulate the array of cellular alterations measured experimentally, are consistent with the experimental observations of Ca^{2+} silencing following RAP remodeling. However, our results indicate that reduced I_{CaL} , rather than increased Ca^{2+} buffering strength, may be the main effector of Ca^{2+} silencing. Ca^{2+} alternans were only observed in two of the remodeled populations (I_{NaCa}^{max} and $Serca2a$ density), and in

IV. A computational study of the effects of rapid atrial pacing-induced remodeling on calcium wave propagation in rabbit atrial cardiomyocytes

a fairly low percentage of the models. This low occurrence of alternans suggests that they are the result of more drastic changes in cellular mechanisms, which were not captured in the remodeled populations constructed here. Overall, the results presented here provide insight into the possible mechanisms of Ca^{2+} silencing in rabbit atrial CMs.

The approach used here to quantify the effects of changing model parameters on model behavior differs from the more traditional approach where a single model is used to represent a certain region of the heart, animal species, or genotype. In contrast, we opted to use a small population of 16 models, obtained by calibrating a population of 3000 models to experimentally measured rabbit electrophysiological parameters. The advantage of the population approach over a single model approach is that it allows to incorporate natural inter- and intra-regional variability observed in the atria. Therefore, this approach provides a more robust analysis of the effects of incorporating electrical remodeling into the model, and how these changes may be related to observed Ca^{2+} wave patterns.

As with any modelling study, the approach developed here has its own limitations and assumptions. We note that, although the approach proposed here, whereby variability in maximum ionic conductances is taken into account, can improve robustness and reliability of simulation results, the control population used in this study is only an abstraction for a real population of myocytes obtained from different specimens and varying regions of the heart. The control population was produced by experimentally calibrating a population of 3000 models against rabbit APs and CaTs characteristics [25], and thus the variation in maximum conductances introduced in the population cannot be verified experimentally as of this point due to the lack of data. A more holistic approach would be to take into account experimental variability in ionic channel expression levels, for instance, and calibrating the simulated population accordingly. However, we also note that this does not invalidate the results presented here in that the control models are still valid representations of healthy rabbit atrial CMs. Furthermore, the methods presented here can be equally applied to other populations and remodeling case scenarios. The population can also be expanded via re-sampling of the maximum conductances, such as introducing perturbations around the baseline values, and recalibrating. Additionally, we also note that the work developed here can be further extended by incorporating variability in the RyR parameters, and J_{up}^{\max} , and Buff_factor as well, thereby producing a population that more reliably captures the full spectrum of Ca^{2+} wave propagation patterns that result from RAP remodeling.

IV.5 Conclusions

This study proposed an approach for analysing the effects of RAP-induced remodeling in a population of healthy rabbit atrial CMs. The remodeling changes were implemented on the population one-by-one to dissect the effects of each remodeled component individually, and simultaneously to reproduced the experimentally observed array of changes.

The results indicate that reduced I_{CaL} was the main determinant of the occurrence of Ca^{2+} silencing, with decreased I_{NaCa}^{max} , increased I_{NaK}^{max} , double RyR open probability, and reduced RyR density also resulting in some cases of Ca^{2+} silencing. Reduction in I_{NCX} , and in Serca2a density also resulted in Ca^{2+} alternans in a small percentage of instances. Furthermore, changes in RyR density largely resulted in unphysiological Ca^{2+} transients. This paper offers some insight on the mechanisms of altered Ca^{2+} wave propagation patterns in rabbit atrial CMs, and provides a framework for assessing effects of cellular remodeling in a cohort of healthy models.

Acknowledgments

This project has received funding from the European Union’s Horizon 2020 MSCA ITN under grant agreement No 675351.

References

- [1] Trayanova, N. A., “Mathematical approaches to understanding and imaging atrial fibrillation: Significance for mechanisms and management”, *Circulation research*, vol. 114, no. 9, pp. 1516–1531, Apr. 2014.
- [2] Grandi, E. and Maleckar, M. M., “Anti-arrhythmic strategies for atrial fibrillation: The role of computational modeling in discovery, development, and optimization.”, *Pharmacol Ther*, vol. 168, pp. 126–142, Dec. 2016.
- [3] Vagos, M., Herck, I. G. M. van, Sundnes, J., Arevalo, H. J., Edwards, A. G., and Koivumäki, J. T., “Computational modeling of electrophysiology and pharmacotherapy of atrial fibrillation: Recent advances and future challenges”, *Frontiers in Physiology*, vol. 9, p. 1221, 2018.
- [4] Blatter, L. A., “The intricacies of atrial calcium cycling during excitation-contraction coupling”, *The Journal of General Physiology*, vol. 149, no. 9, pp. 857–865, 2017.
- [5] Bootman, M. D., Smyrnias, I., Rüdiger, Coombes, S., and Roderick, H. L., “Atrial cardiomyocyte calcium signalling”, *Biochimica et Biophysica Acta (BBA) - Molecular Cell Research*, vol. 1813, no. 5, pp. 922–934, 2011, Including the Special Section: 11th European Symposium on Calcium.
- [6] Keizer, J., Smith, G. D., Ponce-Dawson, S., and Pearson, J. E., “Saltatory propagation of Ca^{2+} waves by Ca^{2+} sparks.”, *Biophys J*, vol. 75, no. 2, pp. 595–600, 1998.
- [7] Trafford, A. W., Clarke, J. D., Richards, M. A., Eisner, D. A., and Dibb, K. M., “Calcium signalling microdomains and the t-tubular system in atrial myocytes: Potential roles in cardiac disease and arrhythmias.”, *Cardiovasc Res*, vol. 98, no. 2, pp. 192–203, May 2013.

IV. A computational study of the effects of rapid atrial pacing-induced remodeling on calcium wave propagation in rabbit atrial cardiomyocytes

- [8] Miura, M., Ishide, N., Oda, H., Sakurai, M., Shinozaki, T., and Takishima, T., “Spatial features of calcium transients during early and delayed afterdepolarizations.”, *Am J Physiol*, vol. 265, no. 2 Pt 2, H439–44, 1993.
- [9] Diaz, M., Eisner, D., and O’Neill, S., “Depressed ryanodine receptor activity increases variability and duration of the systolic Ca^{2+} transient in rat ventricular myocytes”, *Circulation Research*, vol. 91, no. 7, pp. 585–593, 2002.
- [10] Chang, K. C., Bayer, J. D., and Trayanova, N. A., “Disrupted calcium release as a mechanism for atrial alternans associated with human atrial fibrillation”, *PLOS Computational Biology*, vol. 10, no. 12, pp. 1–16, Dec. 2014.
- [11] Bosch, R. F., Zeng, X., Grammer, J. B., Popovic, K., Mewis, C., and Kuhlkamp, V., “Ionic mechanisms of electrical remodeling in human atrial fibrillation.”, eng, *Cardiovasc Res*, vol. 44, no. 1, pp. 121–131, Oct. 1999.
- [12] Liu, T., Xiong, F., Qi, X.-Y., Xiao, J., Villeneuve, L., Abu-Taha, I., Dobrev, D., Huang, C., and Nattel, S., “Altered calcium handling produces reentry-promoting action potential alternans in atrial fibrillation-remodeled hearts”, *JCI Insight*, vol. 5, no. 8, Apr. 2020.
- [13] Voigt, N., Li, N., Wang, Q., Wang, W., Trafford, A. W., Abu-Taha, I., Sun, Q., Wieland, T., Ravens, U., Nattel, S., Wehrens, X. H., and Dobrev, D., “Enhanced sarcoplasmic reticulum Ca^{2+} leak and increased $\text{Na}^+-\text{Ca}^{2+}$ exchanger function underlie delayed afterdepolarizations in patients with chronic atrial fibrillation”, *Circulation*, vol. 125, no. 17, pp. 2059–2070, 2012.
- [14] Voigt, N., Heijman, J., Qiongling, Chiang, D. Y., Li, N., Karck, M., Wehrens, X. H., Nattel, S., and Dobrev, D., “Cellular and molecular mechanisms of atrial arrhythmogenesis in patients with paroxysmal atrial fibrillation”, *Circulation*, vol. 129, no. 2, pp. 145–156, 2014.
- [15] Verrier, R. L. and Nearing, B. D., “Electrophysiologic basis for t wave alternans as an index of vulnerability to ventricular fibrillation.”, *J Cardiovasc Electrophysiol*, vol. 5, no. 5, pp. 445–461, May 1994.
- [16] Rosenbaum, D. S., Jackson, L. E., Smith, J. M., Garan, H., Ruskin, J. N., and Cohen, R. J., “Electrical Alternans and Vulnerability to Ventricular Arrhythmias”, *New England Journal of Medicine*, vol. 330, no. 4, pp. 235–241, 1994, PMID: 8272084.
- [17] Narayan, S. M., Bode, F., Karasik, P. L., and Franz, M. R., “Alternans of Atrial Action Potentials During Atrial Flutter as a Precursor to Atrial Fibrillation”, *Circulation*, vol. 106, no. 15, pp. 1968–1973, 2002.
- [18] Franz, M. R., Jamal, S. M., and Narayan, S. M., “The role of action potential alternans in the initiation of atrial fibrillation in humans: A review and future directions”, *Europace*, vol. 14, no. Suppl 5, pp. v58–v64, Nov. 2012.

- [19] Mackenzie, L., Roderick, H. L., Berridge, M. J., Conway, S. J., and Bootman, M. D., “The spatial pattern of atrial cardiomyocyte calcium signalling modulates contraction”, *Journal of Cell Science*, vol. 117, no. 26, pp. 6327–6337, 2004.
- [20] Greiser, M., Kerfant, B.-G., Williams, G. S., Voigt, N., Harks, E., Dibb, K. M., Giese, A., Meszaros, J., Verheule, S., Ravens, U., Allessie, M. A., Gammie, J. S., Velden, J. van der, Lederer, W. J., Dobrev, D., and Schotten, U., “Tachycardia-induced silencing of subcellular Ca^{2+} signaling in atrial myocytes”, *The Journal of Clinical Investigation*, vol. 124, no. 11, pp. 4759–4772, Nov. 2014.
- [21] Greiser, M., “Calcium signalling silencing in atrial fibrillation.”, *J Physiol*, vol. 595, no. 12, pp. 4009–4017, Jun. 2017.
- [22] Smith, G. L. and Eisner, D. A., “Calcium buffering in the heart in health and disease.”, *Circulation*, vol. 139, no. 20, pp. 2358–2371, May 2019.
- [23] Loughrey, C. M., MacEachern, K. E., Neary, P., and Smith, G. L., “The relationship between intracellular Ca^{2+} and Ca^{2+} wave characteristics in permeabilised cardiomyocytes from the rabbit.”, *J Physiol*, vol. 543, no. Pt 3, pp. 859–870, Sep. 2002.
- [24] Swietach, P., Spitzer, K. W., and Vaughan-Jones, R. D., “Modeling calcium waves in cardiac myocytes: Importance of calcium diffusion.”, *Front Biosci (Landmark Ed)*, vol. 15, pp. 661–680, Jan. 2010.
- [25] Vagos, M. R., Arevalo, H., Heijman, J., Schotten, U., and Sundnes, J., “A novel computational model of the rabbit atrial cell with spatial calcium dynamics”, 2020.
- [26] Aslanidi, O., Boyett, M., Dobrzynski, H., Li, J., and Zhang, H., “Mechanisms of transition from normal to reentrant electrical activity in a model of rabbit atrial tissue: Interaction of tissue heterogeneity and anisotropy”, *Biophysical journal*, vol. 96, pp. 798–817, Feb. 2009.
- [27] Weiss, J. N., Karma, A., Shiferaw, Y., Chen, P.-S., Garfinkel, A., and Qu, Z., “From pulsus to pulseless: The saga of cardiac alternans.”, *Circ Res*, vol. 98, no. 10, pp. 1244–1253, 2006.
- [28] Gaeta, S. A. and Christini, D. J., “Non-Linear Dynamics of Cardiac Alternans: Subcellular to Tissue-Level Mechanisms of Arrhythmia”, *Frontiers in Physiology*, vol. 3, p. 157, 2012.
- [29] Xie, Y., Izu, L. T., Bers, D. M., and Sato, D., “Arrhythmogenic transient dynamics in cardiac myocytes”, *Biophysical journal*, vol. 106, no. 6, pp. 1391–1397, Mar. 2014.
- [30] Workman, A. J., Kane, K. A., and Rankin, A. C., “The contribution of ionic currents to changes in refractoriness of human atrial myocytes associated with chronic atrial fibrillation.”, *Cardiovasc Res*, vol. 52, no. 2, pp. 226–235, Nov. 2001.

IV. A computational study of the effects of rapid atrial pacing-induced remodeling on calcium wave propagation in rabbit atrial cardiomyocytes

- [31] Weber, C. R., Ginsburg, K. S., Philipson, K. D., Shannon, T. R., and Bers, D. M., “Allosteric regulation of Na/Ca exchange current by cytosolic Ca in intact cardiac myocytes”, *The Journal of general physiology*, vol. 117, no. 2, pp. 119–131, Feb. 2001.